Turbulent Switching Arcs and Influence of Design Parameters on Performance of Auto-Expansion Circuit Breakers

by

Haoyu Wang

Thesis submitted in accordance with the requirements of the University of Liverpool for the Degree of Doctor in Philosophy

Department of Electrical Engineering and Electronics

March 2014

Copyright

Acknowledgements

Firstly, I would like to express my special appreciation to my supervisor, Dr. J D Yan, for his guidance, support and assistance throughout my postgraduate study.

I wish to thank Professor M. T. C. Fang who gave much guidance to me in some important and fundamental knowledge. I am particularly grateful to my colleague Mr Q Zhang for his support and help as well as all of my group members for their help and encouragement.

Finally, I dedicate everything to my parents Mr Wang, Jianping and Mrs Zhang, Shufang for all their love and support over the years.

Abstract

Turbulence enhanced momentum and energy transport is an important mechanism in shaping the flow and temperature field of low current turbulent SF_6 (Sulfur-hexafluoride) arcs burning in a nozzle. It is a factor that largely determines the prediction accuracy of the interruption capability of high voltage circuit breakers. Previous study [81] has shown that for SF_6 arcs the parameters in the Prandtl mixing length model and the two equation k-ε model must be adjusted to bring agreement between prediction and measurement. The experimental observation [109] of steep temperature or density gradient exists at the arc edge, where turbulence is usually strongest. The density gradient can be regarded as a result of temperature gradient when the pressure difference across the low current arc column is small.

In previous studies of turbulence models, the effects of large density or temperature gradient have not been considered. In the present work the k-ε model is modified to take into account the effect of the presence of steep local temperature gradient. The model is first applied to the steady state SF_6 nozzle arcs in the current range from 100 A to 1800 A. The performance of the modified turbulence model is assessed by a comparison of the predicted and measured radial temperature profiles at different currents and its behaviours with another two most commonly used turbulence models, the Prandtl mixing length model and the k-ε model. The relevant turbulence parameters of the Prandtl mixing length model are adjusted according to the different nozzle shapes with different values and it has been found that its applicability is limited. The modified k-ε model, which is modified to take into account the effect of large temperature gradient with all default coefficients, can make

reasonable prediction for turbulent arcs in the Aachen nozzle [67, 108] under direct current conditions. The model is then applied to the transient nozzle arcs in a GE nozzle [86] and the Campbell nozzle [85]. Finally, a real puffer-type circuit breaker of 252 kV has been used to verify this model. The predicted arc voltage and pressure agree reasonably well with the measurements at both high and low current levels, justifying the applicability of the modified k-ε turbulence model.

The auto-expansion circuit breaker is a relatively new interruption technique, which creates the required fast gas flow at current zero using the energy dissipated by the arc itself. A design study has been carried out for a prototype 245 kV auto-expansion circuit breaker at 50 Hz, in order to investigate the influence of key design parameters in terms of arcing conditions at the current zero phase and the critical RRRV (Rate of Rise of Recovery Voltage).

Auxiliary nozzle with different lengths, and the severity of leakage from the expansion volume have been implemented for testing the influence of design parameters in an auto-expansion circuit breaker. PC-based arc modelling taking account the effect of nozzle ablation and the mixing process of PTFE vapour with SF_6 has been made for auxiliary nozzle investigation. For the effect of leakage, various sizes of a leakage hole are specified on the valve of the expansion volume. The critical RRRV values for the Ref. Case and the its modifications are used for comparison of its interruption capability in order to estimate the influence of these key design parameters.

The solution of all of the equations in the arc models is based on a commercial computational fluid dynamics package, PHOENICS. PHOENICS has been extensively used at the University of Liverpool to model the arc behaviours since 1992. Before using PHOENICS to simulate the arc behaviour

in this thesis some conditions need to be resolved. These are related with the choice of turbulence model, the computational domain size for electric field, and the influence of the Lorentz force. The differential models for reported works in the thesis is implemented into PHOENICS version 3.6.1. All boundary conditions which are treated as sources terms are discussed in Section 2.3

Table of Contents

List of Figures

List of Tables

List of Acronyms

SF_6: Sulfur-hexafluoride

RRRV: Rate of Rise of Recovery Voltage

PTFE: Polytetrafluoroethylene

CFD: Computational Fluid Dynamic

CTE/LTE: Complete / Local Thermal Equilibrium

MVCB: Medium Voltage Circuit Breaker

HVCB: High Voltage Circuit Breaker

EHVCB: Extra High Voltage Circuit Breaker

UHVCB: Ultra High Voltage Circuit Breaker

IEC: International Electro-technical Commission

GIS: Gas Insulted Switchgear

BBC: Brown Boveri Research Centre

NSA: Non Slender Arc

SA: Slender Arc

NEC: Net Emission Coefficient

BFC: Body Fitted Coordinate

EMTP: Electromagnetic Transient Program

CHAPTER 1
Introduction

1.1 Arc Plasmas and their Applications

Plasma, the fourth state of matter appearing on the earth, was discovered by Davy [1] in 1808. It has unique characteristics in comparison with other states of matter, higher temperature, electrically conducting, and charged particles. In plasmas, electrons are liberated from atoms and catch complete freedom of motion. The freely moving electrons are able to transport electric current, so plasma is a type of conducting gas.

Plasmas can be classified in nature and in the laboratory (man-made) as a result of ionisation. These ionisations are produced by heat, radiation and electric discharge. It is known that the plasma is not a common state on the earth. The main reason that this can be considered is because it is too "COLD" on the earth, and the temperature is normally low. In the thermal equilibrium, the amount of gaseous ionisation is extraordinarily low ($\frac{n_i}{n_n} \approx 10^{-122}$) [2] at room temperature (300 K), which can be known by Saha equation.

$$\frac{n_i}{n_n} \approx 2.4 \times 10^{21} \frac{T^{3/2}}{n_i} e^{-U_i / KT} \tag{1.1}$$

where n_i and n_n are respectively the density of ionised atoms and of neutral atoms. T is the gas temperature, K is Boltzmann's constant, and U_i is the ionisation energy of the gas.

That is why plasmas exist in astronomical bodies with temperatures of millions of degrees, but not on earth.

Plasmas are widely encountered in industrial applications. The most widely used method to obtain plasma is through the electrical gas discharge. Typical examples include: electric sparks, electric arcs, gaseous flash lamps, radio frequency, microwave generated plasmas and so on [3]. The plasmas research in this thesis is all about the application of low temperature plasmas (range of temperature of 2,000-50,000 K).

1.1.1 Plasma characteristics

Plasma is a quasi-neutral gas of charged and neutral particles, which exhibits collective behaviour [2]. It is very different with the common gas behaviour, since plasma is a collection of large amount of charged particles. So these particles will be affected by electric force when these charges of positive and negative give rise to the electric field, and generate current, and magnetic field. And then these particles will affect the other charged particles far away.

An ionised gas is known as plasma if its Debye length is much larger than the average distance between constituting particles, and much smaller than the dimensions of the system. Plasma presents quasi-neutral in macro due to the electric field presence around each charged particle. So a cloud of ions would surround the negative charged particle and a cloud of electrons would surround the positive charged particle. If there is no thermal motions and balance with electrical interaction, the cloud of charges gives rise to the perfect shielding, and no electric field would be present outside of the clouds. The radius of cloud is so called Debye length. It is a measure of the shielding distance of the sheath.

1.1.2 Arc in local thermal equilibrium

Properties of thermal plasma can be described based on the temperature of the system. Plasmas in my research are in the Local Thermal Equilibrium (LTE), and the state of LTE is relative to Complete Thermal Equilibrium (CTE). The characteristics of CTE can be summarised as follows:

1. Unique temperature in the arc,
2. Particles of all velocities and the most probable distribution of these velocities are according to Maxwell-Boltzmann distribution, which is a special case of the Boltzmann distribution,
3. Distribution of internal energy obeys Boltzmann distribution,
4. All chemistry progress in plasma, the number densities of charged particle species are related through the Saha equation, and
5. The magnetic radiation field satisfy the Plank's law about the black body.

Actually, the CTE of plasma only exist in some particular conditions, for example some special planets in the universe. The plasma which is generated in the laboratory almost cannot exist in the state of CTE. In my thesis, it is known that an arc is sustained by Ohmic heating and the non-uniformity of the arc and imposed gas motion lead to mass, momentum and energy transfer. In many cases the arc discharge changing is rapid and the arc is in a transient state. All these cases cannot be considered in CTE state.

So another definition of the state of plasma is needed. That is the state of local thermal equilibrium which is relative to that of CTE. The LTE almost

obeys all the distributions and laws of CTE, except Plank's law. So it can be considered that some parts of gas are in the state of thermal equilibrium, but not all. For a switching arc, it is generated between two separate contacts when an electric current is interrupted. This type of arc discharge is characterised by low voltage drop in the cathode region and large current density at the cathode. The arc column between the cathode and anode is usually in LTE. In common with all LTE plasmas the material properties of an arc gas is determined by two thermodynamic quantities (e.g. temperature and pressure) and the distribution of particle population among different energy levels obeys Boltzmann's distribution. The behaviour of LTE plasma in gas flow is determined by conservation of mass, momentum and energy together with the equation of state, the laws governing electromagnetic fields, charge transport (Ohm's law) and supplementary relations for transport properties (i.e. electrical conductivity, viscosity etc.)

High temperature and high flux are the most important characteristics of the arc plasma. There are many applications of plasma generated by electric discharge. My research will aim to establish an improved mathematical model for arc where turbulence is important, in conjunction with detailed computational results for circuit breakers, which can then be used for optimum product design.

1.2 Background of High Voltage Circuit Breakers

1.2.1 General description

Two main classification of circuit breakers can be made substantially depending on their voltage class, which are the low voltage circuit breakers

(less than 1000 V), and high voltage circuit breakers (1000 V and above). The high voltage circuit breakers, can be further subdivided in to the medium voltage circuit breaker (MVCB) and the high voltage circuit breaker (HVCB). There is no clear division between the MVCB and the HVCB. MVCBs rated between 1 and 75 kV at the present, but it was changeable as the development of HVCB. A further group of HVCB can be classified into extra high voltage circuit breaker (EHVCB) and ultra high voltage circuit breaker (UHVCB) when voltage higher than 230 kV.

High voltage circuit breakers (Fig.1.1) are mainly used for protecting the electrical power transmission networks from various damages caused by overload or short circuit. When a short circuit fault occurs, it has to be detected by fault conditions and interrupt current flow. It is also used to connect and switch between different sets of circuits. The International Electro-technical Commission (IEC) defines the circuit breaker as a mechanical switching device, capable of making, carrying and breaking currents under normal circuit conditions and also making, carrying for a specified time and breaking currents under specified abnormal circuit conditions such as those short-circuit. The circuit breaker is usually intended to operate infrequently, although some types are suitable for frequent operation [4]. It is a good conductor when contacts are closed and an excellent insulator when contacts are separated. It is also needed to interrupt current flow as quickly as possible and to ensure the stability of the system. The speed of the interruption is a very important parameter in high voltage circuit breaker research.

Fig.1.1: LW15-550 outdoor H.V.A.C porcelain SF_6 circuit breaker from XIAN XD high voltage switchgear Co., Ltd.

1.2.2 History and development of high voltage circuit breakers

1.2.2.1 Oil circuit breaker

The air and oil are considered to be the first arc extinguishing mediums in the history of electric power switchgear. For the first forty years, high voltage circuit breaker research was based on oil [4]. The earlier bulk-oil circuit breaker is just simply separating contacts for interruption in oil. The first oil circuit breaker was developed in 1900, and in the following decades, the development of oil circuit breaker improved vastly. Arc is generated when separated contacts, specifically oil molecules dissociate under the high temperature of an arc. The high-pressure hydrogen gas bubbles created by the arc energy are advantageously used to confine, compress, and cool the arc. The breaking capacity is considered very low for this type of circuit breaker.

1.2.2.2 Air circuit breaker

The air circuit breaker was developed initially by the Westinghouse team in 1929. Arc extinction is achieved by magnetically forcing the arc into a chute where the arc is lengthened and cooled. Although the air is a very convenient insulating medium, the use of air as an interruption medium is restricted as long as it is used at a pressure of 1 bar. As the development of high voltage circuit breaker, greater pressure is required. The following air blast type is a further development of air circuit breaker. The arc burning between the contacts cannot be sustained when the applied voltage is less than the sum of the cathode drops of the series of arcs, it is utilized in interruption. The dielectric strength increases when the air is compressed. The switching arc is confined and cooled by the high-speed air flow through an insulating nozzle. It is also widely used in distribution voltage switchgear. The principle of interruption of air blast can be classified into two types, which are the axial blast circuit breaker and the cross blast type [4].

1.2.2.3 Vacuum circuit breaker

Vacuum, as an interruption medium, was first used by Sorensen [5] in 1926. Vacuum interrupter technology was truly practical in the 1960s. For the vacuum circuit breaker, it is no mechanical blast to help cooling of the arc can be applied to vacuum circuit breaker. The only physical process is arc itself. Comparing the oil circuit breaker with the SF_6 circuit breaker, this type of circuit breaker is safe and in fact harmless, but the problem is its relatively low unit voltage and the difficulty of making a unit a high continuous current.

1.2.2.4 SF_6 circuit breaker

SF_6 and air are the two main types of gas used in the gas blast type circuit breaker. In recent years, SF_6 almost replaced air as the main insulated medium. SF_6 is a colourless, odourless, non-flammable, inorganic, extremely potent greenhouse gas, which was discovered and produced by French researchers in 1900 [6]. Due to its excellent dielectric and arc quenching properties, it has been widely used for switchgear since the 1950s. Westinghouse first used SF_6 for real circuit breaker in 1959 [4]. The principle for this type of circuit breaker is very similar with the air circuit breaker. Two types of mechanical structure can be classified as double pressure type and gas blast type (puffer type). The second type, SF_6 circuit breaker, is a double pressure type. Two different levels of gas pressure exist inside the arc chamber. The lower SF_6 pressure of about 3 to 5 bar only has function of insulating and the higher SF_6 pressure of larger than 10 bar is used to blast in compressor. The capacity of arc interruption of this type of circuit breaker is outstanding and the speed of interruption is also very short. However, its structure is extremely complex. Consequently, the puffer type structure is proposed. Its structure is much simpler than the double pressure type structure. Improvement of mechanical structure significantly decreased the mechanical energy requirement for interruption. As the SF_6 type circuit breaker develops, the capacity of interruption of puffer type SF_6 circuit breaker may well be able to go beyond the double pressure type SF_6 circuit breaker. The circuit breaker used in Chapter three is the SF_6 puffer type circuit breaker.

1.2.2.5 Gas insulated switchgear

Gas Insulated Switchgear (GIS) is a further application which is based on the

SF_6 circuit breaker. It uses the dielectric capability of the pressurised gas to reduce the size of the equipment and increase its reliability. The principle of GIS is to insulate all the components (circuit breaker, disconnecting switch, earth switch, current transformer, potential transformer, cable sealing end, main busbar etc.) connected to the busbars of substations with SF_6 gas in a metal enclosure.

1.3 Review of Arc Models

In section 1.1, it is known that the electric arc was discovered at the beginning of the 19^{th} century. However, the fundamental investigation of physical progress of the electric arc was started around the period of the Second World War. The breakthrough of arc research was made by Libermann and Lowke [6] when the radiation characteristics of SF_6 were calculated. After that, the arc model developed rapidly. A detailed overview of the development of the arc models will follow.

1.3.1 Early arc models

The first attempt to describe arc interruption in high voltage circuit breaker was proposed by Slepian [7] in 1928. Slepian's model has successfully investigated the rate of recovery of dielectric strength of the gap increases faster rather than the rate of increase of the reapplied voltage across the two electrodes of the circuit breaker. After that, the first mathematical model of a dynamic arc was proposed by Cassie [8] in 1939. The arc was deemed a cylindrical shape and its temperature distribution is uniform on a cross section.

The diameter of the arc column will be changed as the current in a constant temperature. The gradient of arc voltage is a constant. So the heat loss (N)

depends mainly on convection loss and is proportional to the arc cross sectional area (A). Cassie's model is detailed below:

$$\frac{1}{i}\frac{di}{dt}-\frac{1}{E}\frac{dE}{dt}=\frac{1}{\theta}(\frac{E^2}{E_0^2}-1) \tag{1.2}$$

where i is the current, E the electrical field, t the time, E_0 the electrical field strength of the arc at steady state.

Here $\theta = Q/N$ a time constant of arc, where Q stored heat and N the heat loss. In Eq.(1.2), $E_0^2 = N/G$ where G is arc conductance (G=σA). Cassie's model is considered for analysis of a relatively large current, but not suitable to predict the arc near the current zero period because the arc temperature vary rapidly.

In the Mayr arc model, the arc is also regarded as a cylindrical shape of constant diameter. The arc conductance variation is attributed to a transition in the degree of ionisation. The improvement of Mayr's model is that the temperature can be changed while the power loss per unit length is a constant. It can solve the arc in a relatively small current level.

The conductance R corresponding to the ionisation degree, obtained from Saha's equation is expressed as:

$$R=k \exp(-Q/Q_0) \tag{1.3}$$

where k and Q_0 are constants, Q the heat content and Q_0 is the heat content at a steady state.

The energy balance equation is:

$$EI = \frac{dQ}{dt} + N_0 \tag{1.4}$$

and then, Mayr's expression can be deduced:

$$\frac{1}{R}\frac{dR}{dt} = \frac{1}{\theta}\left[\frac{EI}{N_0} - 1\right] \tag{1.5a}$$

or in another form:

$$\frac{1}{i}\frac{di}{dt} - \frac{1}{E}\frac{dE}{dt} = \frac{1}{\theta}\left(\frac{E_i}{\Gamma} - 1\right) \tag{1.5b}$$

where $\theta = Q_0 / N_0$ with a unit of time is called the arc time constant. Γ is the power loss per unit length. Mayr's model better represents the arc behaviour around current zero period than Cassie's model.

Models by Cassie and Mayr can be considered to predict some specific cases with different assumptions in switch arc and their applicability is quite limited. A further improvement of arc model to combine these two models for generally describing the arc behaviour was made by Brown [9, 10] in 1948. Brown suggests calculating the arc behaviour in period before the final current zero by using Cassie's model and calculating the arc in post current period by using Mayr's model. For Brown's model calculation, the following assumptions are made:

1. Arc voltage is much less than the power supplier voltage;
2. Current at the natural zero crossing point; and
3. A very large gap resistance after arc extinction.

For his proposal of arc model is restricted because the black box nature.

The arc modelling was described in the form of conservation equations by Elenbaas [11] in 1946. This was the first time that the arc behaviour in terms of Ohmic heating for power input and heating conduction for power loss had been described. The conservation equation by Elenbaas is given by:

$$\frac{1}{r}\frac{\partial}{\partial r}(rk\frac{dT}{dr})+\sigma E^2=0 \tag{1.6}$$

where r is the arc radius, T the temperature, k the thermal conductivity, σ the electrical conductivity and E the axial electrical field. From the Eq.1.6 it can be seen that the expression is over-simplified, since some important processes (radiation and convection) are excluded from the energy balance, which are essential for describing circuit breaker arcs. Radiation and convection are important factors that should be considered with regards to gas blast type circuit breakers.

Elenbaas' equation has also been used by Frind [12] to investigate the relationship between arc time constants and physical processes. The arc time constant was proportional to the system dimension and proportional to the thermal diffusivity.

1.3.2 Further development of dynamic arc models

In the 1970s, the arc model developed rapidly as a result of the Cassie and Mayr arc models. However, concepts connected to the Cassie and Mayr arc models are still very rough in physical processes and can only be used in simple models. With the improvement of the accuracy requirement, these simple models are not enough for modelling to describe the arc behaviours of

circuit breaker.

Research surrounding dynamic arc characteristics in jet flow has been become significant as circuit breakers and arc heaters have developed. Based on mass, momentum, and energy conservation equations can determine the temperature, velocity, pressure, and arc radius as the function of space and time. Consideration of the gas properties and the system dimension, the capability of arc interruption of circuit breakers can be predicted by these dynamic arc models on a computer.

Due to strong accelerating flow in the nozzle of high voltage circuit breakers, convection has to be considered as a very important factor. The integral method is a combination of formal analysis and empiricism [13, 14, 15, and 16]. The conservation equations in full differential form are integrated and only axial derivation in the equations. The conservation equations assume that the arcs are axisymmetric. The closure of the conservation equations requires knowledge of the radial temperature and velocity profiles. Numerous researchers have been devoted to the development of the arc model and have contributed to the advancement of the arc model. Details of these arc models will be given below.

The integrated arc model was adopted for arc analysis by Tophamin [17, 18, and 19] which is a specific case of Cowley's model [13]. Swanson and Roidt [16, 20-25] published a series of papers on arc modelling to derive integral arc equations from the differential conservation equations based on boundary layer flow [20]. The energy equation is given below:

$$\rho\frac{\partial h}{\partial t}+\rho u\frac{\partial h}{\partial r}+\rho w\frac{\partial h}{\partial z}=\left[1-\rho\left(\frac{\partial h}{\partial p}\right)_T\right]w\frac{\partial p}{\partial z}$$
$$-q(p,T)+\sigma E^2+\frac{1}{r}\frac{\partial}{\partial r}\left[r\left(\frac{\mu}{p_{rl}}+\frac{\rho\varepsilon_m}{p_{rt}}\right)\frac{\partial h}{\partial r}\right] \quad (1.7)$$

where p_{rl} and p_{rt} are respectively the laminar and turbulent Prandtl number, u the molecular viscosity and ε_m the turbulent diffusivity. w is the axial velocity, h the enthalpy, q the radiation loss, σ the electrical conductivity and E the electrical field strength.

However, their starting conservation equation for energy is generally incorrect, and this is pointed out by Fang [26] that the term $\rho\left(\frac{\partial h}{\partial p}\right)_T$ on the right hand side of Eq.1.7 should be dropped out.

The energy equation to the boundary layer can be integrated and transformed into a differential equation for the steady arc radius [20, 21] (electrically conducting core), obtained from a boundary layer analysis of circuit breaker arc into equations for the heat flux potential [22].

Before current zero, it was assumed that the gas flow weakened the arc column to a small cross sectional area at the current zero and that the axial energy convection can be neglected. The cooling will be mainly by turbulent and molecular diffusion. The effect of radiation is also significant when the arc temperature is higher enough at the current zero.

Swanson and Roidt suggested [22] that the transformation around the current zero is that the thermal energy storage in the arc column is controlled by changes in arc temperature rather than arc area. However, this assumption is

not valid for nozzle arcs at the current zero [27].

In order to calculate the arc temperature by using equations in [22], turbulence parameter was introduced for representing the turbulence influence, and a good agreement between theory and experiments was given in [25].

A mathematical model is derived to describe the current interruption in high voltage gas blast circuit breaker as proposed by Hermann and Ragaller [28] in 1977. Two arc sections with different behaviours have been classified as the high-pressure arc section and the turbulent arc section. Radiation and convection are significant in the high-pressure arc section. Whereas turbulence, produced by the instability of the arc boundary layer, is the main factor to affect the turbulent arc section. In order to describe the exchanges of the turbulent arc section, a three-zone radial temperature profile was used. Zone one is the arc core with an isotherm as boundary (4,000K for SF_6). Zone two is the region surrounding the thermal layer. Zone three is the region around 1,000K to the cold gas. Conservation equations are derived differently for these zones. It is considered a complex and coarse assumption.

Hermann and Ragaller [28] introduced the arc turbulence in the downstream of the nozzle throat, and assumed that the mixing zone (a transient region between the arc core and the thermal layer) is established in the high current phase of the arc flow interaction. The turbulent viscosity was given roughly in [28].

$$\varepsilon = 1.5\times10^{-4} L c f_t \tag{1.8}$$

where L is the effective arc length, c the sound velocity at the arc boundary. It is an additional adjustable factor which needed to match with the experiment

results in [28].

The post arc current measured by Frind et al. [29] is lower than that predicted by Hermann and Ragaller [28] using a similar nozzle. The reason of discrepancy probably caused the treatment of turbulence and the lack of axial variation of arc properties for Hermann and Ragaller's model.

Lowke and Ludwig published a simple model [15] for high current arcs stabilised by forced convection in 1975. It is a significant contribution to the arc modelling development. This simple model is idealised of that (1) radiation and emission coefficient at a given pressure are a function of temperature and independent of the arc radius, (2) the Mach number of the arc plasma is determined by the nozzle shape and independent of the arc current, and (3) plasma kinetic energy is neglected relative to the enthalpy. Therefore, the three principal assumptions of the model are: (1) the arc temperatures are isothermal for arc radius, (2) radiation losses per cm^3 at a given pressure are determined by the net emission coefficient , and (3) the Mach number of the arc plasma is equal to the Mach number surrounding the arc. Tuma et al. [30-32] extended this work related to the transient nozzle arcs after that.

The energy conservation equation appropriate to a unit volume of plasma at the arc centre is shown below:

$$\sigma E^2 = U + \nabla \cdot (\rho h \vec{V}) + \nabla \cdot F_c \qquad (1.9)$$

where E is the electric field, ρ the density, h the enthalpy, V the plasma velocity and F_c the heat conduction flux density. U is the rate of loss of radiation energy per unit volume at the arc centre.

The basic equations are all listed below:

$$\rho c_p \frac{\partial T}{\partial t} = \sigma E^2 - U - \rho c_p w \frac{\partial T}{\partial z} - 4\pi k_{eff} \frac{T}{A} \tag{1.10a}$$

$$\rho h \frac{\partial \theta}{\partial t} = (\sigma E^2 - U_t) A - \frac{\partial}{\partial z}(A \rho h w) \tag{1.10b}$$

$$I = \sigma E A \tag{1.10c}$$

$$w = Mc \tag{1.10d}$$

Eq.1.10a is the energy balance equation for the arc centre, where c_p is the specific heat, A the arc cross sectional area, U the net emission coefficient at the arc centre and k_{eff} the effective thermal conductivity. The term of $4\pi k_{eff} T/A$ in Eq.1.10a indicates thermal conduction losses.

Eq.1.10b is the enthalpy flow equation. Ut is the radiation emitted per cm^3 between arc and surrounding gas.

From the Eq.1.10a and 1.10b, the pressure is independent of time and ρh/p is independent of temperature and time.

Eq.1.10c is simple Ohm's law, where I is the current and σ the electrical conductivity.

Eq.1.10d is the axial velocity expression in arc plasma, where c is the local sound velocity, M the Mach number which is assumed independent of radius.

The arc model above proposed by Tuma and Lowke, took no account of turbulence effects. They considered the turbulence might smear the temperature profile at the arc edge, and a large enough current should not affect the effective average area of the arc. This is also established in Chapter three

by using different nozzle arcs. The arc model does not take into account the turbulence effect, which can give a good result, as demonstrated by the experimental result of the 2000 A arc in nitrogen (N_2).

The integral conservation equation, based on axisymmetrical arc, was proposed by Cowley [13] in 1974. Fang et al. [34, 35] made a further modification based on Cowley's method in 1979 for describing the energy conservation equation in arc core. The integral model by Cowley, Fang and Chan et al. has been used successfully for experimental (e.g. [36]) and computer simulated arcs [35, 37]. This method has also been widely used to investigate the effects of nozzle ablation [26, 38 and 39].

1.3.3 Arc model based on differential method

The rapid development of computer techniques in conjunction with the ability to solve partial differential equations has made it possible to use the arc modelling in full differential form. This approach of developing the differential method for the investigation of transient arcs has been given more attention in recent years. For this approach, the conservation equations of mass, momentum and energy are solved with appropriate initial and boundary conditions for the physical domain. Simplification and approximation work have been made since the complexity of some important mechanisms (e.g. radiation transfer, turbulent mixing and electrode sheath interaction etc.). Therefore, researchers have proposed varieties of models for solving different arcing situations.

Ragaller et al. [40] at Brown Boveri Research Centre (BBC) carried out an extensive investigation on arcs in gas flow. They used a set of boundary layer type differential equations to investigate dielectric recovery of a gas blast arc after current zero. A three dimensional arc model of the transient electrical arc

is given by the following equations:

Mass conservation equation:

$$\frac{\partial \rho}{\partial t} + \frac{\partial}{\partial r}(\rho u) + \frac{\partial}{\partial z}(\rho w) = 0 \tag{1.11a}$$

Axial momentum conservation equation:

$$\frac{\partial \rho w}{\partial t} + \frac{\partial w}{\partial r}(\rho u) + \frac{\partial w}{\partial z}(\rho w) = -\frac{\partial p}{\partial z} + \frac{1}{r}\frac{\partial}{\partial r}(\mu r \frac{\partial w}{\partial r}) \tag{1.11b}$$

Energy conservation equation:

$$\rho c_p \frac{\partial T}{\partial t} + \rho c_p u \frac{\partial T}{\partial r} + \rho c_p w \frac{\partial T}{\partial z} = w\frac{\partial p}{\partial z} + \frac{1}{r}\frac{\partial}{\partial r}(rk\frac{\partial T}{\partial r}) + \sigma E^2 - q \tag{1.11c}$$

Viscous dissipation and axial thermal conduction are neglected in the energy equation. The radial momentum was reduced to a uniform radial pressure distribution. Thus, the surrounding cold flow solely determines the axial pressure distribution.

These equations were transformed into isotherms for radial discretization by Ragaller [41] and Hermann [42] in earlier work to solve the problem of strong non-linearity of the material properties in above equations (Eq.1.11a-c).

A turbulence influence was also introduced in the conservation equations by using the Prandtl mixing length model [40]. In his experimental observation, the turbulence as the main influence develops around the stagnation region at about 30 μs after current zero in steady flow. However, in Graf et al. [43] measurement, the stagnation zone with a much higher axis temperature indicates that the influence of turbulence in the stagnation region of double-flow geometry during dielectric recovery can be neglected.

Mitchell et al. [44] made another approach to solve the partial differential equations for forced convection-stabilized electric arcs. The model solves the LTE conservation equations for mass, momentum and energy using an implicit finite difference method for marching in the axial and time dimensions. It was used to simulate steady state arcs in N_2 and SF_6 and correctly predicts the arcs in upstream region of single or double flow model breakers are cylindrical. The value of net coefficient of Liebermann and Lowke [6] (by a factor of 4) requires increasing significantly which proved by the experiment of the steady state SF_6 arc at 1200 A and 3.6 bar. They investigated the electric behaviour after current zero in laminar flow and assumed that the convection and laminar conduction suffices to cool the stagnation region of the decaying arc. The turbulence, which was confirmed, has a small influence on the upstream temperature recovery and dielectric recovery on the Graf et al. experiment [43].

Meanwhile, Lowke and Lee [45] investigated the interruption of N_2 and SF_6 gases circuit breakers by using a two-dimensional model with laminar flow assumption. The simulation is a transient for the current zero period, which started from a steady state of 2 kA before the final current zero point. However, Lowke and Lee's prediction of critical RRRV for both N_2 and SF_6 did not agree with the experiment given by Hermann and Ragaller [28]. The prediction shows that the N_2 was a better interruption medium than SF_6, which is opposite to the experiment.

Fang and his co-workers [46-48] at the University of Liverpool also applied the differential method to investigate gas blast arcs for both steady state and transient state. The differential equations of Fang et al. [46-48] are similar to those of Ragaller et al. [40], and the temperature in energy equation was replaced by enthalpy which can be seen as below:

$$\rho \frac{\partial h_0}{\partial t} + \rho u \frac{\partial h_0}{\partial r} + \rho w \frac{\partial h_0}{\partial z} = \frac{1}{r} \frac{\partial}{\partial r} (r \frac{k}{c_p} \frac{\partial h_0}{\partial r}) + \sigma E^2 - q \qquad (1.12)$$

where h is the enthalpy, k the thermal conductivity and c_p the specific heat at constant pressure. All others are same as model of Ragaller et al. [40].

The net radiation loss for energy equation is calculated by using the radiation transport model of Zhang et al. [49] which is based on the experimental results of Ernst et al. [50] for wall stabilised nitrogen arcs and from the theoretical prediction of radiation transport calculations for N_2 (by Shayler and Fang [51]) and SF_6 (Liebermann and Lowke [6]).

Solutions to the conservation equations were fixed by the radial profiles of temperature and axial velocity at a certain axial position. It was assumed [46] nearing the nozzle entrance there is a flow stagnation point and the pressure distribution in this region ensures a section of the arc which is axially uniform (i.e. the self-similar arc [49, 52]). Thus, the equations of mass, momentum and energy for describing the transient self similar arc are solved numerically. These solutions provide the required axial boundary conditions [49] for the energy conservation equation of nozzle arcs. The research of Fang et al. [46] is based on the laminar flow. Presence of the turbulence is observed for the SF_6 nozzle arcs and it will be discussed as follows in turbulence.

Further investigations for the arc model in recent decades focused on the case of axisymmetric-flows and to the interaction between the arc and electrodes [57] which plays an important role on the arc behaviour research. Determining the current density distribution over the cathode surface (so-called arc rooting) in a circuit breaker is an extremely complicated phenomenon. Fang et al. [53] predicted the thermal plasma arc in the argon at 200 A which is

based on the semi-empirical radiation transport model by Kovitya [54] for getting the net radiation loss and net emission coefficients of argon [55]. Apart from the physical mechanisms responsible for the non-LTE layer in front of an electrode surface [56], it is known that the arc column is attached to the inner surface of the hollow contacts. The position and size of the arc root is affected by the interaction between the current in the plasma column and the magnetic field produced by the current in the metallic contacts as well as in the external circuit to which the breaker is connected. Normally the arc models assume the distribution of current density over the cathode surface, and neglect the non-equilibrium sheath layer for free burning arcs in the most models. The current density in the vicinity of the cathode, the maximum current density, is derived by the measurement of the size of the molten cathode tip for a given arc current [57]. The theoretical predictions to the current density at the electrode are sensitive. The current density is the main factor in determining the pinch pressure produced by the self-magnetic field of the arc. The pinch pressure drives the convective flow of plasma within the arc and determines arc radii and temperatures. For most models, the boundary condition for temperature at the cathode surface comes from measurements. The current density distribution and heat conduction at the cathode surface are calculated by introducing one dimension conservation equations of electron number density, energy and generalised Ohm's law in the cathode sheath layer [58, 59]. Biehler et al. [60, 61] developed a model by considering mass balance for electrons, ions, neutrals and the change of ions velocity distribution function from Maxwellian to a profile fulfilling the so called Bohm criteria [62].

1.3.4 "AirArc" Static Arc Model

Long arcs are commonly met in transmission line faults, and the arc behaviour of the long arcs is different from the arc in high voltage circuit breakers, which has been introduced in section 1.3.3. The nature of long arcs is complex and its behaviour is affected by various factors. The length variation is an important factor in describing the arc behvaiour. The arc length is determined by the magnetic forces produced by the supply current, the convection of plasma and the surrounding air, and the atmospheric conditions.

Recently, Terzija et al. proposed a new "AirArc" static arc model in EMTP (Electromagnetic Transient Program) based on the real arc behaviour [63]. The arc model introduced the effects of arc elongation, including the length variations. Kizilcay et al. [64] and Johns et al. [65] have modeled long arcs in free air in earlier time. These arc models are very complex due to its nonlinear nature. Terzija et al. simplified these models using an alternative approach based on a stationary arc model with a new derivation of arc resistance [66], which is based on the analysis of measured arc voltage and current. A series of experimental results, which were provided by the high-power test laboratory at FGH-Mannheim, Germany, have been used to verify this "AirArc" static arc model.

The arc is modeled as a current-dependent voltage source with a characteristic-distorted rectangular voltage that elongates nonlinearly over time.

The arc voltage is modeled by the following equations:

$$u_{a0}(t)=\left(U_a+U_b\frac{I_0}{i_b(t)}+R_\delta\left|i_b(t)\right|\right)\mathrm{sgn}(i_a)+\xi \tag{1.13}$$

$$i_b(t)=\begin{cases} I_0 & |i_a(t)|<I_0 \\ |i_a(t)| & |i_a(t)|\geq I_0 \end{cases}$$

(1.14)

where $u_{a0}(t)$ and $i_a(t)$ are the voltage and current of an arc having a constant length. sgn is the sign function sgn (x) = 1 if $x \geq 0$ and sgn (x) = -1 if $x < 0$. is the zero-mean Gaussian noise. U_a is the product of the arc voltage gradient E_a and the length of the arc path L_a (the distance between the arc electrodes). The term $U_b I_0/i_b(t)$ represents the arc ignition voltage, and the term $R_\delta |i_b(t)|$ is a quasilinear part determined by arc current i_a. R_δ is the arc resistance.

The arc voltage is a very important factor to verify the applicability of an arc model. The predicted arc voltage is compared with the measured results, and the accuracy of the arc model is very high. The time-domain and spectral-domain features of the predicted arc were realistic. It was also found that the instances of arcing faults and the transients during the arc's inception and quenching can be detected efficiently.

1.4 Turbulence Models for Electric Arcs

In fluid dynamics, turbulence is a complex three dimensional and rotational flow, which is unsteady, irregular and composed of eddies. It is known that the arcs burning in the supersonic nozzle can become turbulent, especially at the low current [67]. The large size of eddies, is comparable with the scale of the flow, extract energy from the mean flow. The small eddies, in which the viscous effect is important, dissipate the turbulent energy by vortex stretching.

The turbulence effect had almost been neglected by the earlier arc models. Tuma et al. [33] assumed that the turbulence might smear at the arc edge, and they claimed that the neglect of turbulence could be proved by its measurement

of Nitrogen arc [68]. The turbulence effects in the arc quenching during the current zero period was continually disputed in the early seventies. Arc turbulence was observed experimentally, especially in the vicinity of the current zero period for SF_6 arcs [69-72]. The experiment by Hermann et al. [70] recorded the radial arc structure with a fast spinning mirror ± 30 μs in the vicinity of current zero period at different axial positions along the arc and it has been represented in Fig.1.2. Turbulence is not significant at the position in front of nozzle throat, which can be found from figure “a” and “b”. Turbulence is still very weak at the position “c” before current zero and slowly increased after zero point. Turbulence is obviously observed at the position “d” and “e”, especially ± 5 μs around zero point. The effect of turbulence especially around the current zero period will eventually lead to eddies in the flow field. This is represented in Fig.1.3.

SF_6 has recently been used as the most common insulated medium for high voltage circuit breaker because it’s excellent insulated strength and high arc interruption capability. Fang et al. [47] in their research claimed that the SF_6 arcs in laminar flow theory cannot predict satisfactorily the temperature profile and critical RRRV. Fang et al. [48] suggested that turbulence enhanced cooling might have to be taken into account for SF_6 arcs.

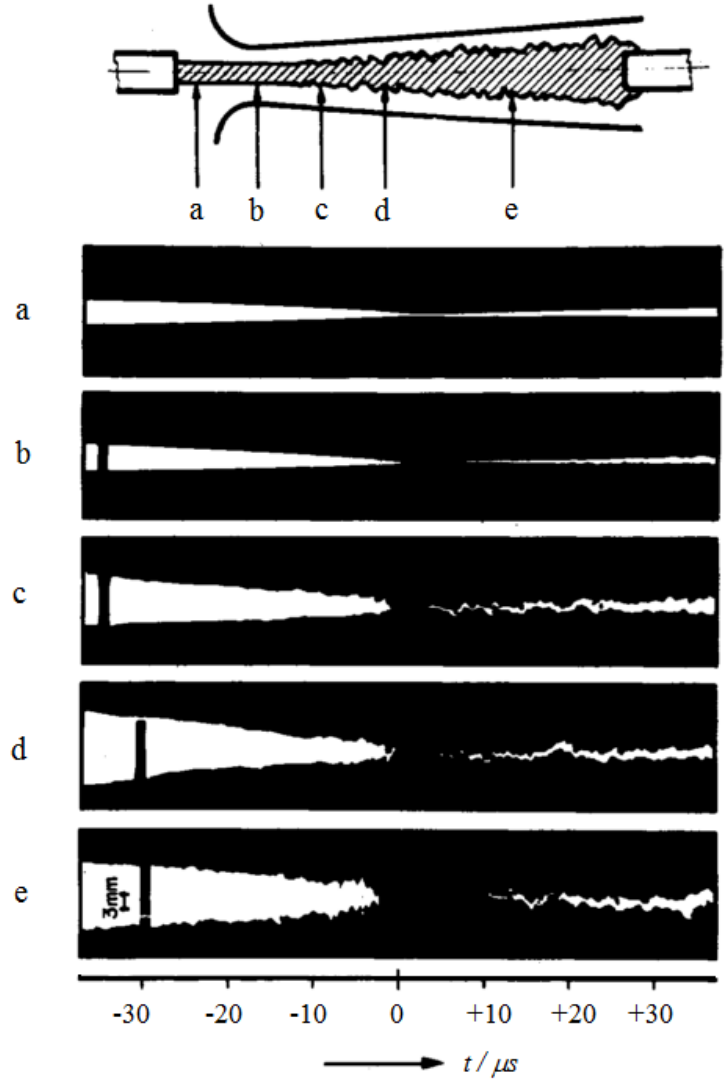

Fig.1.2: Fast streak records of the arc in the vicinity of current zero at different axial positions (N_2, 23 bar, di/dt = -39 A/μs) [70]. Letters of “a” to “e” respectively indicate upstream of nozzle throat, downstream of nozzle throat and three different positions of the downstream of nozzle.

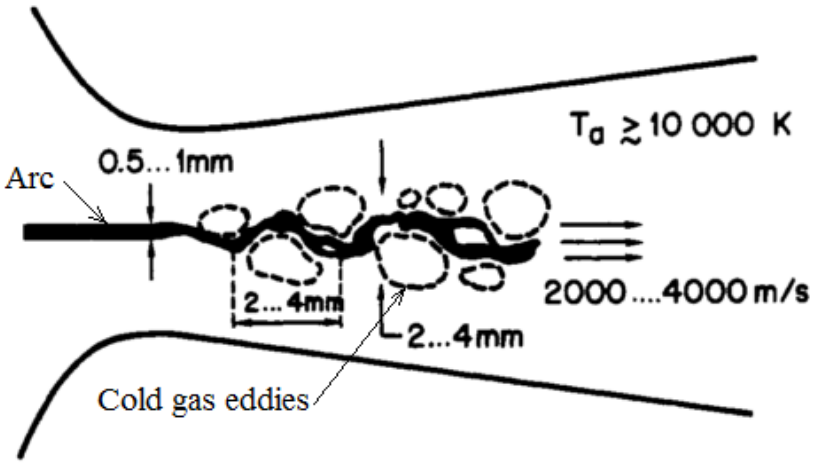

Fig.1.3: Schematic diagram of turbulence eddies in nozzle arc flow.

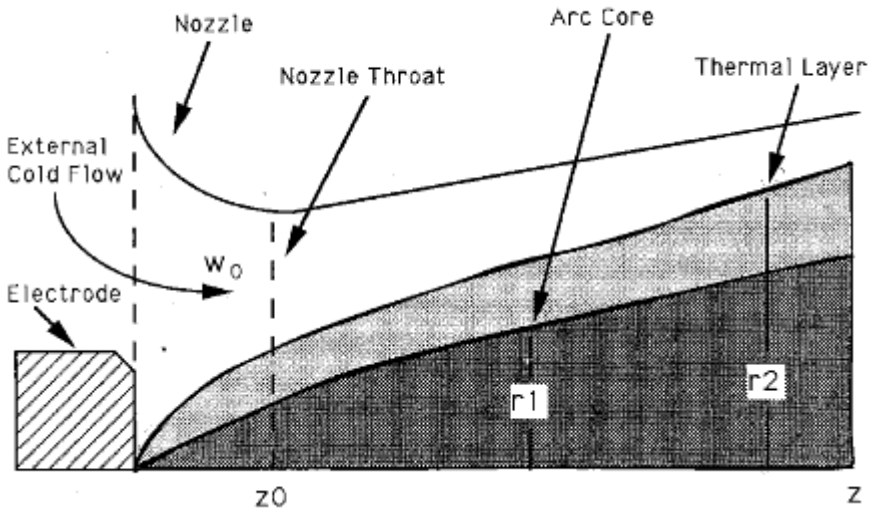

Fig.1.4: Diagram of a gas blast arc inside a supersonic nozzle [49].

The study of Niemyer and Ragaller [76] indicates that the product of the axial pressure gradient and the radial density gradient is a source of generation of turbulence, which often leads to instability as in the case of shear layer instability. For an arc in mainly axial flow, a velocity shear layer is formed between the arc core and the external flow (Fig.1.4), because the radial temperature profile has an extremely high gradient from the highest core temperature (higher than 15,000K) to external cold flow. The low gas density and high temperature gradient lead to the gas velocity reaching a very high speed (few thousand meters per second [49]).

The radial gradient of density is largest where the temperature rapidly reduces to that of external flow, and the density gradient together with the imposed axial pressure gradient by the nozzle generates vorticity in this region. The radial gradient of axial velocity within the region where temperature changes rapidly is also very strong.

The research of boundary layer might be helpful in investigating the arc instability and influence of turbulence. The nozzle arc behaviour is similar with a free rounded jet flow [73]. Thus, the approach of modelling rounded jet flow can be adapted to turbulent arc.

Up until now, the modelling of turbulence arcs is almost always based on the turbulence models for shear layer flows. Swanson [21] (in 1971), Hermann [28] (in 1977) and Tuma [31] (in 1980) etc. had been modelled the arc turbulence, which are based on radial integral conservation equations and the mixing length model of turbulence. For the closure of these equations the radial temperature and velocity profiles have been assumed to be of fixed shape. However, Fang’s results showed that the value of turbulence parameter lead to

a large influence [48]. Ludwig Prandtl [74] developed the mixing length turbulence model in the early 20th century which is a method to describe momentum transfer by using Reynolds stresses with a boundary layer by means of an eddy viscosity.

The application of Prandtl mixing length turbulence model for the supersonic nozzle arcs can be used to successfully predict the thermal interruption capability, but the value of turbulence parameter has to be adjusted when using a different nozzle shape.

1.4.1 K-ε Turbulence Model

K-ε turbulence model is another very popular turbulence model to simulate turbulent conditions. It is also known as the two equations model, as two additional transport equations with variables of kinetic energy and its dissipation rate are included in the model. In the beginning the k-ε model was developed to improve the mixing length model. Launder and Sharma derived the standard k-ε turbulence model in 1972 [75]. The two equations k-ε model can be applied to the near wall region and the region away from the wall boundary, there are five turbulence parameters which do not need to be adjusted and can be used directly as the default value to make a reasonable prediction to the cases where mean pressure gradients are small. As mentioned above the advantage of k-ε turbulence model, when compared against the mixing length model, is its wide range of applicability of these turbulence parameters. However, for the high temperature jet flow cases or mean flow of turbulent jets, which are similar to the nozzle arc, the standard k-ε turbulence model could not provide an accurate prediction [77, 78]. In late of 1970s, Pope [79] suggested that the standard k-ε turbulence model was not capable of

predicting the mean velocity profiles of turbulent axisymmetric jet accurately. Numerous researchers have proposed various modifications based on the standard k-ε turbulence model. An approach of adding or modifying correction terms of the transport equation for obtaining a better agreement has been widely used by many people [80-85]. Theis and Tam [80] used some different values to determine the coefficient of the turbulent transport equations. Yan et al. [86] also used k-ε turbulence model with different coefficients for a comparison study between the mixing length model and k-ε model. These models can successfully make good results for high temperature turbulent flow.

Seiner et al. [77] and Thomas et al. [78] observed that the high total temperature gradient led to the faster mixing and spreading of the jet flow. Abdol-Hamid et al. [87] based this observation on the proposed modified k-ε turbulence model arguing that the density gradient in a turbulent flow would add to instability due to local accelerations in the turbulent velocity field. They chose the total temperature gradient to represent the concept of additional mixing instability and then made a good agreement for high total temperature gradient jet flows.

In recent years, the k-ε turbulence model has been widely used to perform supersonic nozzle arcs or switching arcs in order to consider the turbulent effect as supported by several papers [86, 88]. Recent research indicated that the performances connected to the standard k-ε turbulence model are not very good. In fact, several modifications to the k-ε turbulence model have limitations connected to their particular conditions. In the present work the standard k-ε model is modified to take into account the effect of steep temperature (density) gradient at the edge of arcs in various nozzles or circuit

breakers. The k-ε model with a modified generation term will be introduced in Chapter Two in detail and a large amount of testing has been completed in Chapter Three to support the k-ε model proposed.

1.5 The Objectives of Research and Organisation of Thesis

1.5.1 Introduction and the arc models

Chapter One gives a detailed introduction of the background of the arc plasma, the history of the arc models, the development of circuit breakers, and the history of the turbulence models. These are the fundamental knowledge in the research of the turbulent arcs in circuit breakers, which should be studied in the beginning of the research work.

Chapter Two introduces the arc models which used in my simulation. The governing equations and the calculation for each material property has been detailed. Boundary conditions of inlet, outlet and setting of ablation patches, the Ohmic heating and Lorentz force calculation for different conditions are also introduced. The radiation models and turbulence models are detailed finally. All of them, which are listed above compose the complete arc model. Thus, each of them should be carefully checked and modified to make the prediction of turbulent arc reasonably and accurately.

1.5.2 Turbulence model modifications

It is known that the Prandtl mixing length model has been widely used to perform the supersonic nozzle arcs and switching arcs. However, the value of turbulence parameter needs to be adjusted when using different nozzle shape according to the experimental results. Some researchers often modify its value

with their experience . Therefore, I think the applicability of the Prandtl mixing length model is limited relatively.

The k-ε turbulence model is an empirical model based on model transport equations for the turbulence kinetic energy (k) and dissipation rate(ε). Modelling of turbulent arcs has been exclusively based on the turbulence models for share layer flows. For shear layer flows, the k-ε turbulence model has been popular since the five turbulence parameters which not very sensitive to flow conditions and default values can usually be used to make reasonable predictions. However, the standard k-ε model are often poorly predicted for the turbulent arcs. Thus, the objective of this chapter is to propose an turbulence model based on the k-ε model, which can improve the applicability and accuracy of the k-ε model.

The standard k-ε model is modified to take into account approximately the effect of steep temperature or density gradient at the edge of SF_6 arcs, which based on the experimental evidence that the size of the largest eddies present in turbulent arc flow are comparable to the transverse size of the arc column [43]. The modified k-ε model has been applied to various nozzle and switching arcs, which has been detailed in Chapter Three, for verifying its applicability and accuracy. The turbulence model is first applied to the steady state cases with DC currents from 100 A to 1800 A, and then to the transient cases of GE nozzle arcs [91] and Campbell nozzle arcs [90]. Finally, switching arcs for the 10 kA and 47 kA are used to verify the model.

1.5.3 Design studies for the auto-expansion circuit breaker

The objective of Chapter Four is to investigate the influence of design parameters for the auto-expansion circuit breaker. The design study is based on an ABB 245 kV auto-expansion circuit breaker. Two of key design parameters have been detailed at the present work to investigate the effect by using different length of auxiliary nozzle and gas leakage from the expansion volume. The interruption capability could be affected by the length of the auxiliary nozzle. Leakage problems always exist in reality, the arc simulation should be considered it for accuracy. These parameters are very important in the design of an auto-expansion circuit breaker and quite useful to the optimisation work.

The work is summarised in Chapter Five. It will also detailed suggested future work based on the work in Chapter Three and Four.

CHAPTER 2
The Arc Models

2.1 Introduction

The arc plasma consists of electrons, ions, atoms, and molecules. When a gaseous molecule receives more energy than the bond energy between its component atoms, it dissociates into single atoms. When an atom receives more than its ionisation energy, orbital electrons become free electrons, leading to the plasma state.

The arc plasma can be simulated by one or a series of mathematical models, which included various physical processes, in order to mathematically and correctly represent all these important mechanisms for the behaviours of the system. The local thermal equilibrium is the most important assumption for modelling the arc behaviour of different nozzle and circuit breakers in the present research work. In order to derive the conservation equations for transient axisymmetric nozzle arcs, some basic assumptions are going to be introduced below.

LTE has been introduced in detail in Chapter One, and it greatly simplifies the mathematical description of the arc behaviour.

The arc flow can be assumed to be a continuous medium due to its high density of particles. The stagnation pressure is usually higher than 1 atm, and the collision of particles are frequent in the system.

Most thermal arc and plasma processes of industrial relevance use a mixture

of different gases. When vapour is present in the arcing flow, it is not only carried by gas flow, but also diffuses from a high concentration region to a low concentration region. A combined diffusion coefficient [92] can be used to describe the laminar diffusion of species belonging to one gas in a mixture of gases.

The boundary layer assumption is used to describe a nozzle arc into two distinct regions which are the arc thermal influence region and the external flow. The arc thermal influence region is where the large radial gradients of temperature and axial velocity exist and turbulent mixing occurs. The external flow is assumed to be one-dimensional and laminar. It greatly simplifies the conservation equations for nozzle arcs.

2.1.1 The PHOENICS CFD package

PHOENICS [117], which is a commercial computational fluid dynamics (CFD) package, has been used in my simulation for solving partial differential governing equations of mass, momentum, and energy. The choice of the CFD package is a very strict and important aspect in my research simulation. The most commercial CFD package is the limited user interface, where the user has no right to access the core code if the solution procedure is implemented. In order to attain privacy in the CFD package, much effort is needed to check the solution of well-defined cases against experimental or analytic results. For instance, users have to use the user-defined subroutines to check if the mass, momentum, and energy are balance in the solution. Logical parameters can be set connected to certain active numerical schemes. The parameters should be considered carefully as inappropriate settings can lead to converged and physically incorrect results. In the arc simulation, it is often necessary to

resolve the steep temperature and velocity gradient at the arc edge. In this situation, much more grids are needed in certain regions of the computational domain. However, the presence of large gradients of physical properties together with high gas speed often leads to difficulties in convergence. For example, in the domain of gas with a low temperature and a high density, a weak relaxation is needed and is sufficient to guarantee rapid convergence. In contrast, gas in the arc region always has a very low density due to its high temperature. With highly changeable energy source (Ohmic heating and radiation) the energy and momentum equations require strong relaxation for smooth convergence. Special measures may be required to produce a reasonably well converged solution within affordable computational time.

2.1.2 Functional structure of PHOENICS

The simulation of nozzle arcs and circuit breakers in this thesis are using PHOENICS which requires the user to define the arc model through command and data files. PHOENICS provides a user-interface subroutine written by Fortran. The procedure of performing computer simulation is described in Fig.2.0. Users can only access the "Q1" and the "ground.for" files to generate the grid system and to specify the initial, boundary conditions and source terms.

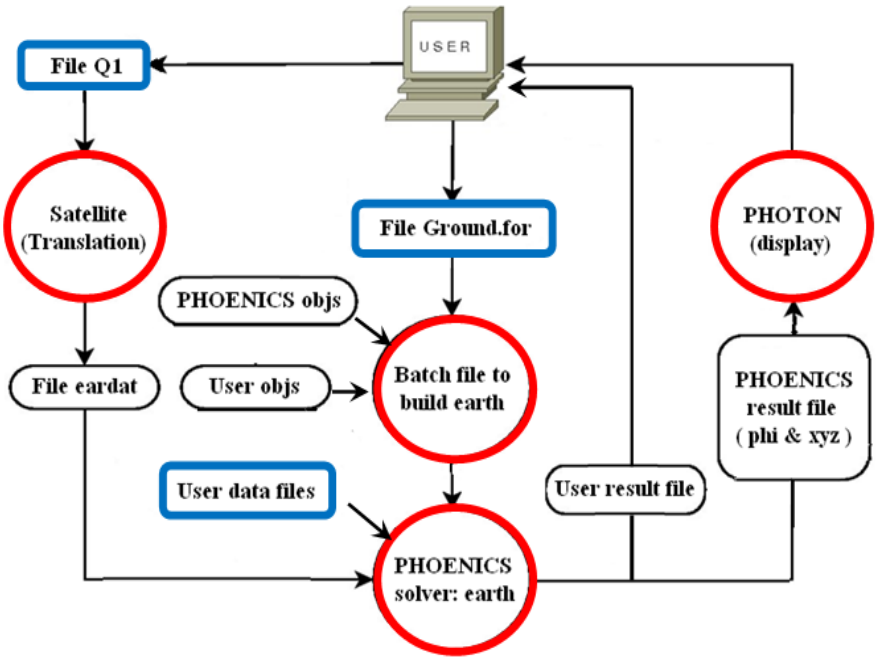

Fig.2.1: Flow chart of computer simulation of switching arcs based on PHOENICS. BLUE (files to be prepared by user), RED (executables to be run in the simulation).

2.2 Governing Equations and Material Properties

2.2.1 Governing equations

The equations, which describe the conservation of mass, momentum and energy, have been derived and simplified by many researchers [93, 94]. The governing equations represent a mathematical description of how different mechanisms interact and work together to control the behaviour of the arc, which represented by the time averaged Navier-Stokes equations. For gas blast arcs, additional terms which take into account of the electromagnetic field (Ohmic heating and Lorentz force) and radiation transport are also included in the conservation equations [95].

The governing equations for turbulent arcs and surrounding flow are the time-averaged Navier-Stokes equations, which can be written in a conservation form as:

$$\frac{\partial(\rho\phi)}{\partial t} + \nabla \cdot \left(\rho \vec{V} \phi\right) - \nabla \cdot \left(\Gamma_\phi \nabla \phi\right) = S_\phi \qquad (2.1)$$

where ρ is the gas density, ϕ the dependent variable to be solved, $\vec{V}$ the velocity vector, Γ_ϕ the diffusion coefficient, and S_ϕ the source term. Details are given in Table 2.1. The subscript l denotes the laminar part of the diffusion coefficient and t the turbulent part. The material and transport properties (μ_l, k_l, σ) of SF_6, its equation of state, and the method of calculating radiation transfer in terms of q (net radiation loss) have been described in [97]. The electric field is obtained by solving the current continuity equation (also represented by Eq.2.1) with a current density of 2.0×10^8 A/ m^2 on the surface of the only electrode in the computational domain.

Equation	ϕ	Γ	S_ϕ
Continuity	1	0	0
Axial Momentum	w	$\mu_l + \mu_t$	$-\partial p/\partial z$ + viscous terms
Radial Momentum	v	$\mu_l + \mu_t$	$-\partial p/\partial r$ + viscous terms
Energy	h	$(k_l+k_t)/c_p$	$dp/dt + \sigma E^2$ - q + viscous terms
Current Continuity	φ	σ	0

Table 2.1: Dependent variables in Eq.2.1. Mass, Momentum and Energy conservation equations for nozzle arcs and switching arcs.

These equations also can be written in cylindrical coordinates (r, z) after simplification of using the boundary layer assumption and electromagnetic terms as:

Mass conservation equation:

$$\frac{\partial \rho}{\partial t}+\frac{1}{r}\frac{\partial}{\partial r}(\rho v r)+\frac{\partial}{\partial z}(\rho w)=0 \tag{2.2}$$

Axial momentum equation:

$$\rho\frac{\partial w}{\partial t}+\rho v\frac{\partial w}{\partial r}+\rho w\frac{\partial w}{\partial z}=-\frac{\partial P}{\partial z}+\frac{1}{r}\frac{\partial}{\partial r}[r(\mu+\mu_t)\frac{\partial w}{\partial r}] \tag{2.3}$$

Energy conservation equation:

$$\rho\frac{\partial h}{\partial t}+\rho v\frac{\partial h}{\partial r}+\rho w\frac{\partial h}{\partial z}=\frac{1}{r}\frac{\partial}{\partial r}[\frac{r}{c_p}(k+k_t)\frac{\partial h}{\partial r}]-q+\sigma E_z^2 \tag{2.4}$$

The term of turbulent diffusion has been changed from $\nabla\cdot(k\nabla T)$ to $\nabla\cdot(\frac{k}{c_p}\nabla h)$ is for the convenience of the numerical calculation.

2.2.2 Temperature calculation

As mentioned above, it is known that temperature is not directly solved in my model, which is derived from enthalpy. For ideal gas, $h=c_pT$ where c_p is a constant. For arcing gas at low temperature (below 1000 K) it requires a reference enthalpy of zero at T = 0 K. Therefore the enthalpy data set obtained from literature [96] for high temperature gas should be carefully checked to match the definition of $h=c_pT$ at the low temperature. The h-T relationship of gas mixture at two pressures of 1 ATM and 10 ATM has been given in Fig.2.2. In our computation, more data enthalpy data are needed, which are obtained by interpolation between different PTFE mass concentrations (0%, 20%, 40%, 60%, 80% and 100%).

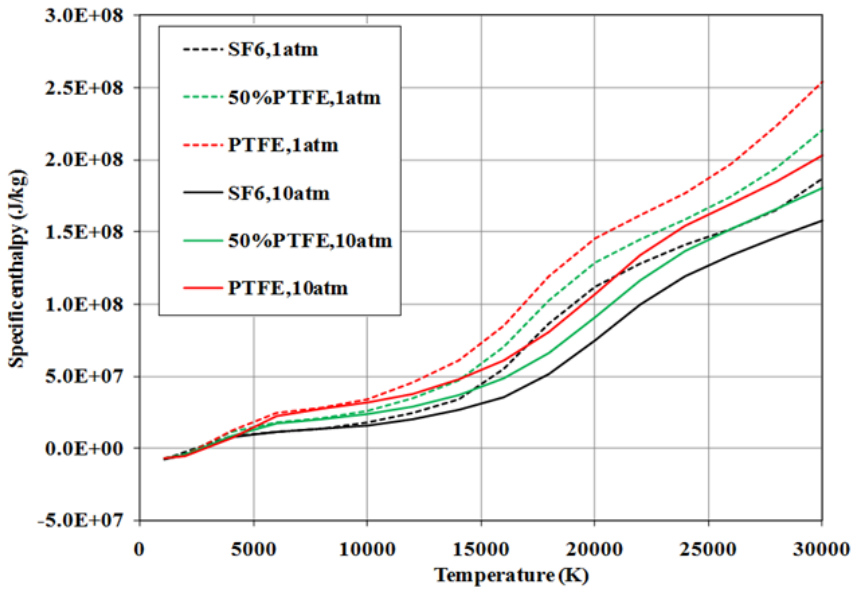

Fig.2.2: Relationship between specific enthalpy and temperature for different PTFE concentrations at two pressures [96].

2.2.3 Density calculation

It is known that the equation of state at room temperature for SF_6 gas takes the form of ideal gas flow with a gas constant of 56 J/kg/K. However, dissociation and ionisation take place and the equation of state will not follow the ideal gas law when the gas temperature is increased. The relationship of density, pressure, and temperature are described by a data set. Enthalpy is used in the energy conservation equation, and it is used to derive the density directly from the enthalpy and pressure. Density can be obtained by interpolation at a particular pressure, enthalpy and PTFE vapour concentration (0%, 20%, 40%, 60%, 80% and 100%). If data is obtained from a source with temperature as the independent variable, then the corresponding enthalpy values should replace the temperature values to form a data set of enthalpy and density at a given pressure.

The gas density can be assumed to a reasonable degree of accuracy to be linearly proportional to pressure at high temperature. Care must be taken to

switch from interpolation to ideal gas law when the enthalpy (temperature) is lower than a threshold, which is obtained by comparing the data from interpolation and from ideal gas law. For low temperature gas, the interval between the enthalpy (temperature) points must be sufficiently small to accurately represent the rapidly increasing density when temperature decreases in the low temperature range (<1,000 K).

2.2.4 Viscous effects of laminar and turbulent

μ_l and μ_t in Table 2.1, which are respectively laminar viscosity and turbulent viscosity, represent the effect of turbulence. The viscous effect of the gas leads to shear forces between layers of gas thus transferring momentum from a fast flowing region to a slow moving region. The process is represented as a diffusion term in the equation, because viscous effect is caused by random motion of gas particles. μ_l is called dynamic viscosity and ν_l is the kinematic viscosity, and the relationship of them as below:

$$\mu_l = \rho \nu_l \tag{2.5}$$

where ρ is the density.

The values of kinematic viscosity are given in ground.for file. It is a function of temperature or enthalpy. Fig.2.3 shows the dynamic viscosity as a function of temperature with different PTFE mass concentrations. The viscosity data for SF_6-PTFE mixture used in my arc model is calculated from fundamental transport theory [97] with PTFE mass concentrations of 0%, 20%, 40%, 60%, 80% and 100%.

The effect of laminar viscosity is much weaker than the turbulence eddy viscous effect. The turbulent viscosity will be described later on in this chapter.

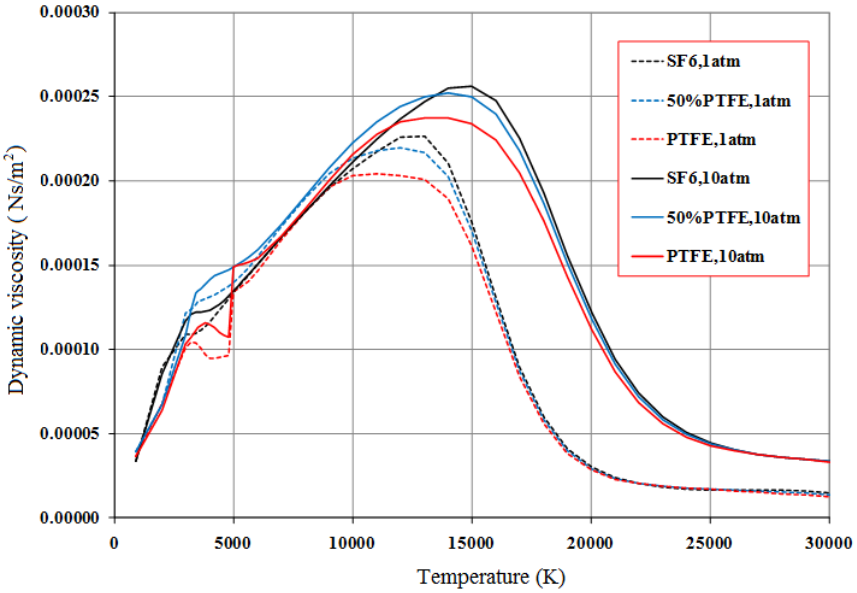

Fig.2.3: Dynamic viscosity of SF_6 – PTFE mixture with three PTFE mass concentrations (0%, 50% and 100%) [96].

2.2.5 Electrical conductivity Calculation

The electrical conductivity of SF_6 in gas can be derived directly from the enthalpy with different PTFE vapour concentration (0%, 20%, 40%, 60%, 80% and 100%). The value of electrical conductivity in metals or transparent contact is set to 1.0E5. The interpolation is used to calculate the conductivity for each PTFE concentration at given pressure. It is used to calculate the electric field and current density and will be detailed later in this chapter.

2.2.6 Ratio of thermal conductivity and specific heat capacity

It is known that the enthalpy is used in the energy equation. The term of representing thermal conduction has to be transformed into a term related to enthalpy gradient. When temperature is used in an energy equation, the diffusion coefficient is k_l (thermal conductivity). However, with the equation of enthalpy, the coefficient has been changed from k_l to k_l/c_p where c_p is the specific heat capacity at constant pressure. Because the value of cp is defined by the enthalpy

and temperature: $c_p = \left(\frac{\partial h}{\partial T} \right)$ in the subroutine of calculating temperature for the present case.

In the PHOENICS, it cannot set k_l / c_p directly and only could be set by using Prandtl number:

$$P_{rl} = \frac{\rho \upsilon_l}{k_l / c_p} \tag{2.6a}$$

The Prandtl number as shown in Eq.2.6a is dimensionless. It represents the relationship of momentum diffusion and energy diffusion, which are both caused by gas particles random motion. The Prandtl number for the enthalpy equation needs to be defined since it is not a constant for arcing gases in a wide temperature range. The value of Prandtl number is calculated by dynamic viscosity and the ratio of thermal conductivity and specific heat capacity as shown in Eq.2.6a.

The Prandtl number is composed of laminar and turbulent, the turbulence enhanced energy transfer, which is so-called turbulent thermal conductivity (k_t), and the turbulent Prandtl number can be defined in Eq.2.6b which is similar with Eq.2.6a.

$$P_{rt} = \frac{\rho \upsilon_t}{k_t / c_p} \tag{2.6b}$$

The turbulent thermal conductivity is related to turbulent viscosity, so its value cannot be directly obtained from the turbulence model. For arc simulation, the value of turbulent Prandtl number assumes 1.0 which is sufficient since adjustable parameters appear in the turbulence model which is to be determined by experimental results for switching arc applications.

2.2.7 Mass concentration and diffusion coefficient for PTFE

The mass concentration of a vapour in a mixture with SF_6 and PTFE is given as:

$$c_m = \frac{n_{PTFE} M_{PTFE}}{n_{PTFE} M_{PTFE} + n_{SF_6} M_{SF_6}} \tag{2.7}$$

where n_{PTFE}, n_{SF6} and M_{PTFE}, M_{SF6} are respectively the molar number and molar mass of the PTFE vapour and SF_6.

The vapour in the arc flow, it diffuses from a high concentration region to a lower region. The diffusion coefficient is expressed by $\rho D_l + \rho D_t$. D_l and D_t are respectively the laminar diffusivity and the turbulent diffusivity which relate to the local laminar viscosity and turbulent viscosity by the laminar and turbulent Schmidt number (Eq.2.33).

2.3 Boundary Conditions

The behaviour of a system can be represented by solution of the governing equations, when the computational domain is determined. The boundary conditions represent the interaction between a system and its environment.

2.3.1 Inlet boundary conditions

Actually, the arcing chamber is enclosed in an insulating tank, so there is not any forced gas inlet. The gas flow in the circuit breaker is generated by piston compression or magnetic force. So in the simulation, a gas inlet will be added to assess the effect of increase gas flow. Inlet energy and momentum can be transferred into the domain by convection, diffusion, and radiation.

The stagnation pressure and temperature of inlet are normally specified which are used to calculate mass, momentum, and energy fluxes into the boundary cells. The equations that relate to the fluxes to the inlet stagnation parameters are as follows:

$$w_{in} = \sqrt{\frac{2\gamma}{\gamma - 1} R_g T_0 [1 - (\frac{P_{\text{cells}}}{P_0})^{\frac{\gamma-1}{\gamma}}]} \tag{2.8}$$

$$\rho_{in} = \rho_0 (\frac{P_{\text{cells}}}{P_0})^{\frac{1}{\gamma}} \tag{2.9}$$

$$T_{in} = T_0 (\frac{P_{\text{cells}}}{P_0})^{\frac{\gamma-1}{\gamma}} \tag{2.10}$$

where γ is the ratio of specific heat at constant pressure (c_p) to specific heat at constant volume (c_v)of the gas. For SF_6, this value is 1.1079. With these three values, the mass, momentum, and energy fluxes can then be calculated. Fig.2.4 illustrates the case where inlet fluxes are related to the stagnation parameters of the gas entering the domain.

The other method of inlet boundary energy and momentum transfer into the domain is through diffusion. Fig.2.5 shows the diffusion effect of the energy equation where the thermal conductivity is given by the term of $-k(\delta T/\delta z)$ or $-(k/c_p)*(\delta h/\delta z)$. The thermal conduction always exists where there is a temperature gradient even if there is no any gas flow. The thermal conduction energy flux must be calculated when there is a very high temperature gradient at the inlet. The temperature gradient along the gas flow direction would be small with a relatively high speed of flowing gas flow. The relationship of convection and diffusion can be represented by the Peclet number, as follows:

$$P_e = \frac{\rho w h}{\frac{k}{c_p}\frac{\partial h}{\partial z}} \approx \frac{\rho w h}{\frac{k}{c_p}\frac{h}{L}} \approx \frac{\rho w L}{k / c_p} \tag{2.11}$$

where L is a length over which the change of h is comparable to its absolute value. It is noted that the diffusion effect is very small and can be neglected when P_e is high. One only needs to specify the sources brought with the gas.

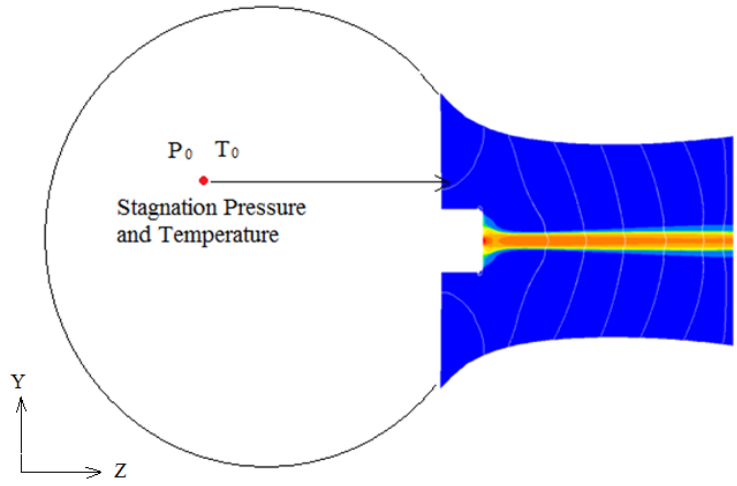

Fig.2.4: The principle of specifying inlet boundary conditions using stagnation parameters.

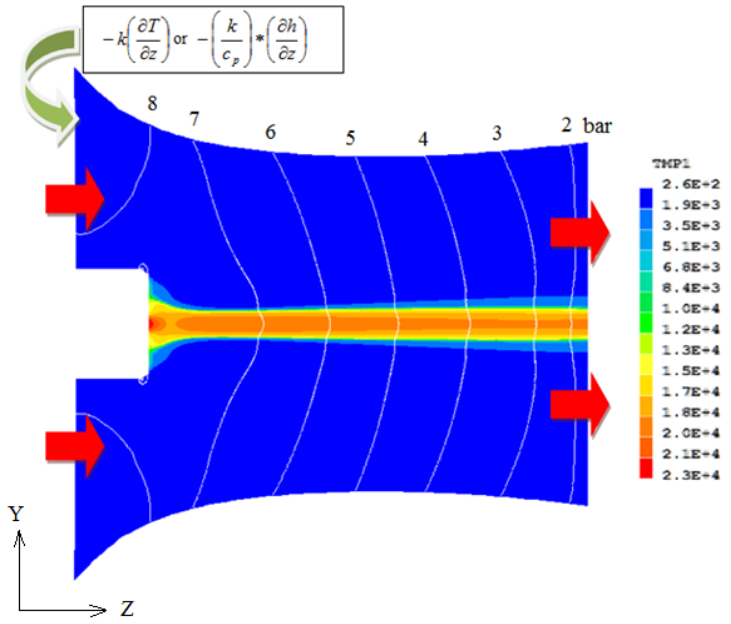

Fig.2.5: A typical nozzle flow with a shock wave in the diverging section.

2.3.2 Flow outlet

In a circuit breaker, there is no gas outlet because gas from the nozzle is exhausted into the background environment in the insulating tank. The whole tank is taken as the system under investigation.

However, the outlet is normally needed when the computational domain is to be restricted to the arcing chamber connected to the same computation time and computer memory. It is expected that gas leaves the domain at a substantial speed, say above 10 m/s with a high Peclet number. Under such conditions, the momentum and energy diffusive fluxes can be neglected in comparison with their corresponding convective terms. As gas leaves outlet boundary cells, it carries away its local momentum and energy automatically. The environment pressure will affect the gas speed in subsonic case. Thus, downstream boundary conditions, other than the pressure at the outlet, will not be necessary.

2.3.3 Ablation

Ablation normally occurs at the PTFE nozzle surface at a high temperature, even before the arcing current reaches its thermal blocking limit. This is indicated by some experimental results [98, 99]. The wall ablation is mainly caused by intense radiation in the circuit breaker [100, 101]. The ablation of PTFE is considered as a quasi-steady process, the amount of evaporated wall material is proportional to the amount of radiation available to the ablating surface.

The ablating PTFE vapour enters into the domain as surface mass, momentum, and energy sources. It adds mass into the domain which will cause the local pressure to increase. The density of mixture gases, material and transport properties including electrical conductivity will be affected. The radiation emission characteristics of the arcing gas will be changed and this affects the arc core temperature. The arc voltage will also be affected.

In the radiation transport calculation, the total radiative energy flux unit length of the arc column, which is the main factor to cause the surface ablation, are determined and stored in variable Q_{ab}. The radiation flux on the cell surface q is shown in Eq. 2.12:

$$q_{low} = \frac{\left|z_o - z_i\right|}{\pi(r_i + r_o)\sqrt{\left(r_o^{\,2} - r_i^{\,2}\right)^2 + \left(z_o^{\,2} - z_i^{\,2}\right)^2}} \mathrm{Q}_{\mathrm{ab}} \tag{2.12}$$

where r_i and z_i are the corner point of a cell closer to the symmetric axis and r_o and z_o are the corner point farther from the axis.

Thus, the ablation surface coefficient depends on the grid system only needs to be calculated once in the simulation;

$$\zeta_{low} = \frac{\left|z_o - z_i\right|}{\pi(r_i + r_o)\sqrt{\left(r_o^{\,2} - r_i^{\,2}\right)^2 + \left(z_o^{\,2} - z_i^{\,2}\right)^2}} \tag{2.13}$$

The ablation vapour mass flux can be written as:

$$m = \frac{\zeta_{low}\alpha Q_{ab}}{h_v} \tag{2.14}$$

where α is a fraction close to 1.0 and (1-α) indicates a small loss of radiation flux reaching the nozzle wall permanently into the environment. In the simulation, the value of α is set as 1.0. h_v is the ablation energy of PTFE which is required to break the chain of PTFE molecules (depolymerisation) and to raise the PTFE from room temperature to 3400 K. Its value is 11.9 MJ/kg in the simulation [101].

The momentum brought with the vapour is the mass flux multiplied the w (r-direction) and v (z-direction). The energy brought with the vapour is the mass flux multiplied enthalpy. The surface ablation patch for a circuit breaker is shown in Fig.2.6.

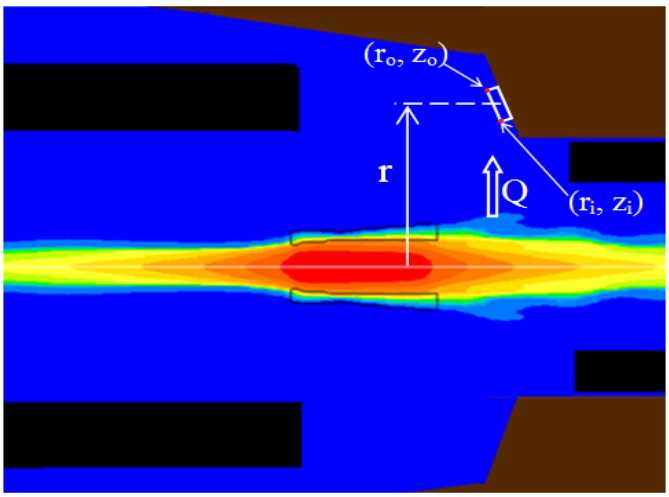

Fig.2.6: Arc temperature and the radiation with the cell position of ablation calculation.

2.4 Ohmic Heating and Lorentz Force

The term of Ohmic heating represents the heat release when electric current through a conductor. It is proportional to the square of the electric field such that: $Q=\sigma E^2$ which is represented in Table 2.1. As mentioned before, the electrical conductivity is a function of temperature and pressure. So the electric field needs to be calculated first. There are two assumptions to consider about the calculation of electric field, involving the non-slender arc model (NSA) and the slender arc model (SA).

2.4.1 Non-slender arc model

When the radial size of the arc column varies along the axial direction significantly and the radial current density component is comparable with the axial current density, the arc is considered “non-slender”. Due to the rapid increasing radial size of the arc column around the upstream electrode, the equal potential lines near the electrode tip are bent to allow for a sufficiently large radial electric field to drive a radial current density. A differential equation based on current continuity has to be solved to obtain the distribution of electrostatic

potential, and then the electric field and current density can be calculated. Considering the fact that across the arc column there is large variation of electrical conductivity and in the solution of the potential equation harmonic averaging of the electrical conductivity is used, it is necessary to first calculate the current density across each cell face. Using a typical grid system shown in Fig.2.7, the current density across each face can be expressed as:

The current density across the cell face H (high) is

$$J^H = -\frac{2}{\frac{\delta z_k}{\sigma_{k,j}} + \frac{\delta z_{k+1}}{\sigma_{k+1,j}}}(\phi_{k+1,j} - \phi_{k,j}) = C^H{}_{k,j}(\phi_{k+1,j} - \phi_{k,j}) \tag{2.15}$$

The current density across the cell face L (low) is

$$J^L = -\frac{2}{\frac{\delta z_k}{\sigma_{k,j}} + \frac{\delta z_{k-1}}{\sigma_{k-1,j}}}(\phi_{k,j} - \phi_{k-1,j}) = C^L{}_{k,j}(\phi_{k,j} - \phi_{k-1,j}) \tag{2.16}$$

The current density across the cell face N (north) can be calculated to a reasonable approximation by

$$J^N = -\frac{2}{\frac{\delta r_j}{\sigma_{k,j}} + \frac{\delta r_{j+1}}{\sigma_{k,j+1}}}(\phi_{k,j+1} - \phi_{k,j}) = C^N{}_{k,j}(\phi_{k,j+1} - \phi_{k,j}) \tag{2.17}$$

The current density across the cell face S (south) can be calculated to a reasonable approximation by

$$J^S = -\frac{2}{\frac{\delta r_j}{\sigma_{k,j}} + \frac{\delta r_{j-1}}{\sigma_{k,j-1}}}(\phi_{k,j} - \phi_{k,j-1}) = C^S{}_{k,j}(\phi_{k,j} - \phi_{k,j-1}) \tag{2.18}$$

where δz is the axial width of a cell and δr the radial width. The Cs are coefficients to relate the current density to the cell centre potential values.

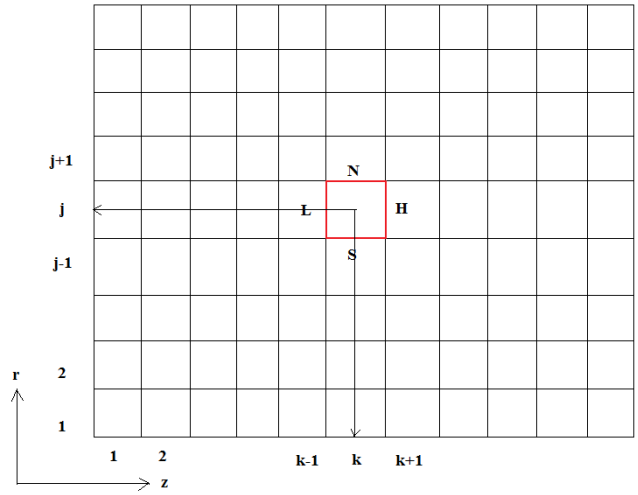

Figure 2.7: Finite volume in a cylindrical polar coordinate system for the calculation of electric field and current density from solution of the potential equation.

The electric field at the cell centre is then calculated by averaging:

$$E_z = \frac{J^H + J^L}{2\sigma_{k,j}} \tag{2.19}$$

$$E_y = \frac{J^S + J^N}{2\sigma_{k,j}} \tag{2.20}$$

2.4.2 Slender arc model

The slender arc model is used to the situation opposite with the non-slender arc model where the radial size of the arc column does not vary significantly along the axial direction and the radial current density is very small when compared to the axial one. In this case, the electric field can be calculated more easily than the non-slender arc model.

$$E_z = \frac{I}{\int_0^{R_c} \sigma 2\pi r dr} \tag{2.21}$$

where R_c is the radius of the conducting column, normally taken as the radial distance from the axis to the point where T = 3,000K. Inside the nozzle the arc

temperature in a slab may be lower than 3000K. In this case R_c will be taken as the nozzle radius. The current density is then σE_z.

2.4.3 Lorentz force

To calculate the Lorentz force, we need to know the current density and magnetic field. The current density has been calculated in the previous Eqs. 2.15-2.18. For the present models, the arc column is rotationally symmetric and the magnetic field is dominated in the azimuthally direction of the axis of the arc column. So the magnetic field can be calculated by:

$$B_\theta = \frac{\mu_0 \int_0^r J_z 2\pi\xi d\xi}{2\pi r} \tag{2.22}$$

where J_z is the axial component of the current density as given in the previous sections. The Lorentz force in radial and axial directions, as volumetric force in Table 2.1, can then be expressed as:

$$f_r = -J_z B_\theta \tag{2.23}$$

$$f_z = J_r B_\theta \tag{2.24}$$

The Lorentz force is calculated based on a uniform axial current density equal to J_{root} . In this case, the Lorentz force is reduced to

$$f_r = -\frac{\mu_0 J_{root}^2}{2} r \tag{2.25}$$

with f_z =0.

2.5 Approximation Method for Radiation Model

Radiation is an important energy transport mechanism for high pressure (above 1 bar) and high temperature arcs (above 12,000 K) [50, 102]. When gas is heated to a very high temperature, the electrons can receive the energy and jump to higher energy levels. However, the states of these electrons are not stable and some of them will return back to the lower energy levels, now a photon is created to account for all or part of the energy difference between the energy levels. This process is called spontaneous emission.

Radiation is a complex phenomenon in physics, and it is very important in the nozzle arcs and arcs of circuit breakers simulation. A comparison study has been done by Dixon et al. [103], for three radiation models, a semi-empirical model based on net emission coefficient [49], the five-band P1 model [104] and the method of partial characteristics [105-107]. The model of Zhang et al. [49] can produce results equally as good as the others for SF_6 nozzle arcs and puffer circuit breakers. At the present research, most computer simulations of electric arcs have accounted for radiation transport by using the net emission coefficient (NEC) [6].

The term of q in Table 2.1 represents the net radiation loss per unit volume and time, it is related to the radiation flux vector:

$$q = \nabla \cdot \vec{F} \tag{2.26}$$

The radiation flux vector, F is the integration of monochromatic radiation intensity Iv over arc's emission spectrum and then over the solid angle.

$$\vec{F} = \int_0^{\infty} \int_0^{4\pi} I_v(\vec{r}, \vec{n}) \vec{n} d\Omega dv \tag{2.27}$$

where $\vec{n}$ is the normal unit vector, Ω is the solid angle, and v the frequency of radiation.

For cylindrical wall stabilised arcs Lowke demonstrated that the use of NEC which is a function of temperature, pressure and the arc radius. It can predict satisfactorily the temperature distribution [6]. It is normally called net emission method. As mentioned before, Zhang et al. [49] has modified this method to calculate the radiation transport of nitrogen arc burning in a supersonic nozzle. For the radiation model, it has been modified to take account of the special feature of an arc affected by wall ablation. Since the model is concerned with radiation transport in radial direction, so it is thus called 1D radiation model or 1D model for later reference.

So for all prediction in this thesis, the radiation model proposed by Zhang et al. [49] is adopted. This model is schematically described in Fig.2.8. It is known that the 1 D radiation model is originally used for a monotonic radial temperature profile [49] (blue) as shown in Fig.2.8. However, it is modified in the present Liverpool arc model to deal with the non-monotonic temperature profile (black curve) in order to produce reasonable profile of radiation transport. Since for most time, the arc in the auto-expansion circuit breakers under the effect of ablation the maximum temperature is off axis.

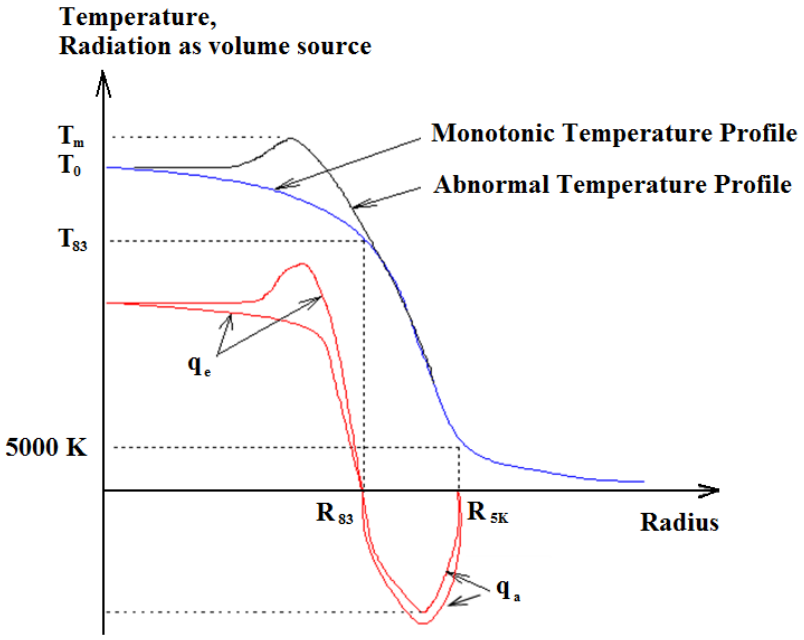

Fig.2.8: Schematic diagram showing the radial temperature profile, the emission and re-absorption zones [49].

The maximum temperature in Fig.2.8 is represented by T_m. T_0 is the temperature on the axis, for the monotonic profile, $T_m = T_0$. The arc core which is defined as the region from the axis to the radial position of the T_{83} isotherm as shown in Fig.2.8, $T_{83} = 0.83^* T_m$ in the arc core region (emission zone), q is a function of radiation radius, temperature and pressure which are the three parameters of NEC. In Fig.2.9, the NEC as a function of temperature in the typical pressure 1 bar is shown.

The radiation radius needs to be chosen carefully, because the NEC is defined in a cylindrical column of uniform temperature whereas in reality there is never such an ideal arc column. In the present case, the radiation radius is between the radius corresponding to $0.83^* T_m$ (R_{83}). For the normal cases, the reference temperature is 4000 K as the boundary of the arc column and 5000 K

for auto-expansion circuit breaker (R_{5K}). The average between the R_{83} and R_{5K} is used as a more realistic arc radiation radius. The net emission coefficient given in [6] is multiplied by a factor of 1.5 because of the non-uniform nature of the arc column.

In calculating the NEC, it is assumed, the plasma is isothermal with a clear boundary defining the radius. Therefore, it is most accurate when the arc temperature is close to isothermal. When the arc is in a real circuit breaker, the maximum temperature is always off axis. The above method of defining an equivalent arc radius is likely to be an over estimate in which case q will be smaller than the actual radiation loss. In order to compensate this net emission coefficient is increased by a factor of 1.5. It has been found during the experiments the value of 1.5 gives the best agreement.

In the region of re-absorption that from the arc core edge (R_{83}) to the 4000 K (5000 K (R_{5K})), the total amount of radiation from the arc core is partly absorbed. It has been found that 80% of the radiation flux from the arc core is re-absorbed at the arc edge. For the auto-expansion circuit breaker arc, the percentage of the radiation is decreased, in the present auto-expansion circuit breaker arcs, 50% is used. The radiation coefficient for this re-absorption region as a function is given below:

$$\frac{q_a(r)}{q_0} = 1.1 - \left(\frac{R_{5K} + R_{83} - 2r}{R_{5K} - R_{83}}\right)^2 \tag{2.28}$$

where q_a is the volumetic radiation source and q_0 the maximum volumetric energy source due to radiation re-absorption in the layer from R_{83} to R_{5K}.
The q_a could be calculated from the Eq.2.28 when q_0 is known. This is the method of semi-empirical which is modified based on the radiation transport

model by Zhang et al. to take account the non-monotonic radial temperature profile.

It is known that the arc is burning in the PTFE nozzle in the auto-expansion circuit breaker. In this case the radiation calculation should be based on the NEC of the PTFE. However at high temperature both SF_6 and PTFE contains a significant propotion of fluorine, their NECs are very close to each other, as shown in Fig.2.9 [108].

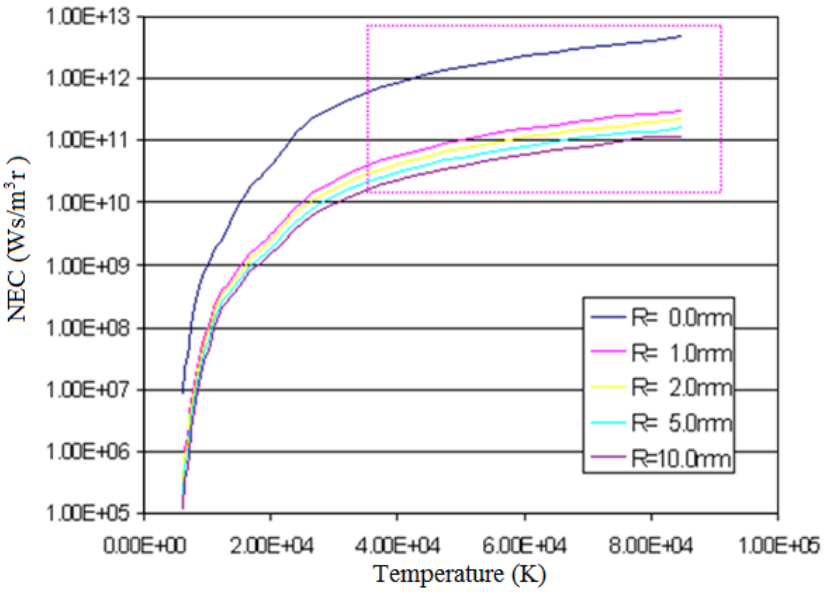

Fig.2.9: Calculated net radiation emission coefficients from cylindrical SF_6 arc plasmas of various radii ($p \approx 1$bar) [96]. Results above 34,000K (enclosed in the doted box) are those extrapolated for numerical stability of the computation.

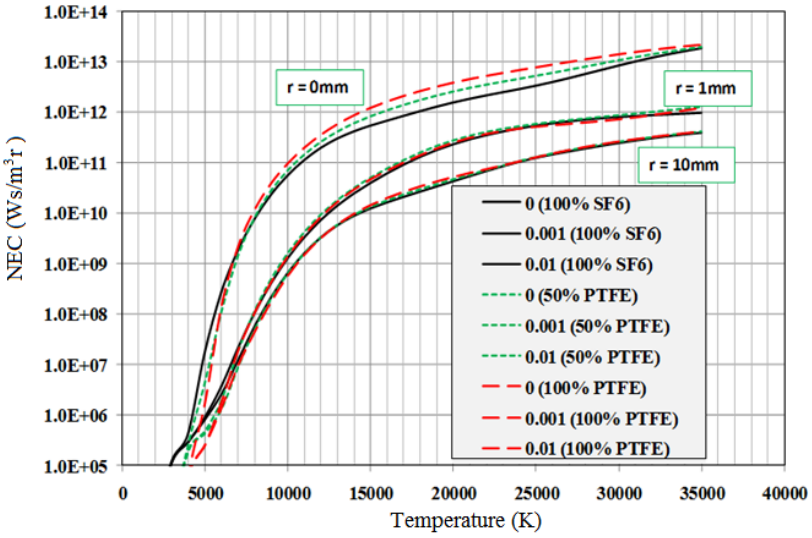

Fig.2.10: NEC as a function of temperature of SF_6 and PTFE in different propotion [108].

2.6 Turbulence Models

Turbulence is one of the most important aspect in SF_6 switching arc modelling because SF_6 arc at low current is unstable with a deformed arc column and entrainment of cold gas into the arc column by eddies. Turbulence enhanced momentum and energy transport has a significant influence on arc behaviour in the low current of SF_6 circuit breaker, especially at the current zero period [43, 70].

Despite the relatively long history since its discovery [109] progress in understanding the underlying mechanisms has been rather slow owing to the complicated nature of the phenomenon. Only limited successful has been achieved with regards to turbulent arcs burning in the nozzles of a specific shape [48, 110].

For arcs in axially dominant flow, the interaction between the arc and its surrounding flow results in turbulent eddies of different scales. A steep temperature gradient exists at the arc edge due to eddy presence. The presence of eddies enhances mass and momentum transfer across regions where velocity and temperature gradient exist. The majority of existing turbulence models is based on the assumption of negligible or mild temperature gradient in the flow domain and as a result the presence of steep temperature (or density) gradient is not explicitly considered in the derivation of the turbulence transport equations.

2.6.1 Prandtl mixing length model

A previous investigation [86] has shown that the simple Prandtl mixing length model has acceptable applicability for a mild converging-diverging nozzle over the current range of 100 A to 1800 A while the standard k-ε model produces unacceptable results at 1800 A when the turbulence parameters are kept at their default values. However the difficulty in the use of Prandtl mixing length model is that the turbulence parameter is unpredictable and needs to be adjusted for nozzles with different shapes. With the Prandtl mixing length model the eddy viscosity is related to the flow field by:

$$\mu_t = \rho l_m^2 \left(\left| \frac{\partial v}{\partial z} \right| + \left| \frac{\partial w}{\partial r} \right| \right) \tag{2.29}$$

where the mixing length for turbulence enhanced momentum transfer is given by:

$$l_m = cR \tag{2.30}$$

where ρ is the density, c the turbulence model parameter and R a characteristic dimension of the arc column, which is defined as the radial distance from the axis to the point of 5000 K for the high current phase. The choice of 5000 K is based on the observation that a large portion of the arcing space can sometimes be filled with hot vapour from nozzle ablation during the high current phase.

The use of a lower temperature such as 3000 K could lead to erroneous values for the characteristic dimension R. For current zero and post arc current simulation, the use of 5000 K will lead to an underestimate of the size of the high-speed jet where turbulence mixing is strong. SF_6 at 5000 K is still conducting. So in the current zero period and the subsequent post arc current calculation, R is defined as the radius of 3000 K isotherm. The choice of the turbulence parameter c is influenced by the definition of R. It has been found that a single value of c is not applicable for both high and low current arcs.

Fang et al. [47, 110] used the simple Prandtl mixing length turbulence model to predict the thermal recovery behaviour of nozzle arcs successfully. The value of turbulence parameter, c, which is a proportional coefficient relating the turbulence length scale to the arc thermal radius R, which is varied when different nozzle geometry used. The thermal radius defined as $\left(\frac{\theta}{\pi}\right)^{1/2}$. θ is given by:

$$\theta = \int_0^{R_{2K}} \left(1 - \rho/\rho_{2K}\right) 2\pi r dr$$

(2.31)

where R_{2K} is the radial distance of the 2000 K isotherm.

The turbulent thermal conductivity k_t is related to the turbulent viscosity through the turbulent Prandtl number, which is assumed:

$$\mathrm{Pr}_t = \frac{\mu_t}{k_t / c_p} \tag{2.32}$$

The turbulent diffusion coefficient is related to the turbulent viscosity through turbulent Schmidt number Sc_t by:

$$D_t = \frac{\mu_t}{\rho Sc_t} \tag{2.33}$$

The magnitude of Sc_t [111] is set to 1.0 in this thesis.

Preliminary results for the 252 kV puffer circuit breaker, indicated that a constant value of turbulent parameter could not accurately predict the rapidly rising extinction peak. So the improvement of the turbulent parameter has to be modified when the size of the arc column experiences significant change, occupies almost the whole of the nozzle hole and there is insufficient cold gas flow around it to promote the development of instability into a fully developed turbulent momentum and energy between the cold flow and the hot arc core.

For a high current phase, the arc column fills most of the nozzle space and cold gas flow only takes a very thin annular layer of the nozzle space. Turbulence cooling does not significantly affect the arc behaviour. When the current decreases to a lower value, the arc column is getting thinner and is surrounded by cold flow. There is more space for the thin arc column to deform freely. In this situation the turbulence parameter c should use a larger value than high current phase. In the simulation, the turbulence parameter is considered in two phases, which are the parameter for the high current phase to the 15,000 A, and the parameter for current zero phase. The turbulence parameter can be defined as:

$$c = \begin{cases} c_H & i > 15kA \\ c_H + \left(1 - \dfrac{|i|}{i_0}\right) * (c_m - c_H) & i \le 15kA \end{cases} \tag{2.34}$$

where c_H is the turbulence parameter of high current phase, i_0 the threshold value of current zero phase. c_m is the maximum turbulence parameter. For the cases of circuit breaker in Chapter Three and Chapter Four, the values of these variables are fixed as: $c_H = 0.05$, $i_0 = 15$ kA, $c_m = 0.3$.

2.6.2 k-ε turbulence model and its modifications

In 2004, Abdol-Hamid et al. [87] applied a temperature gradient correction to the coefficient c_μ of the k-ε turbulence model and used the modified model to simulate a hot jet (stagnation temperature of 1500 K at nozzle inlet) emerging from a supersonic nozzle with an exit radius of 45 mm into open space. Prediction based on the modified model improves the agreement between computed and measured temperature, pressure, and Mach number on the symmetric axis. In the present work the modified k-ε model described in [87] is tested on low current SF_6 arcs in a supersonic nozzle. It was however found that such a temperature gradient correction does not improve the accuracy of the k-ε model for SF_6 nozzle arcs.

The standard k-ε turbulence model is described by the following turbulence transport equations as:

$$\frac{\partial(\rho k)}{\partial t}+\frac{1}{r}\frac{\partial}{\partial r}\left[r\rho v k-r\frac{\rho\nu_t}{\sigma_k}\frac{\partial k}{\partial r}\right]+\frac{\partial}{\partial z}\left[\rho\omega k-\frac{\rho\nu_t}{\sigma_k}\frac{\partial k}{\partial z}\right]=\rho(G-\varepsilon) \tag{2.35}$$

$$\frac{\partial(\rho\varepsilon)}{\partial t}+\frac{1}{r}\frac{\partial}{\partial r}\left[r\rho v\varepsilon-r\frac{\rho\nu_t}{\sigma_\varepsilon}\frac{\partial \varepsilon}{\partial r}\right]+\frac{\partial}{\partial z}\left[\rho\omega\varepsilon-\frac{\rho\nu_t}{\sigma_\varepsilon}\frac{\partial \varepsilon}{\partial z}\right]=\rho\frac{\varepsilon}{k}(c_{1e}G-c_{2e}\varepsilon) \tag{2.36}$$

where k is kinetic energy and ε the dissipation rate. The value of their coefficient respectively are c_{1e}=1.44 and c_{2e}=1.92. The Prandtl number of k and ε with their values being set to σ_k = 1.0 and σ_ε=1.314. The term G represents generation of turbulence eddies as a result of viscous effect in the flow. Its value is given as:

$$G=\nu_t\left[2\left(\frac{\partial w}{\partial z}\right)^2+2\left(\frac{\partial v}{\partial r}\right)^2+\left(\frac{\partial w}{\partial r}+\frac{\partial v}{\partial z}\right)^2\right] \tag{2.37}$$

The turbulence length scale is defined:

$$l=C_D\frac{k^{3/2}}{\varepsilon} \tag{2.38}$$

where C_D has a default value of 0.1643, and the turbulent dynamic viscosity is

given by:

$$\mu_t = \rho \cdot \nu_t = C_v l k^{1/2} = \rho \cdot c_\mu \frac{k^2}{\varepsilon} \tag{2.39}$$

where C_v has a value of 0.5478 and c_μ is 0.09.

Abdol-Hamid et al. [87] proposed a modification to the standard k-ε turbulence model based on qualitative argument to account for the effect of temperature gradient. The term c_μ is multiplied by a term representing the temperature gradient effect:

$$c_\mu = 0.09\left[1 + \frac{\left(\nabla(\mathrm{T_t}) \cdot (k^{3/2}/\varepsilon)/T_t\right)^3}{0.041 + f(M_\tau)}\right] \tag{2.40}$$

where T_t represents the magnitude of the gradient of total temperature T_t, in the simulation the term of $\left(\nabla(\mathrm{T_t}) \cdot (k^{3/2}/\varepsilon)/T_t\right)$ represented by T_g and Cμ = 0.09 Ct. Value of f(M_T) is introduced to extend the model for high speed flow:

$$f(M_\tau) = (M_\tau^2 - M_{\tau 0}^2) H(M_\tau - M_{\tau 0}) \tag{2.41}$$

where $M_\tau = \frac{\sqrt{2k}}{a}$ is the turbulence Mach number with a being the local sound speed.

$H(x)$ is the Heaviside step function and $f(M_\tau) = 0$ for no compressibility correction. $M_{\tau 0}$ = 0.1 is used in the present work.

The modified k-ε turbulence model is applied to the Aachen Nozzle to test its applicability for the nozzle arc. The temperature profiles of the nozzle throat are compared with the measurement for 100 A to 1800 A as shown in Figs.2.11 to 2.13.

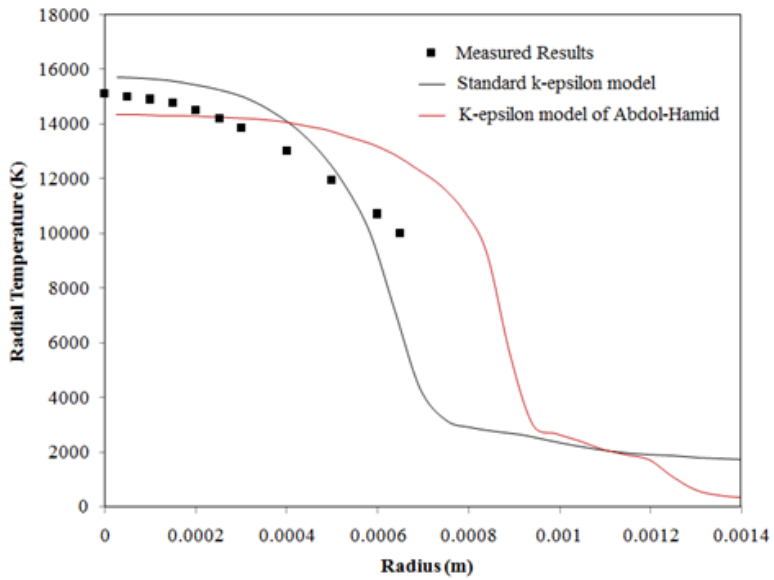

Fig.2.11: Measured [72] and predicted radial temperature distribution of 100A SF_6 arc at the nozzle throat with modified k-ε turbulence model of Hamid.

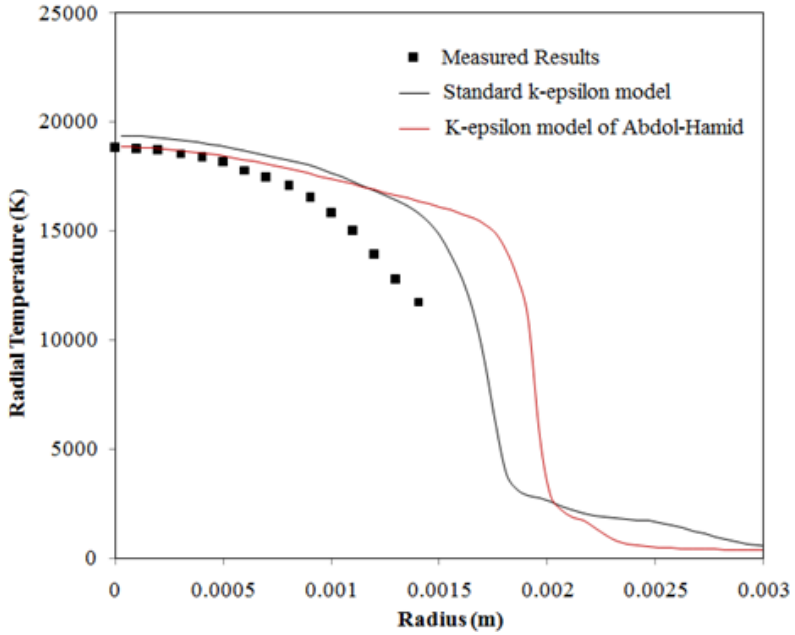

Fig.2.12: Measured [72] and predicted radial temperature distribution of 600A SF_6 arc at the nozzle throat with modified k-ε turbulence model of Hamid.

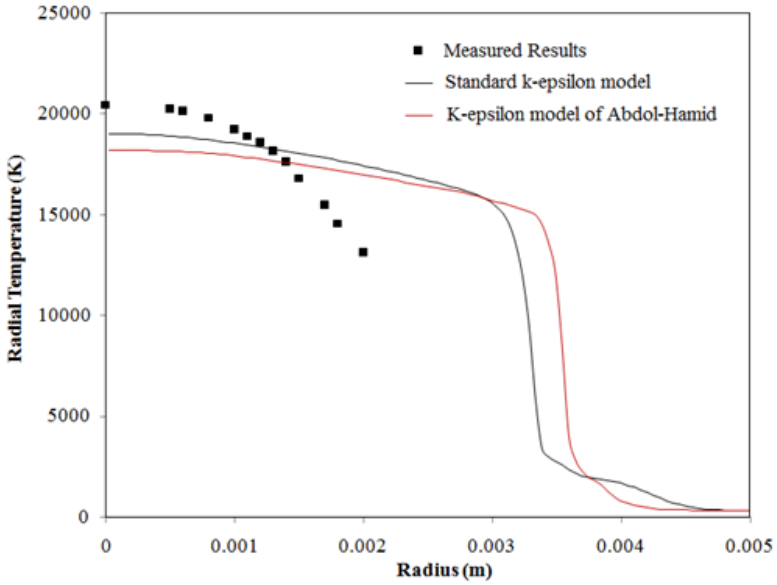

Fig.2.13: Measured [72] and predicted radial temperature distribution of 1800A SF_6 arc at the nozzle throat with modified k-ε turbulence model of Hamid.

When the cases were simulated using the modified k-ε model of [87], it was found that the T_g is in the range of 0.60 to 1.05, and C_μ has a peak value of about 2.6. The c_u is increased, but the ratio of k square and ε is decreased when modification is used in [87]. In the present work, the modified k-ε model described in [87] is tested on low current SF_6 arcs in the supersonic nozzle. It was however found that such a temperature gradient correction does not enhance the turbulence around the arc edge and improve the prediction accuracy of the k-ε model for SF_6 nozzle arcs. In the instance of the 600 A case, the important variables are compared with different turbulence models and are shown in Figs.2.14 to 2.16.

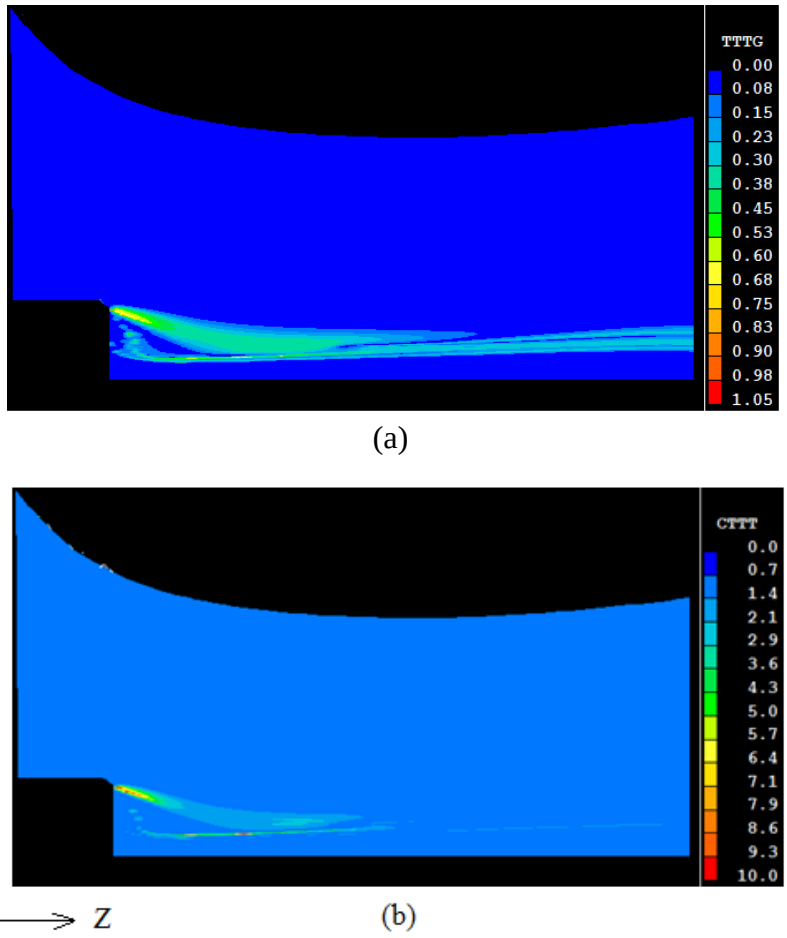

Fig.2.14: (a) Temperature gradient and (b) term c_u without 0.09 of 600A with modified k-ε model of Hamid.

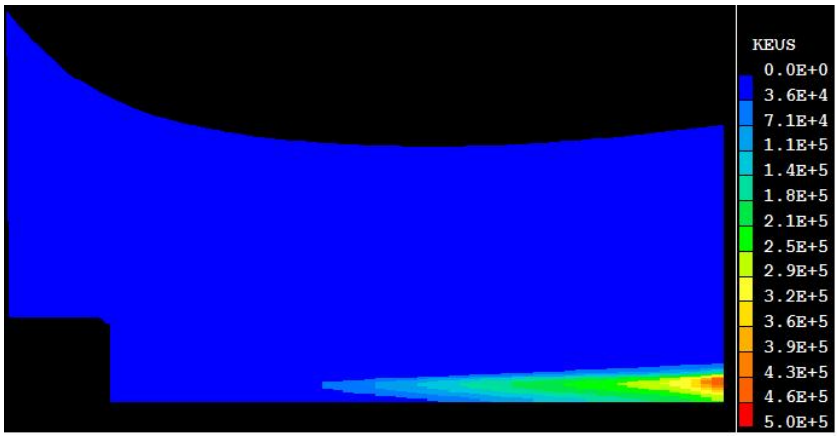

(a)

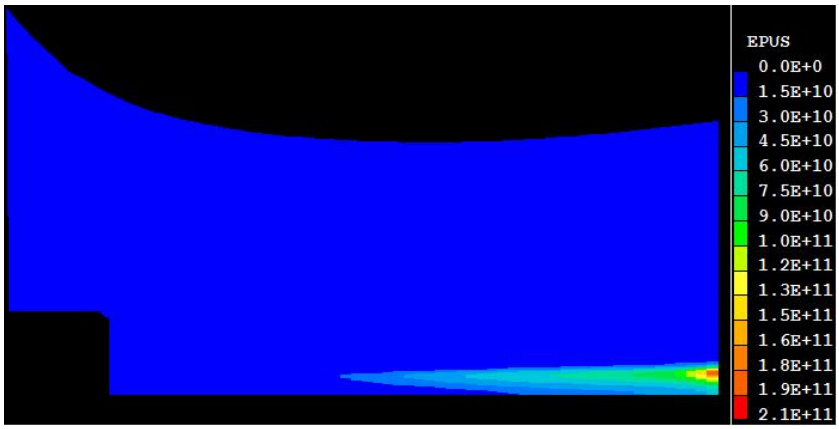

(b)

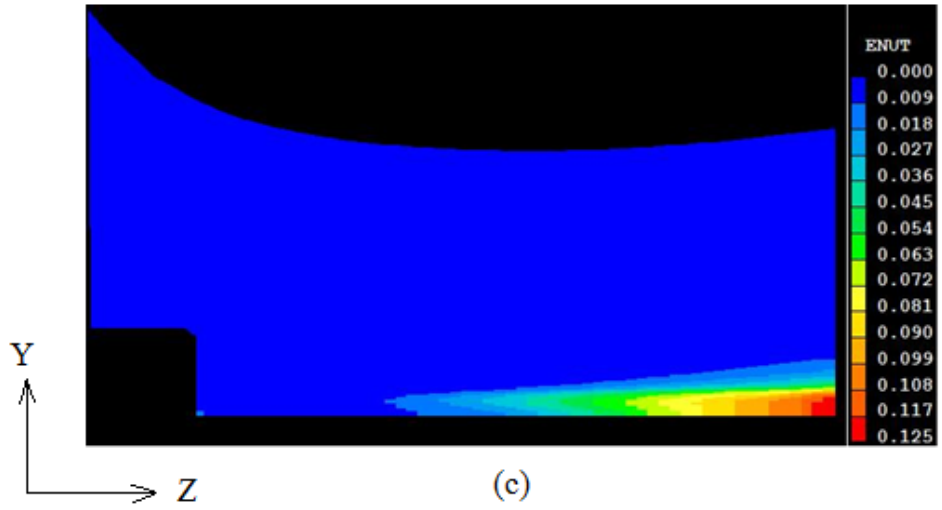

(c)

Fig.2.15: (a) Turbulent kinetic energy, (b) dissipation rate and (c) turbulent viscosity of 600A with standard k-ε model.

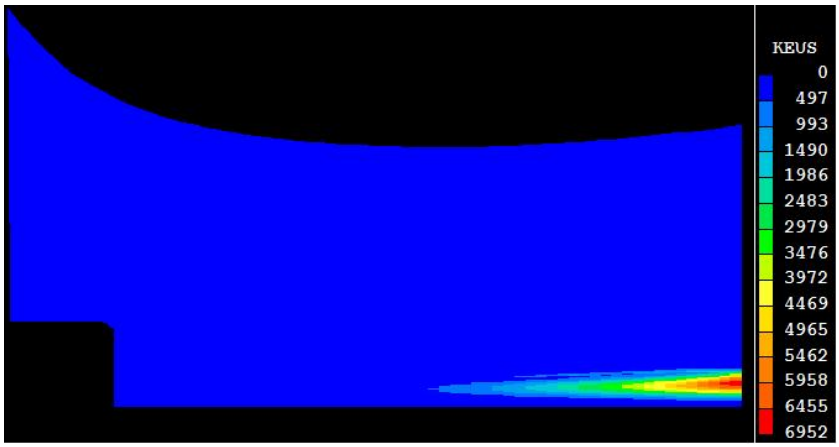

(a)

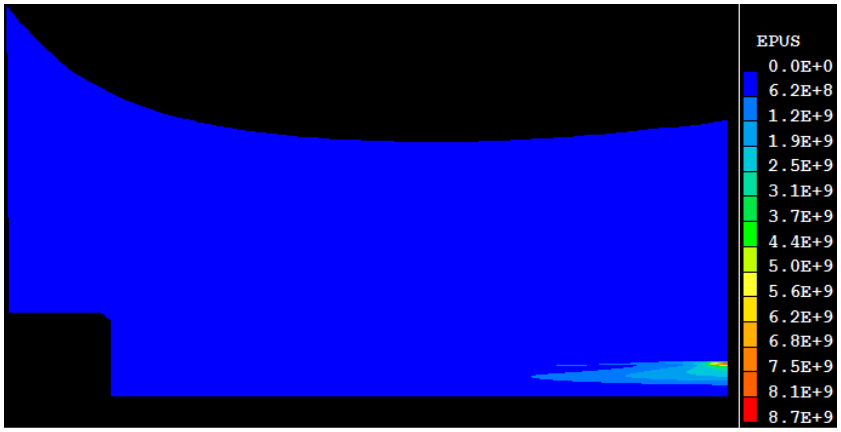

(b)

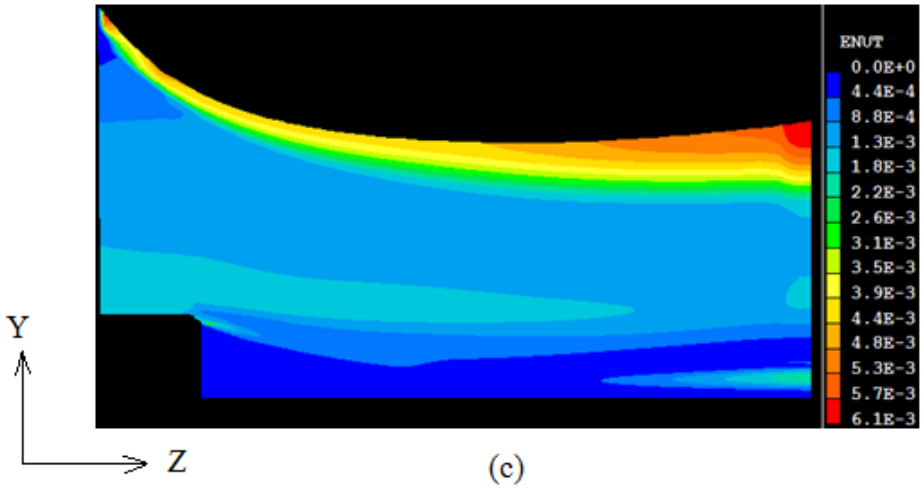

(c)

Fig.2.16: (a) Turbulent kinetic energy, (b) dissipation rate and (c) turbulent viscosity of 600A with modified k-ε model of Hamid.

Another method of adding density gradient terms model based on standard *k-ε* turbulence model has proposed by Tam *et al* [112].

A simple way to incorporate the density effect on turbulent mixing is to allow ν_t to depend on density gradient. The density effect is then characterized locally by *(1/ρ)(dρ/dr)*. While the effect of density on turbulent mixing can be assumed relatively small, as a first approximation, it is reasonable to take the density effect to be a linear addition to the original eddy viscosity. We expect the linear term added to be small so that it may be regarded as a perturbation on the original turbulent mixing. In other words, let ν_t be the combined eddy viscosity (including density effect on flow instabilities). We will assume:

$$\nu_T=\nu_t+\nu_\rho \tag{2.42}$$

where ν_ρ is the density effect and ν_t is the original turbulent eddy viscosity. It will further be assumed that nr is linearly dependent on *(1/ρ)(dρ/dr)*. Now nr must have the dimensions of kinetic viscosity. To ensure dimensional balance in Eq.2.42, note that, within k-ε model, there are only two other quantities, that is, k and ε, available for dimensional adjustment. A simple dimensional analysis yields the following relation:

$$\nu_\rho=\begin{cases} c_\rho \dfrac{k^{\frac{7}{2}}}{\varepsilon^2}\dfrac{1}{\rho}\left|\dfrac{\partial\rho}{\partial r}\right| & \text{if } d\rho/dr \text{ is opposite in sign to } du/dr, \text{ otherwise} \\ 0 \end{cases} \tag{2.43}$$

where c_ρ is 0.035 is used for present simulation.

A comparison study is applied on the Aachen Nozzle with modified *k-ε* model [112] and standard *k-ε* model, the radial temperature profiles at the nozzle throat for using these two turbulence models are shown in Figs.2.17 to 2.19.

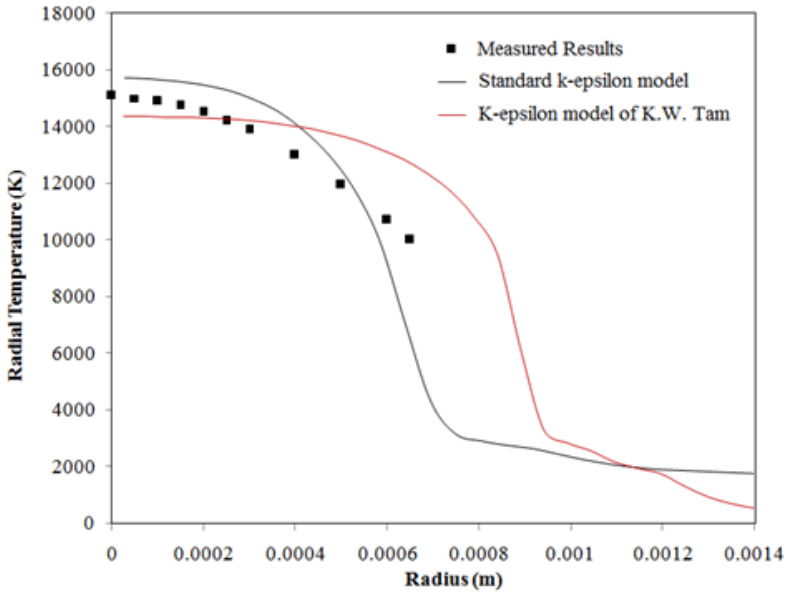

Fig.2.17: Measured [72] and predicted [112] radial temperature profile at nozzle throat in 100A.

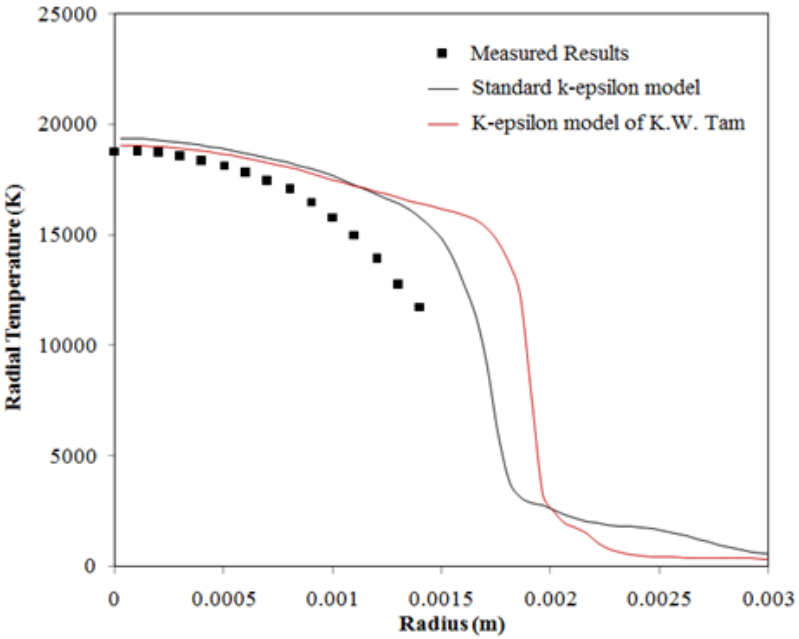

Fig.2.18: Measured [72] and predicted [112] radial temperature profile at nozzle throat in 600A.

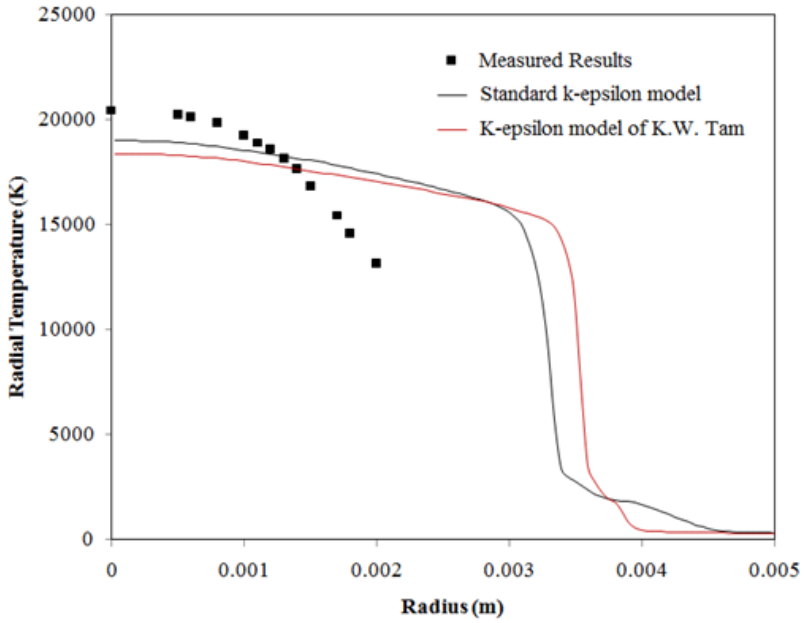

Fig.2.19: Measured [72] and predicted [112] radial temperature profile at nozzle throat in 1800A.

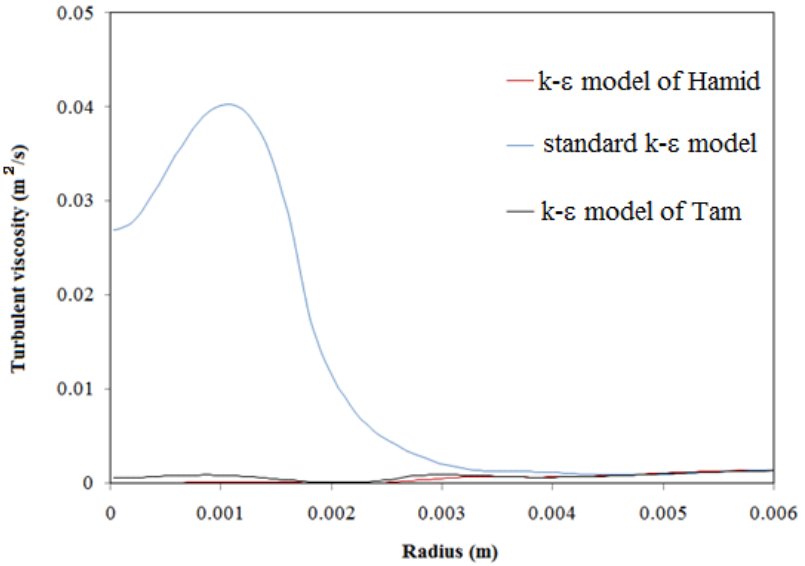

Fig.2.20: Radial turbulent viscosity profiles at the nozzle throat with different turbulence models.

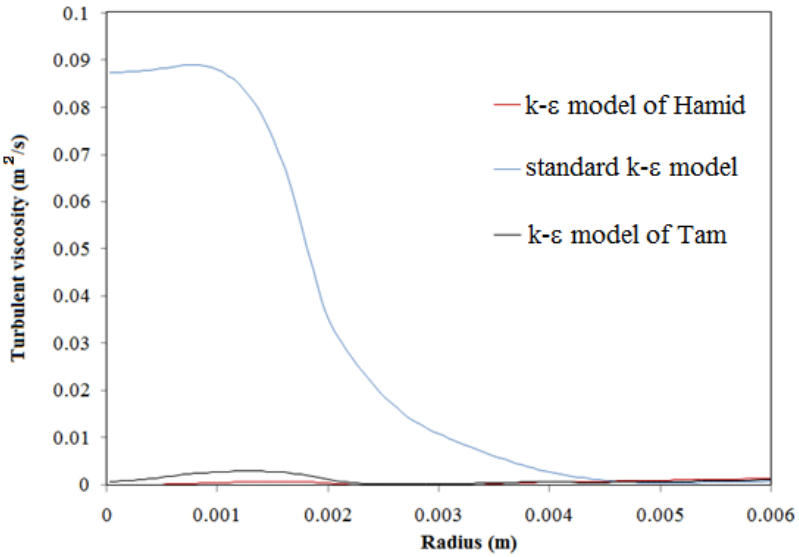

Fig.2.21: Radial turbulent viscosity profiles at the downstream of nozzle with different turbulence models.

The approaches proposed by Abdol-Hamid et al. [87] and Tam et al. [112] both are applied to the nozzle arcs of Aachen nozzle [113]. The predicted radial temperature cannot improve the accuracy at the nozzle throat for both cases. For the cases of 1800 A, the turbulent viscosity is not increased because k and ε increase concurrently and the overall value of cu remains more or less the same, the predicted temperature at the arc core is lower than the measurement by 2000 K or more (as shown in Figs.2.12 and Fig.2.19) with a much broader arc column than that observed in experiment [69, 72]. The turbulence by these two modified k-ε turbulence models is getting smaller when compared against the standard k-ε turbulence model which can be found in Figs.2.20 and 2.21. The radial turbulent viscosity on two slabs (nozzle throat and downstream of nozzle) are recorded to represent the turbulence.

2.6.3 K-ε turbulence model with temperature correction

It is therefore clear that such a modification is not suitable for SF_6 nozzle arcs, which are commonly encountered in high voltage circuit breaker. The standard k-ε turbulence model and two modifications of [87, 112] have similar

performances for the arcs studied in this chapter. A study on the instability of arcs in nozzle flow [114] indicates that the flow can become unstable as a result of the development of large density gradient. Therefore, it is argued qualitatively that the existence of a steep density gradient at the arc edge should contribute to the generation of turbulent eddies. It is thus proposed in the present work that the turbulence generation function given in Eq.2.37 is modified by multiplying a term that represents the effect of density gradient, to replace generation term G in equations of standard k-ε turbulence model in Eqs.2.35 and 2.36, as shown below:

$$G_T = G\,(1+c\,T_g) \tag{2.44}$$

For normal nozzle flows the density gradient as a result of temperature gradient in the radial direction is significant. The presence of this large gradient promotes arc instability and also affects the energy transport process (arc cooling) involving turbulent eddies sitting across large density gradient, such as at the arc edge. With no rigorous mathematical derivation available, it is assumed that the effect of density gradient can be taken into account in a multiplying factor to the turbulence generation term in the k-ε mode, which is $1+cT_g$ where c equals to 0.5 to reflect the enhanced turbulence effect, and

$$T_g = \frac{\left|\overline{\nabla T}\right|}{\overline{T}} \cdot L \tag{2.45}$$

where T_g is a dimensionless temperature gradient in the radial direction of an axisymmetric coordinate system. $\overline{T}$ is reference temperature and L the reference length. In the present work, $\overline{T}$ is taken as the local temperature and L the local radial distance from the symmetric axis, r. The reason for choosing r is based on the understanding that in nozzle arcs the largest eddies have dimensions comparable to the radial size of the arc column and turbulence at the arc edge is most important in arc cooling. Further away from the arc column the temperature gradient is small and the influence of T_g becomes less important.

The modification of the generation term is applied to various nozzle arcs and switching arcs. DC currents of Aachen nozzle with 100 A, 600 A and 1800 A, transient nozzle arcs within GE nozzle [91] and Campbell nozzle [90], 10 kA and 47 kA in circuit breakers. All of these comparison studies are described in detail in Chapter Three.

2.7 Summary

A completed description of the arc model has been detailed in this chapter. The governing equations in the form of conservation of mass, momentum, and energy of a turbulent arc in LTE is the core of an arc model. Because all of the arc behaviours are controlled and reflected by these equations as shown in Eq.2.1. Thus, a good understanding of the meaning of each term in the governing equations is helpful to acquire simulation skills.

At the beginning of the simulation, the computational domain should be established. When determining the boundaries of the computational domain, the boundary conditions for the governing equations should be correctly identified. The mathematic model should be correctly implemented in PHOENICS, a CFD software. Calculation and assignment of material properties are also important, because they are essential in the solution process. The material properties describe the diffusive links between cells. Some common material properties, such as temperature, pressure, laminar viscosity, specific heat capacity, thermal conductivity and electrical conductivity, all these mentioned above can be classified as material properties, because they only depend on the temperature and pressure of the gas under the LTE conditions. The radiation model used in my thesis is part of the Liverpool Arc Model, which detailed in Section 2.5. In my recent research work, most simulate calculations of electric arcs have accounted for the radiation transport

by using the NEC. Because Zhang et al. [49] made good results by this radiation model for SF6 nozzle arcs and puffer circuit breakers.

Investigation of turbulence model is the most important job in my research. Two popular turbulence models of the Prandtl mixing length model and the k-ε turbulence model have been introduced in this chapter. It is well known that the Prandtl mixing length model has been adopted by lots of researchers to perform the turbulent arcs successful. However, the value of turbulence parameter is always hard to decided. Some researchers often modify it with their experience based on the experimental results and the shape of nozzle. Its applicability is limited. The k-ε turbulence model and some of its modifications often poorly predicted for the turbulent arcs. The modified k-ε models of Abdol-Hamid et al. [87] and Tam et al. [112] can predict their own hot jet flow. Two modifications have been applied to the Aachen nozzle [113] for verifying the applicability of turbulent arcs condition. However, the turbulence predicted by these two modified k-ε turbulence models cannot be correctly enhanced in the condition of turbulent arcs. These are only the initial research works in the investigation of turbulence models. Finally, a further modification based on the standard k-ε turbulence model is proposed by author in Section 2.6.3. Previous study [114] indicates that the flow can become unstable as a result of the development of large density gradient. The existence of a steep density (or temperature) gradient at the arc edge should contribute to the generation of turbulent eddies. Thus, the generation function G (Eq.2.37) is modified by multiplying a term into the source term directly that represents the effect of temperature gradient, as shown in Eq.2.44. The applicability of the modified k-ε model based on the temperature correction will be verified in Chapter Three.

CHAPTER 3

K-ε Turbulence Model with Temperature Correction

3.1 Introduction

The applicability of the modified k-ε turbulence model with temperature correction Eq.2.44 is tested in this chapter under different discharge conditions as discussed in Chapter Two. The standard k-ε turbulence model is modified to take into account the effect of steep temperature (or density) gradient, predominantly at the edge of arc column. The turbulence generation function G in the standard k-ε model is multiplied by a factor of $(1+c_T T_g)$ where T_g is a dimensionless temperature gradient as defined by Eq.2.44 in Chapter Two. Prediction is made for the radial temperature at the throat of Aachen nozzle under the steady state current of 100 A, 600 A and 1800 A, arc voltage for puffer circuit breaker arcs at 10 kA and 47 kA, and critical RRRV for two transient nozzle arcs (GE nozzle [91] and Campbell nozzle [90]). Predicted results are compared with available measured results, identifying the applicability of this proposed modification.

There are four sections in this chapter. This modified model was firstly applied to the Aachen nozzle [72, 113]. Yan et al. [86] used this nozzle to carry out a comparative study of the Prandtl mixing length model and standard k-ε model. It was concluded that the k-ε model and Prandtl mixing length model can both give reasonable prediction of the radial temperature distribution of DC SF_6 arcs in the current range of 100 A to 1800 A. However, the turbulence

parameters of the standard k-ε model need to be adjusted. It is our intention not to have any adjustable parameters in the modified model for different nozzle shapes and arc conditions.

Switching arcs in high voltage A.C. circuit breakers are of a transient nature. It is known that the standard k-ε model produces poor prediction accuracy for round jets [120]. Switching arcs, in many aspects, are similar to a round jet despite at low current the arc columns are deformed due to turbulence and other arc instability mechanisms. The presence of turbulence at high current has a limited effect on the arc voltage which determines the overall power dissipation rate in the arc column. It is the low current phase and thermal recovery period that turbulence has the biggest effect on. Its validity should therefore be tested under low current (<15 kA) conditions. The cases of transient nozzle arcs are similar to the switching arcs in circuit breakers.

The assessment of using modified k-ε model tested on the different nozzle arcs or switching arcs will be given in the following sections. The nozzle arc of Aachen nozzle with direct current levels of 100 A, 600 A and 1800 A is detailed given in Section 3.2. The nozzle arcs with two totally different nozzle shapes of GE nozzle [91] and Campbell nozzle [90] with transient steady states are included in Sections 3.3 and 3.4. The switching arcs in a puffer type circuit breaker with 10 kA and 47 kA current levels are detailed in Section 3.5. The conclusion for Chapter Three is given in Section 3.6.

3.2 Turbulence Model Tested on Aachen Nozzle

3.2.1 Introduction

Arcs in a supersonic nozzle usually reach an axis temperature higher than 15,000 K, the radial temperature profile has very large gradient at the arc edge due to radiation absorption there [49]. Gas velocity can reach several thousand meters per second due to the low gas density and high temperature in the arc core [47- 49]. Recent investigations [47- 49, 109] connected to the onset of arc instability argued that the main driving mechanism for arc instability is due to the density fluctuations in the region where the temperature gradient is very high. Thus, the arc edge flow tends to be more unstable and induces stronger turbulence.

The modelling of the turbulence arc has been based on the turbulence models for shear flows. The application of the Prandtl mixing length model to arcs in supersonic flow has had considerable success in predicting the thermal interruption capability of gas blast circuit breakers although the turbulence parameter needs to be adjusted for a given geometry of the nozzle [49].

For ordinary shear layer flows, the k-ε model has long been popular since the five turbulence parameters are not very sensitive to flow conditions. The default values can usually be used to make reasonable predictions.

The k-ε turbulence model has a very wide range of applicability of the turbulence parameters which do not need to be adjusted when compared with the other turbulence models, as introduced of [87, 112] in Chapter Two.

The objective of this section is to carry out a comparative study of these two popular turbulence models and modified k-ε turbulence model to assess the applicability of the latter for turbulent arcs in supersonic nozzle with mild divergence using available experimental results.

3.2.2 Geometry and dimensions of Aachen nozzle

The nozzle was originally used by the University of RWTH Aachen [72, 113]. In the present work, arc temperature measurements at different locations inside of the nozzle and at different current levels were taken using the spectroscopic method. The temperature prediction can be obtained by using the proposed turbulence models, which proposed by Abdol-Hamid et al. [87] and Tam et al. [112], are also applied to the nozzle arcs of Aachen nozzle [72, 113] (it has been introduced in Chapter Two).

The Aachen nozzle has a small diverging angle which prevents flow reversal near the nozzle outlet. Its radius as a function of axial distance from the inlet is given in Fig.3.2.1. The inlet radius is 28.57 mm. The outlet radius is 19.99 mm. The nozzle throat is located at 33 mm from the nozzle inlet with a minimum radius of 18.38 mm.

The nozzle was divided into five sections in the axial direction when the grid system was constructed. Details of the division are given in Table 3.1. The axial position of the cells which are closest to the nozzle throat is needed in order to record the radial temperature distribution in the simulation.

Because of the finite size of the cells, the cell centre may not exactly be at the throat. The axial cell width around the nozzle throat is 1.0 mm. The maximum distance between the cell centre and the throat plane is half the axial cell size which is 0.5 mm in the present case. The computational domain with the grid system for the Aachen nozzle is given in Fig.3.2.2.

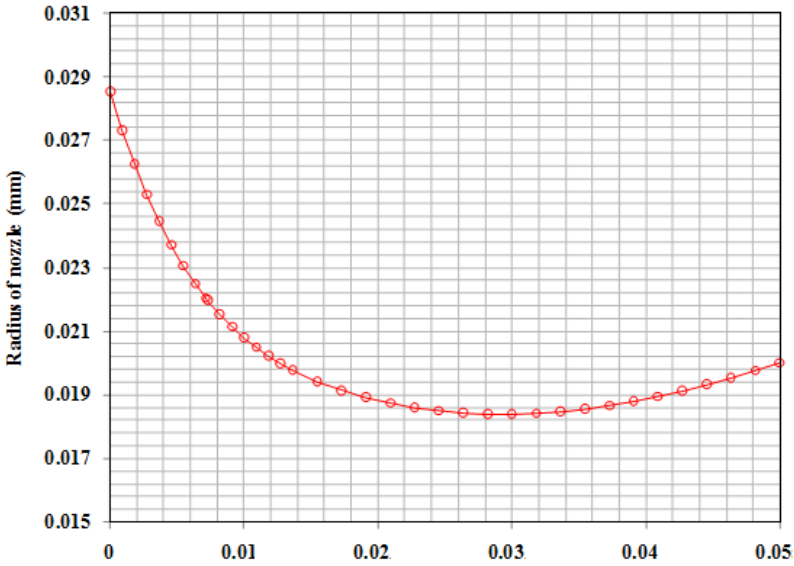

Fig.3.2.1: Aachen nozzle profile. The inlet radius is 28.56 mm, the outlet radius is 19.99mm and the nozzle throat is at 33 mm from the nozzle inlet with a minimum radius of 18.38 mm.

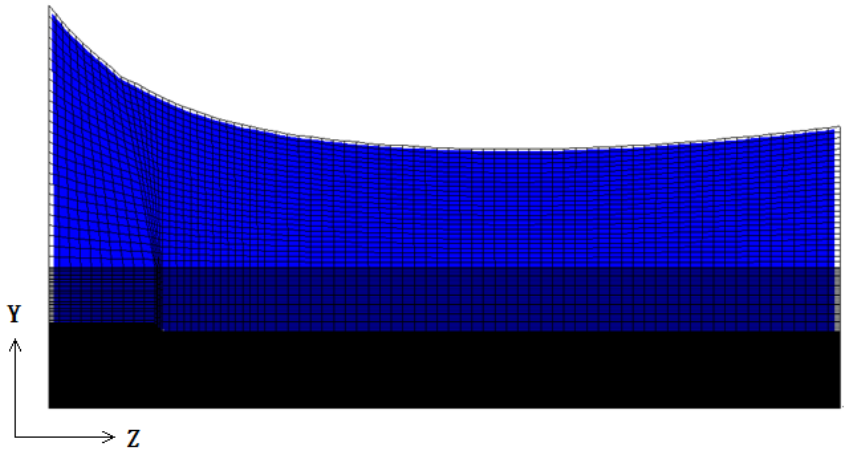

Fig.3.2.2: Computational domain of Aachen nozzle with grid display. The blue part indicates room temperature of 300 K. The number of cells in the axial and radial direction respectively are 80 and 173. The slab of nozzle throat is the 53th in the axial direction.

Points	D1 – DA	DA – D2	D2 – D3	D3 – D4	D4 –D5
Axial coordinates (mm)	0 – 5	5 – 7.86	7.86 – 15	15 – 35	35 – 55
Radius (mm)	28.6 – 23.5	23.5 – 22.0	22.0 – 19.8	19.8 – 18.4	18.4 – 19.9
Radial number of cells	NZ1A (10)	NZA2 (6)	NZ23 (14)	NZ34 (25)	NZ45 (25)
Description	Converging inlet		Converging section	Section containing throat	Diverging section

Table 3.1: Division of the nozzle into different sections and number of cells.

3.2.3 Implementations in PHOENICS

As mentioned in Chapter Two, the governing equations are numerically solved by using a CFD package, PHOENICS [117]. The solutions obtained by PHOENICS were verified by independent software for a self-similar arc [121] and by theory for cold flow shocks in supersonic nozzle.

Axisymmetric boundary conditions are imposed. The radial velocity and the radial gradient of all dependent variables are zero on the axis. Heat fluxes are set to zero for all solid surfaces. The values of k and ε in the cells near the solid surface are sorely determined by the wall shear stress [122].

At the nozzle inlet the pressure and temperature are calculated from the stagnation pressure and temperature using isentropic relations as shown in Eq.2.8-2.10. However, the inlet values of turbulent kinetic energy and its dissipation rate are normally unknown, empirically [122]. The turbulent kinematic energy density, k_{in}, is set to 1% of the kinetic energy associated with the incoming flow, and ε is derived from k by assuming a length scale of 10% of the radial width of the inlet, d_{in},

$$k_{in} = 0.005|\omega|^2 \tag{3.1}$$

$$\varepsilon_{in} = 0.1643 \frac{k_{in}^{1.5}}{0.1 d_{in}} \tag{3.2}$$

The computation has been carried out at three direct current levels (100 A, 600 A and 1800 A) for the Aachen nozzle [72, 113]. The upstream stagnation pressure is 9 bar and the stagnation temperature is set to a room temperature of 300 K. The exit pressure is 2.5 bar. The length of the nozzle is 55 mm and the throat diameter of the nozzle is 36.7 mm. The distance between the inlet and the nozzle throat is 33 mm. The diameter of solid upstream electrode is 10.86 mm and its length is 7.86 mm. The number of cells used in the computation is 173 (radial) by 80 (axial) for all the current levels. Different number of radial cells has been tested as a sensitivity study, the width range from 0.1 mm to 0.01 mm as the cell widths for arc column are used for testing the 100 A and 600 A cases. The predictions of radial temperature at the nozzle throat, which constructed by different cell types are shown in Fig.3.2.4 to 3.2.5 constructed . Finally, 0.05 mm can be used for width of each cell in arc column region.

A body fitted coordinate (BFC) grid system is used to model the curvilinear nozzle surface. The grids are refined in the arc region. The cases for the Aachen nozzle are steady state for the DC current.

3.2.4 Results and discussion

The temperature distributions of these three current levels in the Aachen nozzle are detailed in Figs.3.2.6 to 3.2.8, showing that the radial size of the arc column increases with the current. The flow field of 600 A case is shown in Fig.3.2.3. A non-slander arc model is used to calculate the electric potential field. The upstream arc root is subjected to strong convection cooling. In this case, a differential equation based on current continuity has to be solved to obtain the distribution of electrostatic potential. The electrode field and current

density can then be calculated.

To solve Eq.2.1 with only the diffusion term, the diffusion coefficient can never be zero in order that a solution exists in the whole domain. So for low temperature gas or insulating material, an electrical conductivity of 10^{-3} $\Omega^{-1}m^{-1}$ is used. On all boundary surfaces except that intersecting with current conducting contacts, we assume that no current flows across the boundary. This is in fact the default PHOENICS boundary condition of zero flux. A common approach is to specify current density distribution on one of the boundary and a fixed potential on the other. Fig.3.2.9 shows an example of such boundary conditions. The radius of the circular area (blue box in the green box as figure shown) over which a uniform current density is specified is determined by:

$$R_{root} = \sqrt{\frac{I}{\pi J_{root}}} \tag{3.3}$$

where J_{root} = 5x10^7 A/m^2 to 2x10^8 A/m^2. A value of 1.5×10^8 A/m^2 produces reasonable results.

It is known from Chapter Two that large discrepancies existed between the radial temperature profiles as predicted by the k-ε model and measurements of Leseberg and Pietsch [72, 113]. The results recorded in Figs.3.2.10 to 3.2.12, details all of the turbulence parameters of the k-ε model, which are set to their default values. The figures show that the turbulent energy exchange is slightly over represented for 100A case but seriously under represented for 600A and 1800A cases which can be found from the radial temperature profiles around the arc edge. This also reflects the turbulence effect in arc cooling. The inclusion of the temperature correction factor significantly improves the situation at 1800 A cases as shown in Fig.3.2.12. The arc core temperature predicted by the standard k-ε model is lower than the measurement by almost

30,000 K. The radius of the arc column at the nozzle throat is larger than the measured arc column about 1.2 mm. This is almost 60% of the measured arc column radius. This should be considered to be a large discrepancy in the arc simulation. The predicted temperature at the arc core by modified k-ε model is much closer to the measured arc core temperature, and the discrepancy of the arc radius is only 15% when compared against the measured arc column radius. The prediction for the modified k-ε model is better than the Prandtl mixing length model (the blue curve in Fig.3.2.12) for the 1800 A case. This is also the situation of 600 A case, where the modified k-ε model predicts the radial temperature profile is closest to the measurement in three turbulence models. For the case of 100 A, it is noted that the standard k-ε model has over represented the turbulence effect in arc cooling where the temperature gradient is larger than the experimental result. However, the modified k-ε model still increases the turbulence effect, which is represented by the black curve in Fig.3.2.10. Thus, the arc core temperature is larger than the measured temperature of 6,000 K with a greater temperature gradient at the arc edge. The modified k-ε model does not lead to any improvement at a low current (100 A), because the current modification adds an additional term to the turbulence kinetic equation allowing it to recover to the standard model when the temperature gradient disappears. However, it is generally known that there are possible errors with the measurement, so the measurement for the Aachen nozzle case in some situations must be doubted. This is the reason that I need to use more nozzle arcs and switching arcs to verify the applicability of the modified k-ε model.

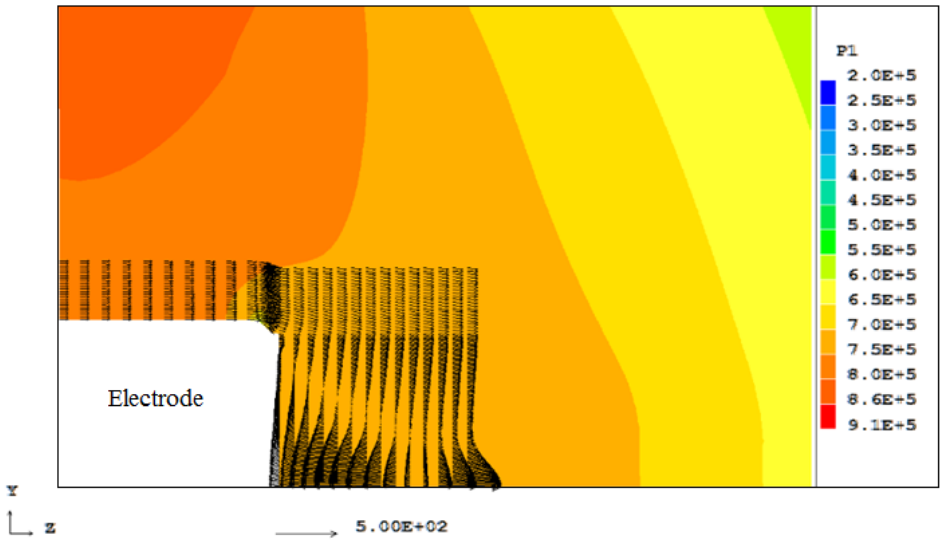

Fig.3.2.3: Flow field around the electrode for 600 A case.

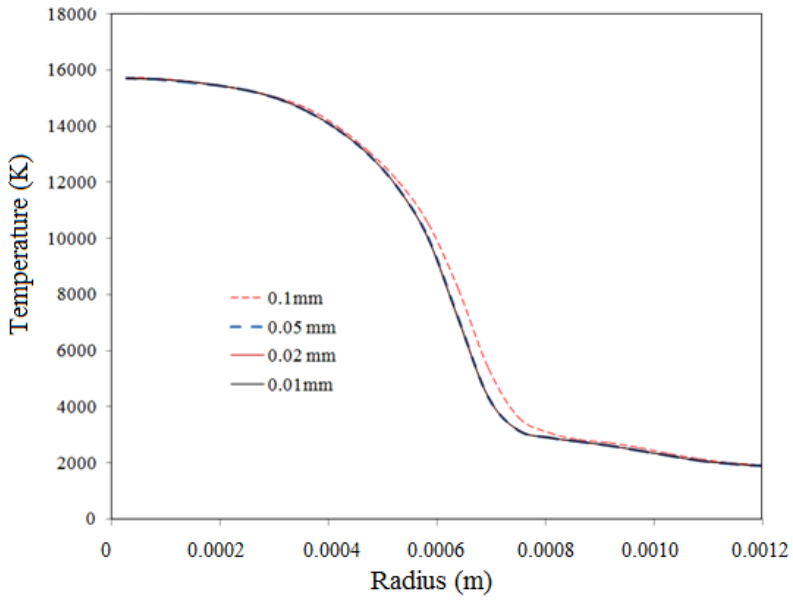

Fig.3.2.4: Radial temperature predictions with different radial cell widths at 100 A case.

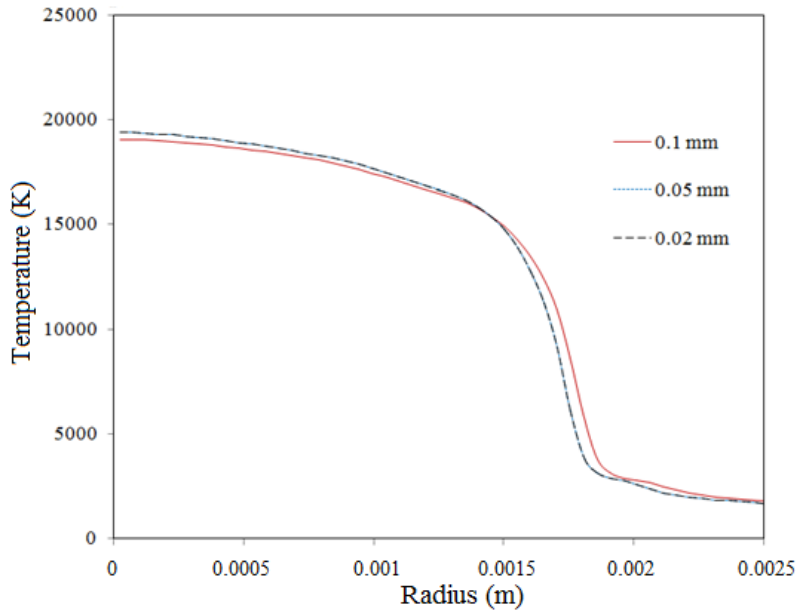

Fig.3.2.5: Radial temperature predictions with different radial cell widths at 600 A case.

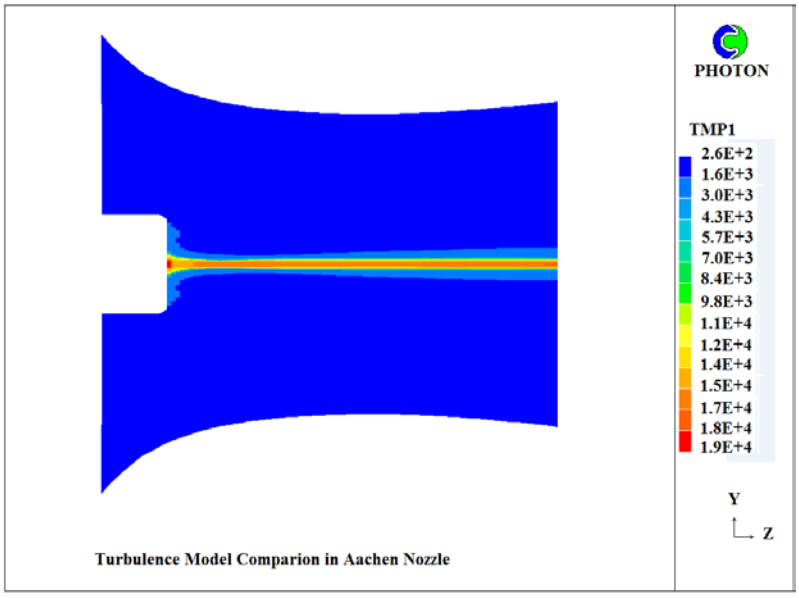

Fig.3.2.6: Temperature distribution of 100 A in the Aachen nozzle.

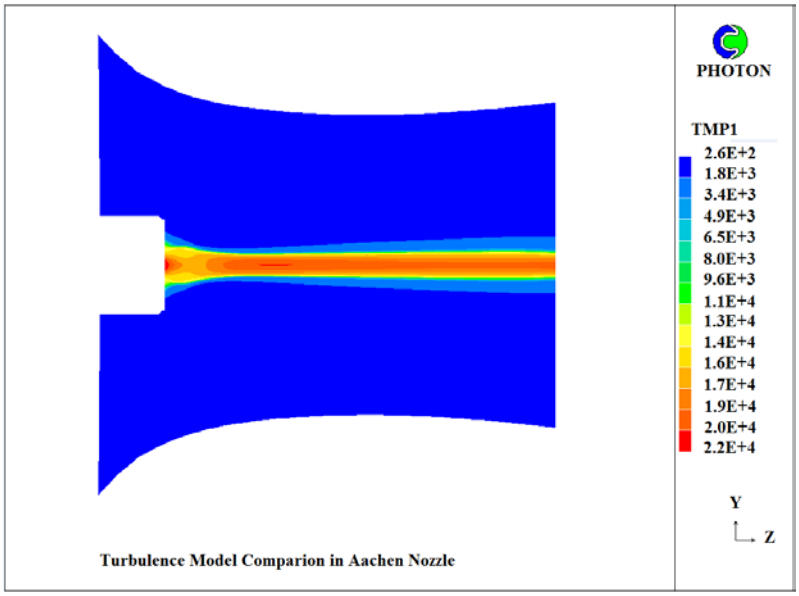

Fig.3.2.7: Temperature distribution of 600 A in the Aachen nozzle.

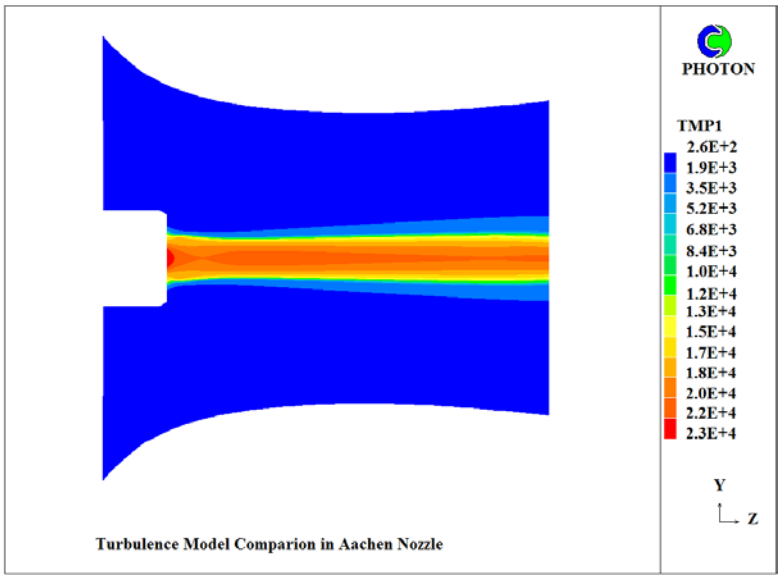

Fig.3.2.8: Temperature distribution of 1800 A in the Aachen nozzle.

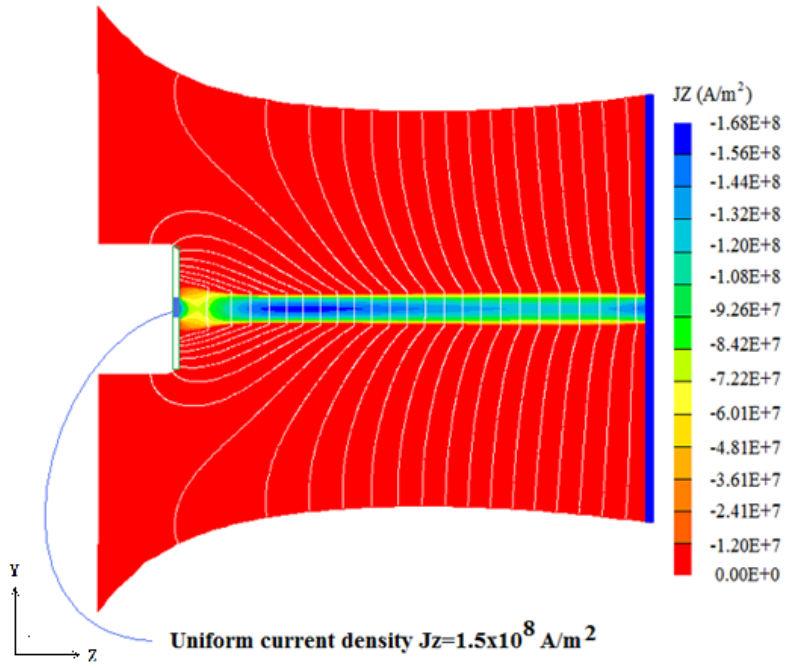

Fig.3.2.9: Diagram showing the boundary conditions for the electrostatic potential equation (current continuity equation). The equipotential lines are perpendicular to the boundary surface representing a zero current density normal to the boundary faces. The uniform current density Jz = $1.5*10^8$ A/m^2.

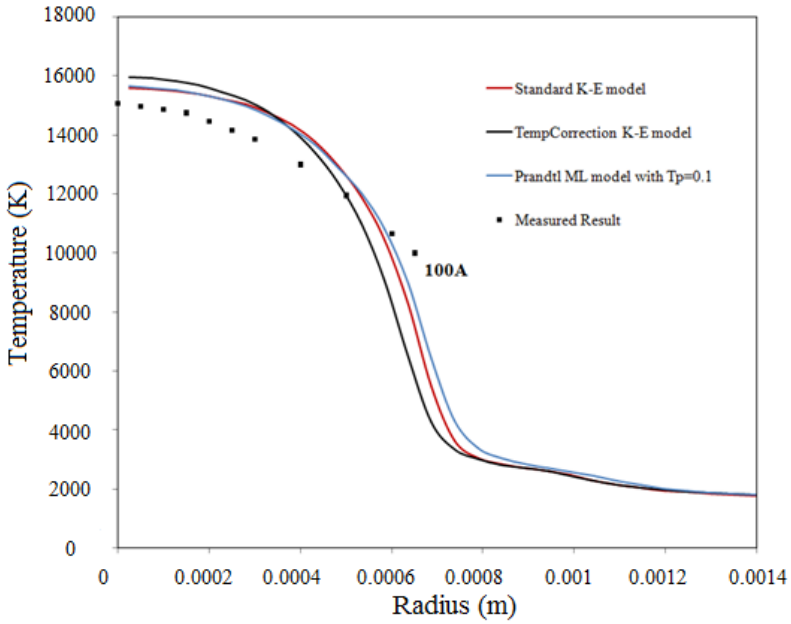

Fig.3.2.10: Measured result [72] and predicted radial temperature at the nozzle throat of 100 A with different turbulence models.

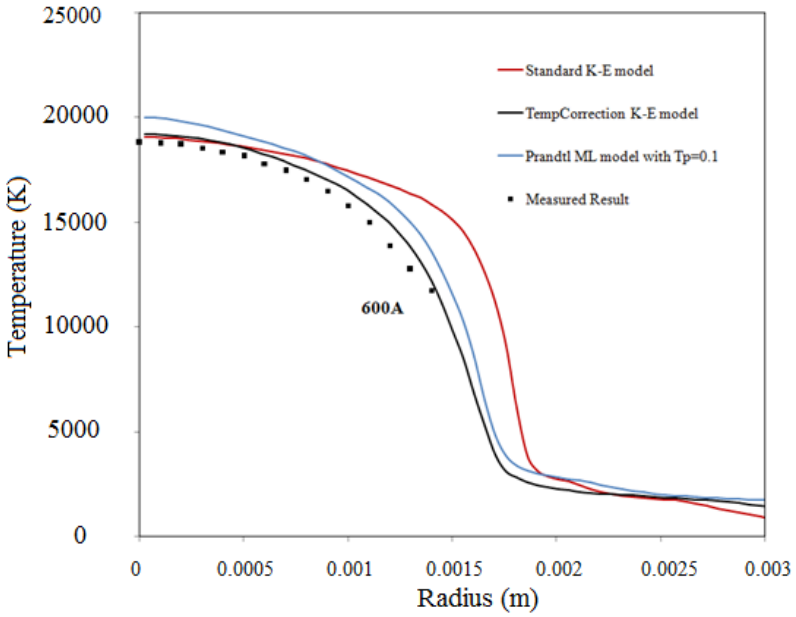

Fig.3.2.11: Measured result [72] and predicted radial temperature at the nozzle throat of 600 A with different turbulence models.

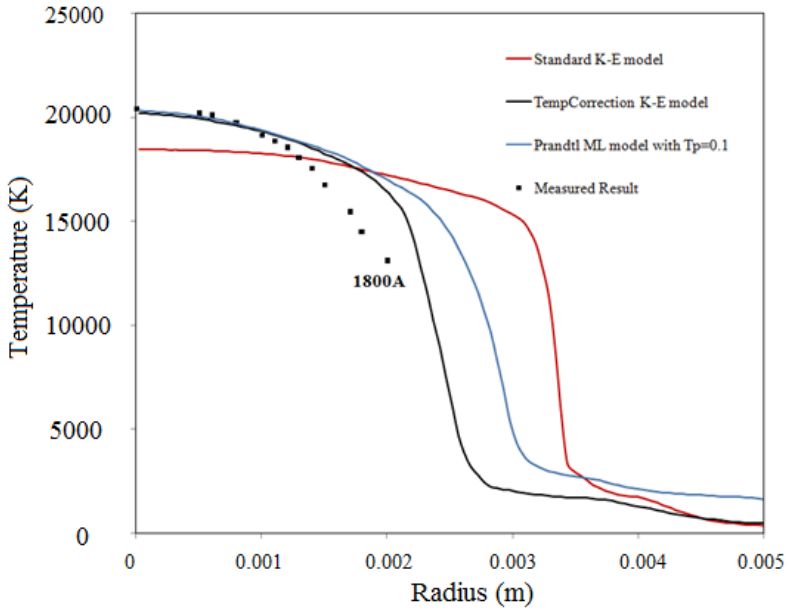

Fig.3.2.12: Measured result [72] and predicted radial temperature at the nozzle throat of 1800 A with different turbulence models.

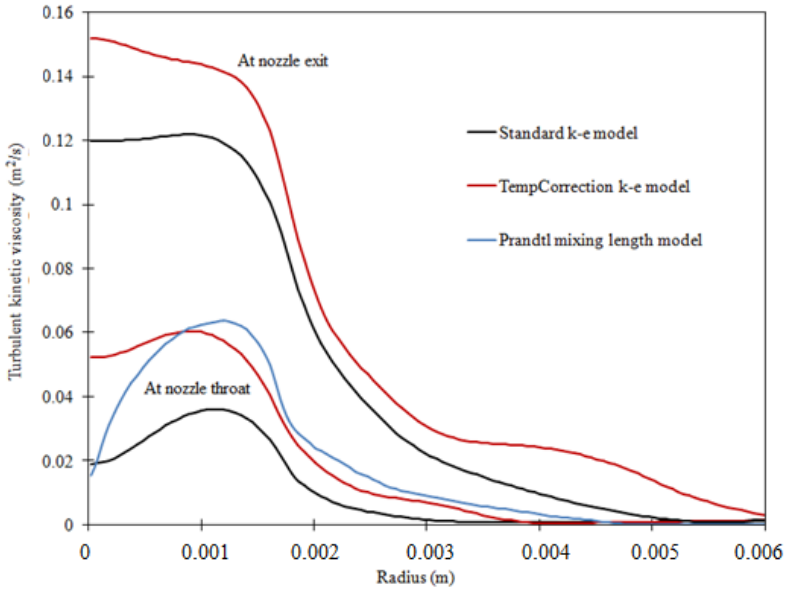

Fig.3.2.13: Radial turbulent viscosity profiles at different axial positions for 600 A.

3.2.5 Energy balance calculation based on integral formulation of energy conservation equation

This part attempts to give more details with respect to the calculation of the balance of energy and mass conservation. Investigations have been performed by taking into account a turbulent nozzle arc at 600 A as a sample, with the effect of turbulence being modelled by a modified k-ε model with a correction term of temperature gradient as described in Eq.2.44 to 2.45.

The governing equations are in steady states, given below as an integral formulation:

$$\int_{CS} \rho h \vec{V} \cdot d\vec{A} + \int_{CS} \rho \frac{V^2}{2} \vec{V} \cdot d\vec{A} - \int_{CS} \frac{k}{c_p} \nabla h \cdot d\vec{A} = \int_{CV} \vec{j} \cdot \vec{E} d\Omega - \int_{CV} q d\Omega \qquad (3.4)$$

It can be seen that the left hand side of Eq.3.4 includes respectively the net flux of enthalpy and the net flux of kinetic energy, which flow out through control volume surfaces, as well as the transport of energy due to

laminar/turbulent heat conduction. Ohmic heating and radiation transport, which are normally considered as source terms, have been available in the right hand side of the above equation. The enthalpy balance for the case of 600 A with the modified k-ε model is shown in the Fig.3.2.14.

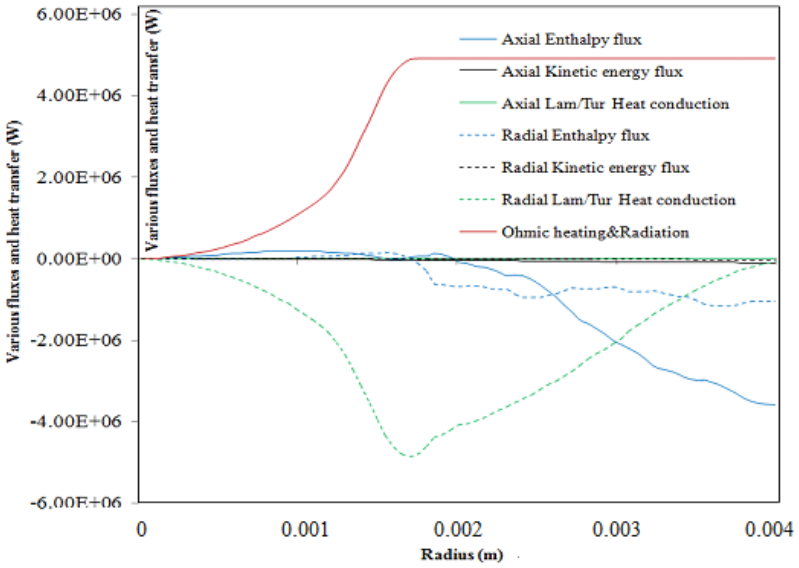

Fig.3.2.14: Radial integrated energy balance on nozzle throat for 600 A case.

Each section of the energy equation in the calculation can be obtained by the following equations, which are slightly different to Eq.3.4:

Axial Enthalpy flux (convection): $-\int \rho w \frac{\partial h}{\partial z} 2\pi r dr$ (3.5a)

Axial Kinetic energy flux: $-\int \rho w V^2 2\pi r dr$ (3.5b)

Axial laminar and turbulent heat conduction: $\int \frac{\partial}{\partial z}\left(\frac{k}{c_p}\frac{\partial h}{\partial z}\right) 2\pi r dr$ (3.5c)

Radial Enthalpy flux (convection): $-\int \rho v \frac{\partial h}{\partial r} 2\pi r dr$ (3.5d)

Radial Kinetic energy flux: $-\int \rho v V^2 2\pi r dr$ (3.5e)

Radial laminar and turbulent heat conduction: $\int \frac{1}{r}\frac{\partial}{\partial r}\left(r\frac{k}{c_p}\frac{\partial h}{\partial r}\right)2\pi r dr$ (3.5f)

Ohmic Heating and radiation: $\int (\sigma E^2 - q)2\pi r dr$ (3.5g)

It can be seen from Fig.3.2.14 that strong Ohmic heating exists in the arc column, which contributes to the significant effect of radiation transport. The radial heat conduction becomes dominant between 0 to 2 mm on radial direction, the values of which are much higher than all other energy fluxes.

In the region of the domain, where r > 2.0mm, neither radiation nor turbulence have significant effect on the energy balance, instead, it is the axial and radial convections that dominate the transport of energy. From Fig.3.2.14 above, it can be seen that the effects are due to the axial and radial kinetic energy fluxes. However, it does seem to be very important throughout the entire domain.

The turbulence kinetic energy and its dissipation rate balance for the Eqs.2.35 to 2.36 with the modification of Eq.2.44 for the case of 600 A are shown in Figs.3.2.15 to 3.2.16. The generation term is significant. Diffusion on radial direction of k and ε are dominant from r = 1.5 mm to 2.0 mm, and the axial diffusion is increased to a large value and significant from 2.2 mm. The relative error for these two energy balance calculations is detailed in Fig.3.2.17, which demonstrates that the relative errors for energy (enthalpy), kinetic energy and its dissipation rate are smaller than 10%, the calculation for the 600 A case with modified k-ε model can be considered accurate and convinced. The cases of 100 A and 1800 A have similar energy balance to the case of 600 A.

Each term of k and ε equations (Eqs.2.35 to 2.36) in Figs.3.2.15 and 3.2.16 are given below:

Axial convection of k: $-\int \rho w \frac{\partial k}{\partial z} 2\pi r dr$ (3.6a)

Axial convection of ε: $-\int \rho w \frac{\partial \varepsilon}{\partial z} 2\pi r dr$ (3.6b)

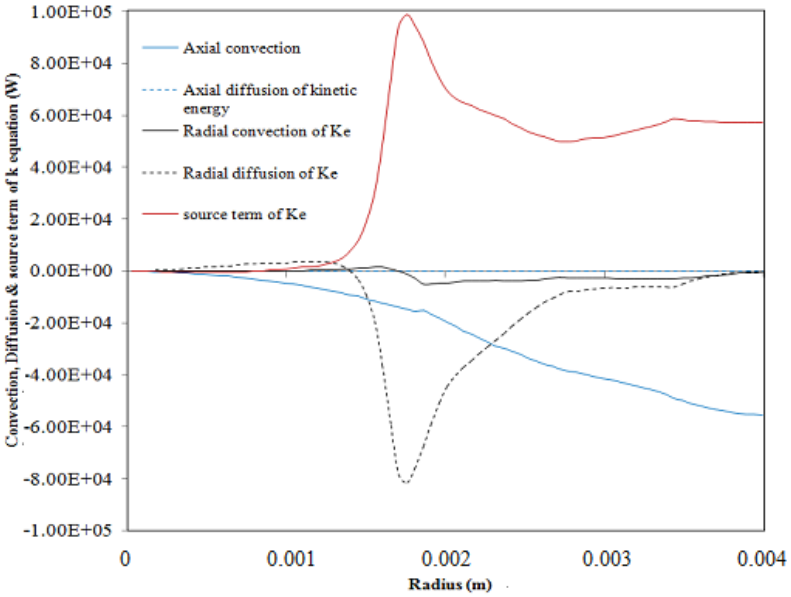

Fig.3.2.15: Kinetic energy balance at the nozzle throat for 600 A case.

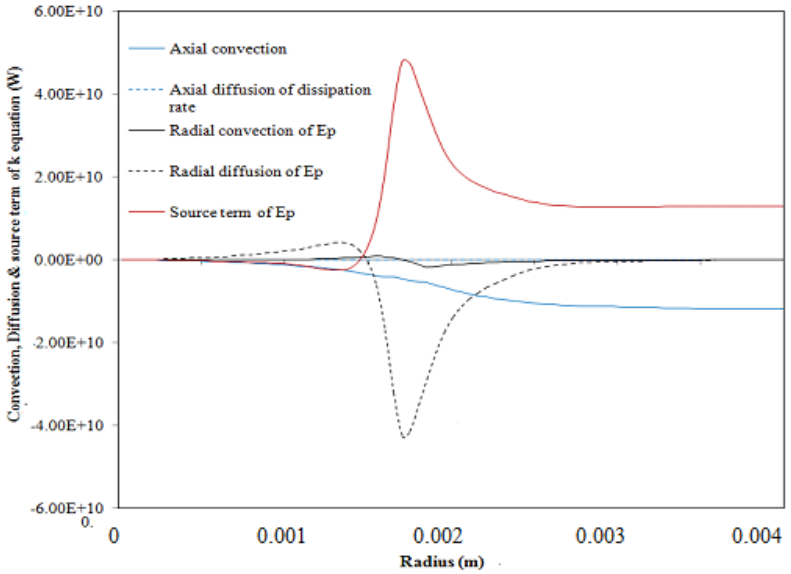

Fig.3.2.16: Dissipation rate balance at the nozzle throat for 600 A case.

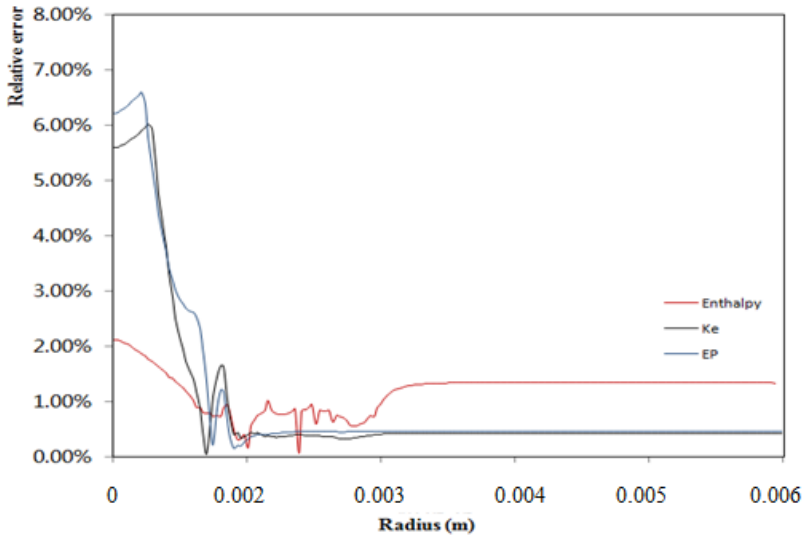

Fig.3.2.17: Relative errors for equations of enthalpy, kinetic energy, and dissipation rate.

Axial conduction of k: $\int \frac{\partial}{\partial z}\left(\frac{\rho \nu_t}{\sigma_k}\frac{\partial k}{\partial z}\right)2\pi r dr$ (3.6c)

Axial conduction of ε: $\int \frac{\partial}{\partial z}\left(\frac{\rho \nu_t}{\sigma_\varepsilon}\frac{\partial \varepsilon}{\partial z}\right)2\pi r dr$ (3.6d)

Radial convection of k: $\int \rho v \frac{\partial k}{\partial r} 2\pi r dr$ (3.6e)

Radial convection of ε: $\int \rho v \frac{\partial \varepsilon}{\partial r} 2\pi r dr$ (3.6f)

Radial conduction of k: $\int \frac{1}{r}\frac{\partial}{\partial r}\left(r\frac{\rho \nu_t}{\sigma_k}\frac{\partial k}{\partial r}\right)2\pi r dr$ (3.6g)

Radial conduction of ε: $\int \frac{1}{r}\frac{\partial}{\partial r}\left(r\frac{\rho \nu_t}{\sigma_\varepsilon}\frac{\partial \varepsilon}{\partial r}\right)2\pi r dr$ (3.6h)

Source term of k: $\int \rho(G-\varepsilon)2\pi r dr$ (3.6i)

Source term of ε: $\int \rho\frac{\varepsilon}{k}(c_{1e}G - c_2\varepsilon)2\pi r dr$ (3.6j)

3.3 Turbulence Model Tested on Campbell Nozzle

3.3.1 Introduction

The modified k-ε turbulence model is then applied a transient nozzle arc case to verify its applicability and accuracy. The nozzle proposed in [90] is completely different compared to the Aachen nozzle [72, 113]. There are two electrodes, both within the nozzle, whose diameters are comparable with that of the nozzle throat. The Body-fitted coordinates are used to match the nozzle and electrode geometry of Campbell et al. [90], as shown as Fig.3.3.1.

Supersonic nozzles are commonly used in modern high voltage circuit breakers. For the nozzle of Campbell et al. [90] used in the present work, the measured critical RRRV are given and could be used to test the modified k-ε model. It is known that the critical rate of rise of recovery voltage (RRRV) is the most important parameter to determine the thermal interruption capability of a circuit breaker.

Arcs burning in a supersonic nozzle with fixed pressure ratios were quite common in the earlier studies [47, 48, and 70]. The arc behaviour was investigated under three inlet stagnation pressures and at different rates of current decay toward zero (di/dt) [47, 48]. The predicted RRRV after current zero decreases with an increase in the magnitude of di/dt and increases with the inlet stagnation pressure. The predicted RRRV for the nozzle of Frind and Rich [115] has been proved the reliability of the experimental results provided that turbulence is introduced for arcs burning in SF_6 [48]. The work in this chapter is to study the behaviour of the modified k-ε model and verify its applicability on the supersonic nozzle of Campbell et al. [90]. A wide range of inlet stagnation pressures and pressure ratios has been used.

3.3.2 Grid system and time steps

A detailed geometry for the nozzle of Campbell et al. [90] is given in Fig.3.3.1 and the grid system is given in Fig.3.3.2. PHOENICS (version 3.6.1), is used to solve the governing equations. The nozzle is 35 mm long with a downstream half divergence angle of 9 degrees. The throat has a diameter of 11.3 mm and is 20 mm away from the nozzle inlet. The upstream electrode is 15 mm long with a diameter of 10 mm and the downstream one is 5 mm long with a diameter of 6 mm. The diameter of the tip is 5 mm for the upstream electrode and 4 mm for the downstream one. The time step used for the computation before current zero is 0.2 μs and 0.01 μs after current zero after a simple test of sensitivity study.

Altogether, 102 cells in the radial direction and 174 cells in the axial direction are used to obtain the results. The minimum value of 0.02 mm and 0.2 mm are used as the radial and axial grid cell size respectively. Efficient computation requires the use of adaptive grids that catch the rapid collapse of the arc toward current zero. A sensitivity study has been carried out, it will be discussed in section 3.3.3.2. However, within PHOENICS, the distribution of grids is not adaptable. Thus, the grid system should ensure that sufficient number of grids in the radial direction is used to compute the temperature profile at current zero.

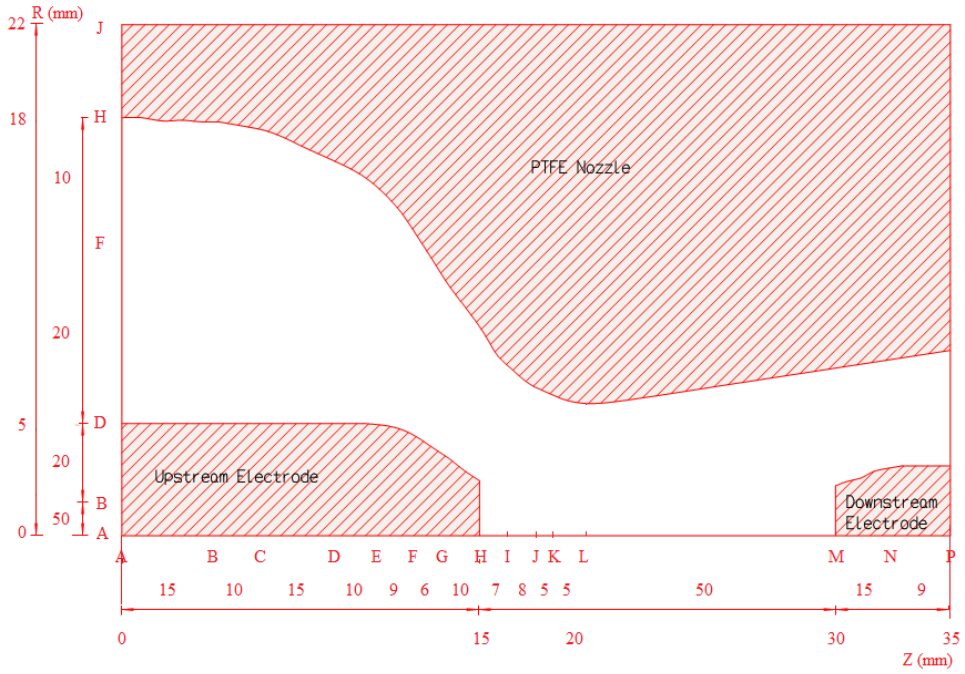

Fig.3.3.1: Nozzle geometry of Campbell nozzle. The number of cells in various regions is also shown.

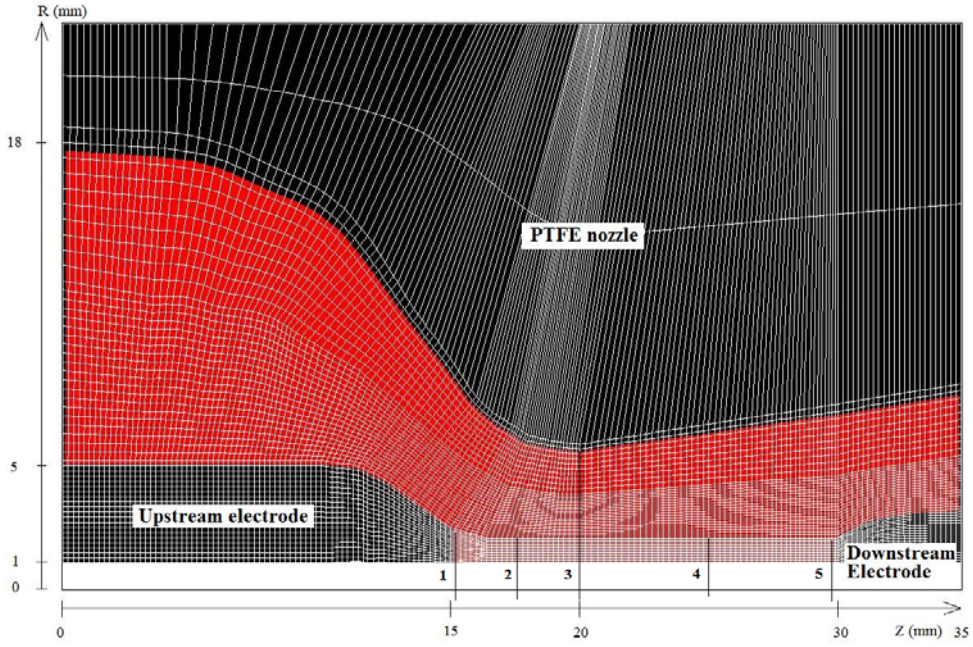

Fig.3.3.2: The grid system of Campbell nozzle and 5 specific slabs are shown.

3.3.3 Results and discussion

Overall 15 cases, which correspond to the experimental cases of Campbell et al. [90], have been computed at three inlet stagnation pressures (3.4, 5.1 and 7.14 bar) and with 5 pressure ratios of 0.1, 0.12, 0.2, 0.33 and 0.5. Detailed information can be found in Table 3.3.1. Case 3 has been chosen as the Ref. Case in the analysis.

The working gas is SF_6. The Prandtl mixing length model was compared with the standard k-ε model and the modified k-ε model. The turbulence parameter for the Prandtl mixing length model is determined by previous research [110]. The value of c = 0.195 is used for all cases with the Prandtl mixing length model.

The analysis is performed in four separated steps. The Case 1 for cold flow is first calculated to obtain the initial flow field for arc simulation. Then the steady state arc of 200 A dc is calculated, e.g. the temperature distribution of the Ref. Case is shown in Fig.3.3.3. A total of 80,000 iterations are used to ensure the convergence of the computation. The third step is to simulate the a.c. arc. A sinusoidal current with a peak of 1.7 kA at 1000Hz was used by Campbell et al. [90]. Initial arc conditions need to be chosen in such a way that the arc at current zero should not depend on the chosen initial conditions. A 200 A dc arc has been found to be satisfactory. The computation follows a sinusoidal waveform with a starting current of 200A as shown in Fig.3.3.4. The rate of change of current di/dt, immediately before the final current zero point, which is a very important parameter influencing the critical RRRV, This has been calculated by Eq.3.7.

Inlet Stag Pressure	7.14 bar	5.1 bar	3.4 bar
Pressure Ratio	Case 1 : 0.1	Case 6 : 0.1	Case 11 : 0.1
	Case 2 : 0.12	Case 7 : 0.12	Case 12 : 0.12
	Case 3 : 0.2	Case 8 : 0.2	Case 13 : 0.2
	Case 4 : 0.33	Case 9 : 0.33	Case 14 : 0.33
	Case 5 : 0.5	Case 10. : 0.5	Case 15 : 0.5

Table 3.3.1: Cases with different pressure ratios and various inlet stagnation pressures.

$$\frac{di}{dt} = -I_{\max}\omega\cos(\omega t + \phi) \tag{3.7}$$

where I_{max} = 1.7 kA, ω = 2π f =6280 and ωt+ϕ=π/2, so di/dt = 10.68 A/μs.

Time steps used for current zero phase is 1.5 μs for each step. In the last 60 μs, a much smaller time step should be set as 0.2 μs due to the coding requires.

The final step is to calculate the post arc current under different RRRV values in order to determine the critical RRRV. The experimental results of critical RRRV were cited in Fang et al.'s paper [110].

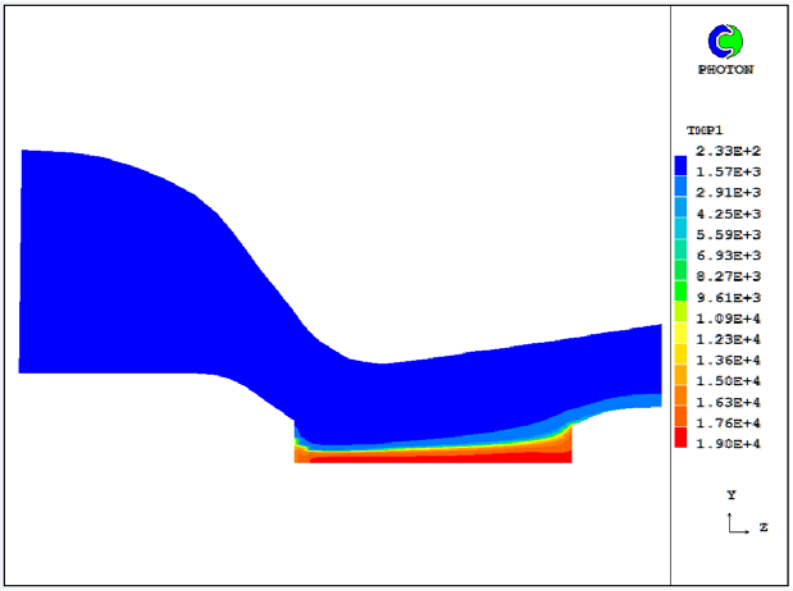

Fig.3.3.3: Temperature distribution of 200 A DC arc in the Ref. Case.

3.3.3.1 Boundary conditions

The boundary conditions for the solution of the governing equations are axisymmetric on the axis. The solid part includes the nozzle and electrodes are thermally insulating, i.e. no heat flux. The boundary conditions for arc at the two electrodes are normally not known, as the equations based on LTE are no longer valid for the region close to the electrode, whose scale is determined by the Debye length.

The effect of the inlet boundary conditions on the arc solution are confined in a small region close to the upstream electrode. The arc voltage is hardly affected by using different upstream boundary conditions as pointed out by Zhang et al. [49].

The temperature boundary conditions at the downstream electrode have little influence on the results for two reasons. One is that convective effect is dominant and secondly, that the influence is again confined within a small region. Energy loss by thermal conduction into the nozzle wall is negligible in the present investigation, since there is a low temperature layer separating the arc from the wall. Ablation of the PTFE nozzle by arc radiation [116] is unlikely to occur because of a very short arc duration.

The boundary conditions at the nozzle entrance are derived from the inlet stagnation pressure and temperature through isentropic relationships. Pressure at the nozzle exit is varied to give a prescribed pressure ratio (P_d/P_u, where P_u is the inlet stagnation pressure and P_d is the exit static pressure) up to 0.5 for three inlet stagnation pressures.

Diffusion of momentum and energy at the exit is small in comparison with convection and is neglected due to the high value of Peclet number at the nozzle exit.

3.3.3.2 Current Zero Phase

The standard k-ε model is initially used for the cases in previous sections. However, the results show that the predicted radial temperature at the nozzle throat does not match well with the experiment. It can be considered that the turbulence is not strong enough at the arc edge, especially at low current or at the final current zero. This situation also occurs for this nozzle arc. The modified k-ε model was applied to the transient nozzle arc. The predicted results are shown in the following sections.

The temperature distributions of the Ref. Case with the standard and modified k-ε model are given in Figs.3.3.6-3.3.9. Five slabs are specified to analyse the results, which can be found in Fig.3.3.2. The upstream electrode tip is labelled by slab 1. The nozzle throat is represented by slab 3. The middle point of slab 1 and 3 is slab 2. The downstream electrode tip is labelled by slab 5, the slab 4 is between the slab 3 and 5. The radial temperature profiles at the different slabs are recorded in Figs.3.3.11-3.3.12 with current peak point and final current zero point.

The results shown in Fig.3.3.11 establishes that the radial temperature profiles predicted by the two models do not differ much at these different axial positions. Temperature distributions for the period of around the current peak point have also been checked by PHOTON. The difference between the two models are small and can be neglected. It can also be considered that turbulence will not affect the arc in high current phase (around 1.5 kA) too much. The results shown in Fig.3.3.12 establishes the radial temperature profile at the final current zero point, it can be seen that there is significant difference in the temperature predicted by the two k-ε models. The temperature at the arc centre is lower with the modified k-ε model. It is also can be found from

Figs.3.3.13 to 3.3.14, the turbulent kinetic viscosity demonstrates that the turbulence predicted by the modified k-ε model is larger than the prediction by standard k-ε model. Thus, the temperature at the arc centre with the modified k-ε model is lower than the one with the standard k-ε model. It can be seen from Fig.3.3.5 that the arc voltage, before the final current zero, is much higher using the modified k-ε model when compared to the one using the standard k-ε model. The arc voltage increases rapidly from the 0.45 ms, because a very small time step is used for the last 50 μs, and the extinction peak of these cases is very high, so all arc voltage are increased from this point. The temperature distribution on the axis is also given in Fig.3.3.15, the temperature on the axis with modified k-ε model is lower than the standard k-ε model which can be proved by the viscosity on the axis as shown in Fig.3.3.16.

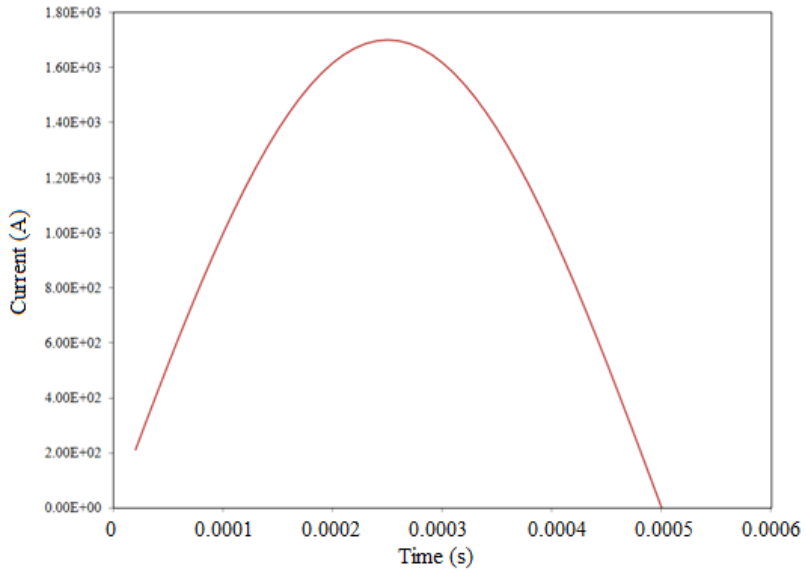

Fig.3.3.4: Current wave (in simulation) of Campbell nozzle [90] from 200A to final current zero.

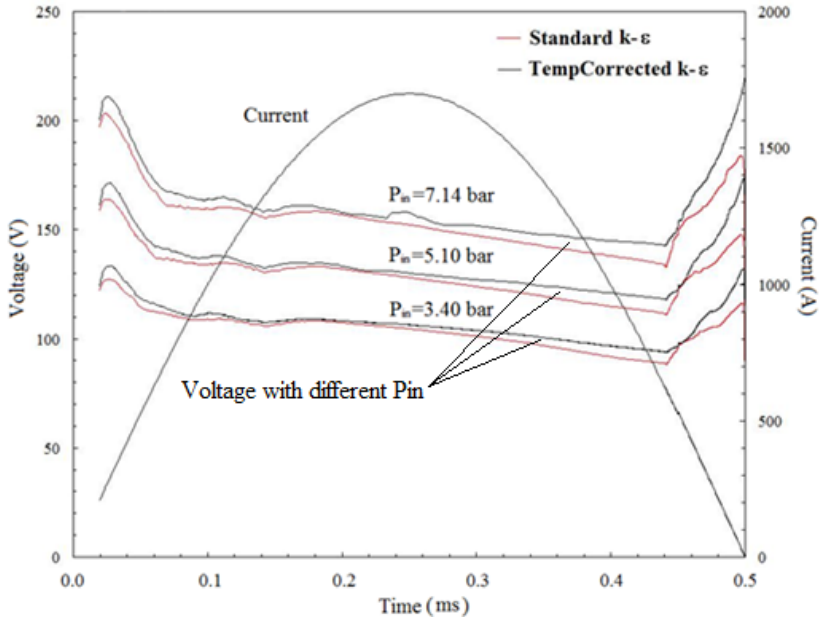

Fig3.3.5: Predicted arc voltage for the whole arcing period at three different inlet stagnation pressures by using different k-ε turbulence model. Pressure ratio is 0.1 for all cases.

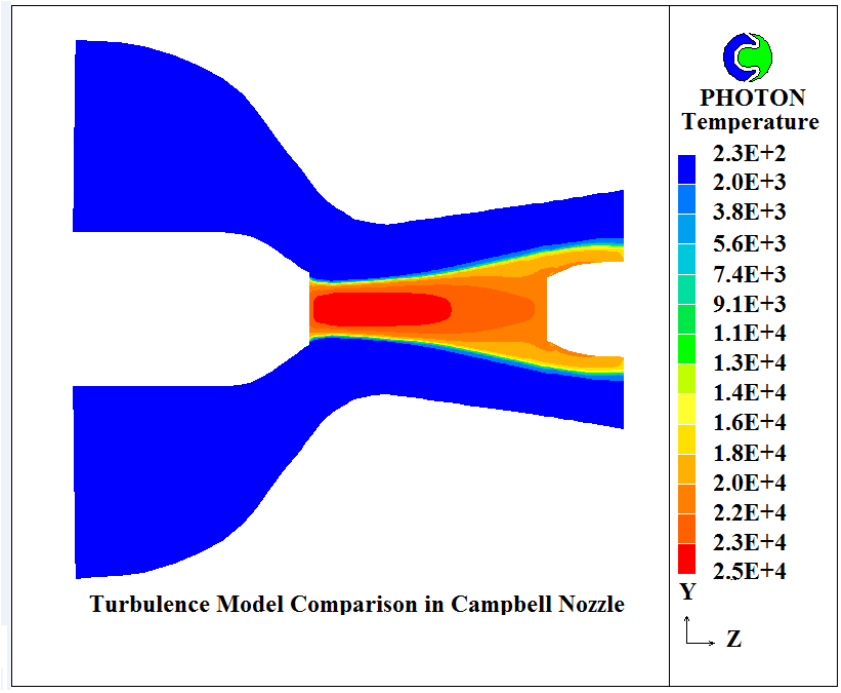

Fig.3.3.6: Arc column at 1.7 kA (current peak) of Ref. Case with Standard k-ε model.

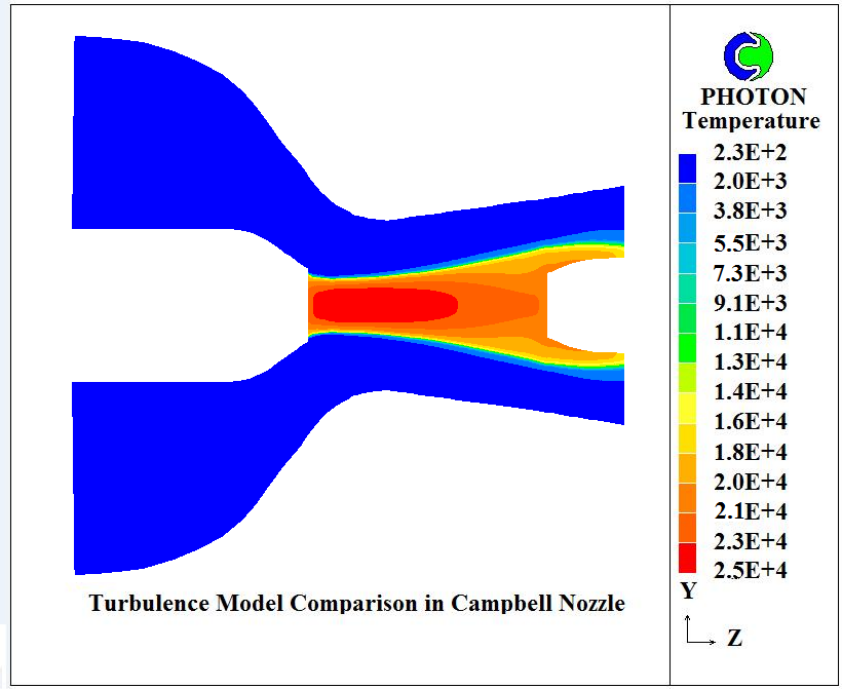

Fig3.3.7: Arc column at 1.7 kA (current peak) of Ref. Case with modified k-ε model.

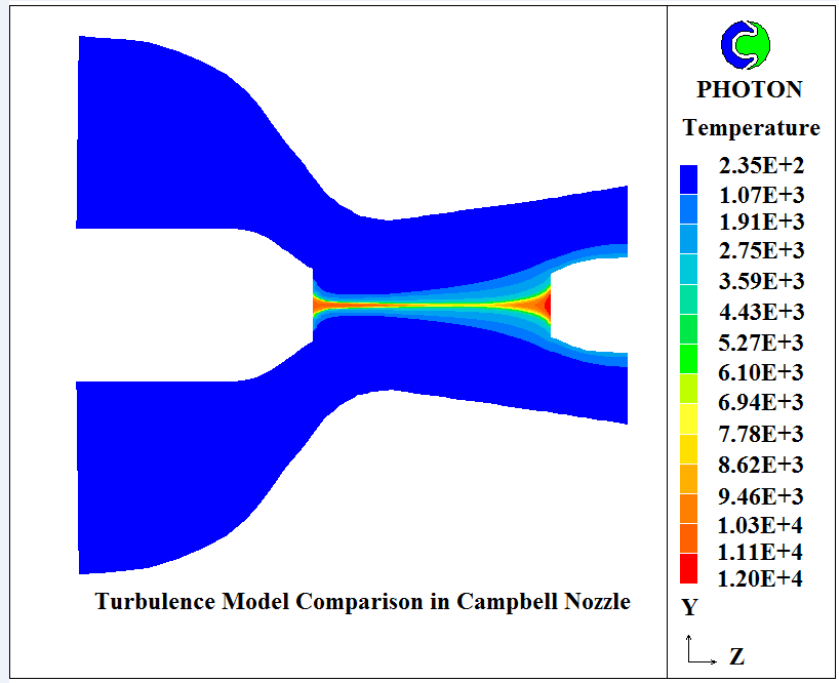

Fig3.3.8: Arc column at final current zero of Ref. Case with Standard k-ε model.

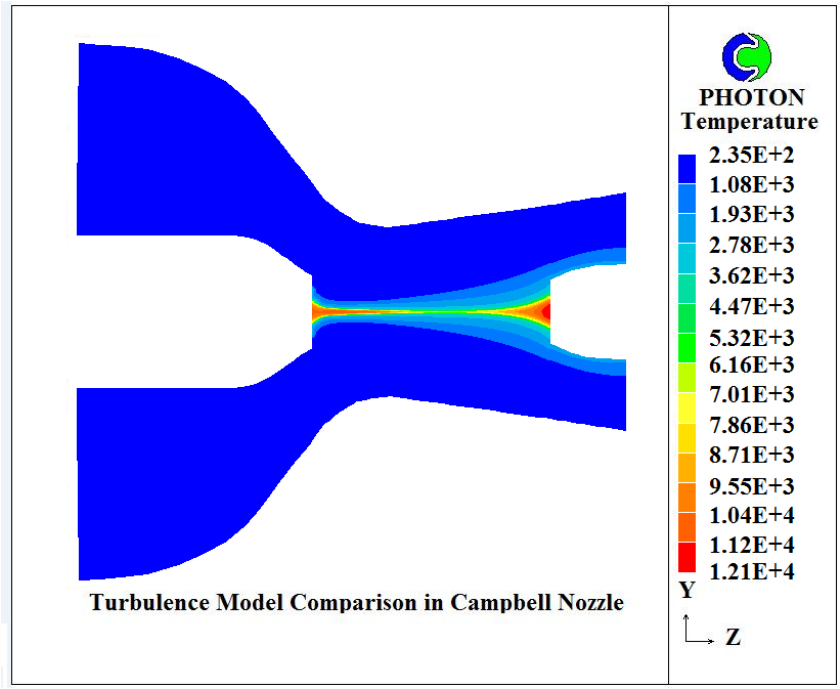

Fig3.3.9: Arc column at final current zero of Ref. Case with modified k-ε model.

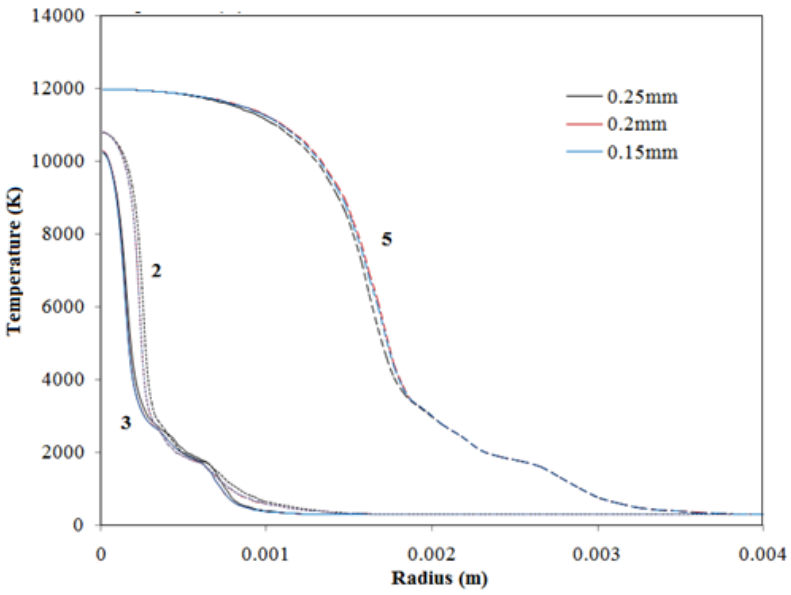

Fig.3.3.10: Radial temperature of Ref. Case near the current zero at three different slabs with different widths of cells in arc column region.

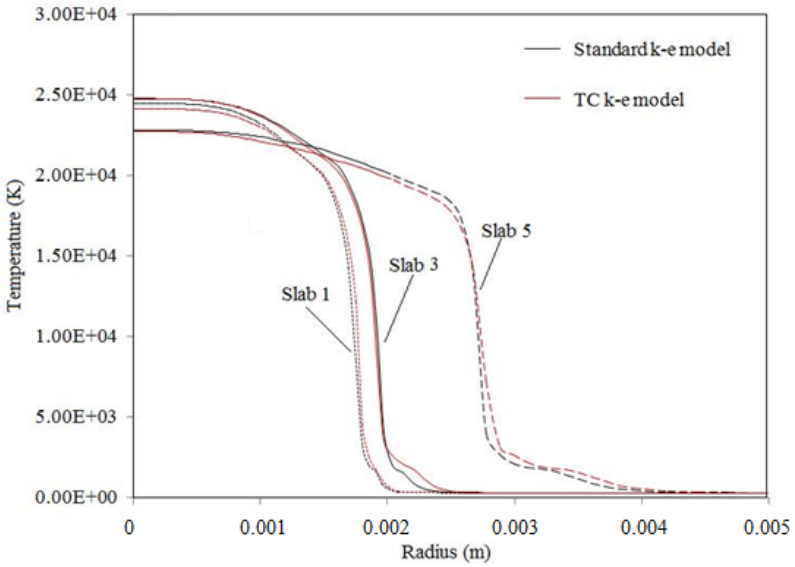

Fig3.3.11: Radial temperature of Ref. Case at three slabs in current peak with standard k-ε model and modified k-ε model.

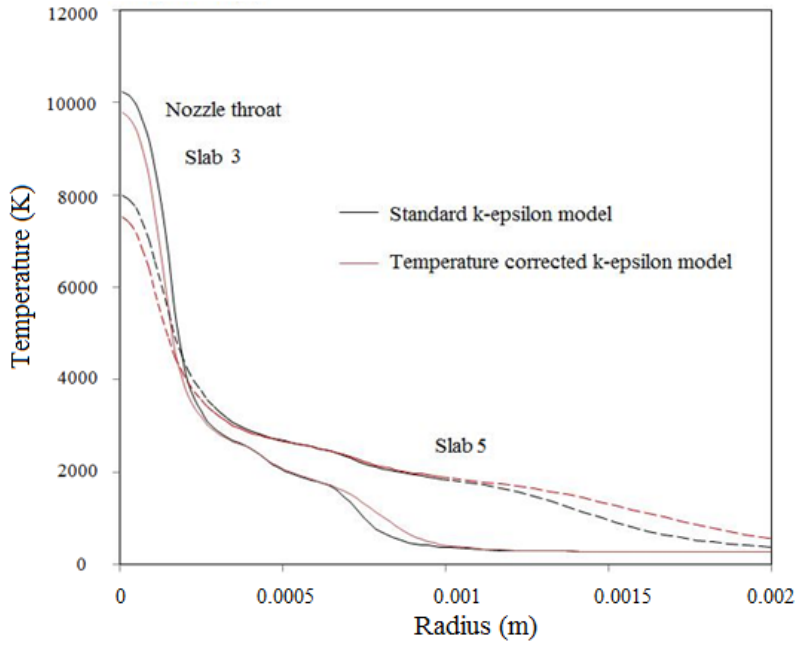

Fig3.3.12: Radial temperature of Ref. Case at two slabs in final current zero with standard k-ε model and modified k-ε model.

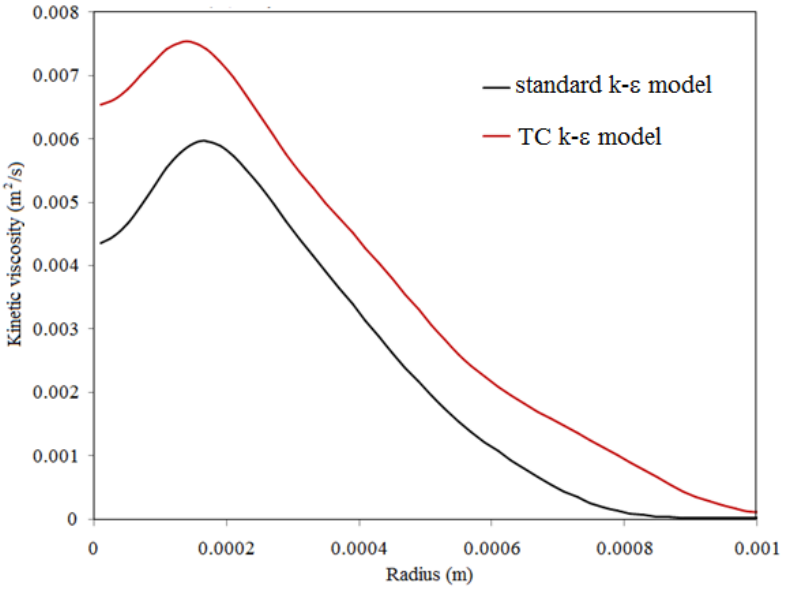

Fig3.3.13: Radial turbulent kinetic viscosity of Ref. Case at the nozzle throat with two k-ε models.

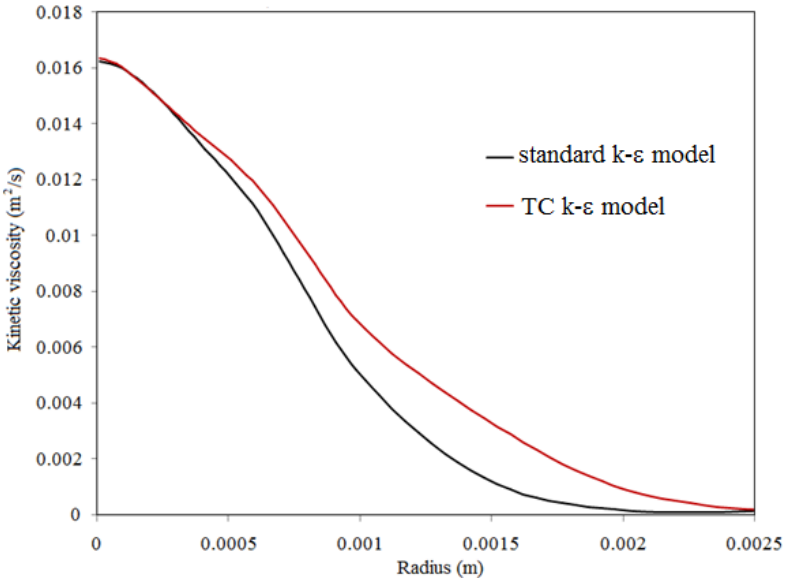

Fig3.3.14: Radial turbulent kinetic viscosity of Ref. Case at the slab 4 with two k-ε models.

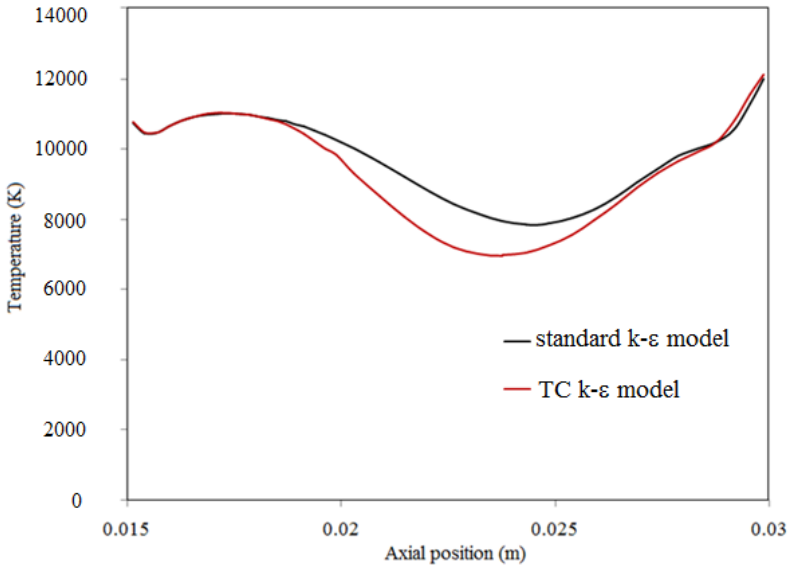

Fig3.3.15: Axial Temperature of Ref. Case on axis with two k-ε models.

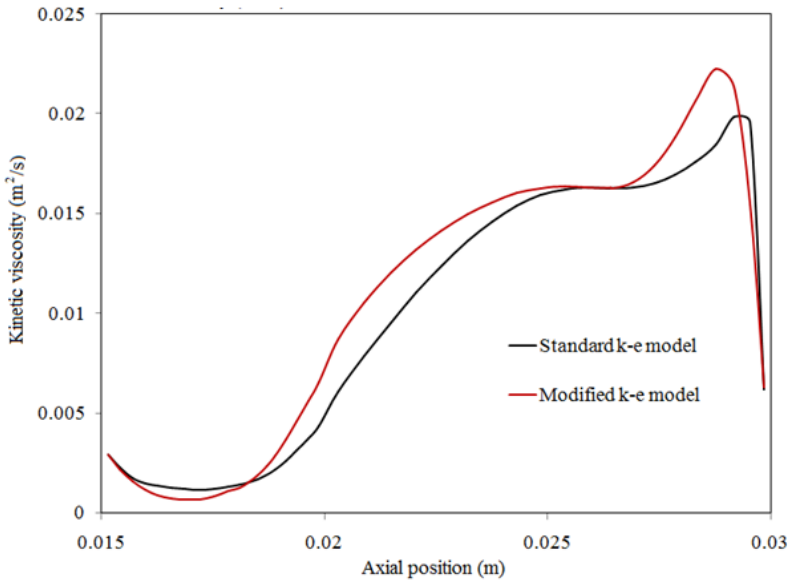

Fig3.3.16: Axial kinetic viscosity of Ref. Case on axis with two k-ε models.

3.3.3.3 Post Arc Current Phase

The thermal interruption capability of a circuit breaker is usually expressed as the critical RRRV. The critical RRRV of the nozzle arc is determined by applying a linearly increasing recovery voltage after current zero.

The rate of rise of the recovery voltage (dv/dt) is increased in small steps until it reaches a value at which the discharge current starts to increase exponentially shortly after current zero, as shown in Figs.3.3.17 to 3.3.20. The pressures of upstream are 5.10 bar (Case 8) and 7.14 bar (Ref. Case) with the pressure ratio of 0.2.

The critical RRRV is defined as the value of dv/dt, above which the arc will reignite. The numerical uncertainty in determining the critical RRRV is less than 5% of its value.

Typical post-arc currents from the two k-ε models are given, respectively, in Figs.3.3.17-3.3.18 for an inlet stagnation pressure of 5.10 bar with the pressure ratio of 0.2. The measured critical RRRV of this case is 2.8 kV/μs (Fig3.3.30), but the prediction from the standard k-ε model is almost 70% lower, same as the cases with an upstream pressure of 7.14 bar (Fig.3.3.29).

The axial temperature distributions predicted by the standard k-ε model and modified k-ε model at different times after current zero are respectively shown in Figs.3.3.21 and 3.3.25, the arc column is rapidly cooled and the current interruption take place successfully, especially in the region of nozzle throat. Figs.3.3.23 and 3.3.27 show the axial temperature distribution by these two k-ε turbulence models when the current interruption fails if the thermally re-ignited. If the rising rate of the recovery voltage dv/dt is higher than the critical RRRV, the temperature at the throat increases rapidly, and then a very high current flows again between the two electrodes. It is thermal failure.

The axial electrical fields are shown in Figs.3.3.22 and 3.3.26 for the Ref. Case. The maximum value appears at the nozzle throat since conductivity decreases due to very strong cooling at this position. When the arc is thermal extinguished, the axis temperature decays rapidly in the first microsecond (eg., dv/dt = 1.4 kV/μs in Fig.3.3.22). When the arc plasma reignites under a higher dv/dt of 1.6 kV/μs, the corresponding electric field distribution is given in Fig.3.3.24. For the case using modified k-ε model, when the dv/dt reaches 3.4 kV/μs, the arc is reignited (Fig.3.3.28).

The computed critical RRRV for the 15 cases in Table 3.3.1 are shown in Figs.3.3.29 to 3.3.31. The measured results are also given in these figures. The predicted results by using the standard k-ε model are lower than the measurements by almost 70% for high pressure ratio cases and more than 50% for other cases. The prediction results using the modified k-ε model produces higher critical RRRV for all the cases. It can be found that the predictions for the pressure ratio of 0.2 to 0.33 match with the measurement very well.

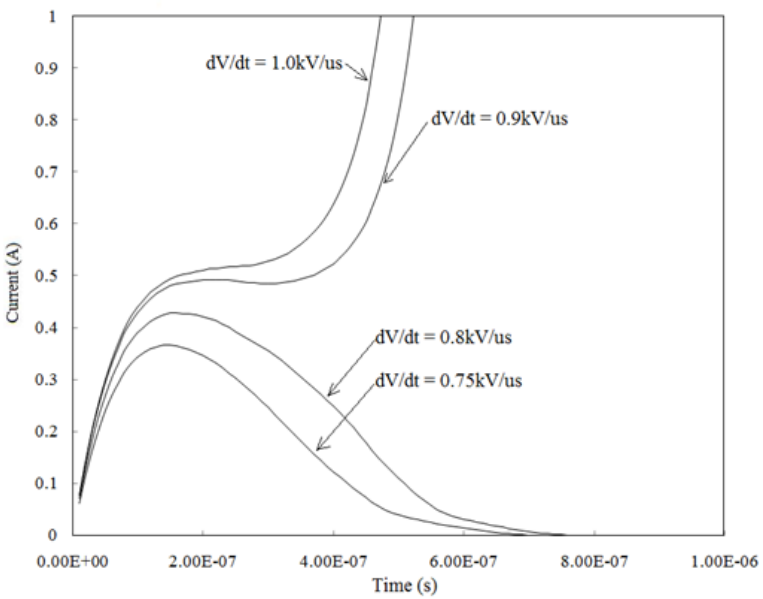

Fig.3.3.17: Post-zero current of Case 8 for different values of dv/dt with standard k-ε model.

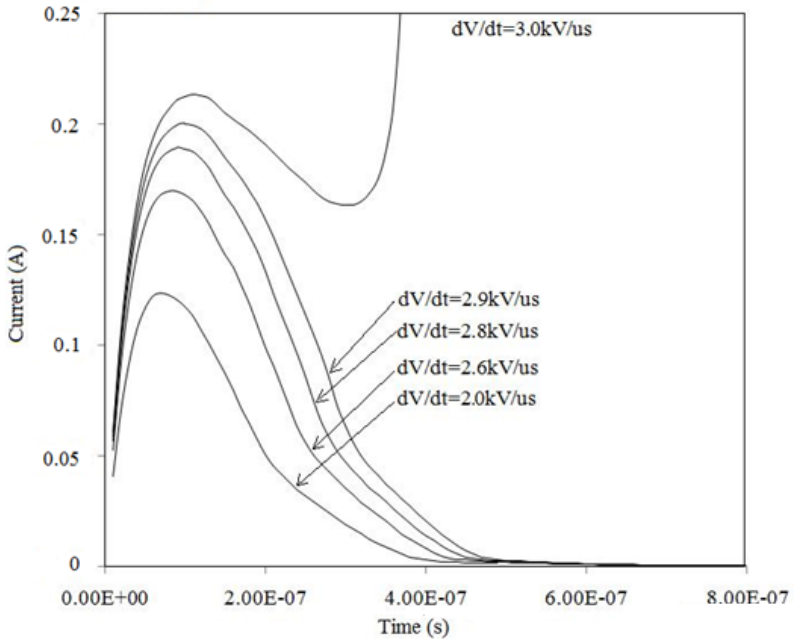

Fig3.3.18: Post-zero current of Case 8 for different values of dv/dt with modified k-ε model.

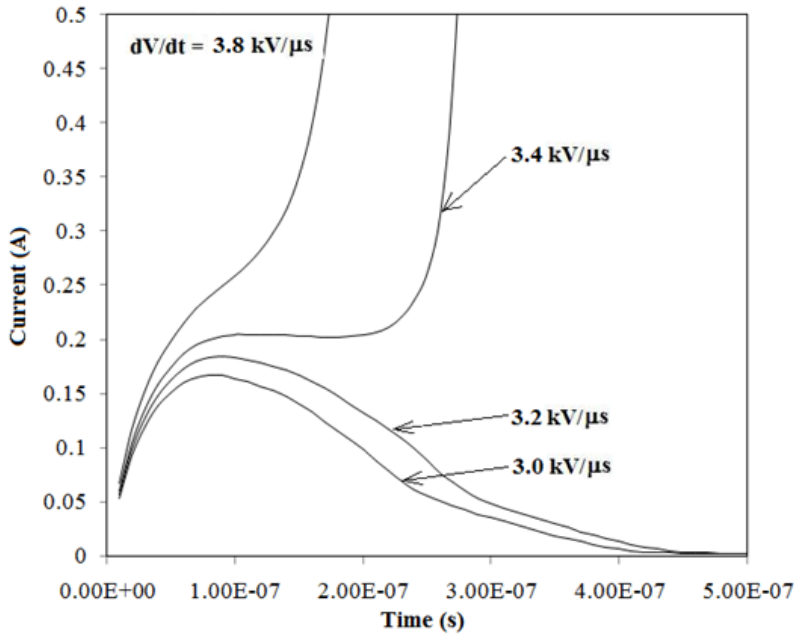

Fig3.3.19: Post-arc current of Ref. Case for different values of dv/dt with modified k-ε model.

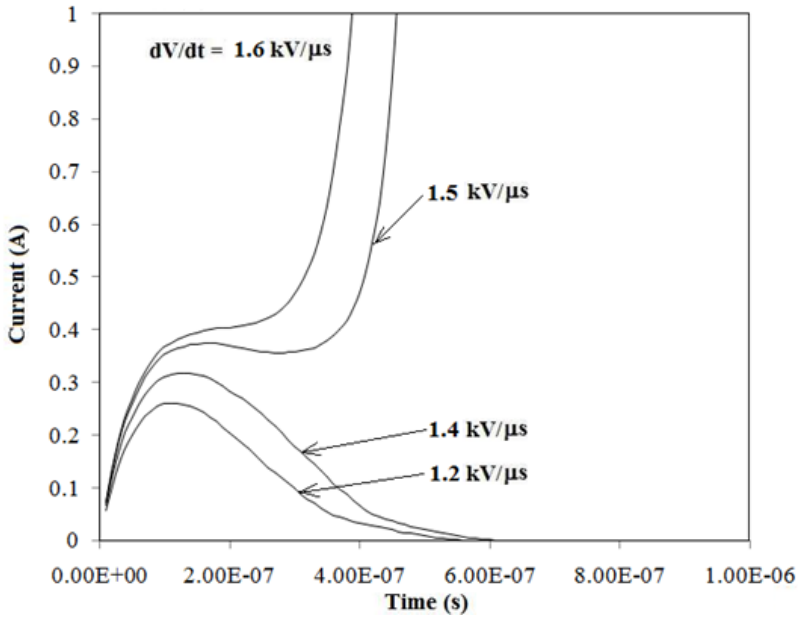

Fig3.3.20: Post-arc current of Ref. Case for different values of dv/dt with standard k-ε model.

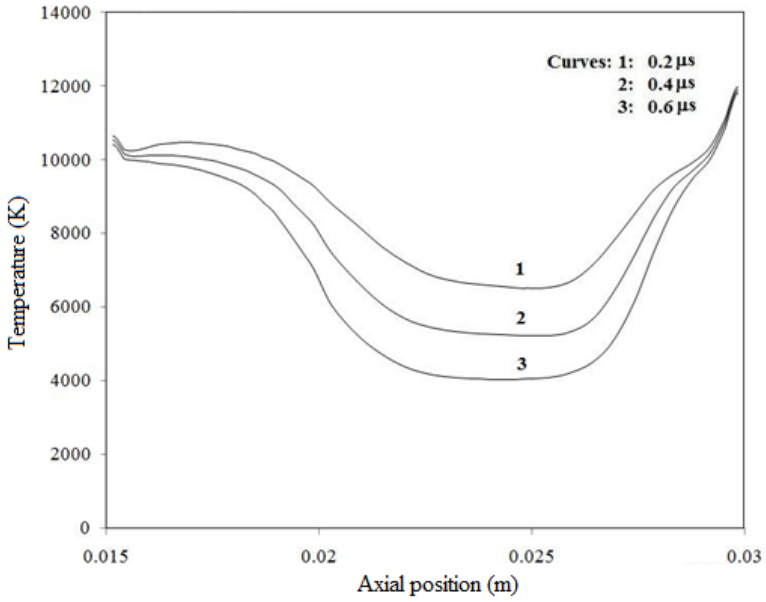

Fig3.3.21: Axial Temperature distribution at various times (dvdt=1.4kV/µs) of Ref. Case with Standard k-ε model.

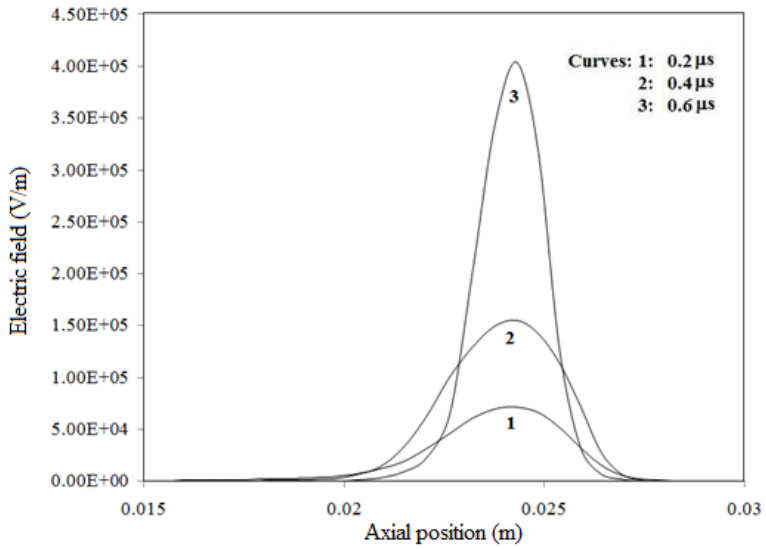

Fig3.3.22: Electrical field distribution at various times (dv/dt=1.4kV/µs) of Ref. Case with Standard k-ε model.

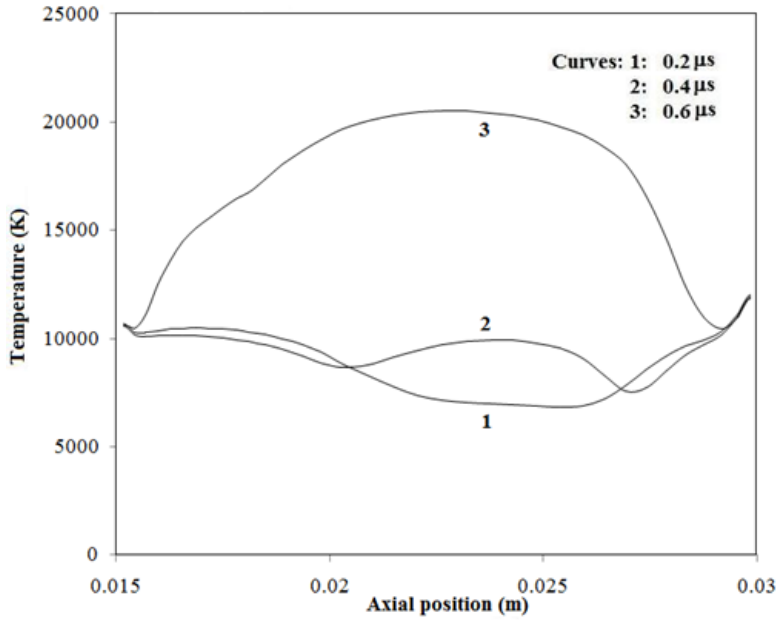

Fig3.3.23: Axial Temperature distribution at various times (dvdt=1.6kV/µs) of Ref. Case with Standard k-ε model.

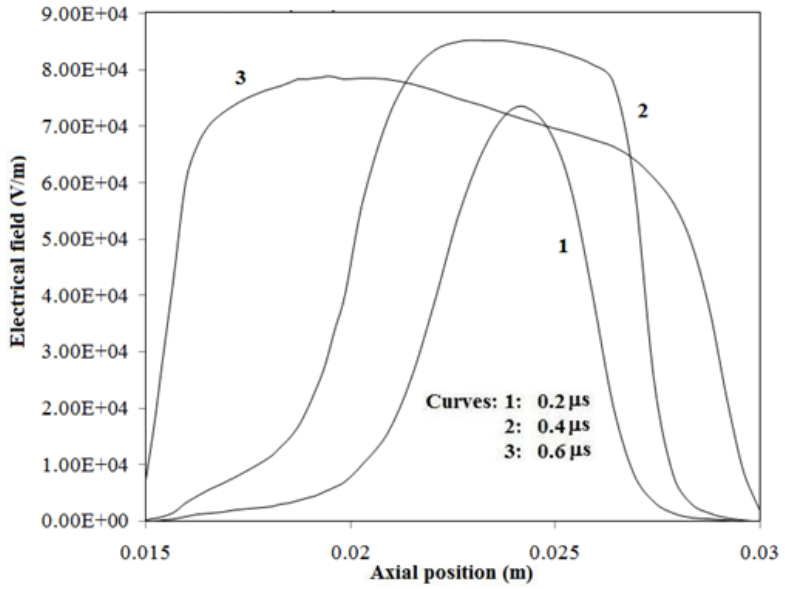

Fig3.3.24: Electrical field distribution at various times (dvdt=1.6kV/µs) of Ref. Case with Standard k-ε model.

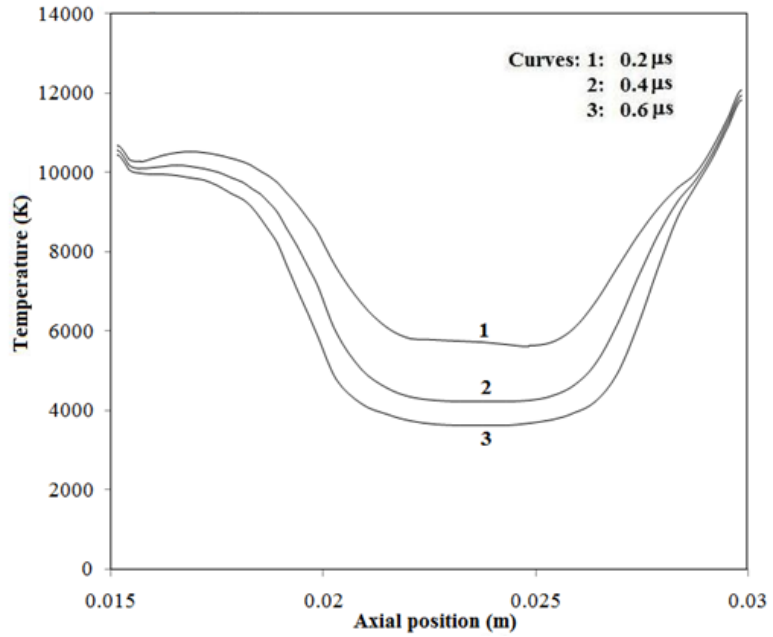

Fig3.3.25: Axial Temperature distribution at various times (dvdt=3.2 kV/µs) of Ref. Case with modified k-ε model.

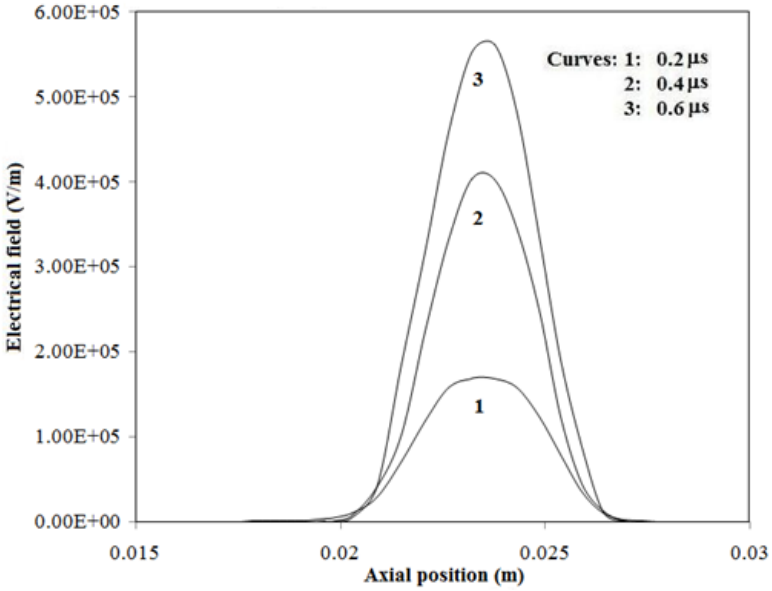

Fig3.3.26: Electrical field distribution at various times (dvdt=3.2 kV/µs) of Ref. Case with modified k-ε model.

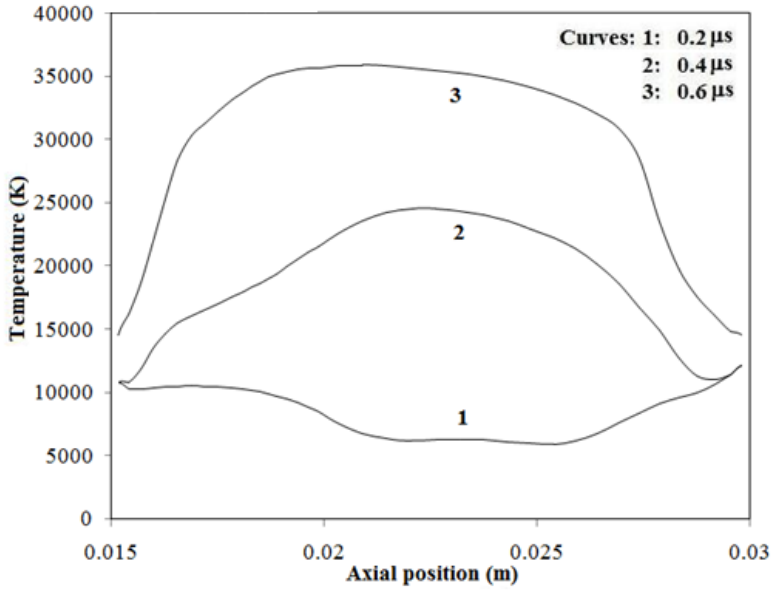

Fig3.3.27: Axial Temperature distribution at various times (dvdt=3.4 kV/µs) of Ref. Case with modified k-ε model.

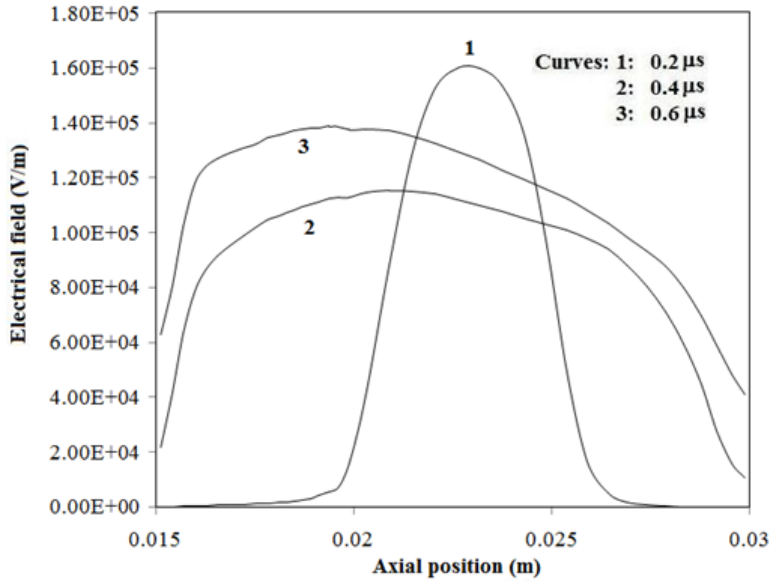

Fig3.3.28: Electrical field distribution at various times (dvdt=3.4 kV/μs) of Ref. Case with modified k-ε model.

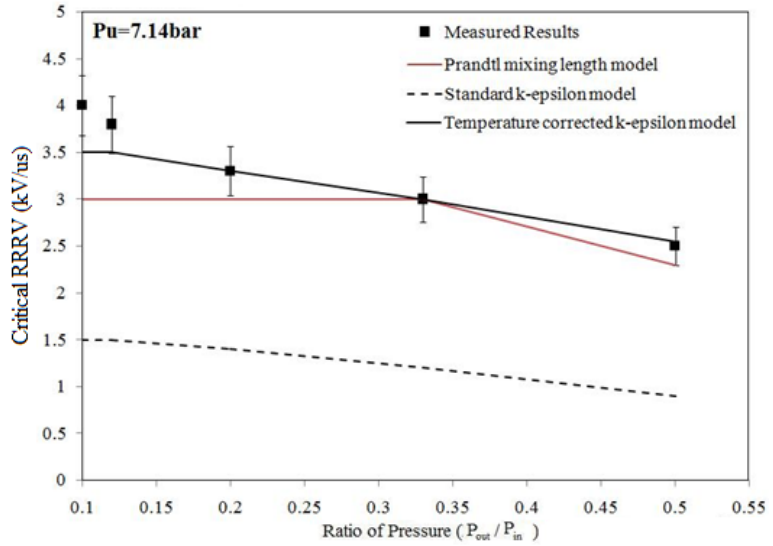

Fig.3.3.29: RRRV as a function of the pressure ratio with inlet stagnation pressure of 7.14bar.

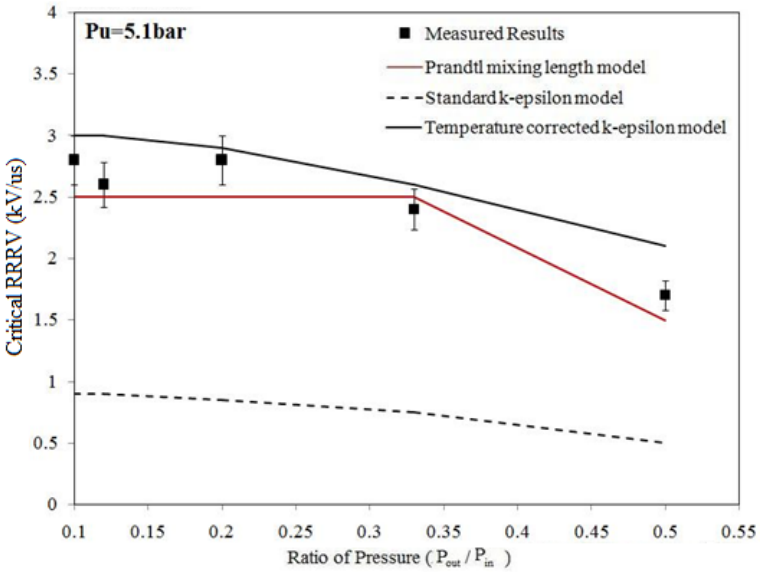

Fig.3.3.30: RRRV as a function of the pressure ratio with inlet stagnation pressure of 5.10bar.

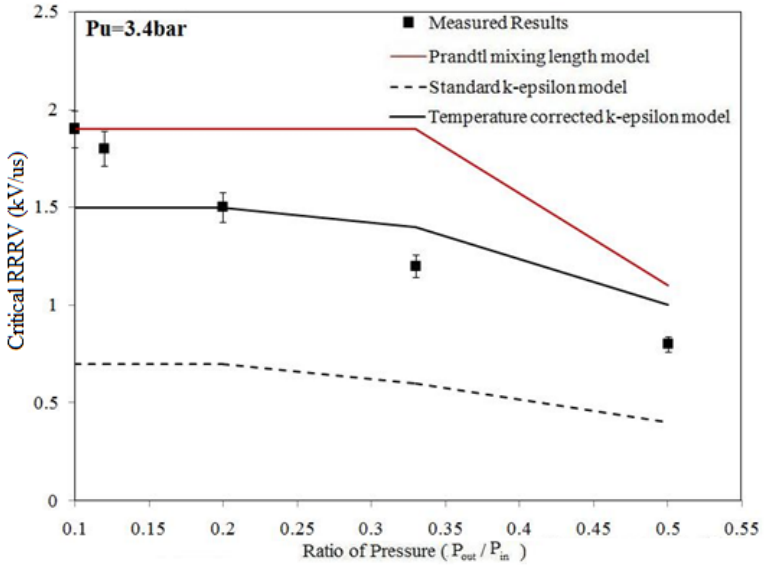

Fig.3.3.31: RRRV as a function of the pressure ratio with inlet stagnation pressure of 3.40bar.

3.4 The Application of the Modified k-ε Model to GE Nozzle

3.4.1 Introduction

The modified k-ε model is then applied to calculate another transient case of nozzle arcs provided by General Electric corporate research and development, so it is called as GE nozzle in this section. This type of nozzle is different when compared with the Aachen nozzle [72, 113] and Campbell nozzle [90] as described in previous sections. There is a long hollow contact at the downstream. This type of nozzle is commonly used in puffer circuit breaker. The BFC are used to match the nozzle and electrode geometry of Frind et al. [91], as shown as Fig.3.4.1. The grid system with the whole computational domain is given in Fig.3.4.2. A transient nozzle arc experimented by Campbell et al. [91] has been studied in section 3.3. The modified k-ε model with the coefficient in the temperature correction term set to 0.5 is able to predict the critical RRRV accurately. The measurements of critical RRRV for the GE nozzle were given in a final report [91]. Thus, the measured critical RRRV will be used to verify the applicability of the modified k-ε model for different nozzle shapes.

Two typical nozzle types are used with different nozzle throat diameters. The two nozzles have identical half diverging angle of 15 degrees, which are shown in Fig.3.4.1(a) and (b). For these two nozzle profiles, several upstream pressures are used. The unit of PSIG (pound per square inch, gauge) and inch were used in the original report [91]. For easy interpretation in this thesis all these units have been converted into standard units. Five upstream pressures were used in [91] which are 100, 150, 200, 250 and 300 PSIG corresponding to standard units of 7.8, 11.2, 14.6, 18.0 and 21.4 bar.

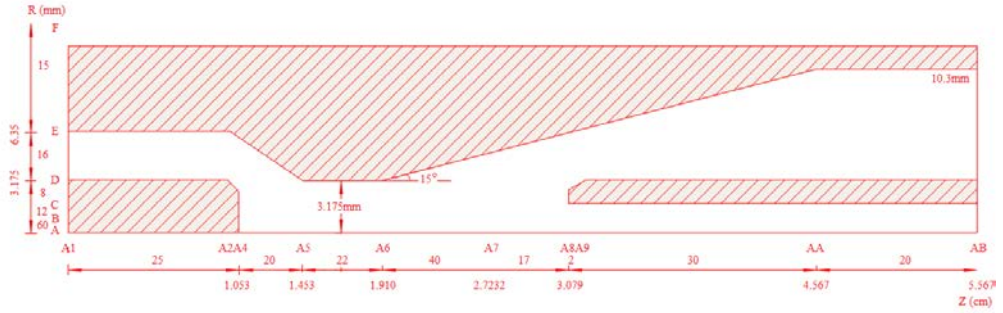

(a)

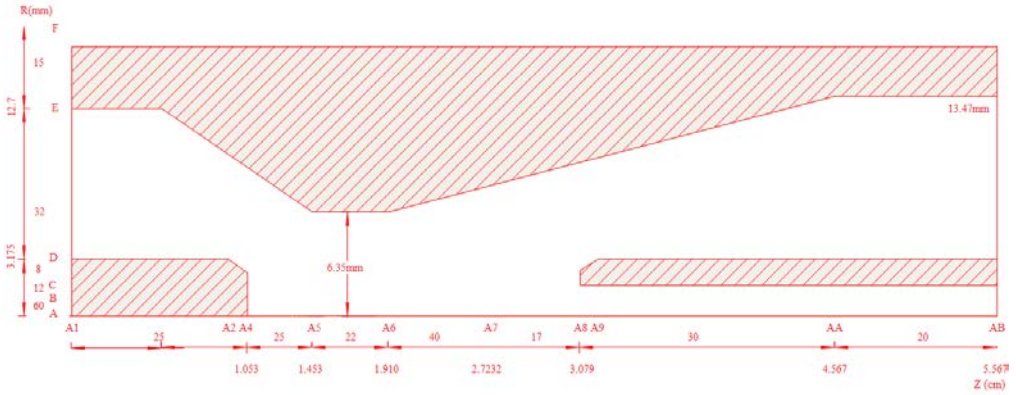

(b)

Fig.3.4.1: Nozzle geometry of GE (a) nozzle 1and (b) 2 with nozzle throat diameter 0.25 inch (6.35 mm) and 0.50 inch (12.7 mm). The number of cells in various regions is also shown.

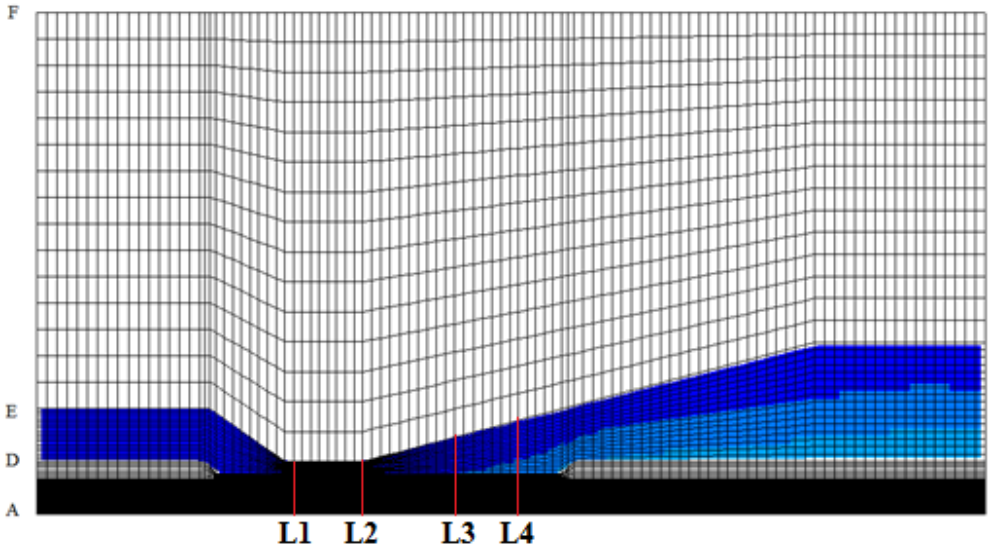

Fig.3.4.2: Whole computational domain and the grid system of GE nozzle 1 with 5 specified slabs for analysis.

3.4.2 Grid system and time steps

The computational domain with detailed information on the grid system for the nozzle with 6.35 mm (0.25 inch) throat diameter is shown in Fig.3.4.2. The Ref. Case nozzle (Nozzle 1 with throat diameter of 6.35 mm) is detailed in the Fig.3.4.1. The nozzle is 5.567 cm long with a downstream divergence angle of 15 degrees. The downstream section of the reference nozzle is longer than the Campbell nozzle. The length from nozzle throat to the outlet is about 3.657 cm. The nozzle throat has a diameter of 6.35 mm and is 14.53 mm away from the nozzle inlet. The upstream electrode is 10.53 mm long with a diameter of 6.35 mm. A transparent contact is used for downstream electrode and its length is 25.0 mm.

The simulation is divided by four steps under PHOENICS package. The period of current zero phase is the most important part in calculation. The time step used for the computation before current zero is 0.05 μs from 4 ms to its final current zero (Fig.3.4.3). There are 600 sweeps are used for each time step before current zero ensuring the convergence of the solution process, and the time step used for the post arc current phase is 0.01 μs.

The BFC grid system is used. The BFC grid system is particularly suitable for flows with smoothly varying irregular boundaries. A grid sensitivity study has confirmed that the fine grid size of 0.03 mm is sufficient for the radial direction. A minimum value of 0.2 mm is used as the axial grid cell size.

3.4.3 Results and discussion

The analysis is performed in several steps depending on the current wave used in the experiments. Two levels of di/dt are used for the GE nozzle 1 case. The current waves are detailed in Fig.3.4.4. For the modelling of GE nozzle arc [91], five steps are needed.

Step One: Initial conditions of pressure and velocity for the cold flow are calculated by MATLAB.

Step Two: Cold flow phase simulation to obtain the initial conditions for arc modelling.

Step Three: The steady state arc, a 1000 A DC steady state arc is reached. A total number of 50,000 sweeps are used to ensure the convergence of the computation, the temperature distribution of 1,000 A is given in Fig.3.4.3.

Step Four: Current zero phase, a period for modelling the arc behaviour before the current zero, from 1000A to the final current zero. The initial conditions are from Step Three. The duration of the arc modelling with standard k-ε model and modified k-ε model requires a computation time of twenty and thirty hours respectively on a PC with i7 CPU processor.

Step Five: Period after current zero, the critical RRRV is determined by calculating the post arc current under different RRRVs.

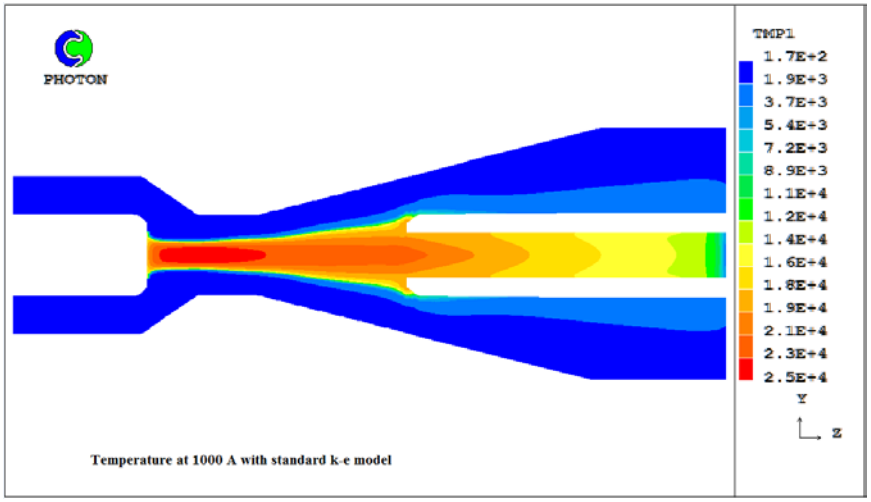

Fig.3.4.3: Temperature distribution at 1000 A as initial state of current zero phase.

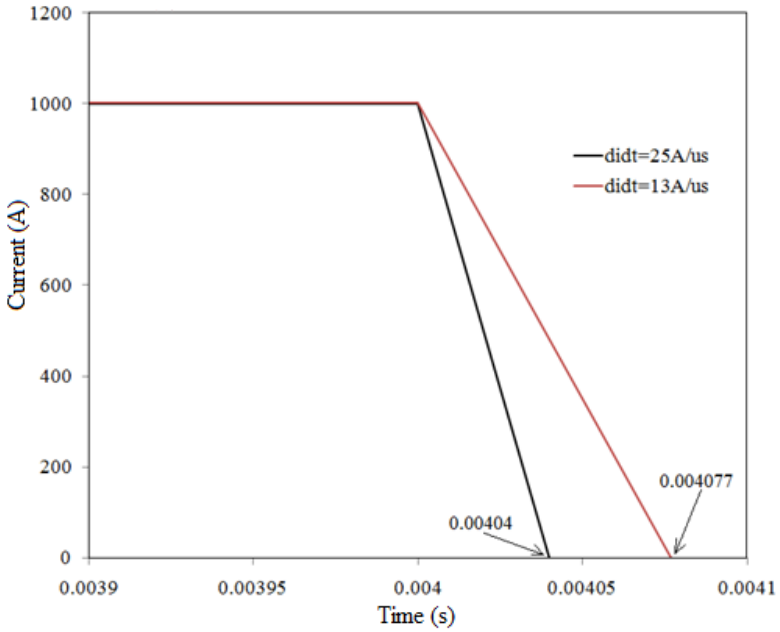

Fig.3.4.4: Current waves with various di/dt.

3.4.3.1 Current zero phase

As mentioned before, two levels of di/dt are applied to test the modified k-ε model. Overall ten cases, which are obtained from the measured results of the GE report [91], have been computed at two levels of di/dt (25 A/μs and 13 A/μs) with two different nozzle throat diameters (as shown in Fig.3.4.1(a) and (b)) in various upstream pressures (100, 150, 200, 250 and 300 PSIG corresponding to standard units of 7.8, 11.2, 14.6, 18.0 and 21.4 bars). Detailed information for all of the cases is given in Table 3.4.1.

di/dt (A/μs)	GE nozzle 1	GE nozzle 2
25	Case 1: 100 PSIG (7.8 bar)	
25	Case 2:150 PSIG (11.2 bar)	Case 6: 150 PSIG (11.2 bar)
25	Case 3: 200 PSIG (14.6 bar)	
25	Case 4: 250 PSIG (18.0 bar)	

25	Case 5: 300 PSIG (21.4 bar)	Case 7: 300 PSIG (21.4 bar)
13	Case 8:150 PSIG (11.2 bar)	
13	Case 9: 200 PSIG (14.6 bar)	
13	Case 10: 250 PSIG (18.0 bar)	

Table 3.4.1: All cases with different nozzle throat diameters (0.25 inch for GE nozzle 1 and 0.5 inch for GE nozzle 2) at two levels of di/dt in various upstream pressures.

The nozzle arc with di/dt of 25 A/μs in GE nozzle 1 with an upstream pressure of 250 PSIG (18.24 bar) is first modelled. In the following analysis section, Case 4 has been used as the Ref. Case. The current zero results for the Ref. Case with two k-ε models will be detailed introduced as below. The arc column size in radial direction predicted by the modified k-ε model is thinner than the prediction of standard k-ε model, which can be found in Figs.3.4.5 and 3.4.6. The maximum value of the temperature connected to the modified k-ε model is lower than the standard k-ε model in hollow contact. For the convenience of this analysis, five slabs are specified in Fig.3.4.2 to analyse the results. The radial temperature profiles at different slabs are given in Fig.3.4.7 for 200 A before the final current zero point and in Fig.3.4.8 for the final current zero point. The radial temperature profiles prediction at 200 A by two k-ε models are lapped closely at these three positions. The arc column size around the nozzle throat are close together which can be found from the L1 and L2 in Fig.3.4.7 that means the upstream of the arc column are similar by using these two k-ε models. In the region ahead of the tip of the downstream electrode the arc column has a mild difference that the size of the arc column predicted by modified k-ε model is smaller than the size of standard k-ε model prediction. It can be considered that the effect of the turbulence starts to grow

stronger at the downstream of the arc column before the final current zero, but it is still not significant. At the final current zero, the temperature profiles have large difference by using these two k-ε models. The axial temperature distribution and the radial temperature profiles at different slabs are both given in Figs.3.4.8 and 3.4.10. The temperature on the axis between the two contacts is from about 1 cm to 3 cm as Fig.3.4.10 shown. The tip of the hollow contact is at 3 cm, which has a peak of temperature of between the two contacts. It is obviously noted that the temperature distribution by modified k-ε model is lower than the prediction of standard k-ε model, it is also can be found from Figs.3.4.5-3.4.6. The comparison of temperature at the radial direction is also given in Fig.3.4.8. The temperature profiles recorded at the same three positions is shown in Fig.3.4.7.They have a totally different situation when at the current of 200 A. It is noted that the modified k-ε model predicts the radial temperature, which is much lower than the prediction of standard k-ε model. All of these comparison show that the turbulence effect of modified k-ε model is much higher than the standard k-ε model, especially at the final current zero. This is also evidenced from the arc voltage prediction, which is given in Fig.3.4.9. The arc voltage predicted by the modified k-ε model is higher than the voltage of standard k-ε model. For a clear comparison of turbulence effects by two k-ε models at the final current zero, some useful variables distribution are also given in Figs.3.4.11 to 3.4.16. The turbulent kinetic viscosity, which is the most important parameter, reflects the turbulence change in the arc region directly. The turbulent kinetic viscosity distributions for the whole computational domain using two k-ε models are presented in Figs.3.4.15 and 3.4.16. The turbulence kinetic viscosity at the tip of the downstream electrode has the highest value due to a maximum velocity being highest at this region.

The kinetic energy is also very high at this point. The related radial turbulence kinetic viscosity distribution is given in Fig.3.4.17. Modified k-ε model predicts a higher viscosity than the standard k-ε model for the entire arc column. The arc edge for current zero is about 0.4 mm around the nozzle throat, which can be found from Fig.3.4.8, so the turbulence kinetic viscosity has a maximum difference between the two k-ε models at the radius of 0.4 mm, it is just around the arc edge. Figs.3.4.18 and 3.4.19 show the difference between the axial velocity and pressure at different slabs predicted by two k-ε models and all these can objectively justify the turbulence effects of the modified k-ε model, which is larger than the standard k-ε model. All of these analyses are from the Ref. Case, the other cases have been checked using similar approaches.

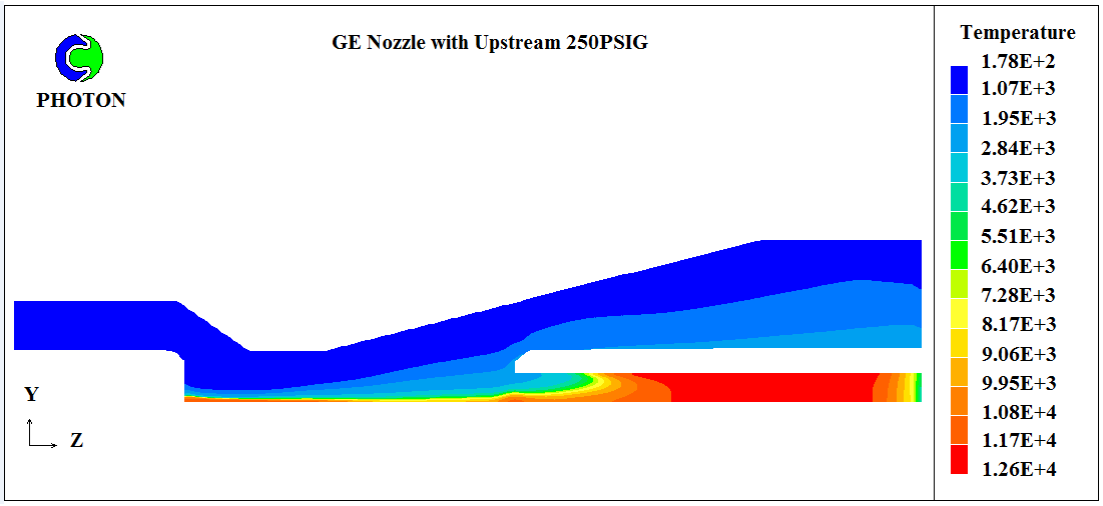

Fig.3.4.5: Temperature distribution at final current zero by using standard k-ε turbulence model. Upstream pressure is 18.24 bar (250PSIG).

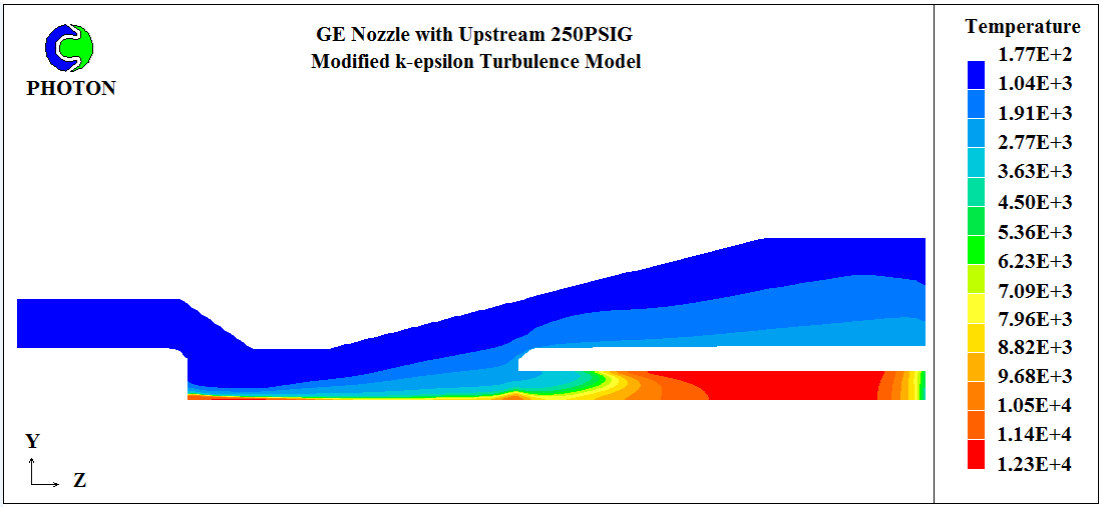

Fig.3.4.6: Temperature distribution at final current zero by using Liverpool k-ε turbulence model. Upstream pressure is 18.24 bar (250PSIG).

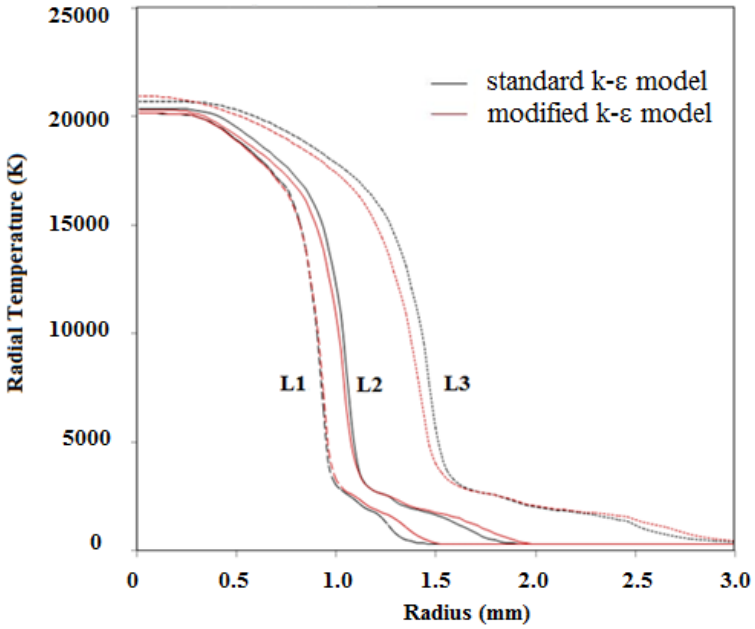

Fig.3.4.7: Radial temperature profile at three different slabs at 200 A with two k-ε models.

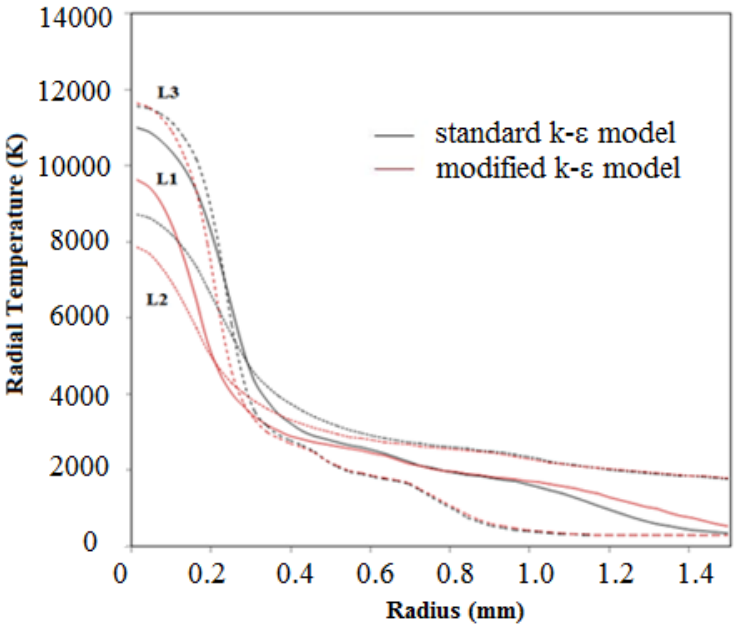

Fig.3.4.8: Radial Temperature profiles at three different slabs at final current zero with two k-ε models.

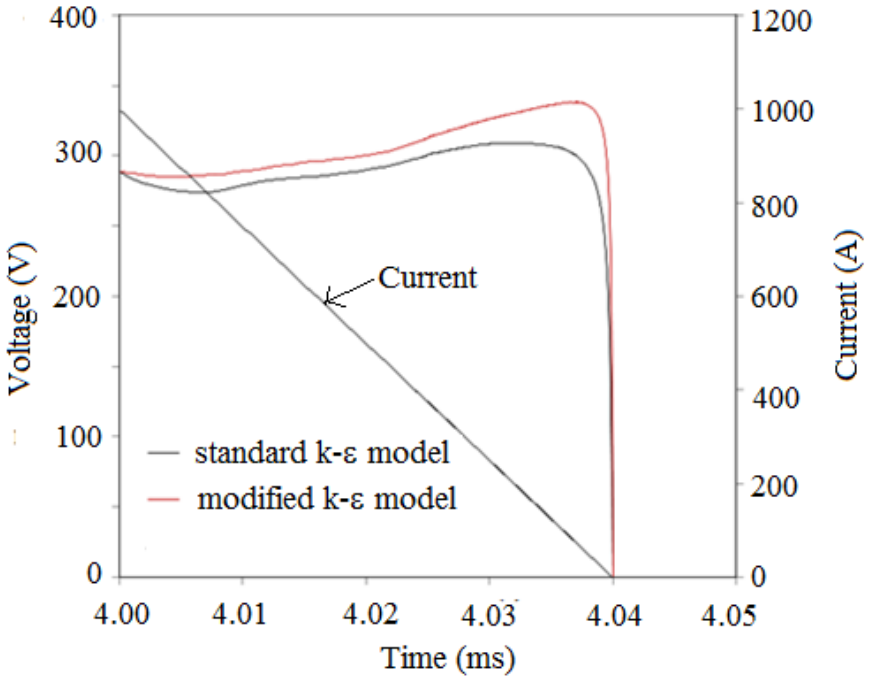

Fig.3.4.9: Current & voltage of upstream pressure of Ref. Case.

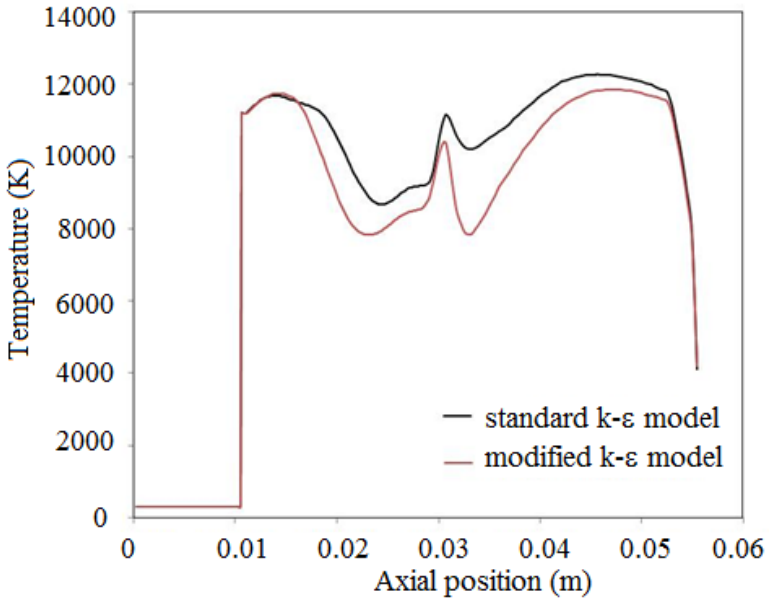

Fig.3.4.10: Axial Temperature on the axis of the Ref. Case with two k-ε models.

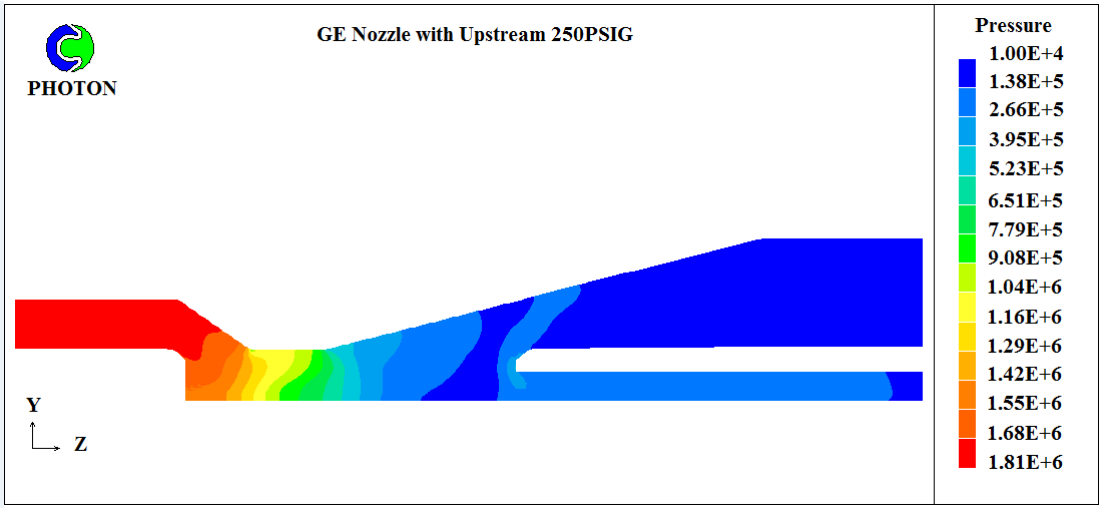

Fig.3.4.11: Pressure distribution at final current zero by using standard k-ε turbulence model. Upstream pressure is 18.24 bar (250PSIG).

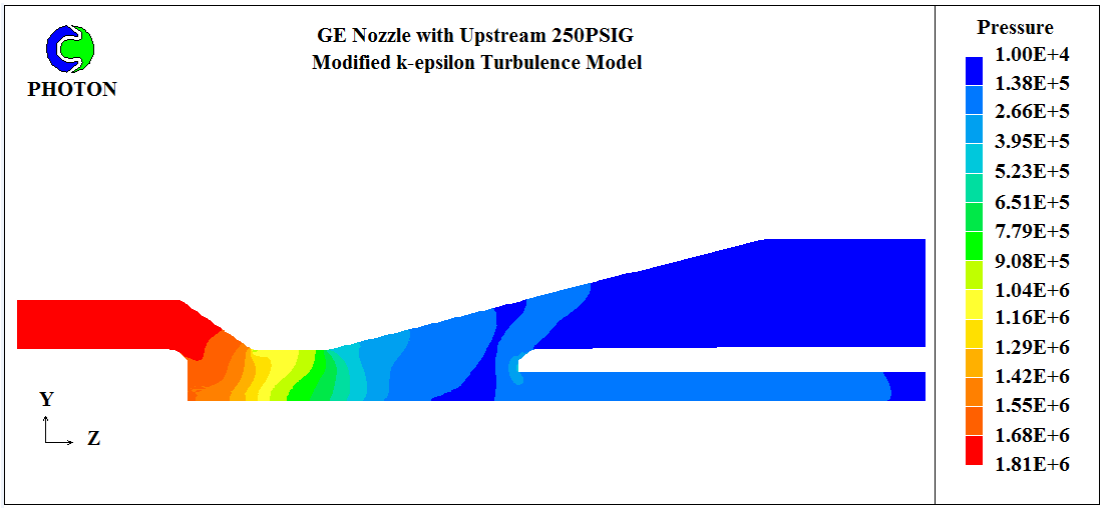

Fig.3.4.12: Pressure distribution at final current zero by using Liverpool k-ε turbulence model. Upstream pressure is 18.24 bar (250PSIG).

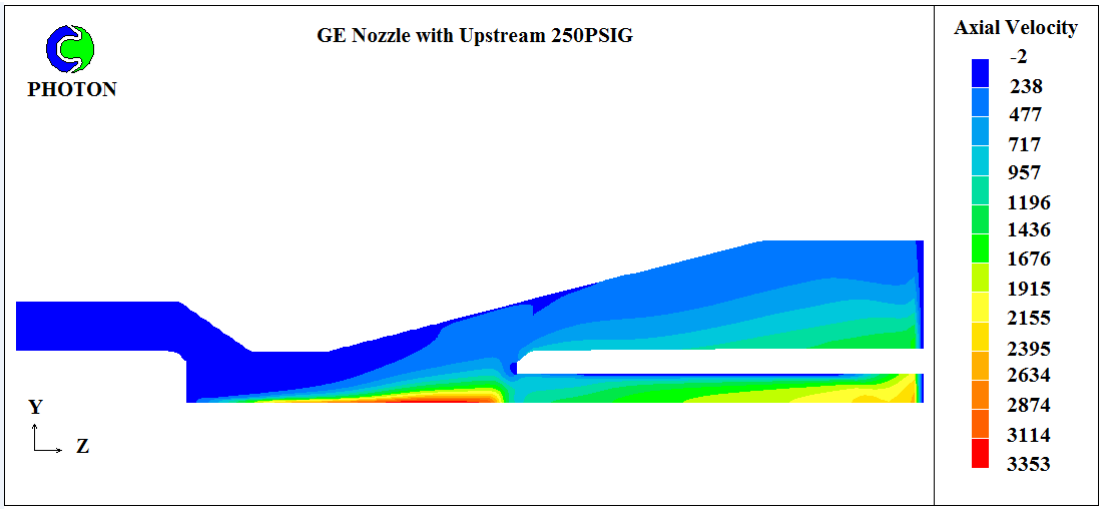

Fig.3.4.13: Axial Velocity distribution at final current zero by using standard k-ε turbulence model. Upstream pressure is 18.24 bar (250PSIG).

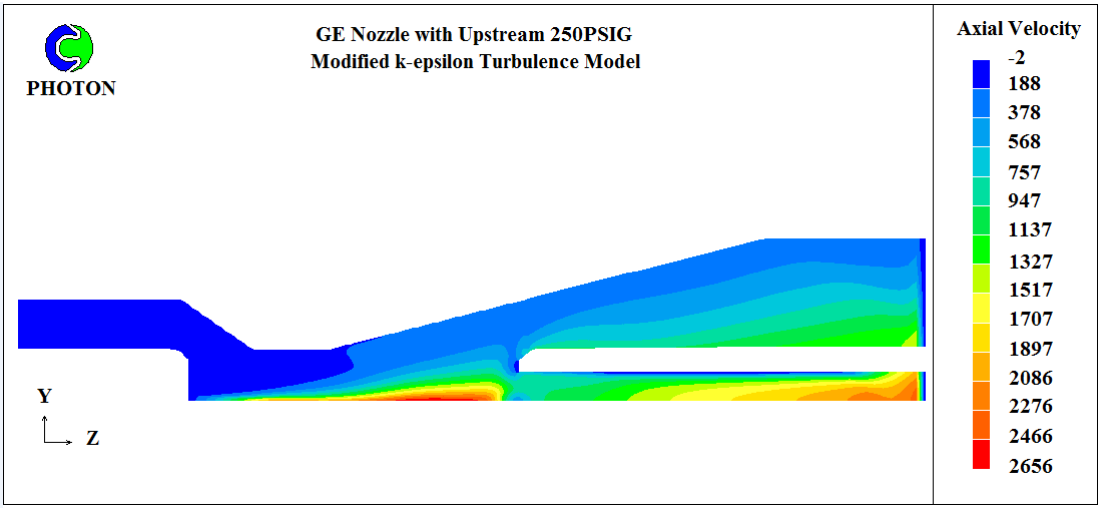

Fig.3.4.14: Axial velocity distribution at final current zero by using Liverpool k-ε turbulence model. Upstream pressure is 18.24 bar (250PSIG).

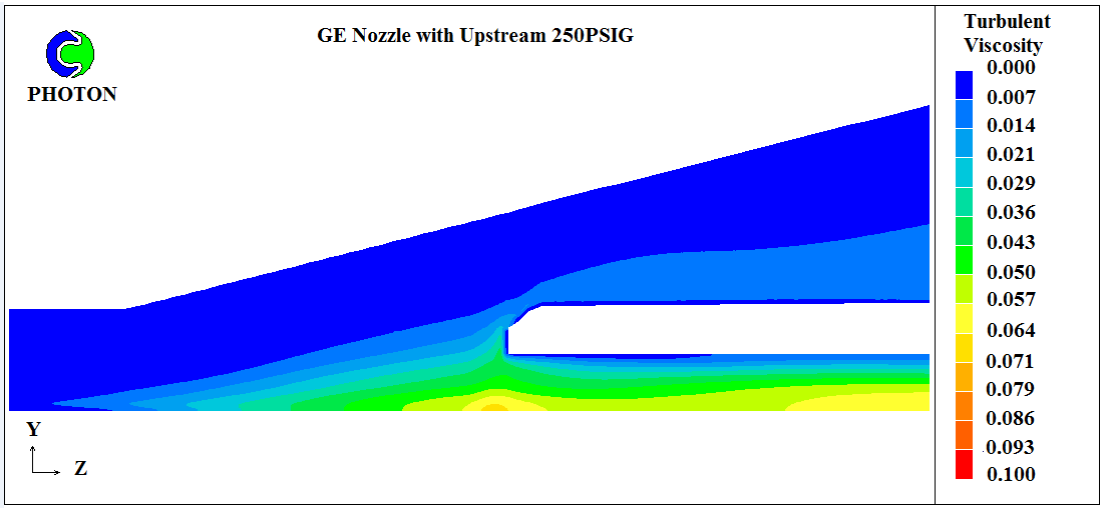

Fig.3.4.15: Turbulent viscosity distribution at final current zero by using standard k-ε turbulence model. Upstream pressure is 18.24 bar (250PSIG).

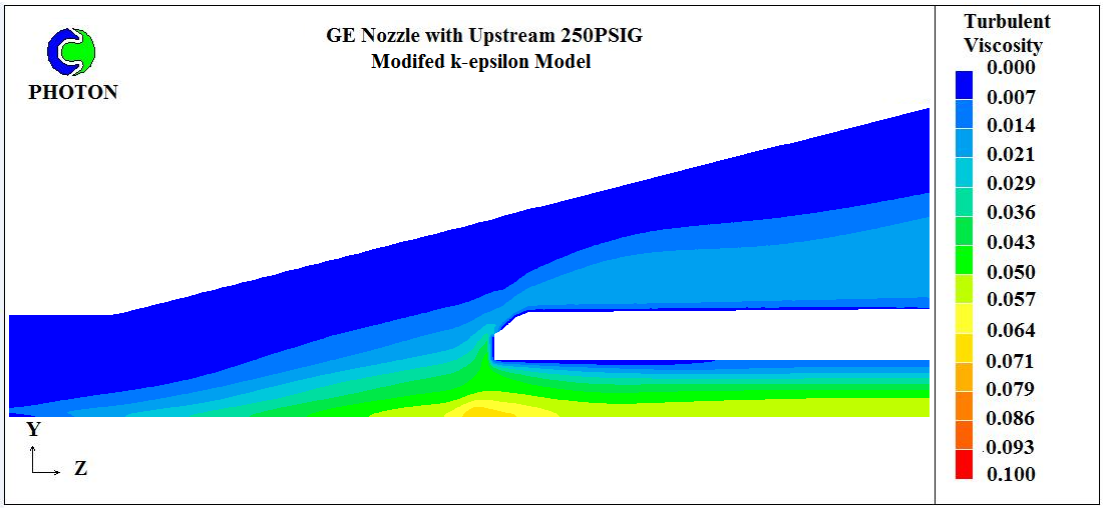

Fig.3.4.16: Turbulent viscosity distribution at final current zero by using Liverpool k-ε turbulence model. Upstream pressure is 18.24 bar (250PSIG).

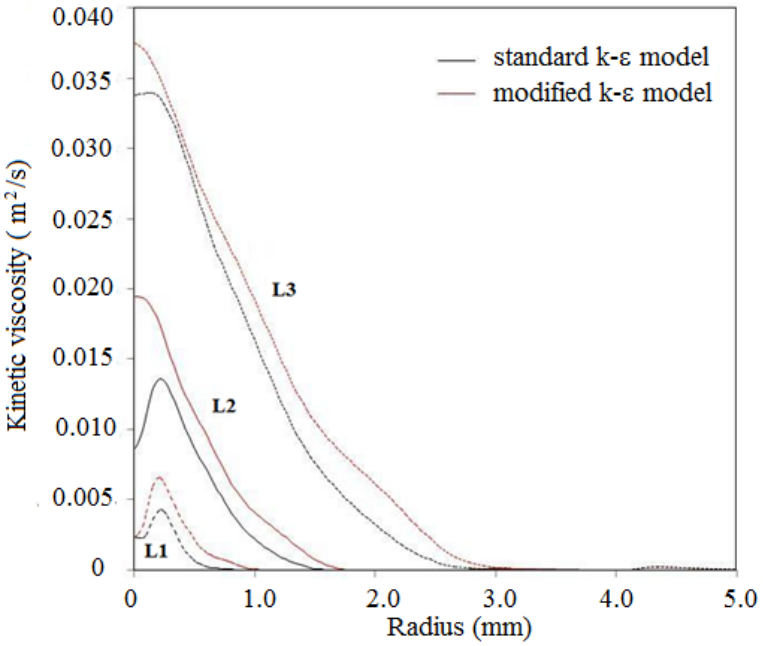

Fig.3.4.17: Radial turbulent viscosity at three different slabs at final current zero with two k-ε models.

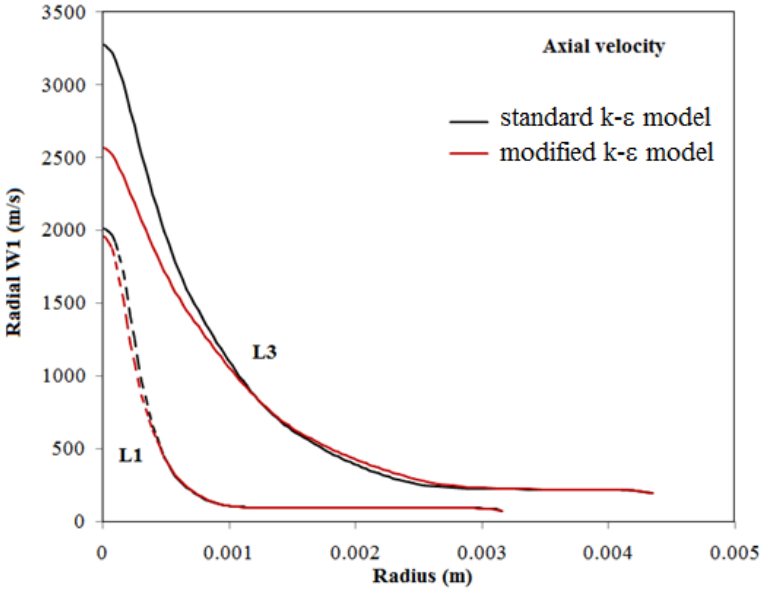

Fig.3.4.18: Axial velocity (w1) on radial direction with two k-ε models at current zero.

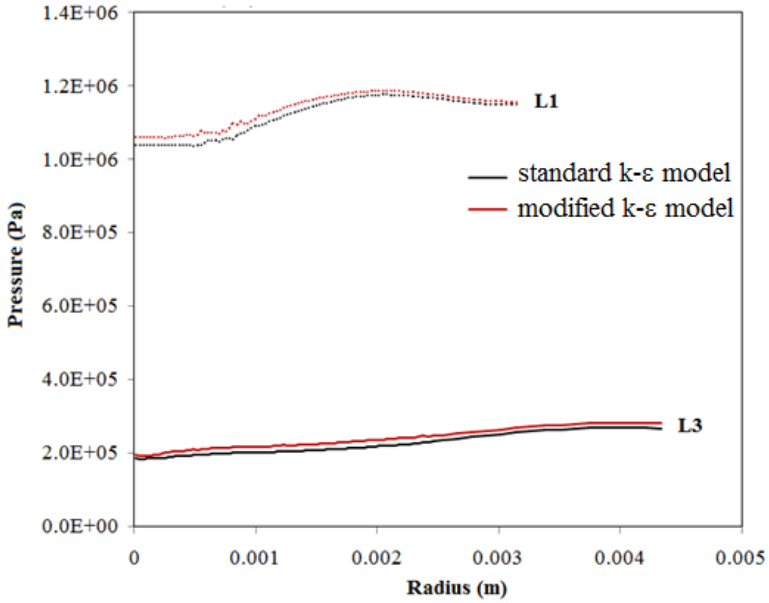

Fig.3.4.19: Radial pressure predictions with two k-ε models at current zero.

3.4.3.2 Post arc current phase

The post arc current phases are calculated with various dv/dt to obtain its critical RRRV for all the cases. The Ref. Case of GE nozzle 1 (0.25 inch nozzle throat diameter) in 250 PSIG (18.24 bar) upstream pressure with di/dt of 25 A/μs is used to introduce the calculation method of critical RRRV. The approach for calculating the critical RRRV for GE nozzle is similar to the calculations in Section 3.3. As mentioned before, the critical RRRV is defined as the value of dv/dt, above which the arc will reignite. The numerical uncertainty in determining the critical RRRV is less than 5% of its value.

Typical post arc currents for the Ref. Case of the two k-ε models are given in Figs.3.4.20 and 3.4.21. The measured critical RRRV of the case with 250 PSIG upstream pressure and di/dt of 25 A/μs for GE nozzle 1 is about 2.7 kV/μs (Fig.3.4.30), but the prediction from the standard k-ε model is only 1.2 kV/μs (Fig.3.4.20). The axial temperature distribution predicted by standard k-ε model at various times for different dv/dt is given in Fig.3.4.22 (success in thermal recovery) and 3.4.23 (failure in thermal recovery). Fig.3.4.22 shows the arc column cooling rapidly between the two contacts. Therefore, the beginning of current interruption occurs successfully in this region. Fig.3.4.23 shows the axial temperature distribution when the current interruption fails. If the rising rate of the recovery voltage, dv/dt, is higher than the critical RRRV, the temperature at the downstream of nozzle throat increases rapidly. Finally, a very large current flows again between the contacts. In this situation, it is thermal failure. The axial electric fields for these two situations are also given in Fig.3.4.24 and 3.4.25. Fig.3.4.24 shows the maximum value of electric field appears at the region of downstream of nozzle throat because the conductivity decrease due to strong cooling at this region. Furthermore, Fig.3.4.24

obviously shows that the failure of thermal recovery. The axial electric field and temperature of success in thermal recovery and failure in thermal recovery for the Ref. case with modified k-ε model are also given in Figs.3.4.24 to 3.4.27. The critical RRRV by modified k-ε model is about 3.5 kV/μs, which increases the value of critical RRRV compared with the standard k-ε model. A comparison of critical RRRV for the Ref. case is shown in Fig.3.4.30. The prediction by modified k-ε model is much closer than the measured results for all others cases with nozzle throat of 6.35 mm diameter. From Fig.3.4.30 shown, the modified k-ε model predicts the critical RRRV much closer than the standard k-ε model. The turbulence in the vicinity of current zero is not sufficient using the standard k-ε model and it has to be enhanced by the modified k-ε model, the critical RRRV values for all the cases in GE nozzle 1 with di/dt of 25 A/μs have justified the modified k-ε model's applicability in this nozzle arc. Case 6 and case 7 in Table 3.4.1 show that the modified k-ε model can make reasonable agreements in different nozzle shapes. GE nozzle 2 is similar with GE nozzle 1, but the diameter of nozzle throat is two times of GE nozzle 1. The critical RRRV value for Case 6 and 7 are shown in Fig.3.4.31. Case 8, 9 and 10 in Table 3.4-1 are using GE nozzle 1 with di/dt of 13 kV/μs. However, the standard k-ε model have over predicted the critical RRRV for these cases, and the modified k-ε model also predicted much higher critical RRRV values for them, because the current changes of di/dt of 13 A/μs slower than the current at di/dt of 25 A/μs. Therefore, at di/dt of 13 A/μs cases, the arc and the transport of k and ε will follow the change of current, and it is possible that k and ε become larger than expected at current zero for di/dt of 13 A/μs case, due to strong radial conduction. For cases with di/dt of 25 A/μs, the arc and transport of k and ε may not be able to follow the current because the

current changes too quickly. This results in the under prediction of k and ε, as well as the eddy viscosity and the final RRRV values.

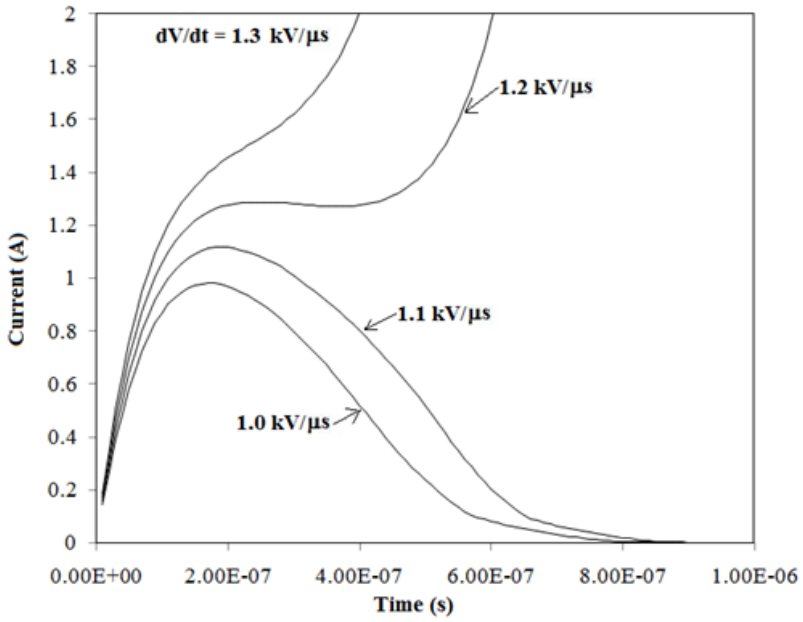

Fig.3.4.20: Calculated post-arc current of Ref. case by standard k-ε model.

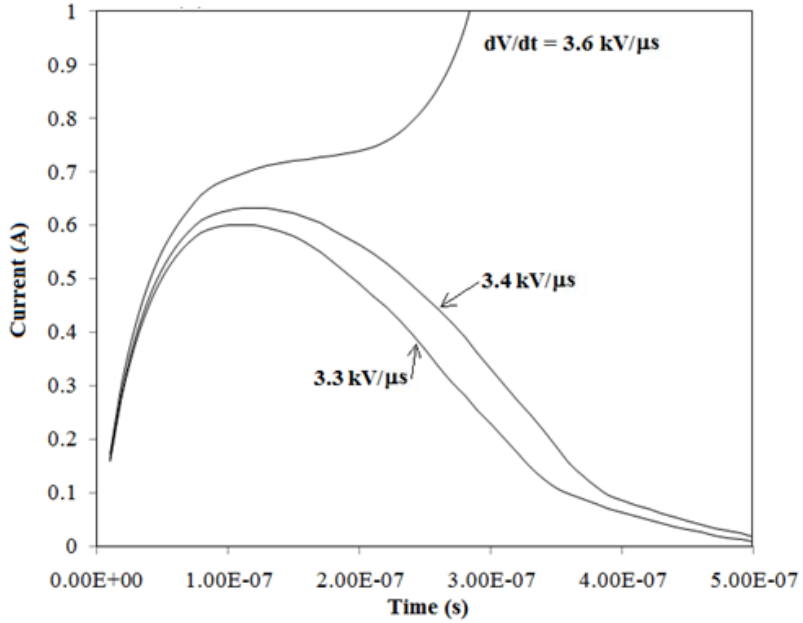

Fig.3.4.21: Calculated post-arc current of Ref. case by modified k-ε model.

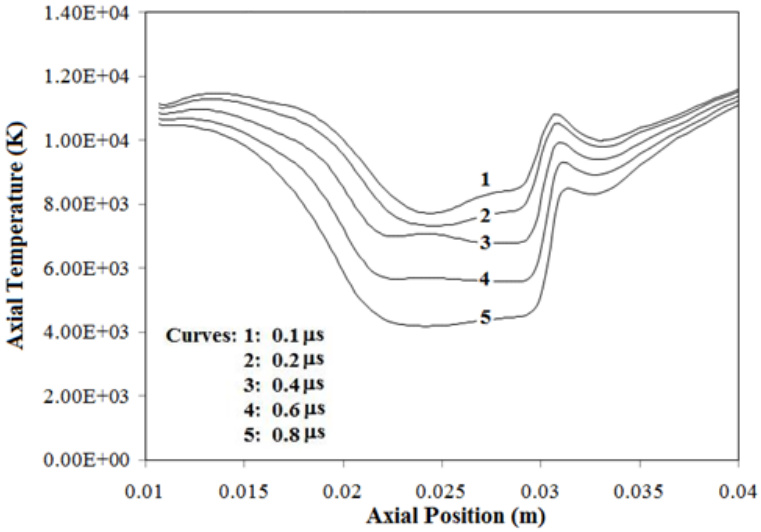

Fig.3.4.22: Axial Temperature distribution at different instants after current zero for Ref. case (dv/dt=1.1kV/μs) by standard k-ε model.

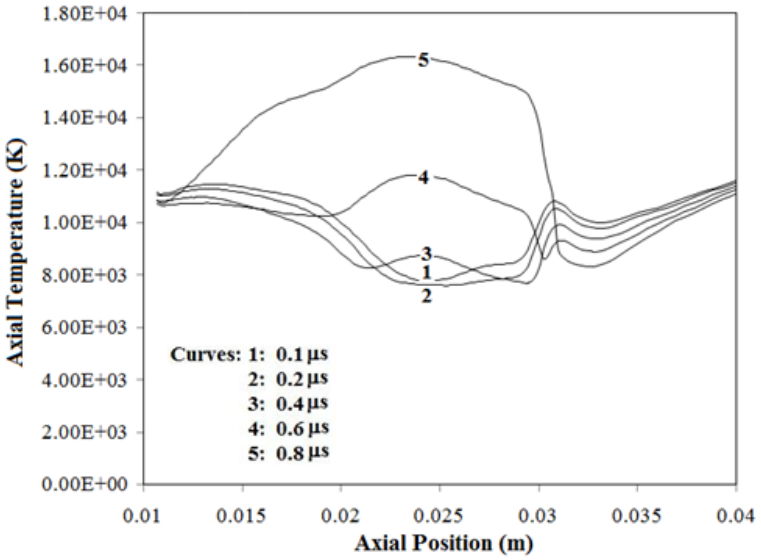

Fig.3.4.23: Axial Temperature distribution at different instants after current zero for Ref. case (dv/dt=1.3kV/μs) by standard k-ε model.

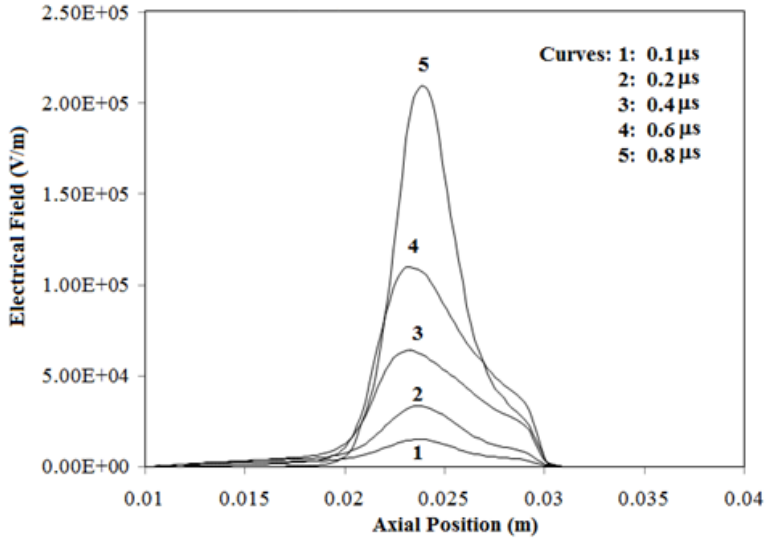

Fig.3.4.24: Electrical field distribution at different instants after current zero of Ref. case (dv/dt=1.1 kV/μs) by standard k-ε model.

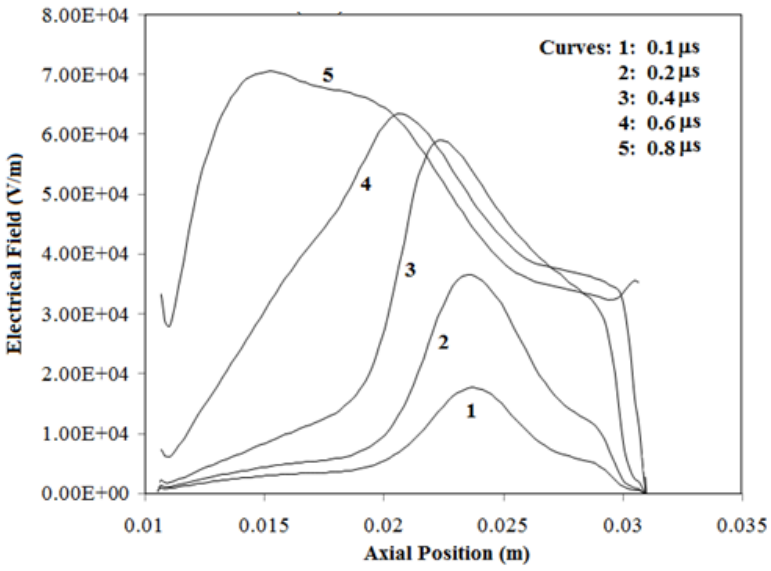

Fig.3.4.25: Electrical field distribution at different instants after current zero of Ref. case (dv/dt=1.3 kV/μs) by standard k-ε model.

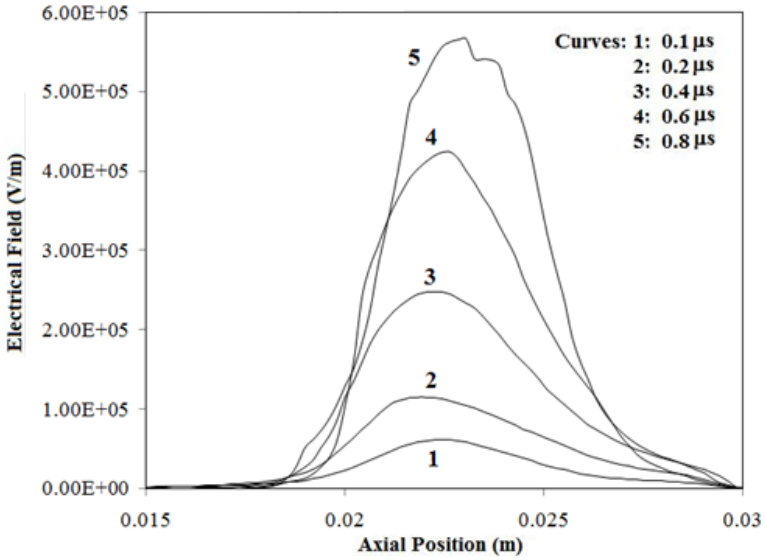

Fig.3.4.26: Electrical field distribution at different instants after current zero of Ref. Case (dv/dt=3.4kV/μs) by modified k-ε model.

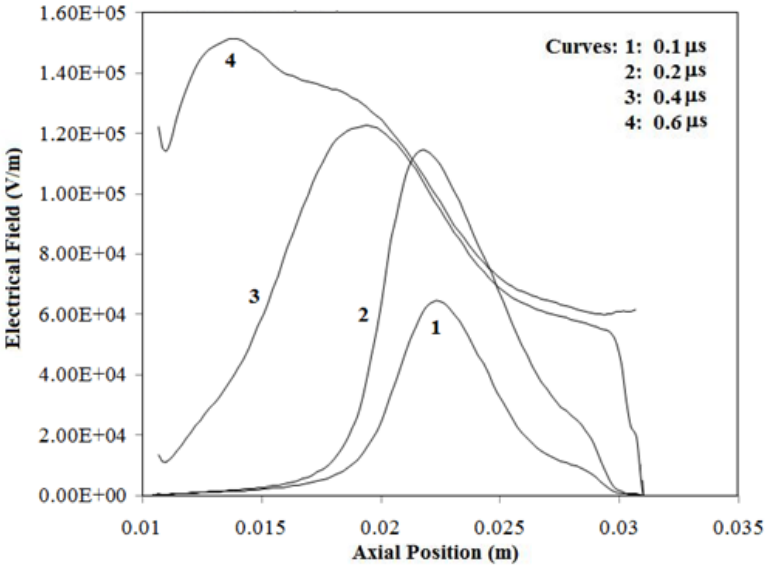

Fig.3.4.27: Electrical field distribution at different instants after current zero of Ref. Case (dv/dt=3.6kV/μs) by modified k-ε turbulence model.

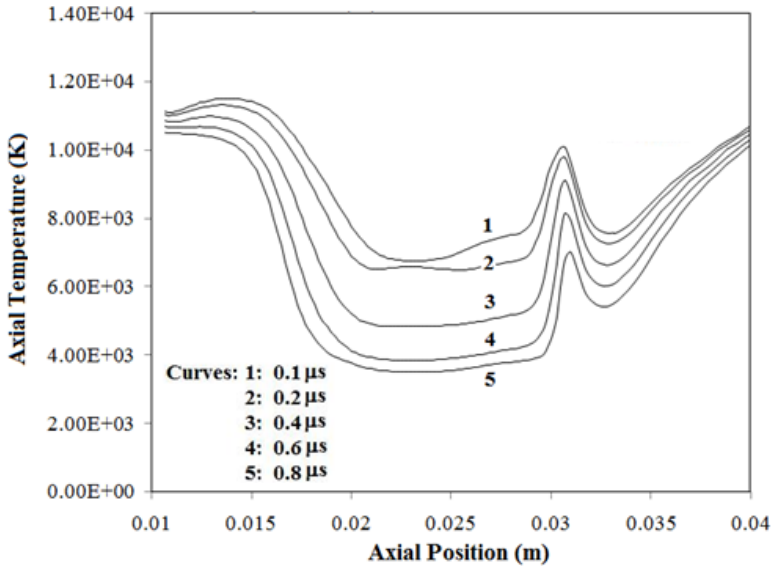

Fig.3.4.28: Axial Temperature distribution at different instants after current zero of Ref. case (dv/dt=3.4kV/μs) by modified k-ε model.

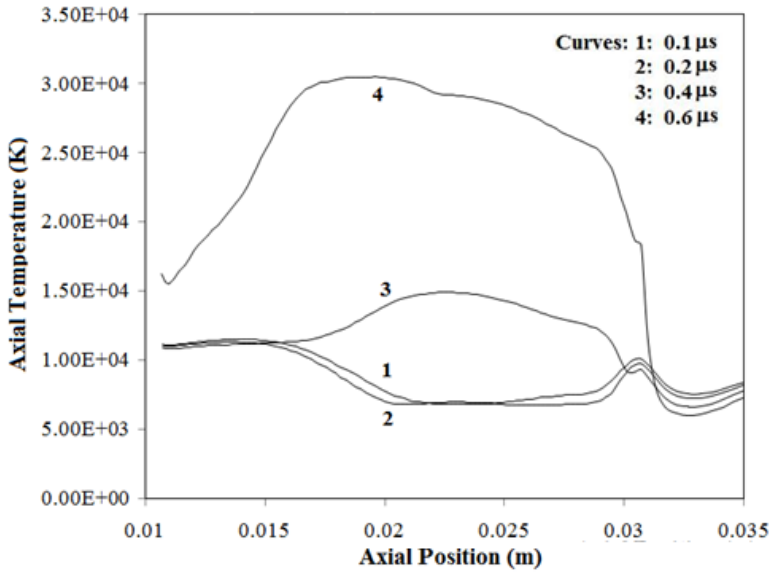

Fig.3.4.29: Axial Temperature distribution at different instants after current zero of Ref. case (dv/dt=3.6kV/μs) by modified k-ε model.

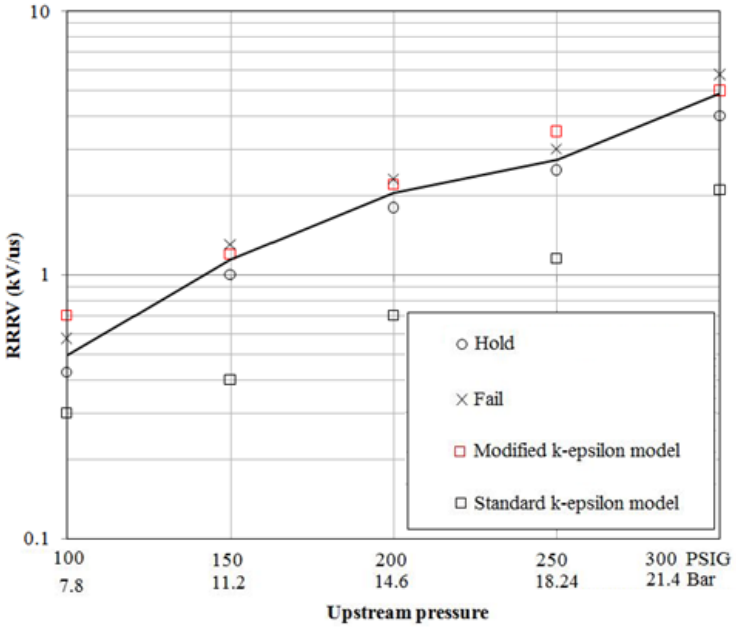

Fig.3.4.30: Critical RRRV with various upstream pressures by two k-ε models in di/dt of 25 A/μs in GE nozzle 1.

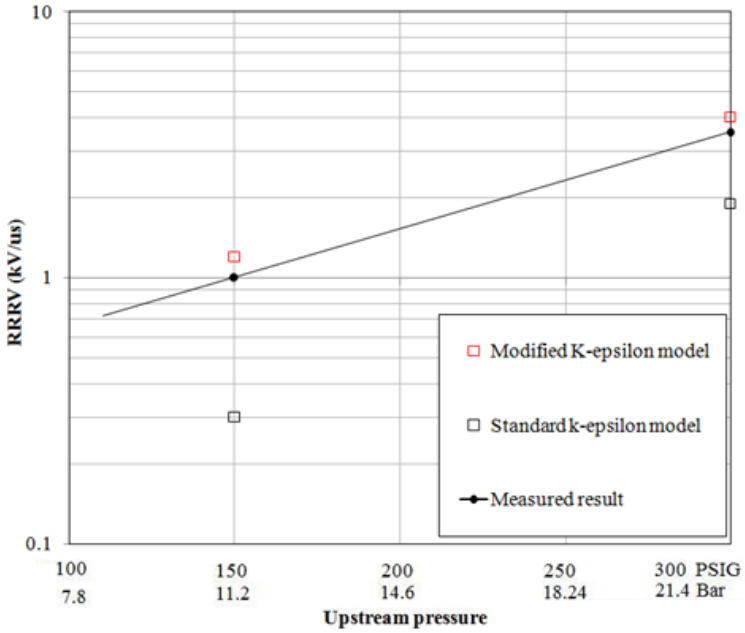

Fig.3.4.31: Critical RRRV with various upstream pressures by two k-ε models in di/dt of 25 A/μs in GE nozzle 2 nozzle(nozzle throat is 0.5 inch diameter).

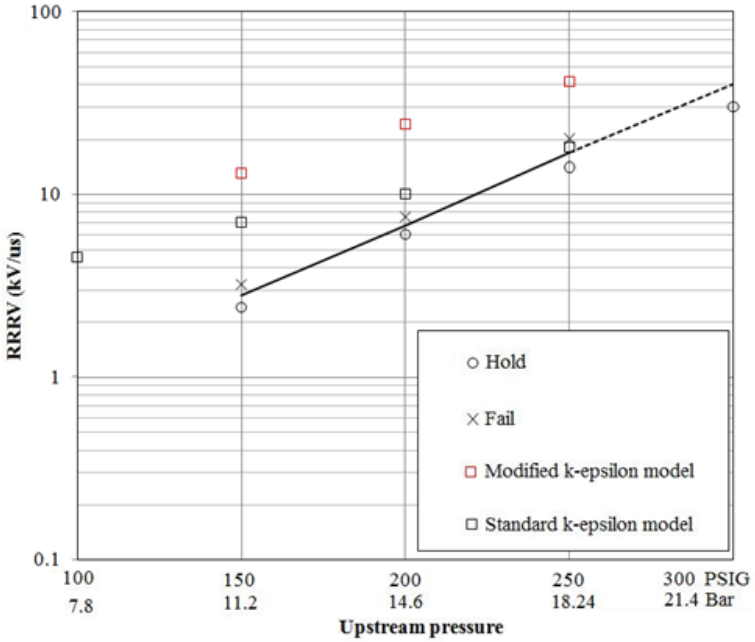

Fig.3.4.32: Critical RRRV with various upstream pressures by two k-ε turbulence models in di/dt = 13 A/μs in GE nozzle 1.

3.5 Turbulence Models Tested on Circuit Breaker

3.5.1 Introduction

The modified k-ε turbulence model was finally applied to a circuit breaker to assess its applicability. The circuit breaker system is a 252 kV puffer type circuit breaker. Two current levels of 10 kA and 47 kA were used.

The structure of the circuit breaker and the computational domain used in the simulation are given in Fig.3.5.1. The arc model is implemented in PHOENICS 3.6.1 [117]. The code consists of three parts similar to the nozzle arcs (Section 3.3 and 3.4). (1) Satellite with an input file of Q1, which contains definitions of all of the important model parameters, grid system, governing equations, boundary conditions and relaxation control. (2) A Fortran file called ground.for where the arc model is coded and compiled to form an executable program called the Earth. (3) Post processing software, PHOTON. The block diagram of the .EXE files and relevant files have been shown in Fig.2.1.

For the simulation of the circuit breaker operations, four steps are needed for the calculation, which are the Cold Flow Phase, High Current Phase, Current Zero Phase and Post Arc Current Phase.

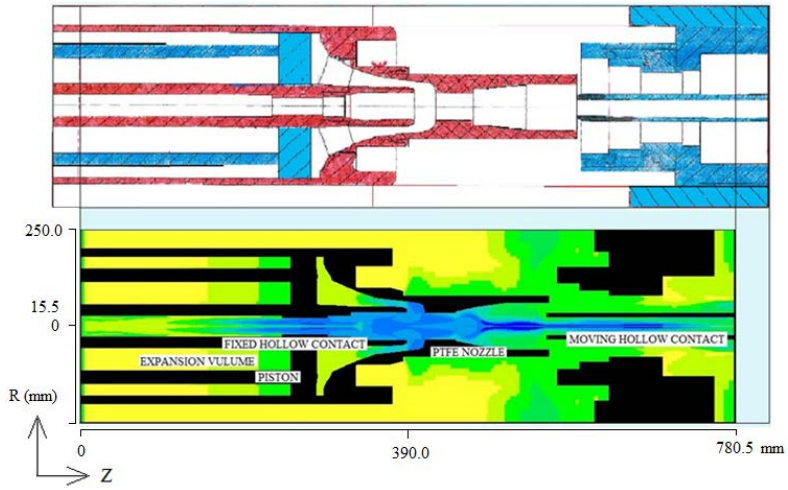

Fig.3.5.1: Geometry of the 252 kV PINGGAO puffer type circuit breaker and the main computational domain used to simulate the arcing.

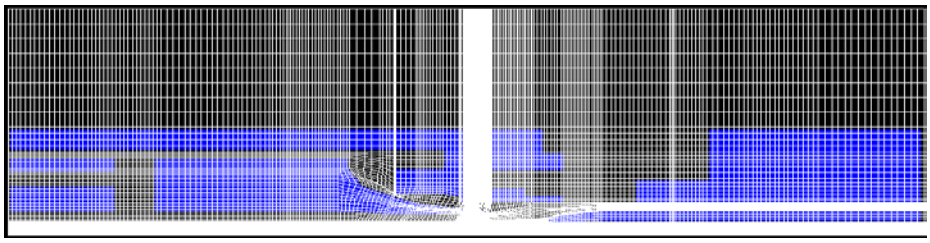

Fig.3.5.2: Whole computational domain and the grid system.

3.5.2 Time length for each phase

According to the measured travel curve as shown in Fig.3.5.3 and 3.5.4, a time zero point on the curve will need to be decided. It is customary to define the time zero as the point, which is only a short while (< 3 ms) before the contact's movement. Ideally the time zero should be the point on the travel curve where the contact, piston and other solid parts are just starting to move with reference to the remaining part of the computational domain. In order to properly use the contact travel file, the recorded current waveform and pressure data should also be consulted before determining the final value of the time zero.

For the High Current Phase, the starting time is obtained from the Cold flow phase when the contact gap length reaches 5 to 8 mm with more than 5 cells in the radial direction between the gap. For 47 kA and 10 kA cases, it is 14.12 ms and 14.1 ms respectively. The simulation duration is decided according to the arc current waveform described in the CURRENT.TXT file as shown in Fig.3.5.5. For this phase, the simulation will stop when the magnitude of the current reaches 15 kA. The grid system will then need to be refined for low current arcs (in the current zero phase). The time step used for this period is 2 μs.

For the Current Zero Period, the starting time is the ending time of the High Current Phase. Its ending time must correspond to the time when the current is

exactly zero. It can be obtained by inspecting the CURRENY.TXT file. In the present model a very small time step at the last 50 μs must to resolve change of arc and flow quantities accurately before the final current zero. In the cases of 47 kA and 10 kA, the time steps are 1 μs for the majority of the period and 0.2 μs for the last 50 μs. An important feature is that special code has been used in the Liverpool model to accurately calculate the current in the last 50 μs before the final current zero. The coding requires that the time step size must remain the same in the last 50 μs.

The critical RRRV is not provided by the experiment. Therefore it will not be considered in this section.

3.5.3 Grid system

The grid system should be defined before the calculation in the Q1 file according to the possible distribution of flow parameters in the domain. In the nozzle the radial number of grids needs to be sufficiently high so there is sufficient spatial resolution in the arc region to resolve the gradient of temperature, density, and other variables.

For the puffer type circuit breaker in the simulation, the length of the whole computational domain is 780.5 mm and the radius is 250.0 mm. The radius of the main nozzle throat is 15.5 mm.

Altogether, 95 cells in the radial direction and 269 cells in the axial direction cells are used for the Cold Flow Phase and High Current Phase. 125 cells in the radial direction and 269 cells in the axial direction are used for the Current Zero Phase. The width of cells in the arc region for the current zero period is 0.05 mm, which is very small and sufficient to calculate accurately. The grid system and the computational domain of the circuit breaker are given in Fig.3.5.2.

3.5.4 Confirmation of the measurement results

First of all, the measured results need to be checked and confirmed. The synchronisation of the record of pressure and arc voltage with different oscilloscopes is maintained by the current signal, so it is necessary to check the current records to make sure that the values from two different sensors are identical.

The current wave can be obtained from the oscilloscope by applying calibration in terms of the equation below:

$$I_{real} = C (V_i - V_{ref}) \quad (3.8)$$

where I_{real} is the current, Vi the measured voltage from the oscilloscope data, V_{ref} the base voltage in zero current, and C is a conversion coefficient.

For the oscilloscope of DL750, the value of C is 160 kA/V provided by the manufacturer and V_{ref} is -0.0493 V by inspecting the raw. The time is different when using different oscilloscopes. For oscilloscopes of DL750 the starting time is -30 ms and the starting time is -5 ms for Tektronix oscilloscope. The electric current obtained from the record of DL750 is shown in Fig.3.5.6 as the broken curve. The peak current in the first half cycle is 65.6 kA and 60.6 kA in the second half cycle. The duration of current is only 19.3 ms. Since its peak value of current is 65.6 kA, which correspond to about 47 kA, and referred to as the 47 kA case in this section.

A different calibration is applied to the Tektronix record with C equals to 11.8 kA/V provided by the manufacturer and V_{ref} set to 0.4 V (Eq.3.8). The current wave of Tektronix is also given in Fig.3.5.6, it is noted that two recorded results are different slightly at the peak value of second half cycle. The value of Tektronix is lower than the DL750 about 5%.

The 10 kA case with two current recorded results is shown in Fig.3.5.7. The green one is measured by the Tektronix oscilloscope, which is shorter than the measurement of DL750 in the second half cycle. However, the recorded result of DL750 does not synchronise with the measured arc voltage (the red curve in Fig.3.5.7), so it cannot be used in the simulation. It is also noted that the recorded current by the Tektronix oscilloscope has serious fluctuation in the measurement. It is modified to a smooth current curve as shown in Fig.3.5.8 which is represented by orange points.

Detailed information of the two cases of 252 kV puffer type circuit breaker of PINGGAO with 10 kA and 47 kA current levels are listed in Table 3.5.1.

Test ID	Arcing duration (ms)	Max contact speed (m/s)	Peak current in last loop (kA)
10 kA	7	9.6	2.5
47 kA	11	9.6	57.6

Table 3.5.1: Test cases for the 252 kV puffer type circuit breaker.

The measurement results of arc voltage, current, and travel for 10 kA and 47 kA cases are shown in Figs.3.5.8 and 3.5.9. The arc voltage for the 47 kA case is relatively smoother than 10 kA case. It is known that the change of the shape of the arc column for 47 kA case is rather smooth. In fact, the actually current for the case of 10 kA is only 2.5 kA at the second half cycle, it is found that the arc voltage in the current below 3 kA with a strong fluctuation. For the period from the beginning of arc generating for the 10 kA case, the measured arc voltage is rather smooth.

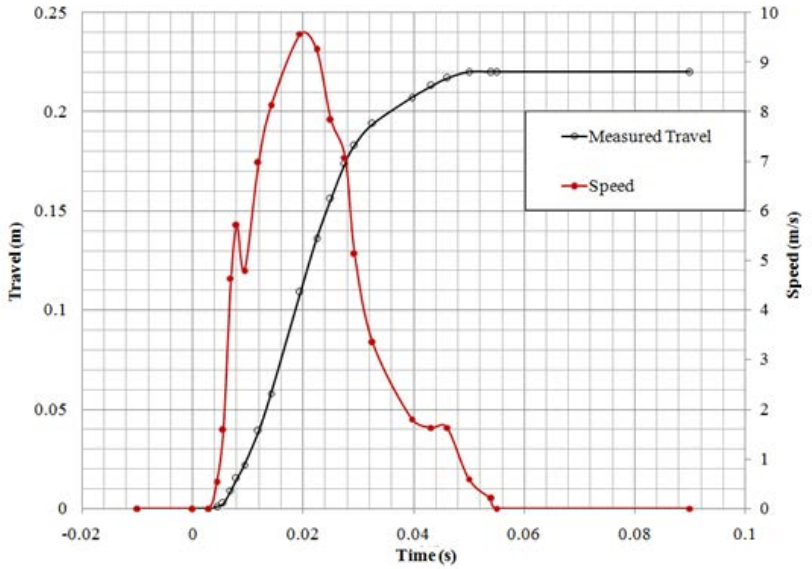

Fig.3.5.3: Contact travel and speed derived from the original record and to be used in the simulation for the 47kA case.

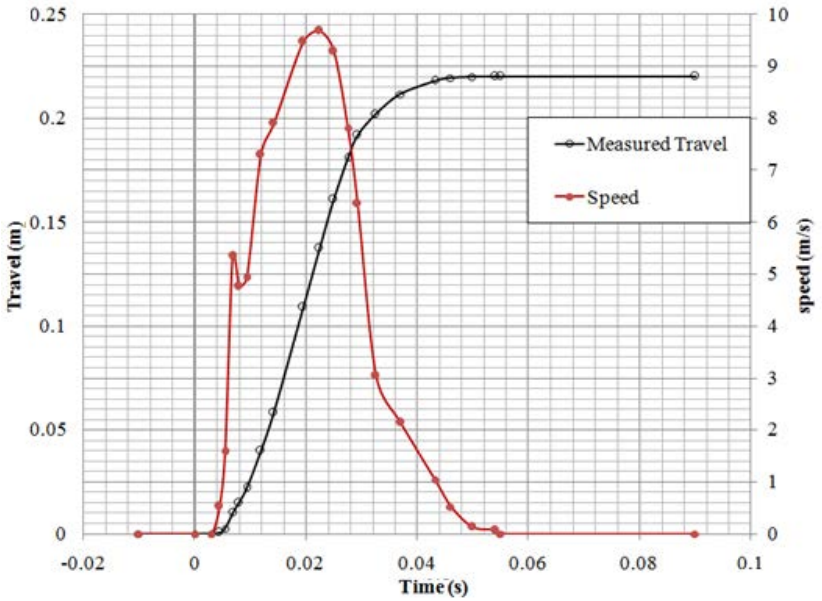

Fig.3.5.4: Contact travel and speed derived from the original record and to be used in the simulation for the 10kA case.

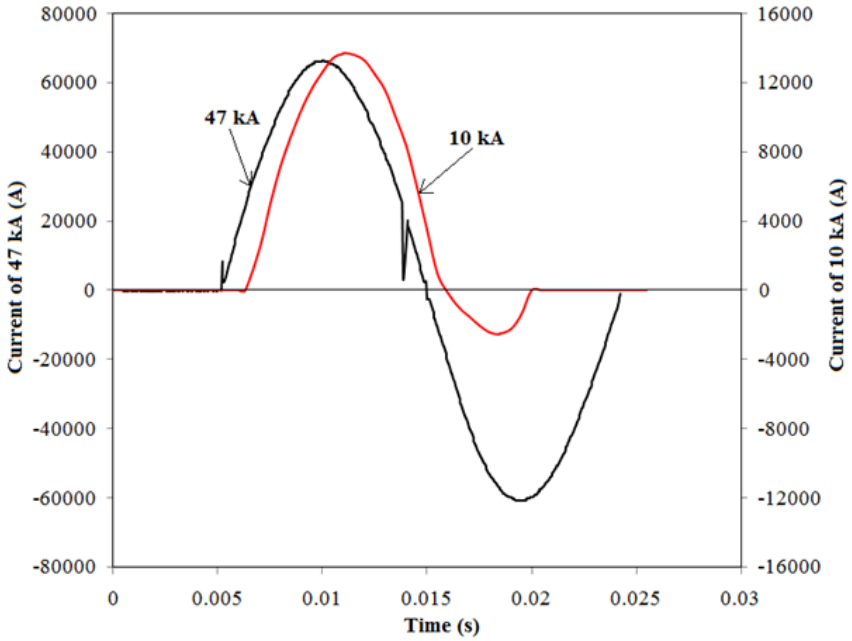

Fig.3.5.5: Current files for the cases of 47 kA and 10 kA.

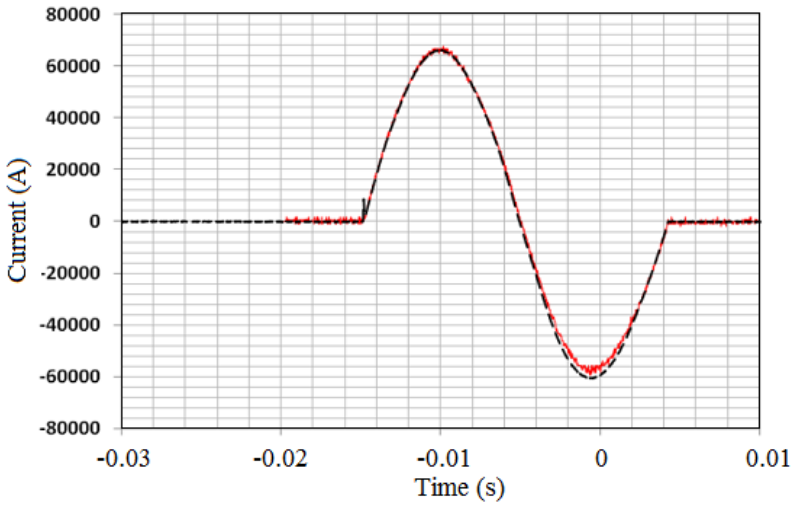

Fig.3.5.6: Comparison of the current waveforms recorded by DL750 (black) and Tektronix (red) for the 47 kA case.

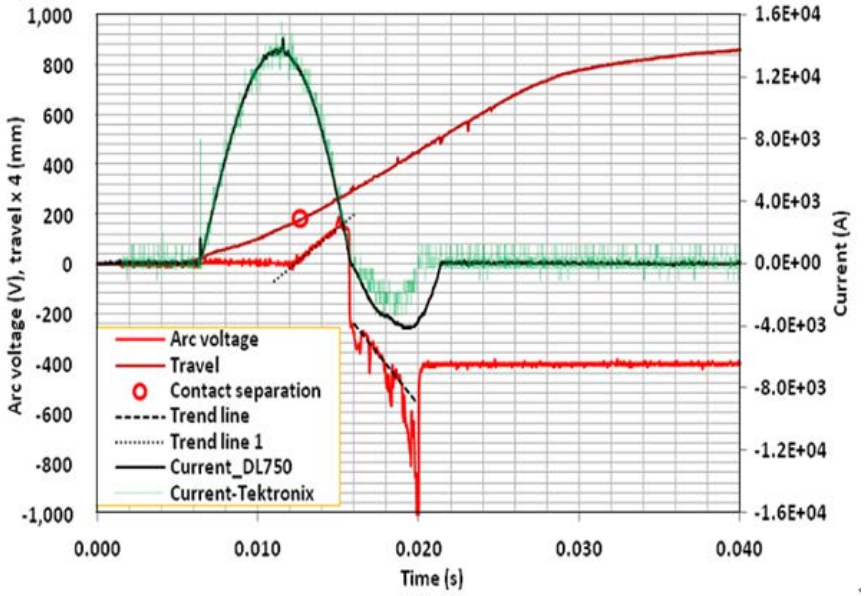

Fig.3.5.7: Current waveform measurement of DL750 (black curve) and Tektronix (green) for 10 kA case.

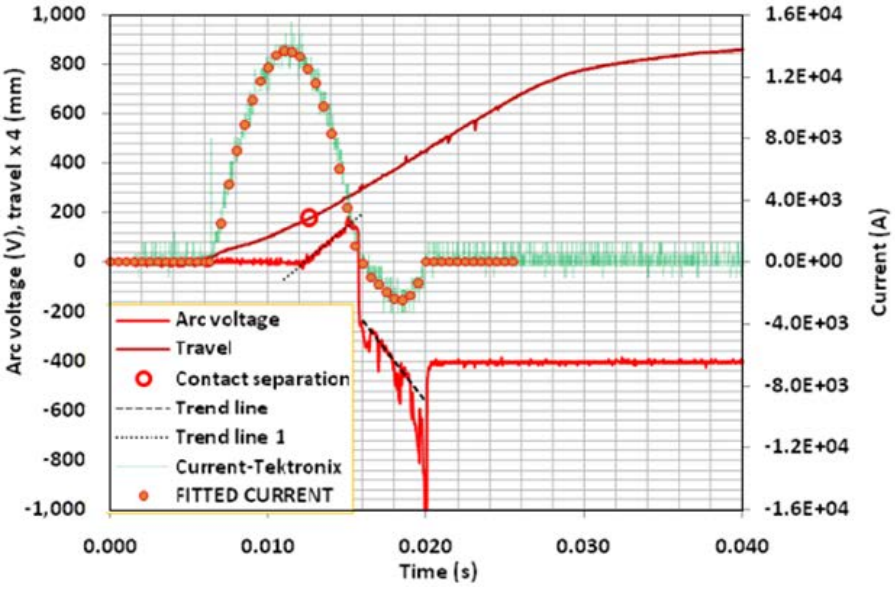

Fig.3.5.8: Current waveform of Tektronix is used in the input current file for 10 kA case. The Arc voltage and contact travel are shown in the figure.

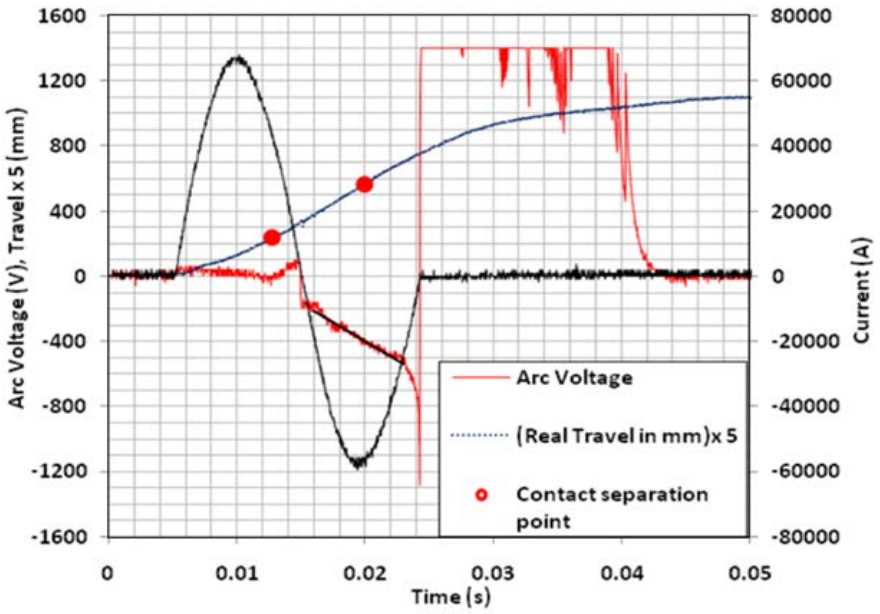

Fig.3.5.9: Current, Travel and measured arc voltage for the case of 47kA.

The extinction peak was observed in both cases for 10 kA and 47 kA as shown in Figs.3.5.8 and 3.5.9. The arc voltage starts to increase rapidly in the very short time before the final current zero. It is very important for investigation of turbulence effect in low current period, and it will be detailed introduced in latter simulation sections.

The pressure is recorded in the cylinder for both cases of 10 kA and 47 kA (Figs.3.5.10 and 3.5.11). Because of the uncertainties in this pressure measurement. The measurement taken in the puffer cylinder will only be used in the comparison with simulation results.

3.5.5 Prediction by different turbulence models

It is known that the arc voltage is extremely important in evaluating the arc model. It directly reflects how satisfactorily the arc column is modelled, the main reasons can be summarised as follows:

1: The arc voltage determines the power dumped inside the arc, which affects

the gas temperature and pressure distribution in the arcing chamber including the puffer for high current phase, and also indirectly in the final current zero period.

2: The temperature in the arc core is largely determined by the balance of radiation and Ohmic heating, the size and shape of the arc column also sensitively affects the arc voltage.

Therefore, the arc voltage prediction should be accurate in the arc modelling. The pressure is also very important in the verification of the simulation model for circuit breakers.

Turbulence and convection are the two most important mechanisms responsible for arc cooling in the period before the final current zero in high voltage gas blast circuit breakers.

In the case of 47 kA, the arcing current has a peak value of 60 kA. The filling pressure of SF_6 is 6.9 bar absolute. The arc is initiated after 14 ms of contact movement. The arc voltage prediction of the modified k-ε model is shown in Figs.3.5.13 to 3.5.14 where the prediction by Prandtl mixing length turbulence model and the standard k-ε model are also given. It can be seen that the predictions by various turbulence models have some difference at the High Current Phase, a much lower arc voltage (50 V) at 17.8 ms is predicted by modified k-ε model, tend of other two models prediction match with the measurement at this point. The prediction of standard k-ε model is slightly larger than the modified k-ε model from 19 ms where the current almost reaches its peak value. There is a very large difference with the standard k-ε model at 21.5 ms, 160 V higher than the measurement value. The prediction of modified k-ε model matches with the measured result around this point, only 12% higher than the measurement. The turbulence effect is not very significant

at the high current phase. The prediction by using the modified k-ε model gives a better match between the predicted and measured arc voltage among predictions using the Prandtl mixing length model and the k-ε turbulence models (Fig.3.5.13).

In the case of 47 kA, when the current falls from 15 kA towards its final current zero point, the arc column shrinks rapidly and the turbulent effect becomes more dominant in arc cooling. The predicted arc voltage in this period corresponds to the extinction peak in the measurement. The predicted results using the standard k-ε model are 20% lower than the measured arc voltage (Fig.3.5.14), and turbulence is enhanced around the arc column when using the modified k-ε model. The arc voltage is much closer to the measurement.

For the 10 kA case, the second half cycle is only 2.5 kA, so the simulation for this case is regarded as a current zero phase. The arc voltage prediction using the modified k-ε model is shown in Fig.3.5.14. In comparison with the predictions by the Prandtl mixing length model and the standard k-ε model are also given in the figure. The arc voltage of using different turbulence models has a similar value before 18 ms where the current almost reaches its current peak. The difference of predictions occurs after 18 ms as the current lower than 2.5 kA, especially around the last 10 ms. Almost 20% difference produced between these predictions. The Prandtl mixing length model with variable turbulence parameter [86] predicts an arc voltage that is much closer to the measurement. The prediction of using the modified k-ε model is much closer to the measured voltage than standard k-ε model, especially near the final current zero (last 10 ms). The trend of arc voltage matches with the measurement the best. The pressure prediction in the cylinder for the High Current Phase and Current Zero Period for 10 kA case is detailed in Fig.3.5.10. The arc column at

current zero for the 10 kA case with the standard k-ε model and modified k-ε model has been compared in Figs.3.5.15 and 3.5.16. It can be found that the arc core temperature (9890 K) in Fig.3.5.16 is lower than the 10,000 K in the prediction by standard k-ε model in Fig.3.5.15. The radial temperature profiles at the main nozzle at the final current zero with two models are given in Fig.3.5.17. The maximum temperature using standard k-ε model is 1000 K higher than that using the modified k-ε model.

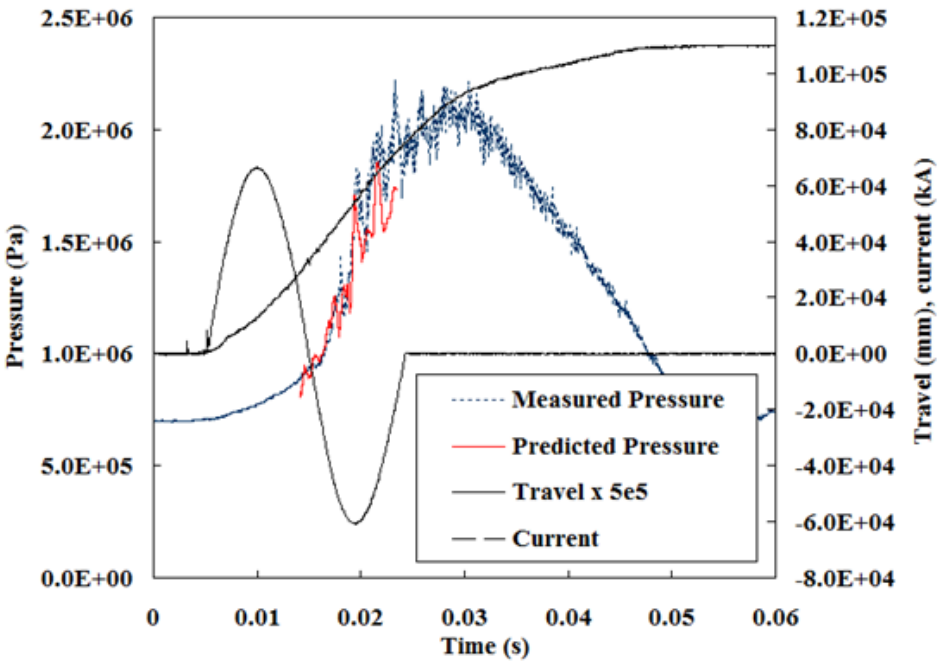

Fig.3.5.10: Predicted pressure by using modified k-ε model in cylinder for the case of 47 kA High Current Phase is represented by red curve. The current and contact travel are also given.

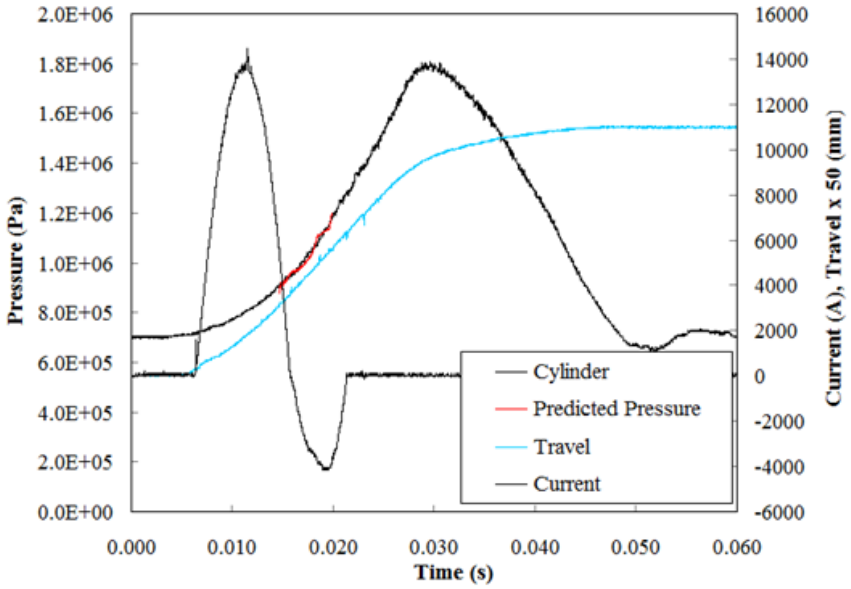

Fig.3.5.11: Predicted pressure by using modified k-ε model in cylinder for the case of 10 kA is represented by red curve. The current and contact travel are given.

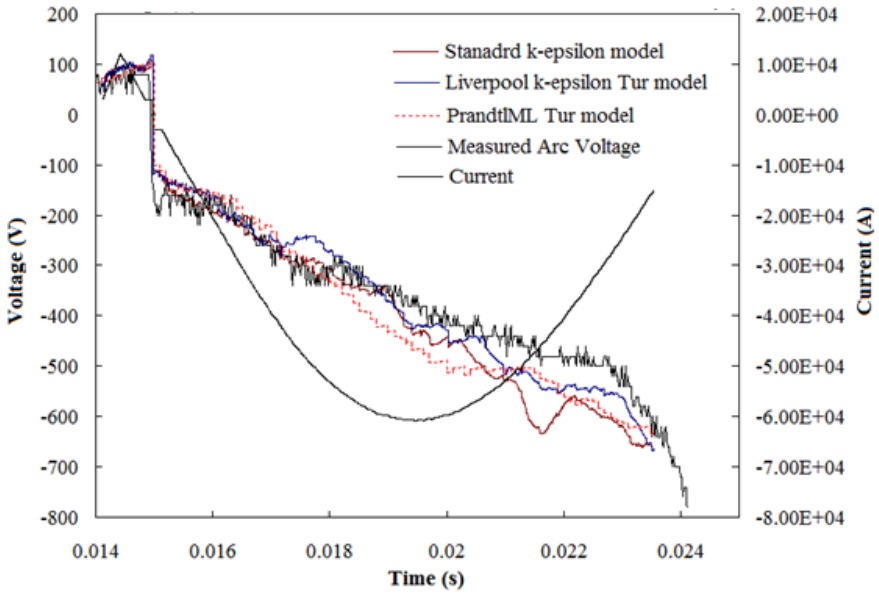

Fig.3.5.12: Predicted arc voltage for the high current phase with various turbulence models of the 47kA case.

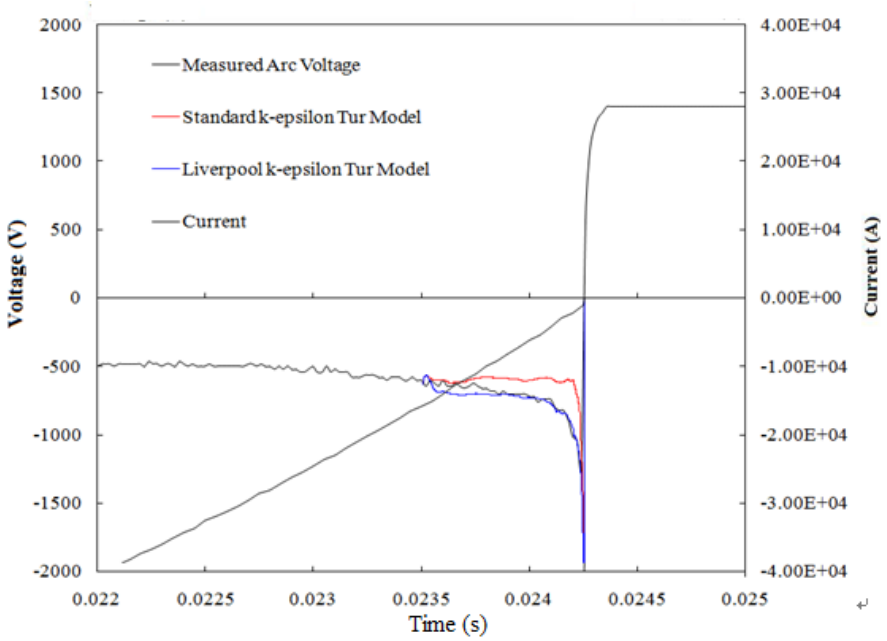

Fig.3.5.13: Predicted arc voltage for the current zero phase with various turbulence models of the 47kA case.

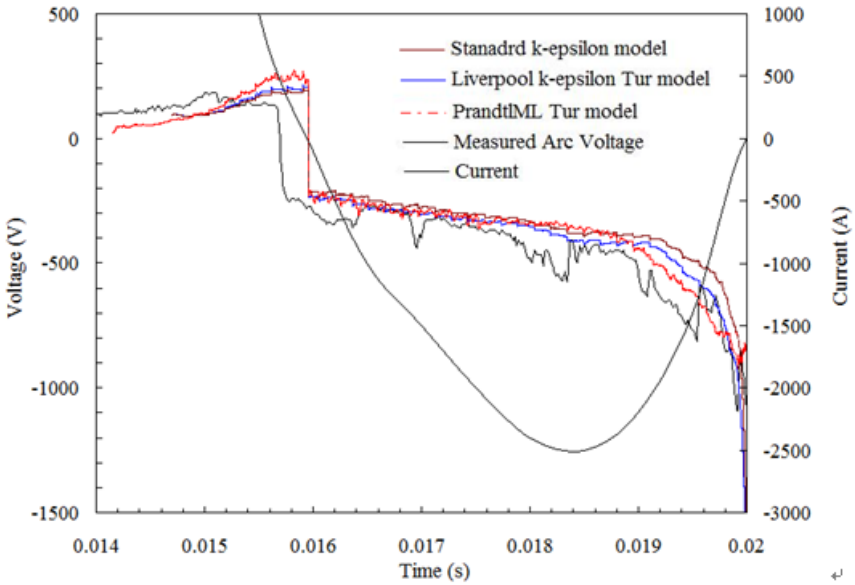

Fig.3.5.14: Predicted arc voltage before the final current zero period with various turbulence models of the 10kA case.

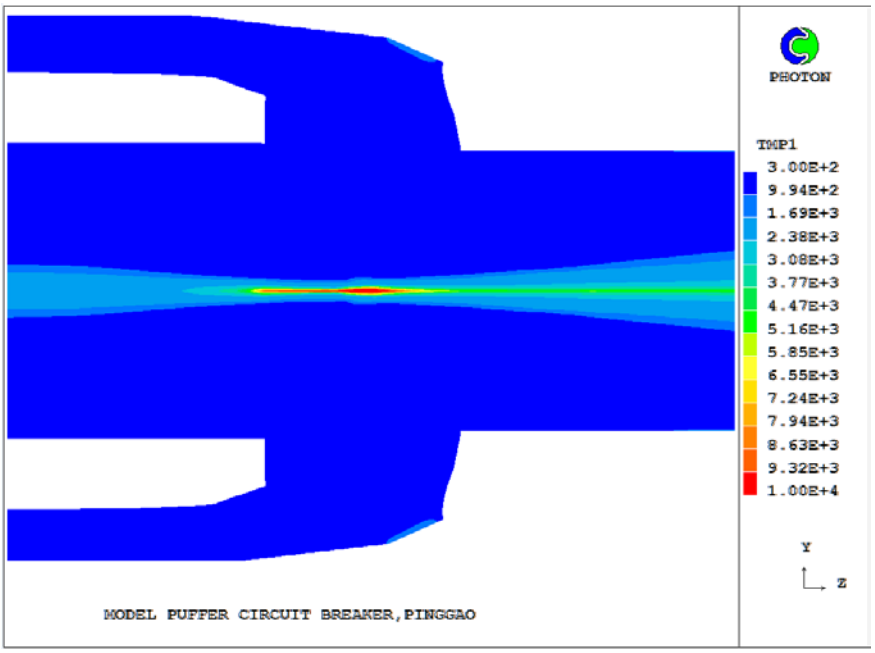

Fig.3.5.15: Temperature distribution by using standard k-ε turbulence model at current zero for the 10 kA case.

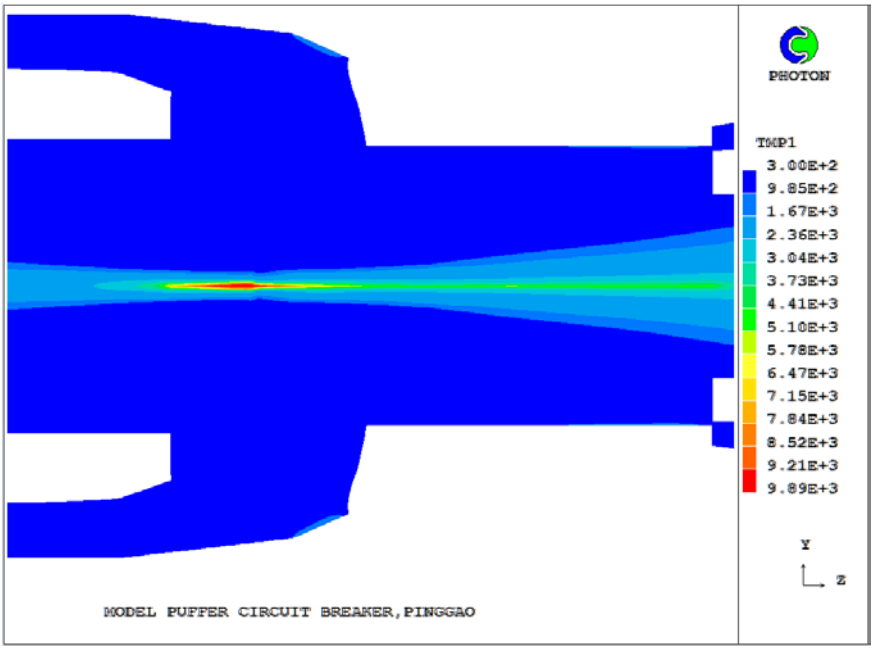

Fig.3.5.16: Temperature distribution by using modified k-ε turbulence model at current zero for the 10 kA case.

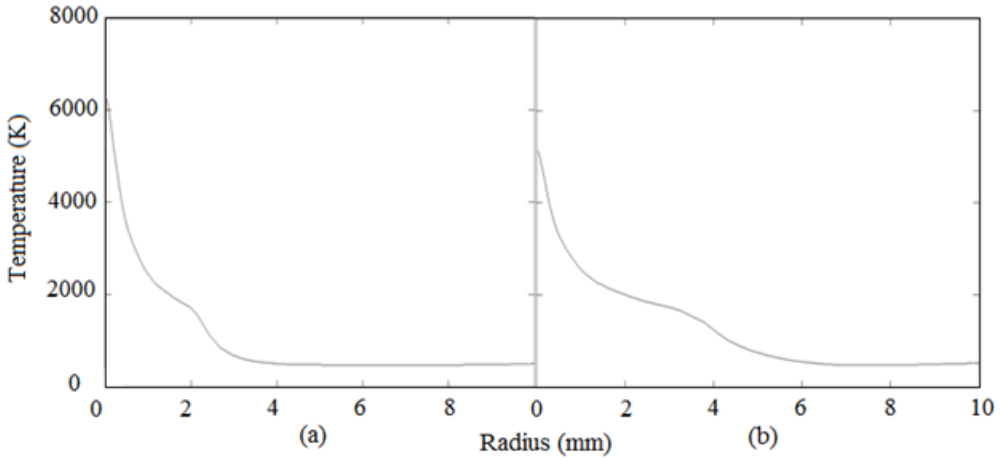

Fig.3.5.17: Radial temperature distribution plotted by PHOTON at nozzle throat by (a) standard k-ε turbulence model and (b) modified k-ε turbulence model.

3.6 Summary

The standard k-ε turbulence model is modified to take into account the approximate effect of steep temperature gradient at the arc edge, which is applied to different types of nozzle arcs and switching arcs to verify its applicability and accuracy in this Chapter.

The radial temperature profile measurement provided by RWTH Aachen University is first used to verify the modified k-ε model. The standard k-ε model under-represents at 1800 A and over-represents at 100 A the turbulence effect in arc cooling. The modified k-ε model significantly improves the prediction at 1800 A. The modified k-ε model can correctly predict reasonable results for the 600 A and 1800 A cases as good as the prediction of the Prandtl mixing length model, and without the problem of adjustable parameter. Its applicability is considered better than the Prandtl mixing length model, the accuracy of the modified k-e model is acceptable for the Aachen nozzle cases.

The modified k-ε model is then applied to the transient cases of Campbell nozzle [90] and GE nozzle [91]. These two nozzles have two completely different nozzle shapes and structures. The modified k-ε model can predict accurately the most cases for these two nozzle arcs within all default settings. A detailed conclusion will be given in Section 5.1.1.2 and 5.1.1.3.

The modified k-ε turbulence model was finally applied to the PINGGAO 252 kV puffer type circuit breaker with two current levels of 10 kA and 47 kA. For 10 kA case, the prediction of arc voltage by standard k-ε model is lower than the measured voltage. The arc voltage predicted by the modified k-e model is much larger than the arc voltage predicted by standard k-ε model, especially around the final current zero. For the 47 kA case, the arc voltage predicted by the modified k-ε model is much closer than the standard k-ε model. Both cases proved that the turbulence effect is increased successful by the modified k-ε model when compared to the standard k-ε model, especially near the final current zero.

The applicability and accuracy of the modified k-ε model can be verified by the most cases in this chapter. The coefficient of temperature gradient is not sensitive, which does not need to be adjusted when using different nozzle and switching arcs. For the applicability of the k-ε turbulence model, it is a major advance.

CHAPTER 4
Influence of Design Parameters on the Performance of Auto- Expansion Circuit Breakers

4.1 Introduction

Auto-expansion circuit breaker, a new technique of arc interruption, using arc's energy to generate the flow and thermal conditions for arc quenching. Two important factors affecting the thermal interruption performance and the subsequent dielectric recovery process are the pressure build-up in the expansion volume in the high current phase and the flow reversal in the heating channel before current zero to establish necessary flow conditions for arc cooling [118].

Pressure build-up in the expansion volume only creates a global condition for arc quenching at current zero. The formation of the flow and thermodynamic environment in the arcing chamber can be divided into three groups, especially in the contact space.

1) The pressurisation in the expansion volume is a result of the incoming energy flux instead of mass flux.

2) The dimension and geometry of the auxiliary nozzle are important in shaping of the pressure variation.

3) The pressure variation in the contact space is a result of the race of two competing processes.

It is known that the arc interruption mechanism is complicated in the auto-expansion circuit breaker. Regarding the design of the circuit breaker, the pressurisation of the expansion volume is one of the most important issues which is influenced by many factors, such as the interruption current, the arcing time, speed of contact, volume of expansion volume, dimension of heating channel, length of auxiliary nozzle, and the structure of the nozzle.

Apparently, simulation can highly reduce the cost and time in the development and optimisation for an auto-expansion circuit breaker. Several attempts [124, 125] based on the high voltage auto-expansion circuit breaker have been made to study the influence of design parameters. However, there is not sufficient in-depth analysis were given on the effects of design changes on the arc and flow behaviour in the whole arcing period and the effect of the interruption capability.

This chapter is concerned with the development of the PC based computer simulation and design tools for auto-expansion circuit breakers. PHOENICS, has been chosen to develop the arc model for the auto-expansion circuit breaker. By applying a commercial CFD package for the simulation of circuit breaker is still very new [126]. Rutten [127] firstly published a simulation work for circuit breaker in 1992. Classens et al. [128] coded a simplified, 2-zone arc model for high current phase by a CFD package, which it is restrictive and only valid for ablation dominated arcs of auto-expansion circuit breaker.

The present investigation in this chapter aims at obtaining the optimised key design parameters on auto-expansion circuit breaker performance in terms of the arcing conditions at current zero as well as the critical RRRV. The work is based on an ABB prototype auto-expansion circuit breaker rated at 245 kV at 50 Hz. The effects of using different auxiliary nozzle lengths and gas leakage

from the expansion volume are studied in this section. The influence of other design parameters was studied previously [129]. The arc model has been described in Chapter 2 and implemented in a commercially computational fluid dynamics (CFD) package, PHOENICS [117].

4.2 Geometry and Grid System

Geometry of the ABB auto-expansion circuit breaker 170PM40 arcing chamber is shown in Fig.4.1 and Fig.4.2. The expansion volume is 8.8×10^{-5} m^3 and the volume of heating channel is 1.1×10^{-5} m^3. The length of the heating channel is about 83 mm. The expansion volume has a length (horizontal dimension) of 86.5 mm and a radial span of 36.25 mm. The main nozzle has a diameter of 22 mm. The diameter of the auxiliary nozzle is 19.1 mm and that of the solid contact (moving contact) in simulation is also 19.1 mm.

In previous studies, the round tip of the solid contact was approximated by a flat tip due to restrictions imposed on moving objects (Fig.4.3(a)). This approximation leads to a change of the flow field in front of the contact tip as well as the effective flow cross sectional area between the solid contact and the nozzle.

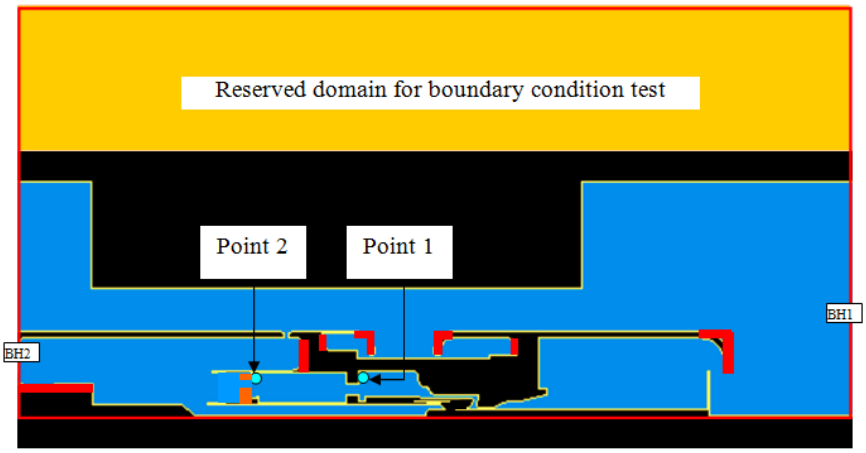

Fig.4.1: Geometry of 245 kV ABB 170PM40(SW10) auto-expansion circuit breaker.

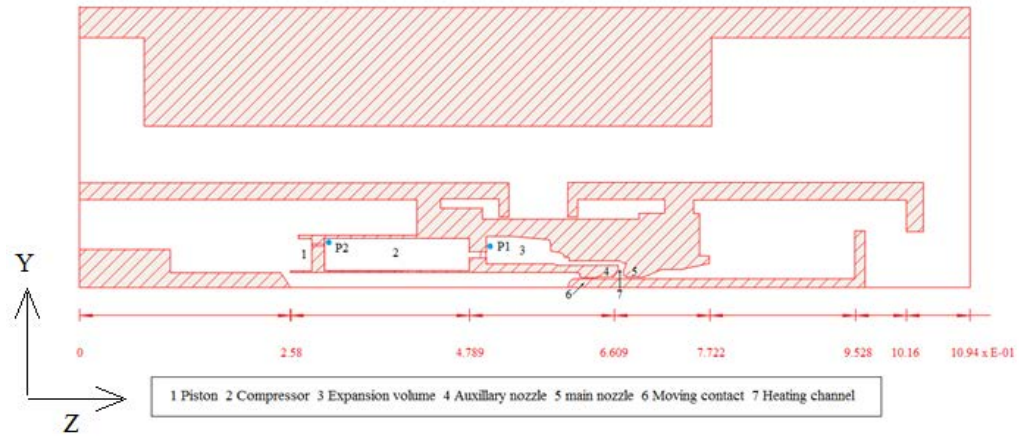

Fig.4.2: Schematic diagram of the ABB Auto-Expansion Circuit Breaker.

In the present work, the shape of the contact tip is modelled using multiple patches (Fig.4.3(b)) to represent the shape of the round tipped contact in arc simulation. Thus, more patches are needed to be used in the Q1 file and more settings to be made in the ground.for file. Two transparent arc roots are used in front of each contact tip to represent arc attachment on both contacts (as shown in Fig.4.3) and especially in the presence of hollow contact, from shrinking to an unreasonable small radius as a result of unrealistic magnetic pinch and axisymmetric treatment of the arc column, in particular the arc root. Transparent contacts in Fig.4.4 (red part on the left) have the highest value of $1.0\times10^{5}\ \Omega^{-1}m^{-1}$. The radius of the circular region covered by the transparent arc root (Fig.4.4) which has a typical value of $1.0\times10^{4}\Omega^{-1}m^{-1}$. A uniform current density is specified as the boundary condition of the electrostatic potential equation determined by:

$$R_{root} = \sqrt{\frac{I}{\pi J_{root}}} \tag{4.1}$$

where J_{root} = $5x10^{7}$ A/m^2 to $2x10^{8}$ A/m^2. A value of 1.5×10^{8} A/m^2 produces reasonable results for circuit breaker arcs.

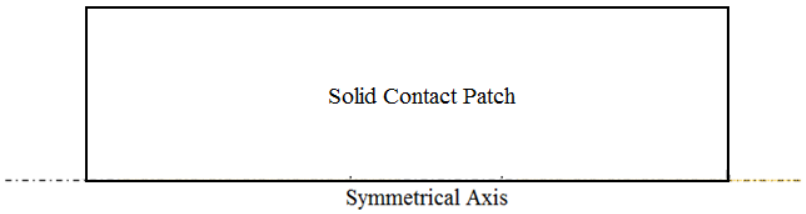

(a)

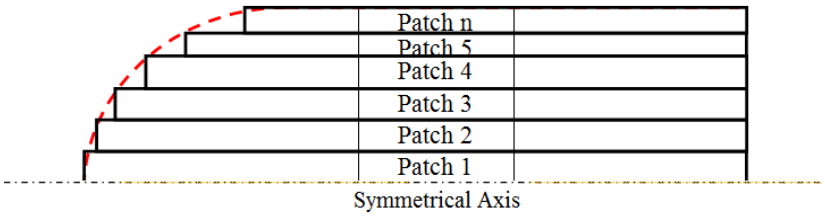

(b)

Fig.4.3: (a) Square corner solid contact with only one patch; (b) Formation of rounded solid moving contact by flat-tipped longitudinal cylinders.

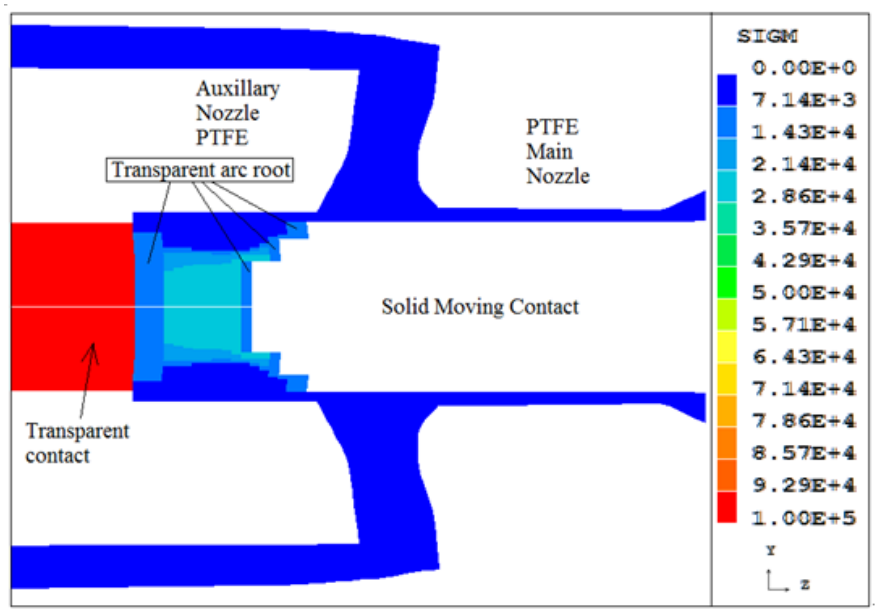

Fig.4.4: Schematic diagram of the transparent arc root implemented in front of the transparent contacts.

A BFC grid system (Fig.4.5) is used to model the complex geometry of the auto-expansion circuit breaker. The number of grids is 151 (radial) by 436 (axial) for the period from Cold Flow Phase to the end of the High Current Phase (15 kA before final current zero). Another number of grids of 236 (radial) by 436 (axial) are used for the Current Zero Period, and Post Arc Current Phase. This is because more grids are needed to resolve the rapid change of quantities in spare in Current Zero Phase, especially at the final current zero, when the arc column is extremely thin (Fig.4.6).

In the arc region, a radial cell size of 0.02 mm is used to resolve the change of flow and thermodynamic quantities (Fig.4.5). The pressure measurement points of P1 and P2 are given in Fig.4.1 and 4.2 with the circuit breaker at its fully closed position.

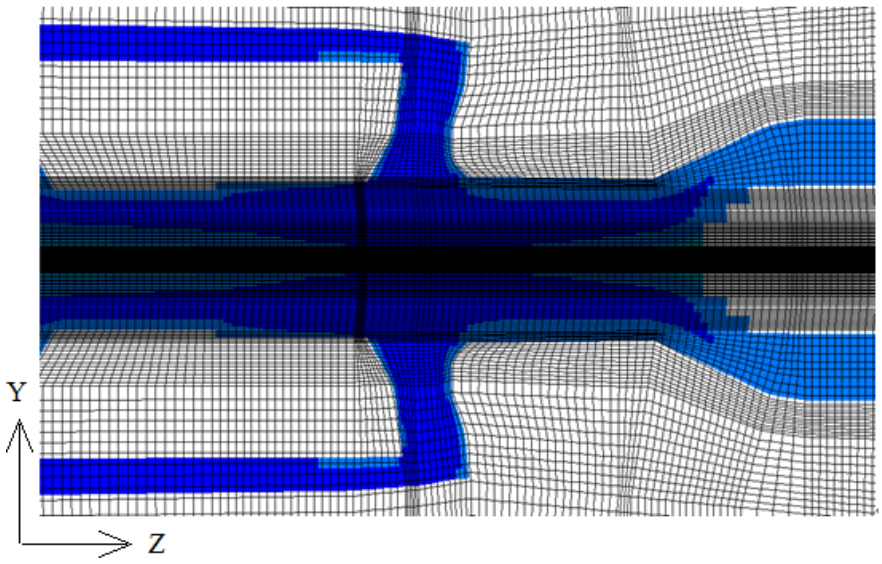

Fig.4.5: Grid system of the main nozzle part at Current Zero Phase.

Fig.4.6: Computational domain with temperature distribution before the current zero and the locations of three lines (L1, L2 and L3) are also shown.

4.3 Arcing Process before the Final Current Zero

The measured travel curve is shown in Fig.4.7 and the input file of travel is also compared with the measurement in Fig.4.7. According to the curve of travel, a time zero point will need to be decided and has been introduced in Section 4.5. The starting time of the high current phase is obtained from Cold Flow Phase when the contact separates about 5 to 8 mm with more than five cells in the radial direction.

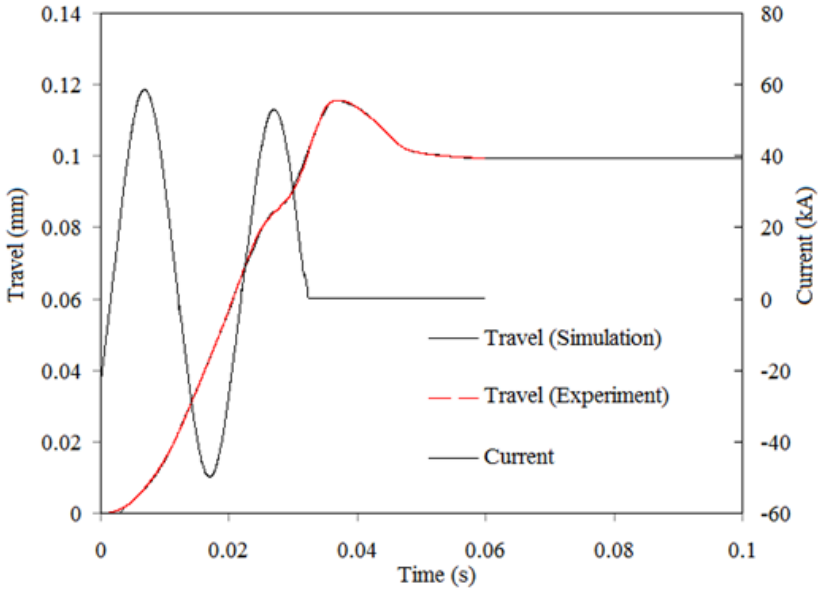

Fig.4.7: Comparison of Contact travel of using in experiment and simulation for the Ref. Case. Whole current wave is shown.

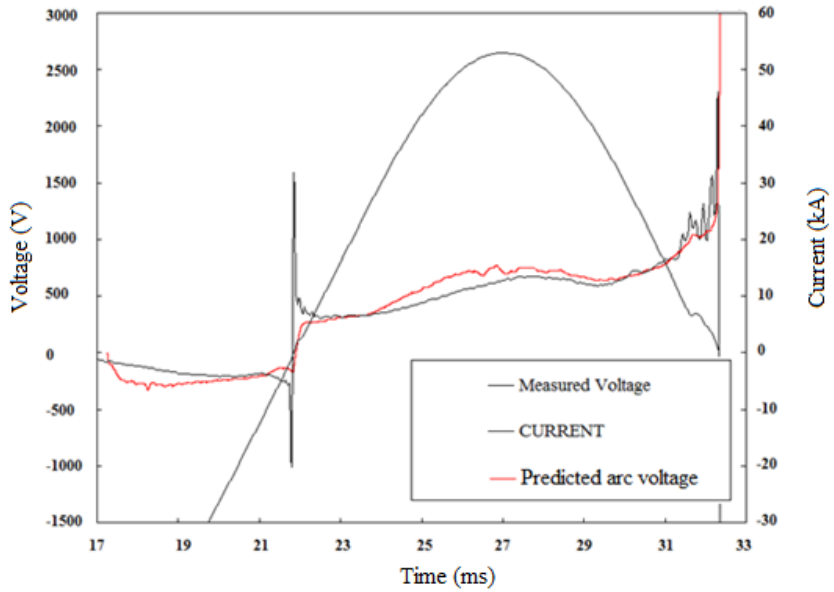

Fig.4.8: Current, measured and predicted voltage before the current zero for the Ref. Case.

A switching case with the test results available was simulated first. This case is referred to as the Ref. Case. The current waveform and predicted arc voltage of the Ref. Case is shown in Fig.4.8. The arc is initiated from 17.25 with a contact gap length of about 8 mm. The current is ramped up from 3 kA to about 48 kA in 0.3 ms to establish the arc. In the first two million-seconds (17 ms-19 ms), the predicted arc voltage is much higher than the measurement although the magnitude of the voltage is low. This is a consequence of the arc in initiation process at a small gap length. The largest difference between the prediction and the measurement is at 26.0 ms (1.0 ms before the peak current is reached). The predicted value is 702 V and the measured value is 555 V. The over prediction can be caused by different reasons, for example, the lack of accurate data of electrical conductivity at high pressure, the uncertainty in radiation re-absorption at the arc edge.

At 26.0 ms, the pressure inside the main nozzle is shown in Fig.4.9. It is more than 10.0 bar higher than the pressure in the expansion volume (Fig.4.10). There is pressure fluctuation in the expansion volume, which is due to a number of reasons. Firstly, there is change in the arc column size when the current changes. Secondly, the arc length increases when the live contact moves. These two factors cause pressure change in the contact space. As a result the pressure change propagates towards the expansion volume. The pressure wave is reflected at the walls of the expansion volume and as a result pressure fluctuation is generated. This type of pressure fluctuation is also observed in pressure measurement in commercial circuit breakers (Chapter 3, Fig.3.5.10 as an example). Since the use of accurate method to calculate radiation transfer in a circuit breaker is not computationally affordable, approximate models are normally used. With the current 1D radiation model, a

percentage of radiation absorption has to be assumed. A constant value of 50% is used in the present work. Figs.4.11 and 12 show that strong ablation of the nozzle by arc radiation generates vapour in flow towards of the arc column and confines the arc column to a radius of about 8 mm. by theory the resistance of the arc column is rather sensitive to the radius of the arc column since a change of δr will lead to a change of conduction area of $2\pi r\delta r$. the arc temperature immediately in front of the solid contact tip is rather high, reaching 38,000 K at an instantaneous current of 50 kA. Since the main nozzle is blocked, a stagnant region is formed in front of the contact tip with strong injection of vapour in the radial direction. It is reasonable to argue that radiation re-absorption at the arc edge for ablation dominated arcs at 30 kA or above should be more than 50 % of the radiation from the arc core.

The pressure variation inside the expansion volume which is recorded at Point 1 (P1) in Figs.4.1 and 4.2 is given in Fig.4.10. It can be found that the pressure changes smoothly with only small ripples superposed on it, which is caused by pressure wave propagations associated with contact movement and changing current. The predicted pressure variation follows closely the measurement. In the period up to 24 ms, the prediction is generally higher than the measurement by an average 1.5 bar. In the period of 25.0 ms to 27.0 ms, strong pressure waves are present which leading to higher predicted pressure in the expansion volume, in response to the higher predicted arc voltage. After the pressure peak, predicted pressure has a delayed drop in comparison with the measurement by 0.7 ms, despite the fact that the rate of change of pressure is more or less the same between 30.0 ms and 32.0 ms.

Dimension and length of auxiliary nozzle are very important parameters for design of auto-expansion circuit breaker. Two main reasons need to be

considered:

1) Ablation on its surface in the High Current Phase (Fig.4.18) enhances blockage of the gas flow through the auxiliary nozzle. Thus, it helps to build-up a high-pressure zone in the contact gap to pump thermal energy into the expansion volume.
2) It helps shape the gas flow around the arc column at current zero in a section of insulating nozzle. This is particularly important for short arc duration switching duties (Figs.4.13 and 4.14).

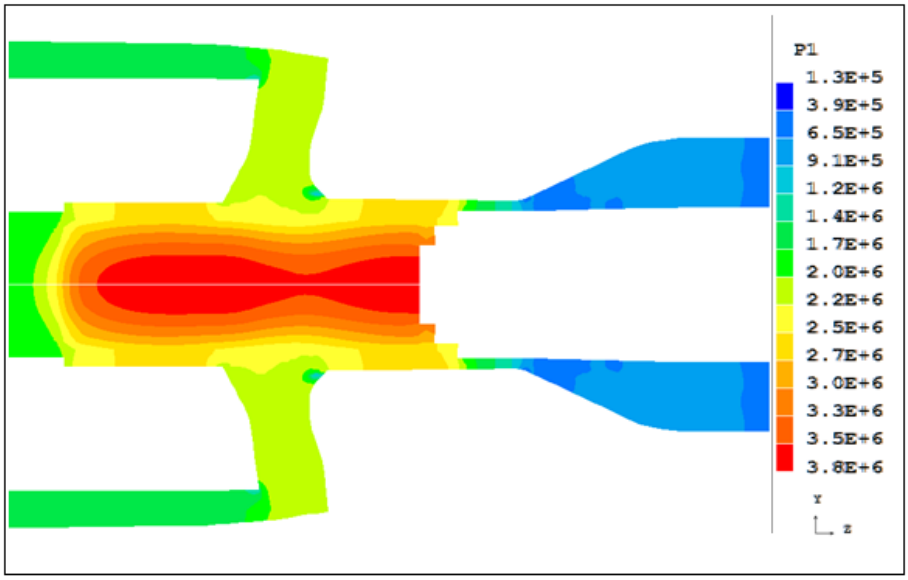

Fig.4.9: Pressure distribution inside the main nozzle at 26.0 ms.

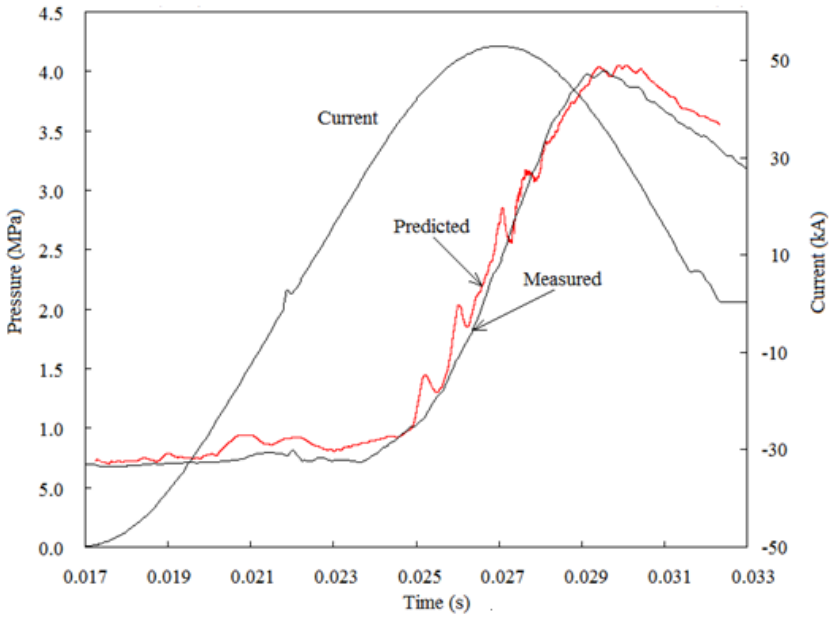

Fig.4.10: Measured and predicted pressure with current waveform in the expansion volume for the Ref. Case.

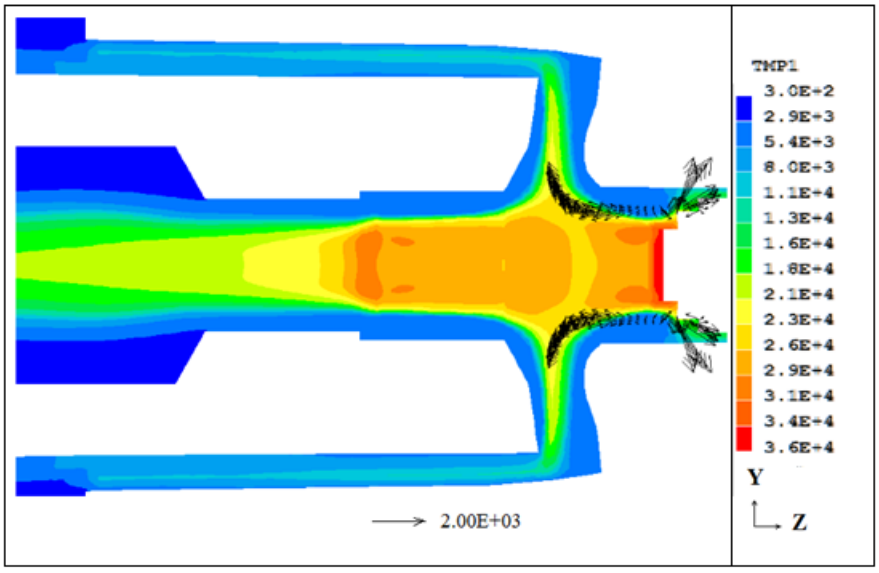

Fig.4.11: Temperature and velocity field at 25ms with a current of 42.5 kA for Ref. Case.

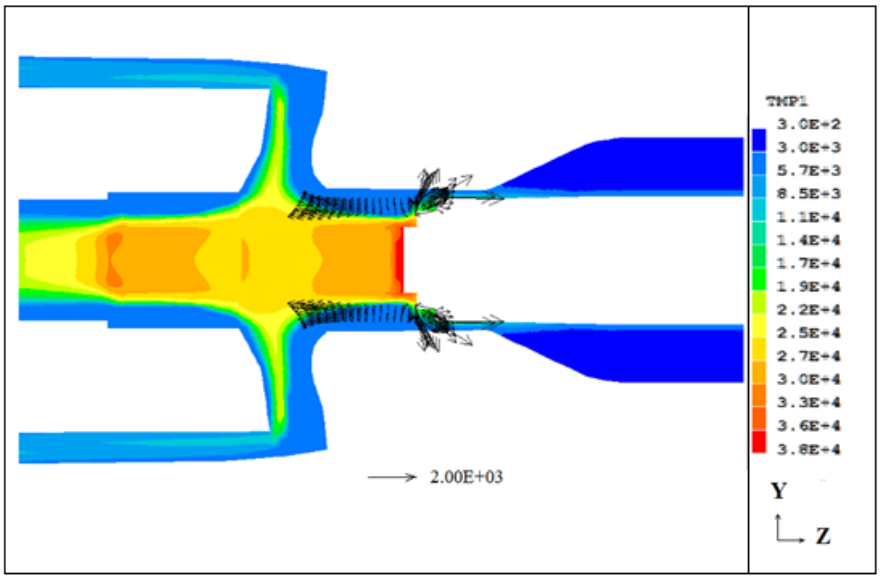

Fig.4.12: Temperature and velocity field at 26ms with a current of 50 kA for Ref. Case.

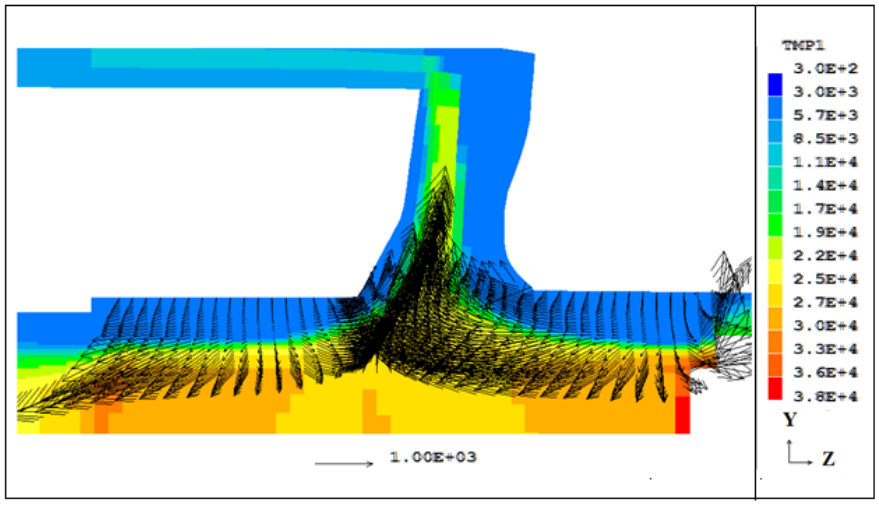

Fig.4.13: Arc column at high current phase with flow field.

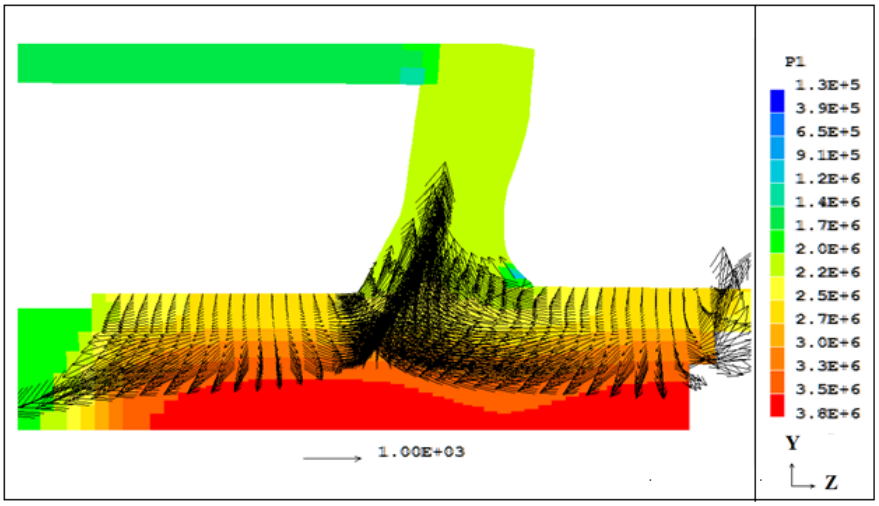

Fig.4.14: Pressure distribution in main nozzle with flow field.

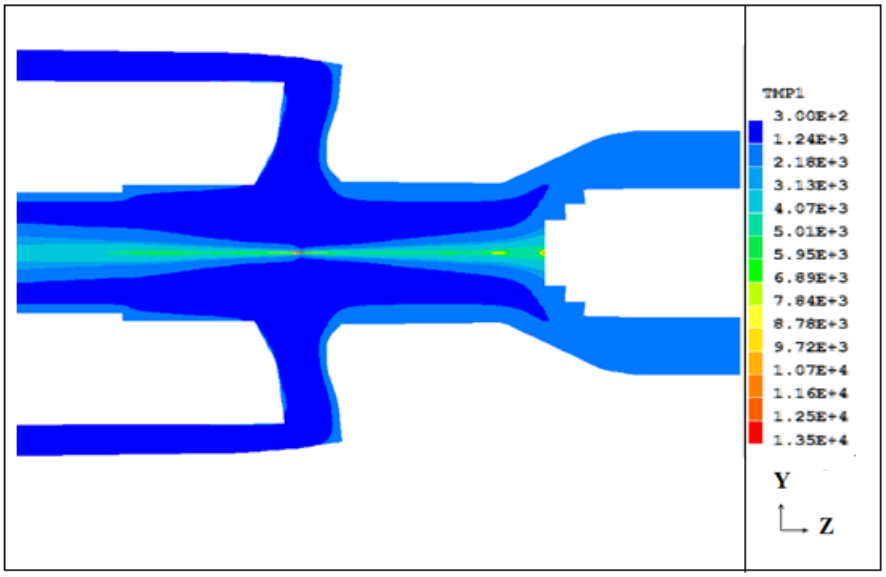

Fig.4.15: Temperature distribution at the final current zero for Ref. Case.

For the Ref. Case the predicted arc voltage agrees well with the measurement after the current peak, especially for a current lower than 30 kA. In a previous research of my group [119] on this circuit breaker, the arc voltage prediction is much lower than the measurement when the current approaches its final current zero displaying no sign of the extinction peak. This is a consequence of not property addressing the role of turbulence at low current. In the present work, the turbulence parameter is defined by:

$$c = c_H + (1 - \frac{|i|}{i_0})(c_0 - c_H) \tag{4.2}$$

where c_H is the turbulence parameter used for the High Current Phase, c the turbulence parameter used for the Current Zero Phase and the Post Arc Period, i_0 a threshold value defining the start of the Current Zero Phase. For this circuit breaker, $c_H = 0.05$, $c_0 = 0.3$ and $i_0 = 15$ kA.

The flow field and thermodynamic environment around current zero start to form when the gas flow reversal occurs in the heating channel occurs. This takes place after 29.5 ms as shown in Fig.4.16. Flow reversal is a result of reduced ablation strength after the current peak (i.e. Fig.4.17). When the current decreases towards its final current zero, the arc column becomes thinner and more cold gas from the expansion volume fills the arc surrounding area to build up strong turbulence flow for arc extinction. Figs.4.19 to 22 give a series of arc temperature distribution before current zero. A typical velocity field at current zero is given in Fig.4.23. The gas temperature in the arc surrounding region is only about 10,000 K and speed is 100.0 m/s.

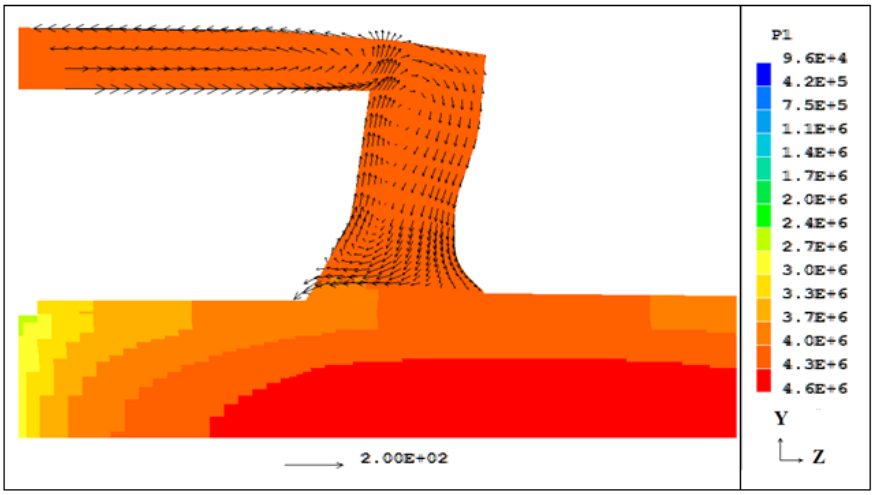

Fig.4.16: Flow field in heating channel at 29.5 ms.

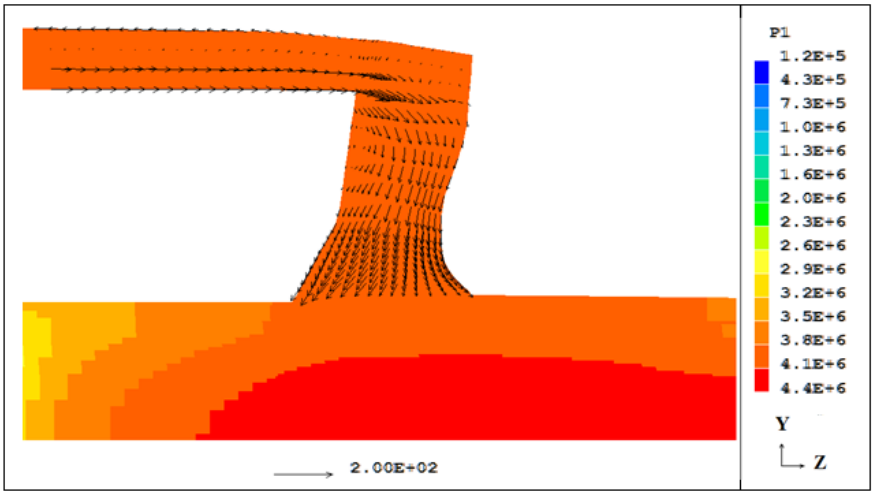

Fig.4.17: Flow field in heating channel at 30.0 ms.

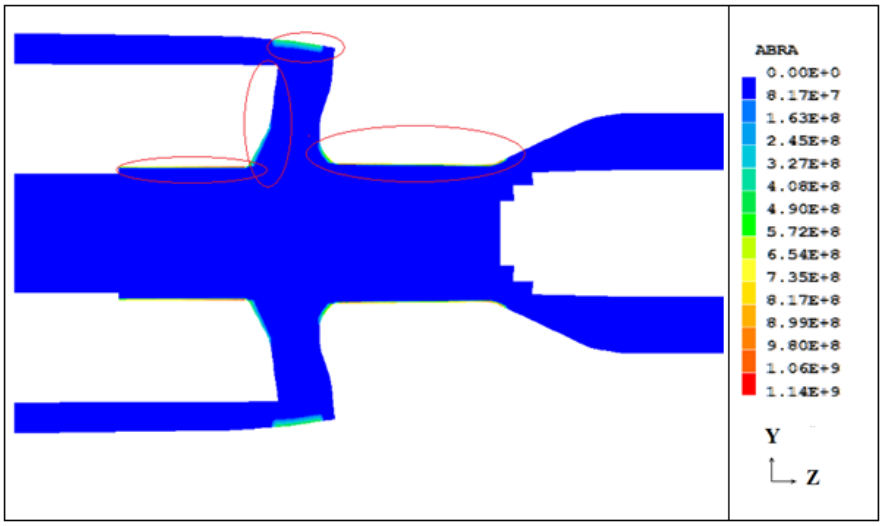

Fig.4.18: Ablation patches of Ref. Case where highlighted by red circle.

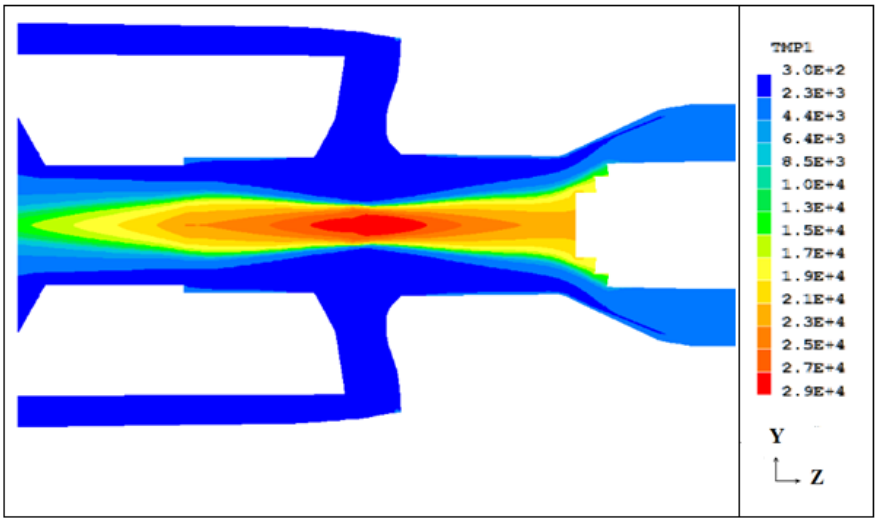

Fig: 4.19: Temperature distribution at 31.36 ms with a current of 10 kA before the final current zero.

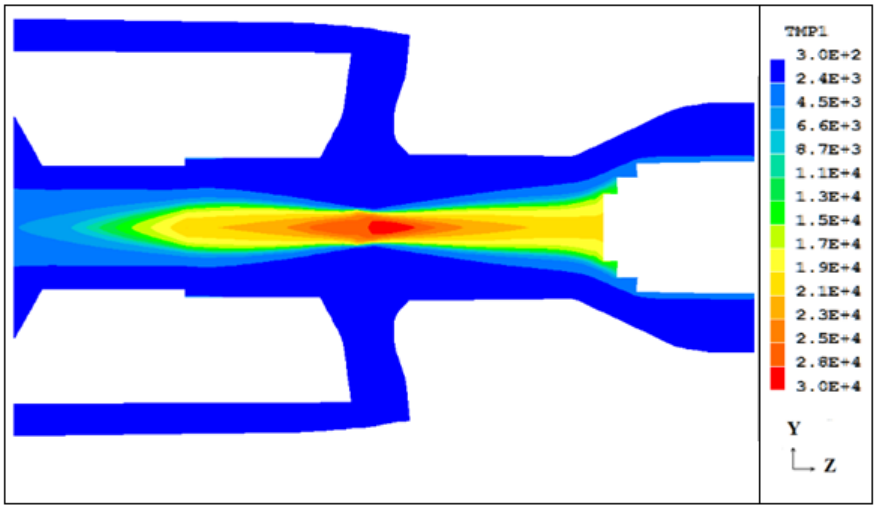

Fig.4.20: Temperature distribution at 31.76 ms with a current of 6.8 kA before the final current zero.

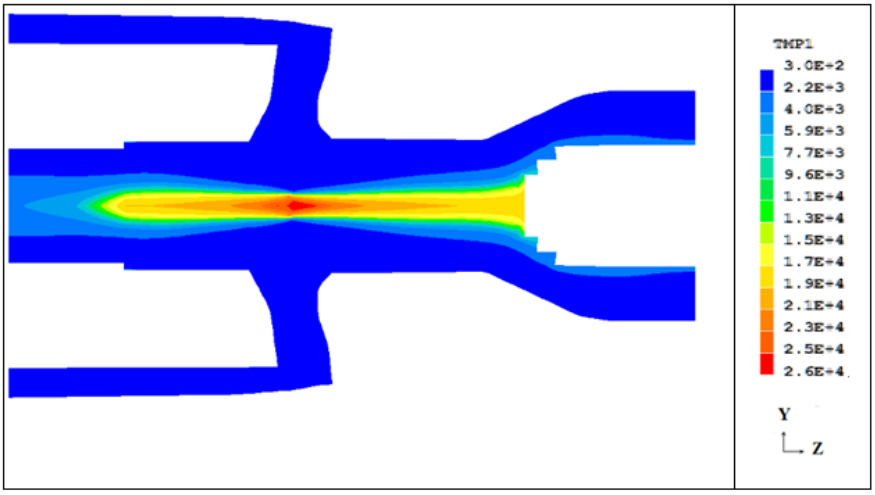

Fig.4.21: Temperature distribution at 32.16 ms with a current of 3.2 kA before the final current zero.

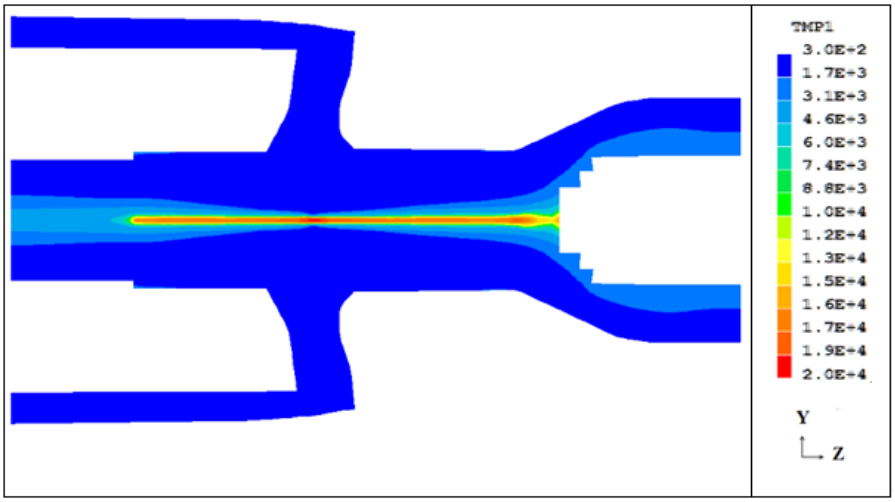

Fig.4.22: Temperature distribution at 32.3 ms with a current of 337 A before the final current zero.

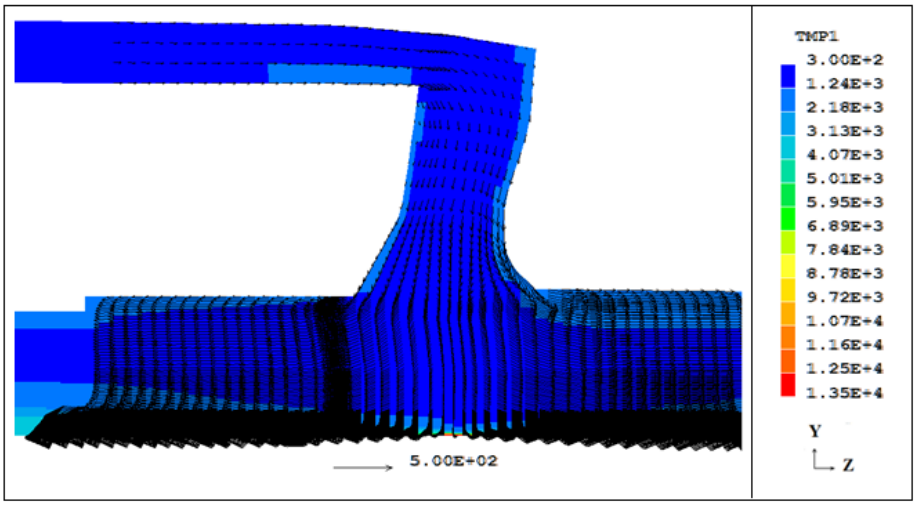

Fig.4.23: Velocity field at the final current zero.

4.4 Influence of Design Parameters

Design studies are divided into two parts. Part A is to investigate the influence of the length of the auxiliary nozzle, which will be introduced in Section 4.4.1. Four cases are studied which are listed in Table 4.1. Part B assesses the effects of interruption performance when a valve in the expansion volume has leakage. This detailed information is represented in Section 4.4.2. Another three cases are studied and representing in Table 4.2.

4.4.1 The effect of the length of the auxiliary nozzle

It is known that the length of auxiliary nozzle of Ref. Case is 2.0 cm. Three modified lengths of auxiliary nozzle have been represented in Fig.4.24. The ablation patch is surrounded to the inner surface of auxiliary nozzle (blue patch in Fig.4.24) and its length is depended on the length of auxiliary nozzle. It is shown that Case 0 which is the Ref. Case with a 2.0 cm length of auxiliary nozzle; a case of 18% longer length of auxiliary nozzle is represented as Case 1 with a 2.32 cm length. Case 2 and Case 3 have lengths of 1.64 and 1.0 cm, which is 18% and 50% shorter of the Ref. Case.

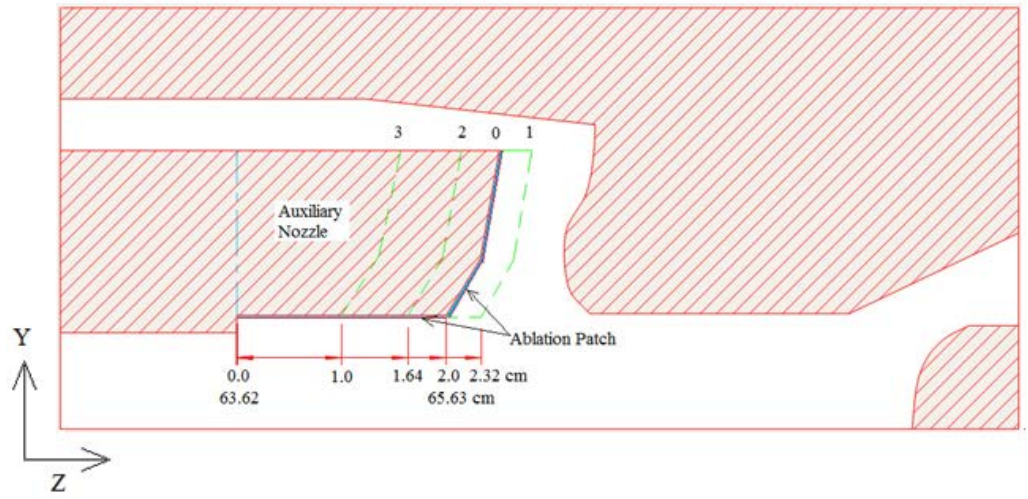

Fig.4.24: Auxiliary nozzle of Ref. Case (red) with three modifications (green).

Cases No.	Length of auxiliary nozzle (cm)
Case 0 (0)	2.0
Case 1 (1)	2.32
Case 2 (2)	1.64
Case 3 (3)	1.0
Case 4 (4)	0.0

Table 4.1: Cases with different lengths of auxiliary nozzle. One longer and two shorter auxiliary nozzles are used. The exact length depends on the number of cells selected. Case 4 only changed the length of the ablation patch to zero, the shape and length of the hollow contact is unchanged.

The pressure in the expansion volume for all of these cases are recorded and represented in Fig.4.25. It is noted that the maximum pressure of Ref. case is 4 bar and the Case 1 (with the longest auxiliary nozzle) is 4.25 bar, which is larger than all other cases. In Cases 2 and 3, the length of the auxiliary nozzle is shorter than the Ref. Case by 18% and 50%. The maximum pressure of Case 2 is 5% lower than the Ref. Case and almost 20% lower for Case 3. The maximum pressure of Case 4 is only 20 bar, 50% of that in Ref. Case.

The enthalpy flow rate for these cases in the heating channel (axial location is indicated by L1 (Fig.4.6)) is shown in Fig.4.26. The enthalpy flow rate is defined as:

$$H = \int_{R1}^{R2} w\rho h \cdot 2\pi r \delta r \tag{4.3}$$

where H is the enthalpy flow rate of the cross sectional area in heating channel at L1. R1 and R2 is the radial position of solid surface.

From Fig.4.26, the enthalpy flow rate of Case 1 is larger than other cases from 23 ms to 30 ms that means the enthalpy flow into the expansion volume is more than other cases. When the current reaches the peak, the gas flow into the expansion volume is the highest. The Ref. Case is slightly smaller than Case 1.

Case 2 is lower than the Ref. Case but not by too much. Case 3 lower than the Ref. Case about 20%. Case 4 is much lower than all other cases, only 7.0×10^6 J/s as the maximum value, lower than the Ref. Case about 60%. It can also be noted that gas flow back into the expansion volume of Case 3 is earlier than other cases after 17 ms. After this Case 2, Ref. Case and Case 1 start to flow back into the expansion volume one by one. The gas flow back into the expansion volume is affected by length of the auxiliary nozzle.

The change in arc voltage is directly associated with the change in arc column length, radius and temperature. The use of a longer auxiliary nozzle leads to stronger ablation and radial confinement of the arc column, as Fig.4.28 shows.

A longer auxiliary nozzle gives rise to a larger arc voltage. The results in Fig.4.27 show that the arc voltage at high current is no longer sensitive to ablation in the auxiliary nozzle once the length of the auxiliary nozzle is cut by 50%. The two overlapped arc voltages of Case 3 and Case 4 around the current peak evidence this. The difference in arc voltage at the current peak between Case 1 and Case 4 is 80 V, which is 11% of the measured arc voltage. Clearly in Case 4, the gas flow in the nozzle is weaker than in the other cases when the current approaches the final current zero point leading to weaker convection and turbulent arc cooling. The radial distribution of the dynamic viscosity at the middle point of the main nozzle is shown in Fig.4.29, as a result the arc resistance in Case 4 is lower, leading to a lower predicted extinction peak.

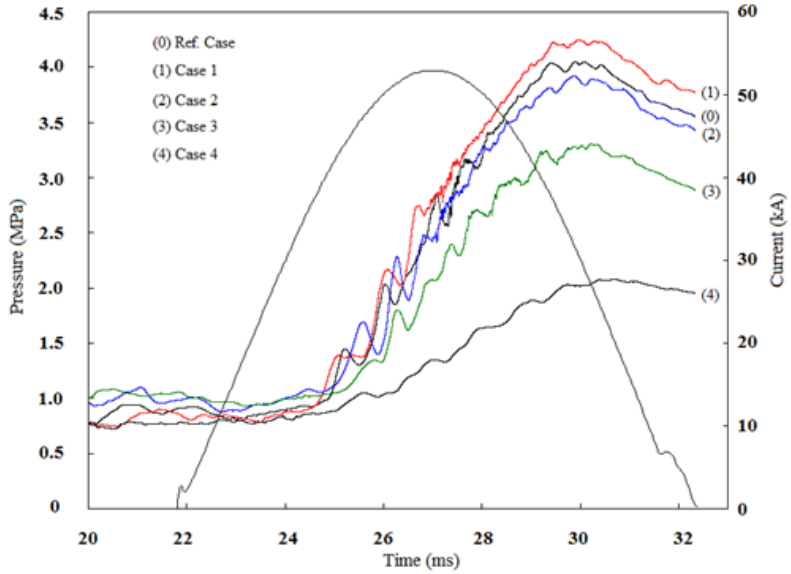

Fig.4.25: Predicted pressure rise in the expansion volume for various effective lengths of the auxiliary nozzle.

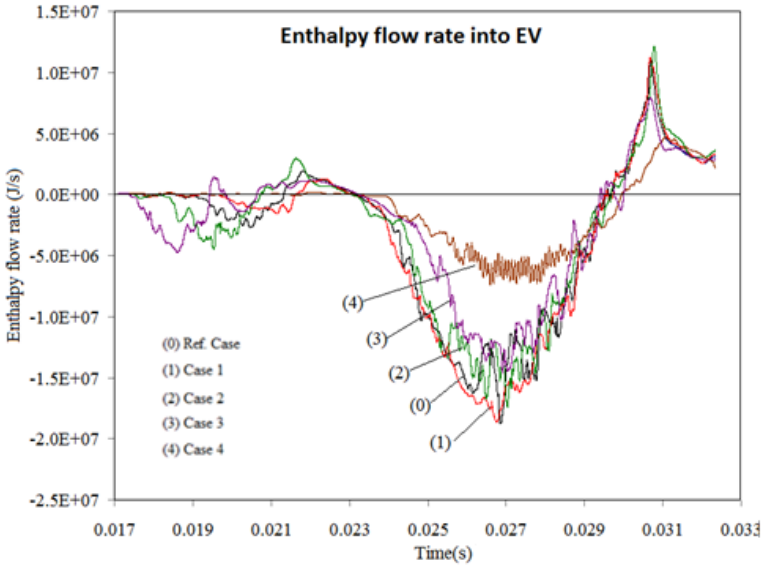

Fig.4.26: Enthalpy flow rate evaluated along Line L1.

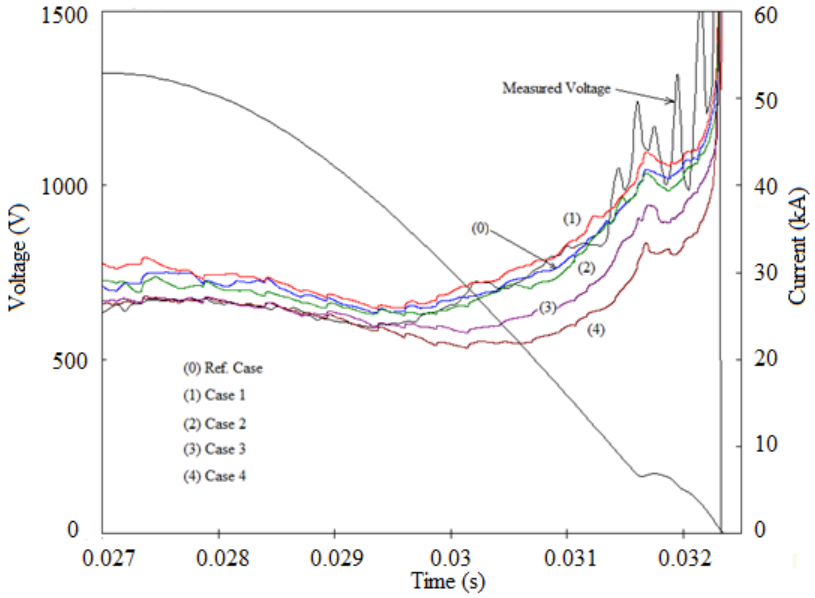

Fig.4.27: Measured and predicted arc voltage from the last current peak to the final current zero with extinction peak.

In Cases 1, 2, 3 and 4, the length of the auxiliary nozzle is different to give rise to different amount of PTFE vapour. Understanding the influence of the auxiliary nozzle length is important in the design of auto-expansion breakers. With a longer auxiliary nozzle (Case 1) the pressure increases rapidly to the peak value faster than other cases (Case 2, 3 and 4) which have shorter auxiliary nozzles, due to a larger amount of mass and energy flowing into the expansion volume. The mass and enthalpy flow rate at the outlet of flat throat of main nozzle (L3 in Fig.4.6) and that into the hollow contact (L1 in Fig.4.6) are plotted against time for the period shortly before the final current zero in Figs.4.30 to 4.33. While the mass flow rate increases with time. The enthalpy flow rate decreases, implying a shrinking arc column. By using a shorter auxiliary nozzle, less mass or energy is taken out of the main nozzle (Figs.4.32 to 4.33), which results in a fatter arc radius at the current zero when compared with the Ref. Case.

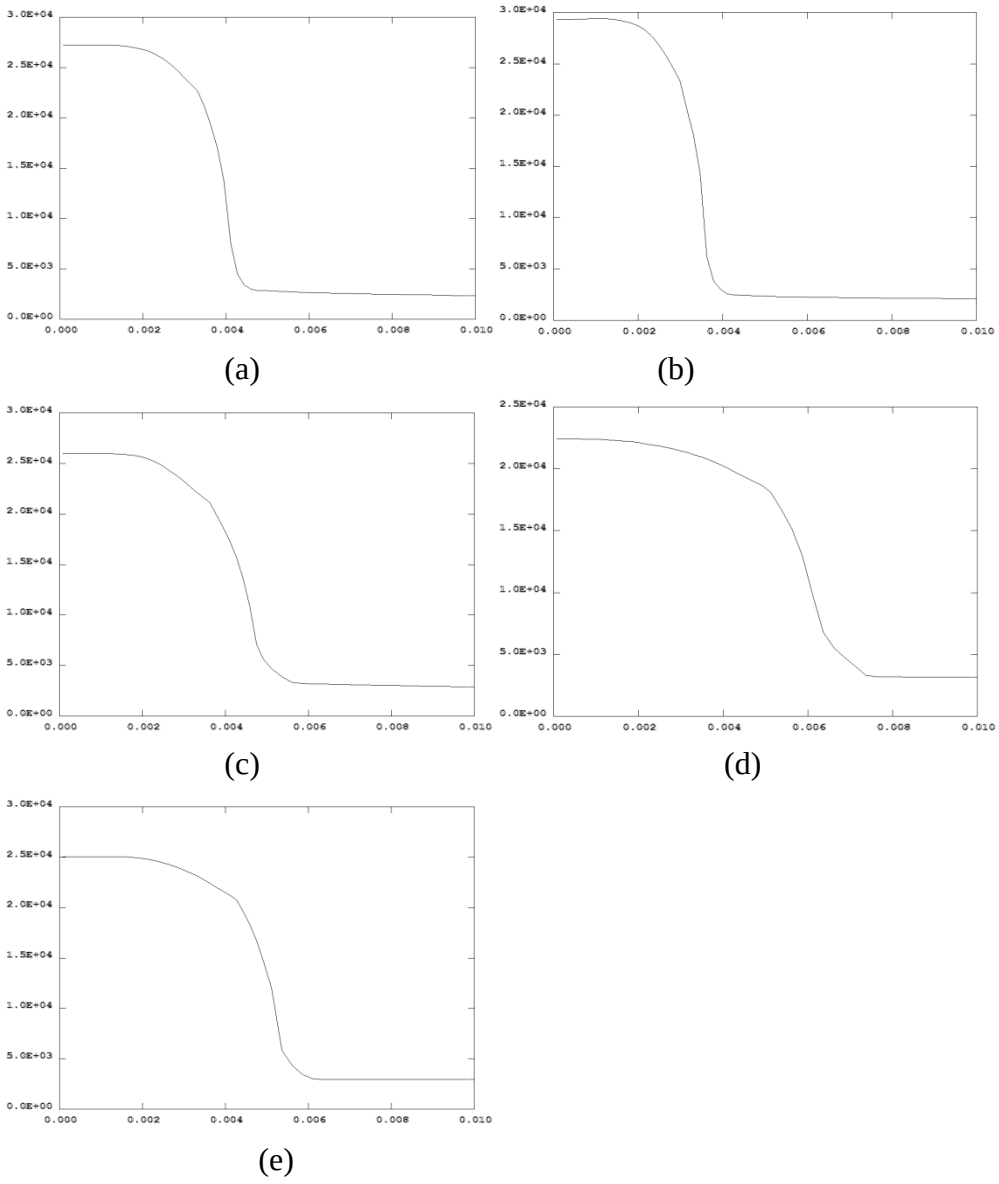

Fig.4.28: Radial temperature profile at nozzle throat at 31 ms. (a) Ref. Case (b) Case 1; (c) Case 2;(d) Case 3; (e) Case 4.

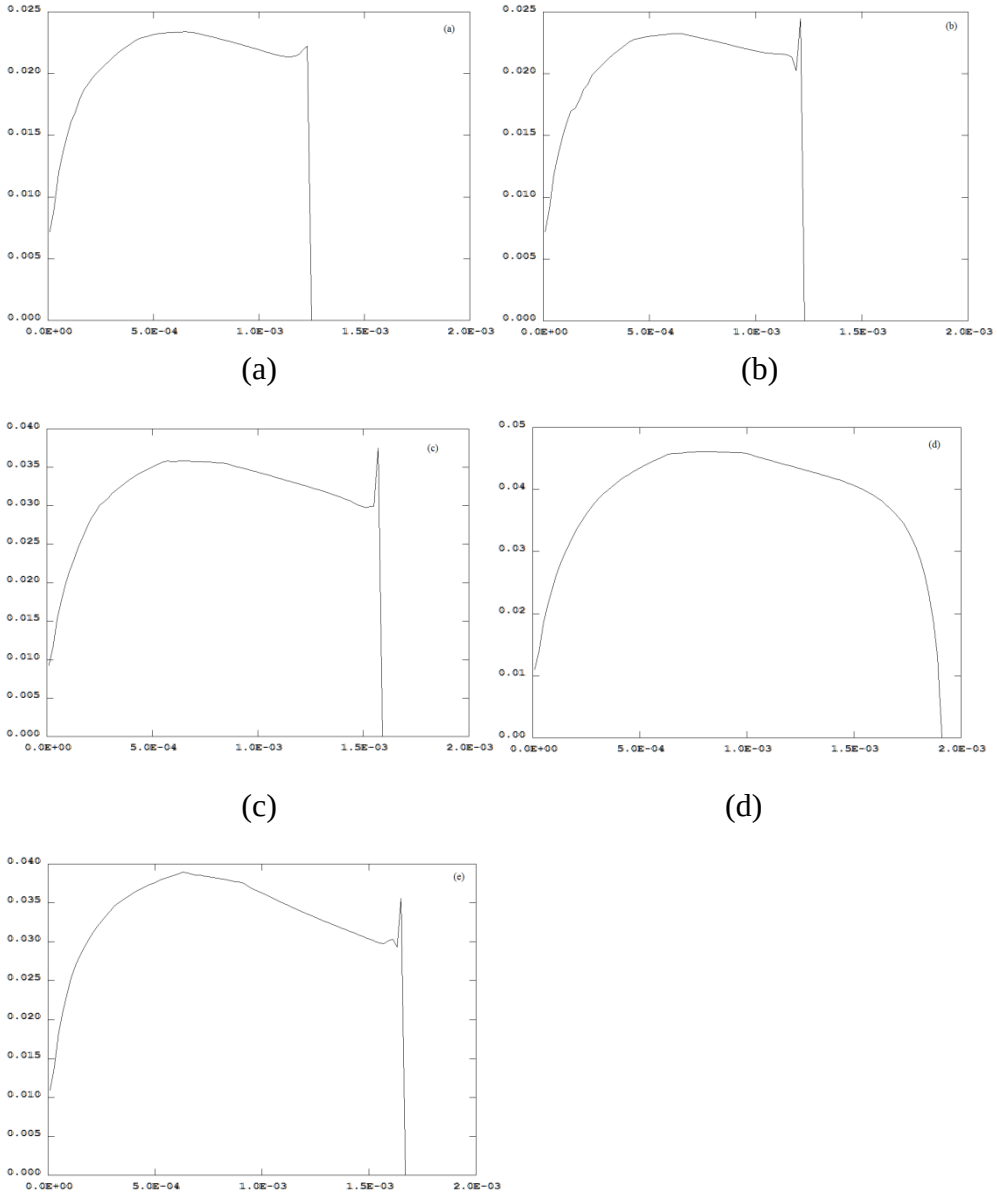

Fig.4.29: Radial distribution of the dynamic viscosity at the middle slab of the nozzle throat. (a) Ref. Case (b) Case 1; (c) Case 2 ; (d) Case 3; (e) Case 4.

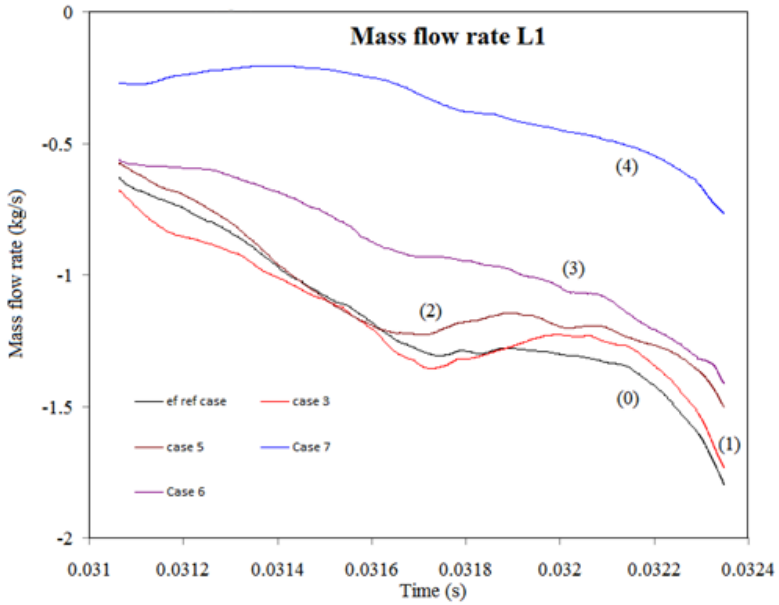

Fig4.30: Mass flow rate evaluated along Line L1 (in hollow contact).

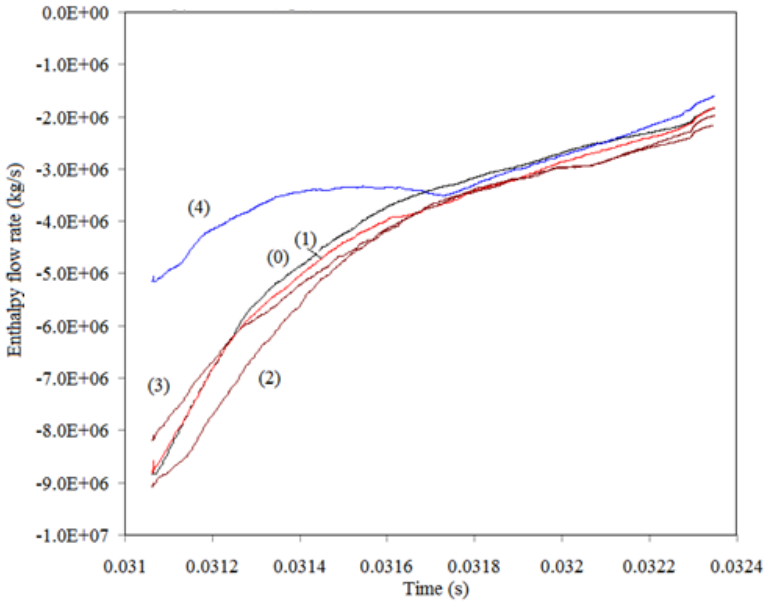

Fig.4.31: Enthalpy flow rate evaluated along Line L1 (in hollow contact).

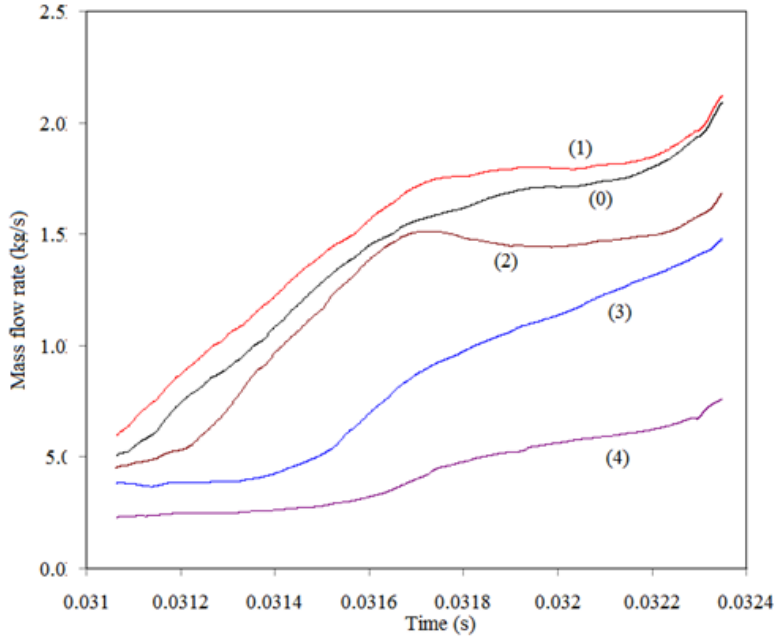

Fig.4.32: Mass flow rate evaluated along Line L3 (Main nozzle).

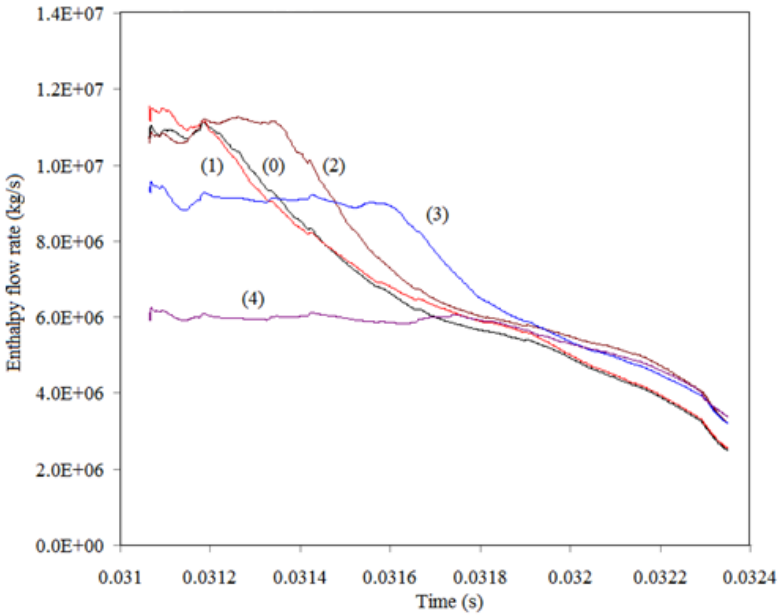

Fig.4.33: Enthalpy flow rate evaluated along Line L3 (Main nozzle).

4.4.2 Prediction of critical RRRV

Starting from the solution obtained at the end of the current zero period simulation, the behaviour of the plasma left between the two contacts can be assessed by applying different RRRV. The post arc current under different RRRVs can be obtained by running a number of simulations. A RRRV can be found below which will eventually be decreased by the Post Arc Current following an initial rise in a time scale about 10 μs to 20 μs. This RRRV is called the critical RRRV and is a direct measure of the thermal interruption capability of the circuit breaker under investigation. For the ABB auto-expansion circuit breaker, there is no measured result for the critical RRRV. So it is difficult to reliably predict the thermal interruption capability. The time scale of post arc current period is set as 20 μs to obtain a critical RRRV result of the Ref. Case (Fig.4.34), it is a criterion to compare with other cases.

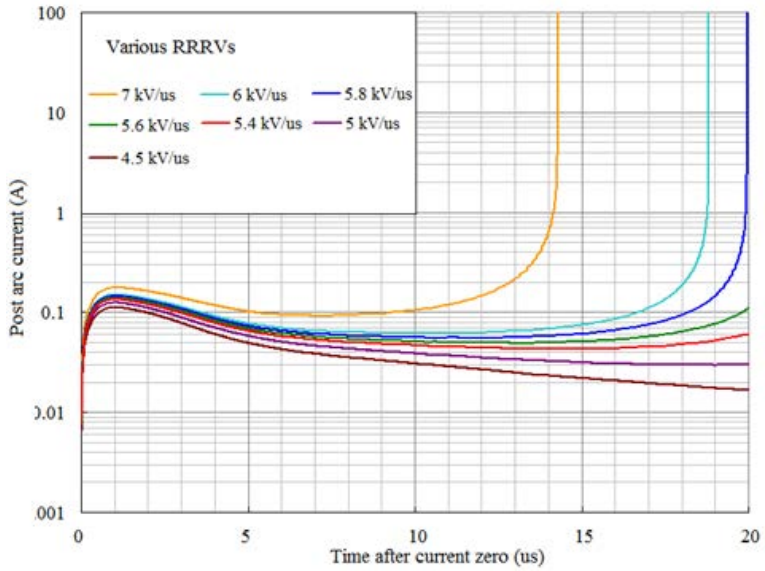

Fig.4.34: Post arc current as a function of time at different RRRV for the Ref. Case. The critical RRRV is between 5.4 kV to 5.6 kV.

The critical RRRV predicted for each case of Part A has been summarised in Table 4.2. The critical RRRV of Ref. Case is between 5.5 kV and 5.7 kV, 5.6 kV/μs is used as its critical RRRV. In Case 1, the critical RRRV is increased by 10% with the length of auxiliary nozzle, which is 18% longer than the Ref. Case. The interruption capability is increased when using a longer auxiliary nozzle. The predicted critical RRRV of Case 2 has very similar RRRVs with the Ref. Case, because of the sensitivity of prediction the critical RRRV of Case 2 is 5.6 as well. The critical RRRV is not affected too much when using a slightly shorter auxiliary nozzle. A much shorter auxiliary nozzle of Case 3 shows that the critical RRRV is much lower than the Ref. Case 10%. The interruption capability is significantly decreased when using a hollow contact without an auxiliary nozzle, it is can be found in Case 4, and the critical RRRV is much lower than the Ref. Case 25%. The pressure in the expansion volume of Case 4 is much lower than the Ref. Case as well. It is noted that the length of auxiliary nozzle is an important design parameter in auto-expansion circuit breaker. The interruption capability is increased when a slightly longer auxiliary nozzle is used, however its interruption capability is lowered when further reducing the length of the auxiliary nozzle due to much lower amount of PTFE vapour generated from the nozzle region. This is due to a relatively lower pressure in the arc region compared with the Ref. Case (Fig.4.35).

Cases No.	Critical RRRV (kV/μs)
Ref. Case	5.6
Case 1	6.2
Case 2	5.6
Case 3	5.0
Case 4	4.2

Table 4.2 Predicted RRRV with different auxiliary nozzle length.

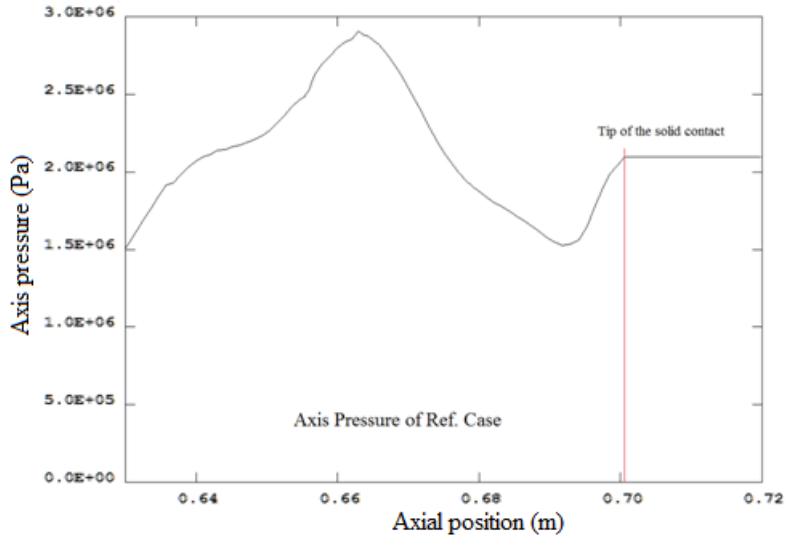

(a)

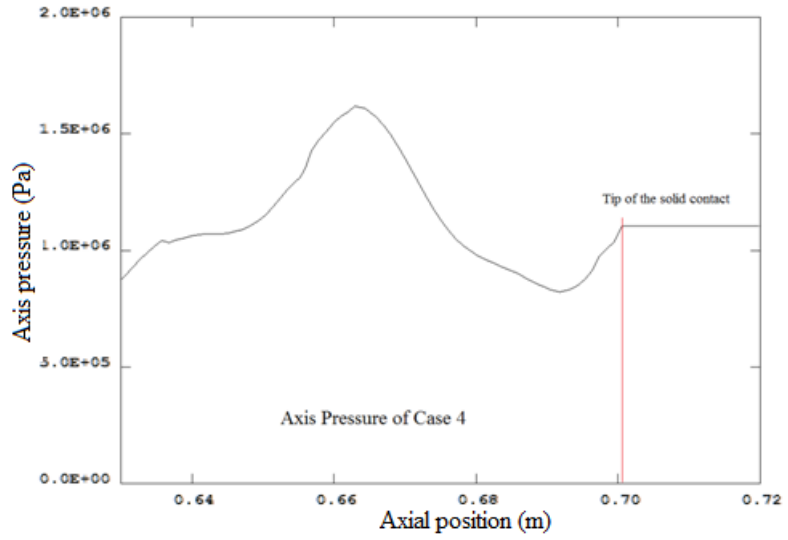

(b)

Fig.4.35: Comparison of pressure distributions on the axis for the Ref. Case (a) and Case 4 (b) at current zero. It is plotted by AUTOPLOT function of PHOENICS.

4.4.3 Leakage in expansion volume

Valve operation is an important aspect of simulation of the interruption process in an auto-expansion circuit breaker. In reality, the operation of over-pressure or unidirectional valves involves the movement of solid surface away or towards an annular opening located in a wall, as shown in Fig.4.36(a). The valve plate is pushed by a spring mechanism on the base plate. In simulation, the movement of the valve plate is not directly simulated. Instead its effect is considered. Assuming a pressure difference between the two faces of the valve plates exists, the net force is related to the effective flow area by consideration of gas dynamics. Thus, in the simulation, the size of the valve hole is controlled and varied according to the pressure difference. In the Liverpool model, I use the method of filling and evacuating of the annular holes based on the pressure difference in regions L and H and the area of the valve plate as shown in Fig.4.36(b). To simulate the changing gap in reality between the wall and the valve plate, the hole in the present simulation can be blocked at different percentage of its maximum cross sectional area.

When the valve hole increases its cross sectional area as a result of increased pressure difference between slab L and slab H, the solid cells need to be changed into gaseous cells. The mass required to fill the evacuated cells and the associated momentum and energy are drawn region H by decreasing the pressure in the cells proportional to the mass to be taken away. When cells in the hole are to be blocked due to reduced pressure differences between L and H, the mass, momentum and energy of the gas in the cells to be blocked are dumped into region H by proportionally increasing the pressure. The subroutine used to set up a valve on an annular plate is SUBMC02() in ground.for file which can be used for a valve on a moving or fixed plate. There

are two valves in the ABB auto-expansion circuit breaker (Fig.4.1 and Fig.4.2). The valve in the expansion volume is used for investing the effect of gas leakage.

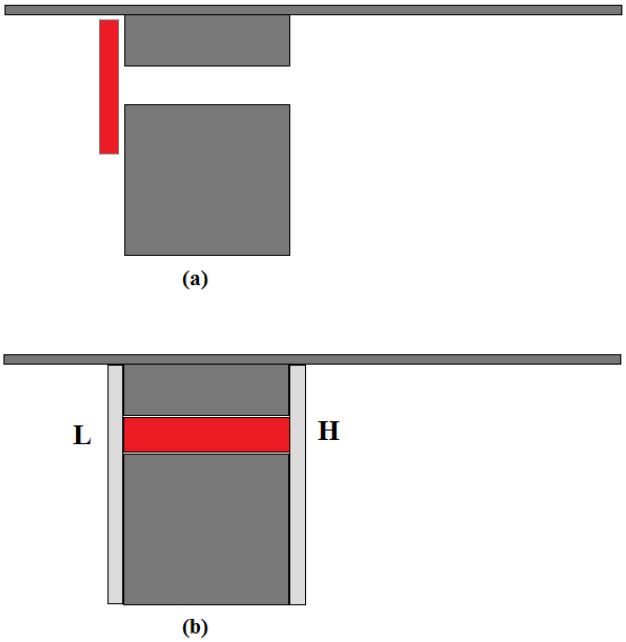

Fig.4.36: Diagram shows the difference of the valve (a) in reality and (b) simulation.

The cross sectional area of the ABB auto-expansion circuit breaker is difficult to draw. Thus, a simple structure of sample circuit breaker cross sectional area is drawn in Fig.4.37 to introduce the leakage effect in the expansion volume. As Fig.4.37 shows that the area from “o” to “a” is the nozzle interrupter region; the area from “a” to “d” is the wall of the expansion volume, and the area of “b” to “c” is the annular hole which is blocked by the valve patch. The area from “c” to “d” is the hole of leakage, where is always filling by gas. For convenience, the area of “b to c” is called as annular hole and “c to d” is called as leak hole (yellow area (region B) in Fig.4.37).

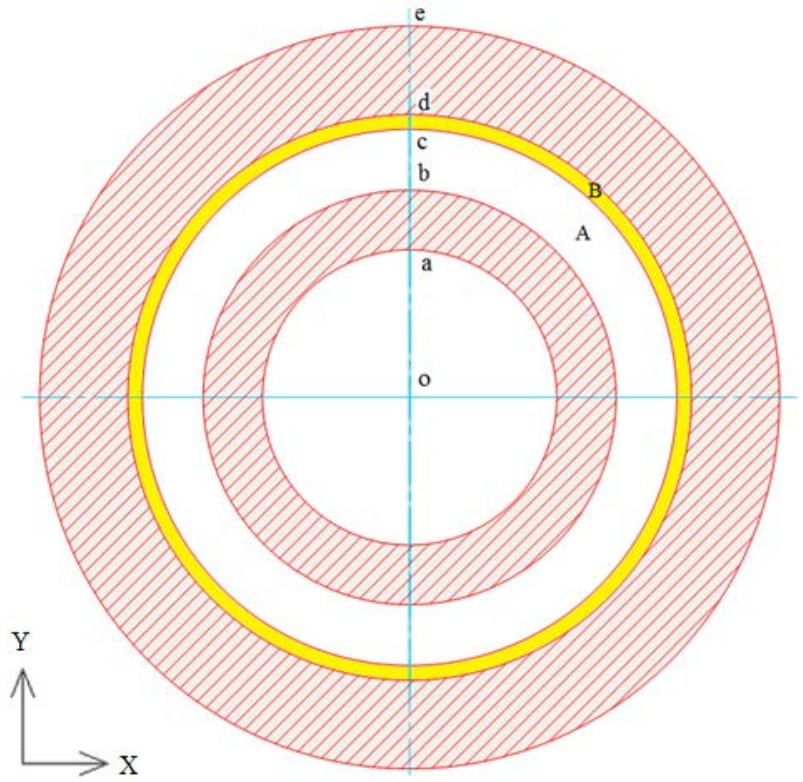

Fig.4.37: Cross sectional area of a sample circuit breaker with a valve.

The severity of leakage is modelled in three cases as shown in Table 4.3. The leak hole is close to the annular hole at the “NORTH” which has an annular area of 7, 10 and 15% of the area of the annular hole. In reality the ABB auto-expansion circuit breaker, the radial length of the annular hole is approximately equal to 1.25 cm (length of “b” to “c” in Fig.4.37). The cross sectional area of annular hole is about 30.0 cm^2. So the cases of L Case 1, 2 and 3 have their own cross sectional area of approximate 3.0, 2.1 and 4.5 cm^2. The level of leak depends on the minimum width of cells surrounding the annular hole.

Case Numbers	Percentage of leakage of valve
L Case 1 (1)	10%
L Case 2 (2)	7%
L Case 3 (3)	15%

Table 4.3: Cases with different percentages of valve leakage of expansion volume.

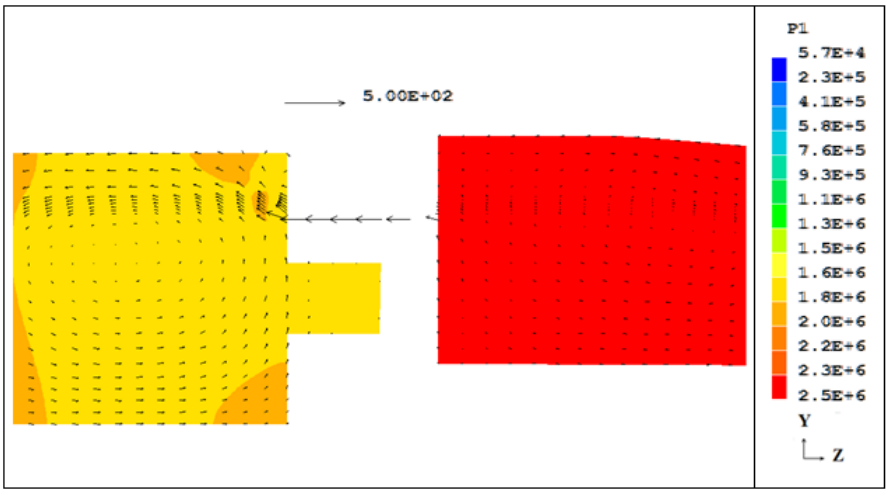

Fig.4.38: Pressure distribution and velocity field in the expansion volume and compression chamber.

Gas leaks from the expansion volume into the compression chamber are shown in Fig.4.38. Due to the display error of PHOTON of PHOENICS, the gaseous cells of leak hole cannot accurately display. The flow field through the leakage can be easily found in Fig.4.38.

A comparison study has been carried out for these cases with different severity of leakage. The predicted pressure in the expansion volume for these three cases and the Ref. Case is shown in Fig.4.39. The predicted pressures for all the cases shown in Fig.4.39 are more or less the same up to 27.0 ms. Because before the current peak, the gas flow back into the expansion volume continually and rapidly, the difference of total amount of stored mass and energy are almost same as shown in Figs.4.41 and 4.42.

The difference occurs obviously after 27 ms. It is known in previous section, the maximum pressure in the expansion volume is higher than 40 bar around 3.0 ms. The maximum pressure decreases as the leakage area increases. Mass and enthalpy leakage flow rate through the leak hole is given in Fig.4.43. The total amount of mass and energy in the expansion volume for the whole arcing process for all cases are recorded in Fig.4.41 and 4.42, and the flow rate of mass and energy though the leak hole is given in Fig.4.43. The calculations for these are given below:

Total amount of mass: $\int_{z1}^{z2}\int_{r1}^{r2} \rho \cdot 2\pi r dr \cdot dz$ (4.4)

Total amount of energy: $\int_{z1}^{z2}\int_{r1}^{r2} \rho h \cdot 2\pi r dr \cdot dz$ (4.5)

Mass flow rate: $\int_{r1}^{r2} \rho w \cdot 2\pi r dr$ (4.6)

Energy flow rate: $\int_{r1}^{r2} \rho w h \cdot 2\pi r dr$ (4.7)

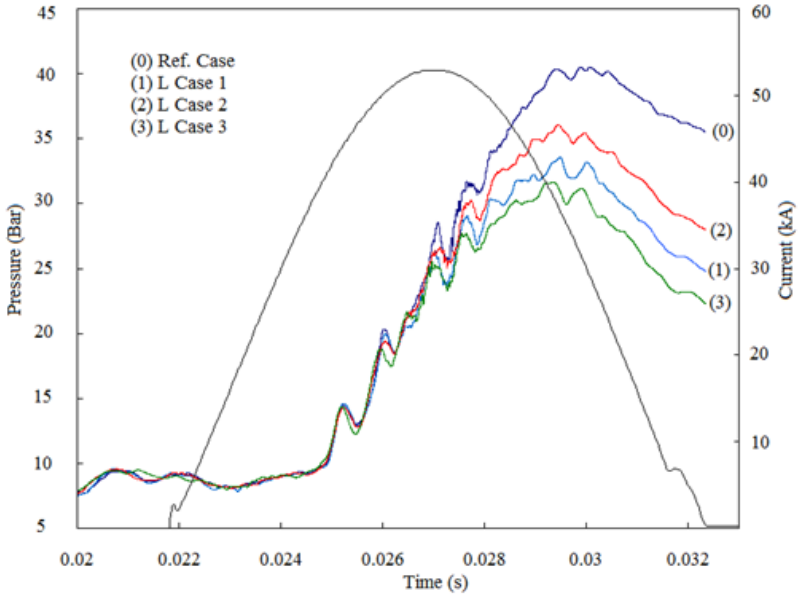

Fig.4.39: Predicted pressure rise in the expansion volume for leakage investigation.

The arc voltages for LCase 1, 2 and 3 are smaller than the Ref. Case (Fig.4.40). It can be seen that the arc voltage and pressure are both inversely proportional to the leakage area. The amount of mass and energy leaked through the leak hole increases when the area is bigger (Fig.4.43-4.44). The stored mass and energy in the expansion volume are getting less when the leakage area is larger.

The maximum value of stored total mass and energy at about 30 ms, when a 7% leakage area exists, the total mass and energy in the expansion volume are respectively 13% and 13% less than the Ref. Case. When a 10% leakage area occurs, the total mass and energy in the expansion volume are respectively 20% and 17% less than the Ref. Case. When a 15% leakage area is developed, the total mass and energy in the expansion volume are 26% and 22% less than the Ref. Case. Fig.4.42 shows that the total stored energy in expansion volume for these 4 cases are almost same before 27 ms. It is the reason why pressure in expansion volume for these cases are not too much difference before 27 ms. The mass and energy flow rate through the leak hole are shown in Fig.4.43 and 4.44. Both of these two figures show that the mass and energy flow rate are rapidly increased at 27 ms. It is also noted that the mass and energy flow rate at the current zero for the LCase 3 are lower than the LCase 1, because the velocity with a large leak hole (15% leakage) is lower than the LCase 1 or LCase 2 which has a smaller leak hole. Yet, it is not affected by the total mass and energy in expansion volume.

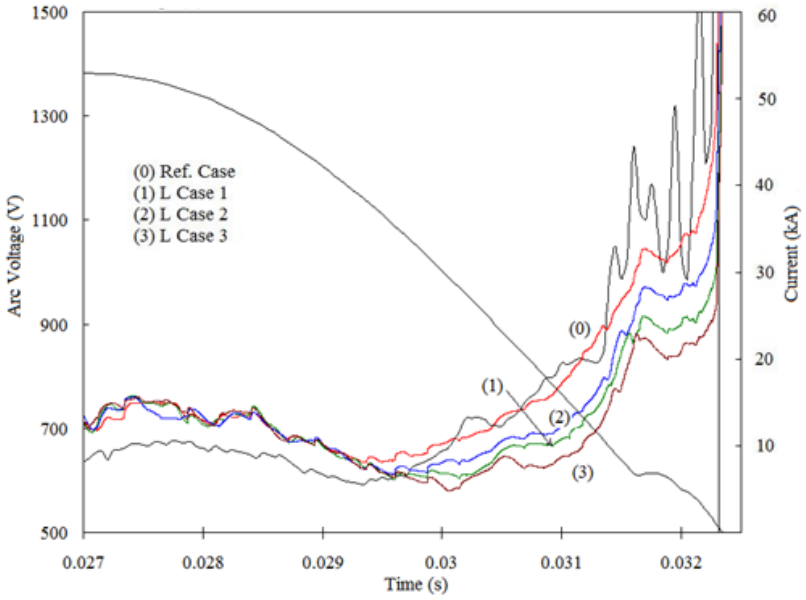

Fig.4.40: Measured and predicted arc voltage from the current peak to the final current zero with extinction peak.

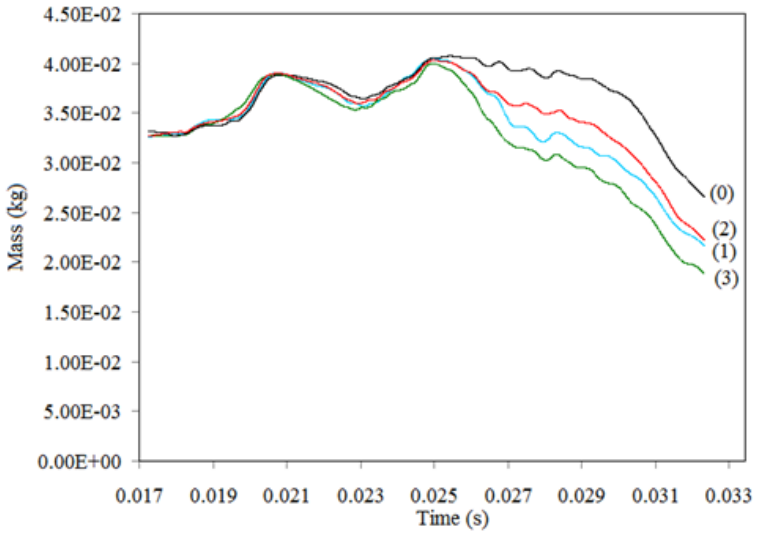

Fig.4.41: Stored total mass in the expansion volume.

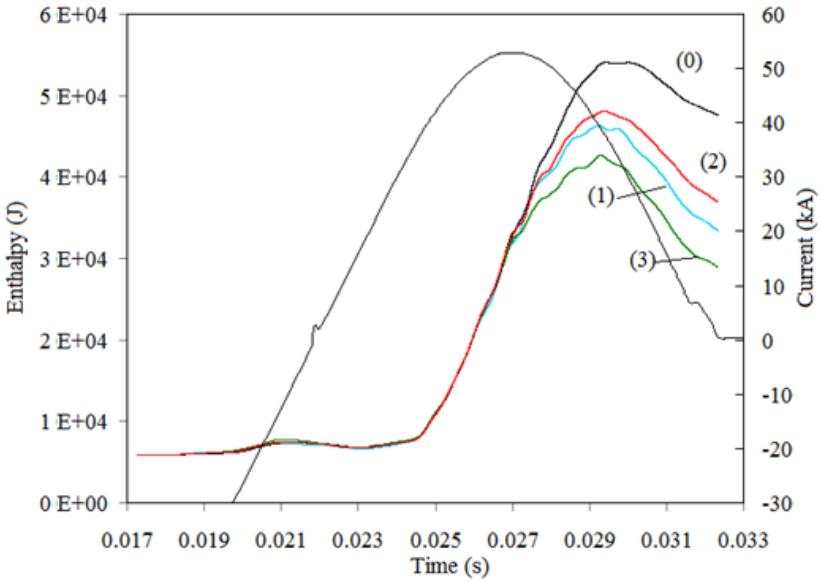

Fig.4.42: Stored total enthalpy in the expansion volume.

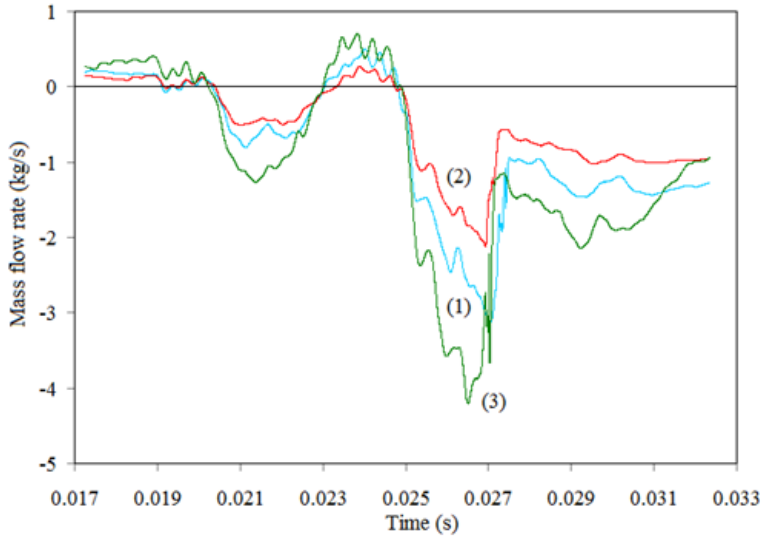

Fig.4.43: Mass flow rate through the leak hole.

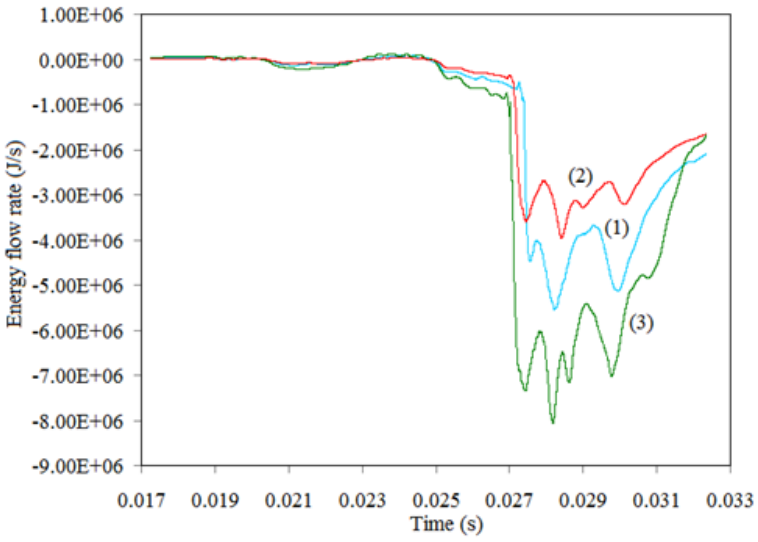

Fig.4.44: Energy flow rate through the leak hole.

The influence of gas leakage from the expansion volume cannot be neglected, as demonstrated by the results in Table 4.4. The interruption capability in terms of the critical RRRV has been reduced by almost 20% with a leakage percentage of 10%, and a reduction of 30% for a leakage percentage of 15%. In type test a valve with severe leakage would lead to interruption failure. Simulation results show that the decrease in interruption capability is linearly proportional to the leak area on the valve plate, as shown in Fig.4.45.

For these three cases, it is known when the leak exists in the expansion volume. The interruption capability of auto-expansion circuit breaker would be decreased and it is proportional to the leak area on the valve plate.

Cases	Critical RRRV (kV/μs)
Ref. Case	5.6
L Case 1 (10%)	4.4
L Case 2 (7%)	4.6
L Case 3 (15%)	4.0

Table 4.4: Predicted critical RRRV for Leakage cases.

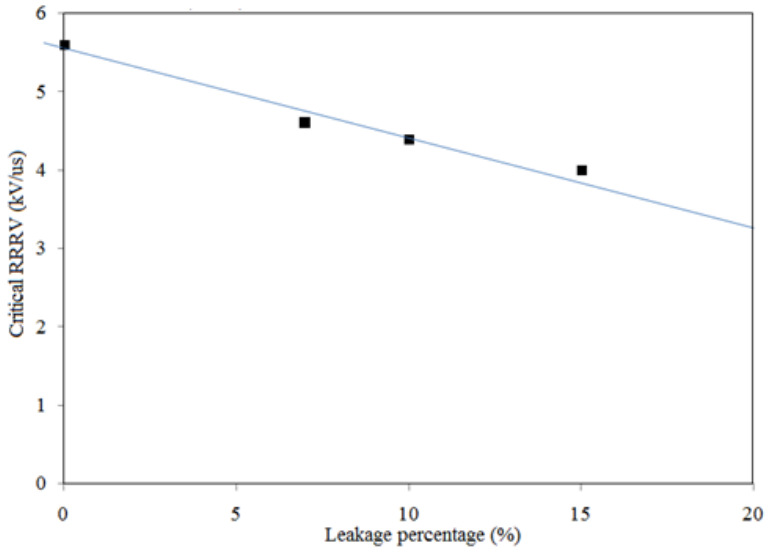

Fig: 4.45 Critical RRRV for the cases with different leakage percentages.

4.5 Summary

The whole arc processing in a 245 kV auto-expansion circuit breaker with Cold Flow Phase, High Current Phase, Current Zero Phase, and Post Arc Current Phase are represented in this chapter. The arc model can accurately predicted the arc processing for the Ref. Case with the newest version. The arc voltage prediction, especially near the current zero period, matches the measurement better than previous works. The pressure variation prediction in the expansion volume also agrees with the measured pressure as well. Design studies based on the accurate arc model is carried out for ABB auto-expansion circuit breaker. The critical RRRV was not provided by the manufactory, as the critical RRRV for the Ref. Case is predicted by my model to compare all the design cases to assess the interruption capability. The influence of interruption capability with different length of the auxiliary nozzle is significant in design of auto-expansion circuit breaker. The leakage problem always exists in reality, it has been proved that the effect is dominant in this chapter and it cannot be

neglected in the design of the circuit breakers.

For the research of leakage from the expansion volume into the compressor in this thesis is limited. There are still lots of parameters for leakage problem such as leakage from compressor, or leakage at the edge of the piston etc.. These problems are also very important, which cannot be neglected in reality. Future work should be considered these in the simulation to assess its influence of interruption capability.

CHAPTER 5
Conclusion and Future Work

5.1 Summary of the Work

5.1.1 Modified k-ε model with different arcs

The simulation of nozzle arcs and switching arcs is an important aspect in switchgear research. PHOENICS, a commercial CFD package is used to solve the arc flow governing equations for modelling arc behaviour. Turbulent arcs in previous studies were modelled using either the Prandtl mixing length or the k-ε models. The Prandtl mixing length model and its modifications can achieve good results for most nozzle arcs. However, the difficulty in the use of the Prandtl mixing length model is that the turbulence parameter c in the turbulence length scale needs to be adjusted for nozzles with different shapes. Thus, the applicability of the Prandtl mixing length model is considerably limited.

In recent years, the k-ε model and its variants have been used to perform the supersonic nozzle arcs and switching arcs. Yet, the performances are not satisfactory, and several modifications based on the standard k-ε model can only make reasonable results in particular conditions. A modification of the k-ε model, proposed by the author, takes into account the approximate effect of the steep temperature (density) gradient at the arc edge. It has been tested on various nozzle arcs and switching arcs with different conditions. Its applicability has been validated for the most cases, which are detailed in Chapter Three.

5.1.1.1 Aachen nozzle arcs

The modified k-ε model was firstly applied to the Aachen nozzle with three direct current levels (1800 A, 600 A and 100 A). The radial temperature profiles obtained from the experiment are used to compare with the predicted results. The standard k-ε model under-represents at 1800 A and over-represents at 100 A the turbulence effect in arc cooling. The inclusion of a temperature correction factor significantly improves the situation at 1800 A. There is also significant improvement in the predicted radial temperature profile, in comparison with the result from the standard k-ε model. For the 600 A case, with the modified k-ε model the predicted radial temperature profile is closest to the measurement with a maximum difference of 7% at a radius of 1.2 mm, whereas with the standard k-ε model the difference is 33% at a radius of 1.4 mm and the predicted arc column is 25% wider than the measurement by comparing the isotherm of 12,000 K. For the 1800 A case, with the modified k-ε model, the predicted radial temperature profile is also closest to the experimental result with a maximum difference of 23% at a radius of 2.0 mm, whereas with the standard k-ε model the difference is 30% at a radius of 2.0 mm and the predicted arc column is 55% wider than the measurement by comparing the isotherm of 13,000 K. For the 100 A case, with the modified k-ε model the predicted radial temperature profile is not match to the measurement with a maximum difference of 25% at a radius of 0.65 mm, and the standard k-ε model makes a relative closer prediction with a maximum difference of 15% at a radius of 0.65 mm. The modified k-ε model predicted arc column is 12.5% thinner than the measurement by comparing the isotherm of 10,000 K. The improvement on the 100 A case cannot be judged properly because of the smaller arc radius, lower axis temperature and uncertainty in the experimental

error. It can be concluded that the modified k-ε model is able to predict turbulent effect in D.C SF_6 arcs for nozzle with mild change of their cross sectional area along axial direction.

5.1.1.2 Campbell nozzle arcs

A reasonable turbulence model for switching arcs should be both steady state and transient arcs. The modified k-ε model was then applied to transient nozzle arcs in Campbell [90] and GE [91] nozzles. The predicted critical RRRVs have been compared with the measurement. For the cases using the Campbell nozzle which has a large diverging angle, three inlet stagnation pressures were used with a di/dt of 10.68 A/μs in simulation by the two k-ε models (standard k-ε and modified k-ε models). The standard k-ε model under-predicted the turbulence effect in the current zero period and led to a critical RRRV more than 50% lower than the measured results for all cases with different inlet stagnation pressures. The modified k-ε model enhances the turbulent effect at the current zero and accurately predicts the critical RRRVs for all cases. For cases with inlet stagnation pressure of 7.14 bar, with the modified k-ε model the predicted critical RRRV is closest to the measurement with a maximum difference of 6% in ratio of pressure of 0.1. Whereas with the standard k-ε model the difference is 62.5% in ratio of pressure of 0.1. For cases with inlet stagnation pressure of 5.10 bar, with modified k-ε model the predicted critical RRRV is also closest to the measurement with a maximum difference of 20% in ratio of pressure of 0.12. Whereas with the standard k-ε model the difference is 67% in ratio of pressure of 0.1. For cases with inlet stagnation pressure of 3.40 bar, with modified k-ε model the predicted critical RRRV is closest to the experimental result with a maximum difference of 21% in ratio of pressure of 0.1. Whereas with the standard k-ε model the difference is 65% in ratio of

pressure of 0.1.

5.1.1.3 GE nozzle arcs

For the cases using the GE nozzle [91] with a di/dt of 25 A/μs for different nozzles, the standard k-ε model under-predicted the turbulence effect in arc cooling, and the modified k-ε model improved the accuracy of prediction of k-ε model. With the modified k-ε model, the critical RRRVs are match to the measurement with a maximum difference of 40% in upstream pressure of 7.8 bar and less than 20% for other cases, whereas with the standard k-ε model, the minimum difference is more than 40% in upstream pressure of 7.8 bar with nozzle throat of 0.25 inch diameter.

5.1.1.4 Switching arcs

The modified k-ε model was finally applied to the real circuit breaker of 252 kV puffer type with 10 kA and 47 kA current levels from PINGGAO Ltd. The arc model is first applied to a complete circuit breaker system. The structure of a circuit breaker is much more complex when compared to the simple nozzle. Thus, the calculation of switching arcs is rather more complicated. The computational domain is bigger, more complex distribution of electric field and flow field, the movement of piston and contacts, there are also other kinds of aspects should be considered in a switching arc. With the standard k-ε model, the predictions of arc voltage, especially around the current zero, are lower than the measurement, which means the arc column was too fat and temperature was higher than in reality. The modified k-ε model effectively enhanced the turbulence effect before the final current zero when the current is low to make better predictions for cases with two current levels. For the 47 kA case, the prediction of arc voltage with modified k-ε model is closest to the measurement, especially near the current zero. The maximum difference is 12.5%

at 22 ms, whereas the predicted arc voltage with standard k-ε model has a maximum difference of 26% at 21.5 ms. For the 10 kA case, the arc voltages before the final current peak with two k-ε models are closed and the difference is produced after 18 ms. the maximum difference with modified k-ε model is only 25% at 19.4 ms and with the standard k-ε model is 43% at 19.4 ms. The pressure in cylinder for both cases are also matched to the measurement with the modified k-ε model.

The modified k-ε model with the temperature gradient coefficient c_T which has a fixed parameter of 0.5, its applicability has been validated by large amount of cases in Chapter 3, and it can be used in most cases without any adjusting except under some particular conditions.

5.1.2 Influence of design parameters in an auto-expansion circuit breaker

The auto-expansion circuit breaker to be simulated is provided by ABB Ltd. In the present work, the calculation of the whole arcing process has been modelled. The Prandtl mixing length model is used to predict the turbulence effect. The critical RRRV was used to compare cases with different parameters.

5.1.2.1 Auxiliary nozzle with different lengths

The auxiliary nozzle is a very important part in the auto-expansion circuit breaker. Ablation on the surface of the inner side of the auxiliary nozzle enhances blockage of the gas flow through the auxiliary nozzle, and helps to build-up a high pressure zone in the interruption nozzle to pump thermal energy into the expansion volume. It also affects the arc column at a low current in the interruption nozzle. The interruption capability is greatly affected by the length of the auxiliary nozzle. A slightly longer auxiliary nozzle (16%) with more ablation vapour could improve the interruption capability 10.7%. An 18% shorter auxiliary nozzle would not affect the interruption capability too

much (1% lower). However, cases with length of 50% of the original auxiliary nozzle and auxiliary nozzle with no ablation have much lower (10.7% and 25% lower), interruption capability as demonstrated in Chapter Four.

5.1.2.2 Expansion volume leakage

Gas leakage from deformed value plates or defects in welded parts can lead to interruption failure, as evidenced in type tests of auto-expansion circuit breakers. Thus, it is necessary to study the consequence of such leakage in auto-expansion circuit breakers. Three different levels of leakage (7%, 10% and 15%) were considered in Section 4.4.3. Results show that leakage from the expansion volume into the compressor affect the interruption capability significantly. For the case of 15% leakage, the interruption capability is reduced by 28% when compared against the Ref. Case. It greatly affects the interruption capability when gas leakage exists. Therefore, the problem of gas leakage in the design studies for an auto-expansion circuit breaker cannot be neglected.

5.2 Future Work

5.2.1 Further improvement of turbulence model

There are two major parts in this thesis, the first one deals with investigation of the turbulence model in the nozzle and switching arcs. The other one involves studying the influence of design parameters for an auto-expansion circuit breaker. The modified k-ε model was applied to several turbulent arcs to assess its applicability. Its prediction is sufficiently accurate in most cases, yet inaccurate for some cases. When the cases of GE nozzle with di/dt of 13 A/μs, the standard k-ε model has over predicted the turbulence effect and the modified k-ε model much over predicted as well. For this case, a further check on the experimental conditions and correctness of experimental results needs to

be carried out in order to draw a conclusion on the poor applicability. Additionally, there is a need to find out why for this particular di/dt the modified k-ε model fails to predict. It is perhaps because the current changes of di/dt of 13 A/μs are slower than the di/dt of 25 A/μs. So at the di/dt of 13 A/μs case, the arc, and the transport of k and ε can follow the change of current. Thus, it is possible that k and ε become larger than expected at the current zero for di/dt of 13 A/μs case, due to stronger radial conduction than expected. For di/dt of 25 A/μs case, the arc and transport of k and ε may not be able to follow the current because the current changes too quickly. In addition to this case, more experimental results such as arc voltage, temperature and dimensions under well defined experimental conditions are essential for the verification of turbulence models.

5.2.2 Further design parameters investigation

The design studies for the ABB auto-expansion circuit breaker in this thesis are limited. The length of auxiliary nozzle is only one of the important design parameter in the whole system, the capacity of the expansion volume, diameter of main nozzle, diverging-converging angle of the main nozzle, etc are also important in the design of an auto-expansion circuit breaker. The design parameters mentioned above could be considered in future work. It is very helpful for the design studies to optimise the research work. Gas leakage from expansion volume prediction in auto-expansion circuit breaker is proposed first by the author, as there are still lots of parameters for the leakage problems, such as leakage from the compressor, leakage at the edge of the piston etc.. These problems cannot be neglected in reality. The arc model, which is introduced in this thesis, can be used to assess the effect of its interruption capability.

References

[1] Davy H. “Elements of Chemical philosophy,” Vol.1, smith and elder, London, 1812, pp152.

[2] F. F. Chen, “Introduction to plasma physics,” Plenum Press, New York and London, 1974.

[3] D. A. Frank-Kamentskii, book of “Plasma the fourth state of matter,” 1972, pp9.

[4] K. Nakanishi, book of “Switching Phenomena in high Voltage Circuit Breakers,” 1991.

[5] W. Sorensen and H. E. Mendenhall, “Vacuum Switching Experiments at California Institute of Technology,” American Ins. of Electrical Eng. Trans. Vol XLV. 1926.

[6] R. W. Liebermann and J. J. Lowke, “Radiation emission coefficients for sulphur hexafluoride arc plasmas,” J. Quant. Spectrosc. Radiat. Transfer, 1976, 17: pp253-264.

[7] J. Slepian, “Extinction of an A-C arc,” Trans. AIEE, 1928, 47:pp1398-1408.

[8] A. M. Cassie, “Arc rupture and circuit breaker severity: A new theory.” Technical report 102, International des Grands Reseaux Electrigues’a Haute Tension (CEGRE), Paris, France, 1939.

[9] J. T. E. Brown, “A study of arc behaviour near current zero by means of mathematical models,” AIEE Trans, 78 (Part III): 1948, pp141-143.

[10] J. T. E. Brown, “An approach to mathematical analysis of a.c. arc extinction in circuit breakers,” AIEE Trans, 78 (Part III): 1958, pp15081-1517.

[11] W. Elenbaas. Phillips Research Report. 1(5), 1946.

[12] G. Frind, “Time constant of flat arcs cooled by thermal conduction,” IEEE Trans. On Power Apparatus and Systems, 1965, 84:pp1125-1131.

[13] M. D. Cowley, “Integrated methods of analysing electric arcs: I. Formulation,” J. Phys. D: Appl. Phys., Vol. 7, 1974, pp2218.

[14] M. T. C. Fang, S. K. Chan and M. D. Cowley, “Transient behaviour of interrupted arc in laminar flow,” J. Phys. D: Appl. Phys., Vol. 9, 1976, pp1757.

[15] J. J. Lowke and H. C. Ludwing, “A simple model for high current arcs stabilised by forced convection,” J. Appl. Phys., Vol. 46, 1975, pp3352.

[16] B. W. Swanson and R. M. Roidt, “Boundary layer analysis of an SF_6 circuit breaker arc,” IEEE Trans., Vol. PAS-90, 1971, pp1086.

[17] D. R. Topham, “The electrical arc in constant pressure,” J. Phys. D:Appl. Phys., vol.4, 1971, pp1114.

[18] D. R. Topham, “The characteristics of axial flow electric arcs subject to pressure gradient,” J. Phys. D:Appl. Phys., vol.4, 1972, pp533.

[19] D. R. Topham, “Scaling laws for the interaction of a gas-blast circuit breaker arc with an electric circuit,” Proc. IEE, Vol.119, 1972, pp1469.

[20] B. W. Swanson, R. M. Roidt and T. E. Browne, “Arc cooling and short line fault interruption,” IEEE Trans., Vol. PAS-90, 1970, pp1094.

[21] B. W. Swanson and R. M. Roidt, “Some numerical solutions of the bound-

ary layer equations for an SF_6 arc," IEEE Trans., Vol. 59, 1971, pp493.

[22] B. W. Swanson and R. M. Roidt, "Thermal analysis of an SF_6 circuit breaker arc," IEEE Trans., Vol. PAS-91, 1972, pp381.

[23] B. W. Swanson, R. M. Roidt and T. E. Browne, "A thermal arc model for short line fault interruption ," Z-A, Bd.93, 1972, pp375.

[24] B. W. Swanson, IEE Winter Power Meeting, Paper c-74.

[25] B. W. Swanson, "Nozzle arc interruption in supersonic flow," IEEE Trans., Vol. PAS-96, 1977, pp1679.

[26] M. T. C. Fang, "A review of gas blast circuit breaker arc modelling," Arc Research Project Report, ULAP-T75, University of Liverpool, 1983.

[27] M. T. C. Fang and W. Y. Lin, "Current zero behaviour of a gas-blast arc Part I: Nitrogen," IEE Proc., Vol.138, No.1, 1991, pp71.

[28] W. Hermann and K Ragaller, "Theoretical description of the current interruption in HV gas blast breakers," IEEE Trans., vol. PAS-96, No.5, 1977, pp1546.

[29] G. Frind, L. E. Prescott and J. H. Van Noy, "Measurements of post-zero current and of power loss in air-blast arcs," J. phys. D: Appl. Phys., Vol. 12, 1979, pp133.

[30] F. R. El-Akkari and D. T. Tuma, "Simulation of transient and zero current behaviour of arcs stabilised forced convection," IEEE Trans., PAS-96, 1977, pp1784.

[31] D. T. Tuma, "A comparison of the behaviour of SF_6 and N_2 blast arcs

around current zero," IEEE Trans., Vol.PAS-99, No. 6, 1980, pp2129.

[32] D. T. Tuma and H Fong, "Current zero deformation by interaction of gas blast arc with the test circuit," IEEE Trans., Vol.PAS-99, 1980, pp976.

[33] D. T. Tuma and J. J. Lowke, "Prediction of properties of arcs stabilised by forced convection," J. Appl. Phys., Vol.46, 1975, pp3361.

[34] M. T. C. Fang, D. Brannen and G. R. Jones, "An analytical method for the design of circuit breaker nozzles," Symposium on High Voltage Switching Equipment, 1979.

[35] S. K. Chan, M. D. Cowley and M. T. C. Fang, "Integral methods of analysing electric arcs: III. Shape-factor correlation for low radiation and laminar flow," J. Phys. D., Vol.9, 1976, pp 1085.

[36] V. R. Malghan, M. T. C. Fang and G. R. Jones, "Investigation of quasi-steady state high current arcs in an orifice air flow," J. Appl. Phy., Vol.48, 1977, pp2331-2337.

[37] M. T. C. Fang, S. K. Chan and M. D. Cowley, "Transient behaviour of interrupted arc in laminar flow," J. Phys. D: Appl. Phys., Vol.9, 1976, pp1757.

[38] M. T. C. Fang and W. H. Bu, "Investigation of ablation dominated AC nozzle arcs," IEE Proc. A, Vol.138, 1991, pp71-77.

[39] W. H. Bu, M. T. C. Fang and Z. Y. Guo, "The behaviour of ablation dominated DC nozzle arcs," J. Phys. D: Appl. Phys.23, 1990, pp175-183.

[40] K. Ragaller, W. Egli and K. P. Brand, "Dielectric recovery of an axially blown SF_6-arc after current zero: Part II Theoretical investigation," IEEE Trans., Vol.PS-10, No.3, 1982, pp154.

[41] K. Ragaller, W. R. Schneider and W. Hermann, “A special transformation of the differential equations describing blown arcs,” ZAMP, Vol.22, 1971, pp474.

[42] W. Hermann, “Computation of decaying wall-stabilised arcs,” Z. Naturforsch., Vol. 28a, 1973, pp443.

[43] H. P. Graf, H. P. Meili, E. Fisher and H. J. Schoetzau, “Axially blown SF_6 arcs around current zero,” Appl. Phys., B., Vol.36, 1985, pp33-40.

[44] R. R. Mitchell, D. T. Tuma and J. F. Osterle, “Transient two dimensional calculation of properties of forced convection stabilized electric arcs,” IEEE Trans., Vol.PS-13, No.4, 1985, pp207.

[45] J. J. Lowke and H. E. Lee, “A numerical study of a two dimensional circuit breaker arc during current interruption,” Proc. of gas discharge and their applications, Oxford, 1985, pp 54-56.

[46] M. T. C. Fang and W. Y. Lin, “Current zero behaviour of a gas blast arc, Part I: nitrogen,” IEEE Proc., 137, Part A(4); 1990, pp175-183.

[47] M. T. C. Fang and Q. Zhuang, “Current zero behaviour of an SF_6 gas blast arc. i. laminar flow,” J. Phys. D: Appl. Phys. 25(8), 1992, pp1197-1204.

[48] M. T. C. Fang, Q. Zhuang and X. J. Guo, “Current zero behaviour of an SF_6 gas blast arc. ii. Turbulent flow,” J. Phys. D: Appl. Phys. 27(1), 1994, pp74-83.

[49] J. F. Zhang, M. T. C. Fang and D. B. Newland, “Theoretical investigation of a 2 kA DC nitrogen arc in a supersonic nozzle,” J. Phys. D., 1987, pp368-379.

[50] K. A. Ernst, J. G. Kopainsky and H. H. Maeker, “The energy transport including emission and absorption in N_2 arcs of different radii,” IEEE Trans., 1973, PS-1, pp3-16.

[51] P. J. Shayler and M. T. C. Fang, “Flow near the upstream electrode of gas-blast arcs,” J. Phys. D: Appl. Phys., Vol.11, 1987, pp1743.

[52] W. Hermann, V. Kogelschatz, L. Niemeyer, K. Ragaller and E. Schade, “Investigation of the physical phenomena around the current zero in HV gas blast breakers,” IEEE Trans., 1976, PAS-95, pp1165-1176.

[53] M. T. C. Fang, J. L. Zhang and J. D. Yan, “On the use of Langmuir probes for the diagnosis of atmospheric thermal plasmas,” IEEE Trans., Vol. 33, No. 4, 2005, pp 1431-1442.

[54] P. Kovitya and J. J. Lowke, “Two-dimensional analysis of free burning arcs in argon,” J. Phys. D: Appl. Phys., 18(1985), pp53-70.

[55] J. Menart, J. Heberlein, and E. Pfender, “Theoretical radiative emission results for argon/ copper thermal plasma,” Plasma Cham. Plasma Pros., Vol. 16, 1996, pp245S-265S.

[56] Rethfeld, J. Wendelstor, T. Klein and G. Simon, “A self-consistent model for the cathode fall region of an electric arc,” J. Phys. D: Appl. Phys. 29, 1996, pp121-128.

[57] K. C. Hsu, K. Etemadi and E. Pfender, “Study of the free-burning high intensity argon arc,” J. Appl. Phys. 54(3), PAS-52, 1983, pp1293-1301.

[58] J. J. Lowke, P. Kovitya and H. P. Schmidt, “Theory of free burning arc columns including the influence of the cathode,” J. Phys. D: Appl. Phys., 25,

1992, pp1600-1606.

[59] P. Y. Zhu, J. J. Lowke and R. Morrow, “A unified theory of free burning arcs, cathode sheaths and cathodes,” ,” J. Phys. D: Appl. Phys., 25, 1992, pp1221-1230.

[60] S. Biehler, G. Ecker and K. U. Riemann, “Theory of the presheath in a weakly ionised plasma with hot neutrals,” Phys. Fluids, Vol. 31, Issue 7, 1999.

[61] M. S. Benilov, M. D. Cunha and G. V. Naidis, “Modelling interaction of multi-species plasmas with thermionic cathodes,” Plasma Source Sci., Technol, Vol. 14, 2005, pp517-524.

[62] B. Rethfeld, J. Wendelstorf, T. Klein and G. Simon, “A self-consistent model for the cathode fall region of an electric arc,” J. Phys. D: Appl. Phys. Vol. 29, 1996, pp121-128.

[63] V. Terzija, G. Preston, M. Popov and N. Terzija, "New static "AirArc" EMTP model of long arc in free air, " IEEE TRANS. ON POWER, VOL. 26, No. 3, 2011

[64] M. Kizilcay and T. Pniok, "Digital simulation of fault arcs in power systems," Eur. Trans. Elect. Power, VOL. 1, No. 1, 1991.

[65] A. T. Johns, @. K. Aggarwal, and Y. H. Song, "Improved techniques for modelling fault arcs on faulted EHV transmission systems," Proc. Inst. Elect. Eng., Gen. Transm. Distrib., VOL. 141, No.2, 1994.

[66] V. Terzija and H.-J. Koglin, "On the modeling of long arc in still air and arc resistance calculation," IEEE Trans. Power Del., VOL. 19, No. 3, pp.1012-1017, 2004.

[67] E. Schade, “Recovery of switching arcs,” Proc. XVIIth Int. Conf. Phenomena Ionised Gases, 1985, pp277-297.

[68] W. Hermann, U. Kogelschtz, L. Niemyer, K. Ragaller and E. Schade, “Experimental and theoretical study of a stationary high-cuurent arc in a supersonic nozzle flow,” J. Phys. Phys. D., Vol.7, 1974, pp1703.

[69] D. Leseberg and G. Pietsch, “Optical investigation on a SF_6 switching arc inside a glass nozzle,” Int. Conf. on Gas Discharges and Their Applications (London), 1982, pp9-12.

[70] W. Hermann, U. Kogelschtz, L. Niemyer, K. Ragaller and E. Schade, “Investigation on the physical phenomena around current zero in HV gas blast breakers,” IEEE Trans. Power Appar. Syst. 96, 1977, pp1165-76.

[71] A. Kobayashi, S. Yanabu, S. Yamashita and Y. Ozaki, “Experimental investigation on arc phenomena in SF_6 puffer circuit breakers,” IEEE Trans. Power Appar. Syst. 8, 1980, pp339-43.

[72] D. Leseberg and G. Pietsch, “Interferometrische Unterschungen von Schaltichtbogen in stromendem SF_6,” 1982.

[73] H. Scheichting, book of “BOUNDARY LAYER THEORY,” 1968.

[74] L. Prandtl, “Z. angew,” math. Mech. 5(1).

[75] B. E. Launder and B. I. Sharma, “Application of the energy dissipation model of turbulence to the calculation of flow near a spinning disc,” Letters in Heat and Mass Trans., Vol.1, No. 2, 1974, pp131-138.

[76] L. Niemyer and K. Ragaller, “Development of turbulence by the interaction of gas flow with plasma,” Z. Naturforsch., 28a., 1973, pp1281.

[77] J. M. Seiner, M. K. Ponton, B. J. Jansen and N. T. Lagen, “The effects of temperature on supersonic jet noise emission,” DGLR/AIAA 14^{th}

Aeroacoustics Conf., Aachen, Germany, AIAA, 2001, pp92-02-046.

[7783] R. H. Thomas, K. W. Kinzie and S. P. Pao, “Computational analysis of a pylon chevron core nozzle interaction,” AIAA, 2001, pp2001-2185.

[79] S. B. pope, “An explanation of the Turbulent round-jet/plane-jet anomaly,” AIAA Journal, Vol.16, No. 3, 1978, pp.279-281.

[80] A. T. Theis and C. K. W. Tam, “Computation of turbulent axisymmetric and Non-axisymmetric jet flows using the k-ε model,” AIAA J., 34, pp309-316.

[81] C. K. W. Tam and A. Gancsan, “A modified k-ε model for calculating the mean flow and noise of hot jets,” AIAA, Jan 2003, pp1064.

[82] A. B. Lebedev, A. D. Lyubimov, V. P. Maslov, B. I. Mineev, A. N. Seeundov and F. Birch Stanley, “The prediction of three dimensional jet flows for noise applications,” AIAA, 2002, pp2422.

[83] R. M. C. So and T. P. Sommer, “An Explicit algebraic heat flux model for the temperature field,” Int. J. Heat fluid flow, 7, 1995, pp455-465.

[84] M. Ronki and T. B. Gatski, “Predicting turbulent convective heat transfer in fully developed duet flows,” Int. J. Heat fluid flow, 22, 1995, pp381-392.

[85] K. Abe, T. Kondoh and Y. nagano, “A two equation heat transfer model reflecting second moment closures for wall and free turbulent flows,” Int. J. Heat fluid flow, 17, 1995, pp228-237.

[86] J. D. Yan, K. I. Nuttall and M. T. C. Fang, “A comparative study of turbulence models for SF_6 arcs in a supersonic nozzle,” J. Phys. D: Appl. Phys. 32, 1999, pp1401-1406.

[87] K. S. Abdol-Hamid, S. P. Pao, S. J. Massey and Alaa Elmiligui, "Temperature corrected turbulence model for high temperature jet flow," Trans. Of the ASME, Vol. 126, 2004, pp 844-850.

[88] K. D. Song, B. Y. Lee and K. Y. Park, "Calculation of the post arc current in a supersonic nozzle using the k-ε turbulence model," J. Korean Phys. Society, Vol. 45, No. 6, 2004, pp1537-1543.

[89] H. Wang, Y. Zhan, J. D. Yan and M. T. C. Fang, "Modelling of low current turbulent nozzle arcs with temperature gradient correction," in Proc. 18th Int. conf. gas Discharges, Greifswald, Germany, 2010, pp90-93.

[90] L. C. Campbell, J. F. Perkins, and J. L. Dallachy, "Effect of nozzle pressure ratio on SF_6 arc interruption," in Proc. 4th Int. conf. Gas Discharges, Swansea, UK., 1976, pp. 44-47.

[91] G. Frind, R. E. Kinsinger, R. D. Miller, H. T. Nagamatsu and H. O. Noeske, "Fundamental Investigation of arc interruption in gas flow," EPRI EL-284 (Project 246-1), 1977.

[92] A. B. Murphy, "A comparison of treatments of diffusion in thermal plasma," J. Phys. D, Appl. Phys., vol. 29, 1996, pp1922-1932.

[93] H. Schlichting, "Boundary layer theory," 7th Edition, McGraw-Hill Book Company, 1979.

[94] Liepmann and Roshko, "Elements of gas dynamics," Wiley, 1957.

[95] K. Nakahashi and G. S. Deiwert, "Self-adaptive-Grid Method with Application o airfoil flow," AIAA Journal, Vol.25, 1987, pp513.

[96] J. D. Yan, "Computer simulation of switching arcs and model implem-

entation in PHOENICS," internal report of University of Liverpool.

[97] J. L. Zhang, J. D. Yan, A. B. Murphy, W. Hall and M. T. C. Fang, "Computational investigation of arc behaviour in an auto-expansion circuit breaker contaminated by ablated nozzle vapour," IEEE Trans. On Plasma Sci., Vol.30, 2002, pp706-719.

[98] M. T. C. Fang and D. B. Newland, "Liverpool University Arc Research Project Rept ULAP T-69," 1981.

[99] M. R. Smith, J. R. Leclerc and G. R. Jones, "Liverpool University Arc Research Project Rept ULAP-T66," 1980.

[100] M. T. C. Fang and D. B. Newland, "DC nozzle arcs with mild wall ablation," J. Phys. D: Appl. Phys. 16, 1983, pp793-810.

[101] C. B. Ruchti and L. Niemyer, "Ablation controlled arcs," IEEE Trans. On Plasma Sci., Vol. PS-14, 1986, pp 423-434.

[102] W. Hermann, U. Kogelschatz, K. Ragaller and E. Schade, "Investigation of a cylindrical axially blown high-pressure arc," J. Phys. D: Appl. Phys., Vol. 7, 1974, pp607.

[103] C. M. Dixon, J. D. Yan and M. T. C. Fang, "A comparison of three radiation models for the calculation of nozzle arcs," J. Phys. D: Appl. Phys. 37, 2004, pp 3309-3318.

[104] S. D. Eby, J. Y. Trepanier and X. D. Zhang, "Modelling of radiative transfer in SF_6 circuit breaker arcs with the p-1 approximation," J. Phys. D: Appl. Phys., 1998, 31:pp1578-1588.

[105] V. Aubrecht and J. J. Lowke, "Calculations of radiation transfer in SF_6

plasmas using the method of partial characteristics," J. Phys. D: Appl. Phys., 1994, 27:pp2066-2073.

[106] V. G. Sevastyanenko, "Radiation transfer in a real spectrum: Integration over frequency," J. Eng. Phys., 1979, 36: pp138-148.

[107] V. G. Sevastyanenko, "Radiation transfer in a real spectrum: Integration with respect to the frequency andangles," J. Eng. Phys., 1980, 38: pp137-139.

[108] V. Aubrecht, private communication

[109] G. R. Jones and M. T. C. Fang, "The physics of high power arcs," Rep. Prog. Phys., Vol.43, 1980, pp1415-1465.

[110] J. L. Zhang, J. D. Yan and M. T. C. Fang, "Investigation of the effects of pressure ratios on arc behaviour in a supersonic nozzle," IEEE Trans. on Plasma Sci., Vol.28, 2000, pp1725-1734.

[111] A. B. Murphy and P. Kovitya, "Mathematical model and laser-scattering temperature measurements of a direct-current plasma torch discharging into air," J. Appl. Phys., 1993, 73: pp4759-4769.

[112] K. W. Tam. Christopher and G. Anand, "Modified k-ε turbulence model for calculating hot jet mean flows and nosie," AIAA Vol. 42, No. 1, 2004, pp26-34.

[113] D. Leseberg, "Holographische interferometrie undoptische spektroshopie an einem SF_6 schaltlichtbogen," PhD thesis, RWTH Aachen, 1982.

[114] R. E. Blundell, M. T. C. Fang and A. Vourdas, "Stability of a DC SF_6 arc in accelerating flow," IEEE Trans. Plasma Sci. 1997, 25: pp852-859.

[115] G. Frind and J. A. Rich, "Recovery speed of axial flow gas blast interrupter: Dependence on pressure and di/dt for air and SF_6," IEEE Trans. Power App. Syst., vol. PAS-93, 1974, pp. 1675-1684.

[116] J. D. Yan, M. T. C. Fang, and W. B. Hall, "The development of PC based

CAD tools for auto-expansion circuit breaker design", IEEE Trans. Power Delivery, vol. 14, 1999, pp.176 -181.

[117] CHAM. PHOENICS. Bakery House, 40 High Street, Wimbledon Village, London, SW19 5AU, UK.

[118] T. M. Wong, J. D. Yan, X. Ye, J. Abrahamsson and M. T. C. Fang, "Global thermal and aerodynamic environment in high voltage auto-expansion circuit breakers," Proceedings of the XVIIth Symp. On Phys. of Switching Arcs, Czech Rep. 2007, pp 37-46.

[119] T. M. Wong, thesis of PhD, "Computer simulation and visualisation of complex system: Arcs and hot gas flow in auto-expansion circuit breaker," Department of Electrical Engineering and Electronics, the University of Liverpool, 2008.

[120] F. Raizadeh and H. Dwyer, "A use of sensitivity analysis in k-ε turbulence round jet modelling," Symp. of Turbulent shear flows, 4th 1984, pp12-14.

[121] S. Kwan, PhD Thesis, "Computer simulation of arcs in gas-blast circuit breakers." Department of Electrical Engineering and Electronics, the University of Liverpool, 1996.

[122] PHOENICS notes on the modelling of turbulence

[123] H. Y. Wang, J. D. Yan, J. Wu and Y. Li, "Turbulence models for transient switching arcs," in Proc. 19th Int. conf. Gas Discharges, Beijing, China, 2012, pp194-197.

[124] J. B. Kim, C, H Yeo and Y Yoshioka, "Effects of various factors on gas blast characteristics of auto-expansion circuit breaker," IEEE Trans. Power Delivery, 25, 2010, pp1538-46.

[125] T. Shinkai, T. Koshiduka, T. Mori, T Uchii, T Tanaka and H Ikeda,

"Improvement of thermal interruption capability in self-blast interrupting chamber for new 245-kV 50-kA GCB," Electrical Eng. in Japan, 67, 2009, pp9-17.

[126] M. T. C. Fang and J. D. Yan, "Common problems encountered in computer simulation of gas blast arcs," Proc. of the third Int. Conf. on Electrical Contacts, Arcs, Apparatus and Their Applications, Xi'an, China, Vol. I, 1997, pp1-7.

[127] U. Rutten, "Simulation of switching arc-gas interaction in SF_6 circuit breakers," Proc. of 10^{th} Int. Conf. on Gas Discharges and their applications, Swansea, UK, 1992, pp140-143.

[128] M. Claessens, R. von Starck, and H. Thiel, "Simulation of gas flow phenomena in high-voltage self-blast circuit breakers at high fault current interruption," IEEE Trans. On Plasma Sci., Special Issue on High-Pressure Arcs and High-Frequency Thermal Plasma, Vol.25, No.5, 1997, pp1001-1007.

[129] Q. Zhang, J. D. Yan and M. T. C. Fang, "Computer aided design studies of auto-expansion circuit breakers," Proc. of 19^{th} Int. Conf. on Gas Discharges and their applications, Beijing, China, 2012, pp82-85.

Appendix

Appendix I

USER defined k-ε model

For further modification of standard k-ε model, a user defined k-ε model is established. In the previous studies, the modified k-ε model is added an additional term into the KETMD (standard k-ε turbulence model in PHOENICS). It is not convenient to modify some coefficients or parameter in standard k-ε model. This USERKE model is aimed to modify the standard k-ε turbulence model easier and efficient.

Two additional variables of kinetic energy and its dissipation rate are replaced by KEUS and EPUS from KE and EP.

To order the solution of the equations of mass, momentum and energy the PIL command **SOLVE (<var>)** is used. in Q1 file (which has been introduced in Chapter 2) the command of **SOLVE(KE,EP)** has been replaced by **SOLVE(KEUS,EPUS).**

User defined equations for length scale (LEN1) and turbulent kinetic viscosity (ENUT) can be defined by:

LEN1=CD*KEUS**1.5/EPUS

ENUT=CMU*KEUS**2/EPUS

where CD is the coefficient of length scale equals 0.1643 and CMU, the coefficient of turbulent viscosity, equals 0.09.

The source term of the k-ε equations can be defined as KELIN command, in the KETMD is default, but in the user k-ε model, it defined by patches of KEUS and EPUS (Fig.3.15, 3.16).

```
  136 CONTINUE
C------------------- SECTION  7 ------------- coefficient = GRND6

      IF((NPATCH.EQ.'KESO').AND.(INDVAR.EQ.LBNAME('KEUS'))) THEN
       CDEE=RG(133)
       CMEW=RG(134)
       CCUSER=CDEE/CMEW
       CALL FN31(CO,VIST,LEN1,CCUSER,1.0,-2.0)
      ENDIF

      IF((NPATCH.EQ.'KESO').AND.(INDVAR.EQ.LBNAME('EPUS'))) THEN
       C2EE=RG(132)
       CDEE=RG(133)
       CMEW=RG(134)
       CCUSER=C2EE*CDEE/CMEW
       CALL FN31(CO,VIST,LEN1,CCUSER,1.0,-2.0)
      ENDIF

      RETURN
 1317 CONTINUE
C------------------- SECTION 18 ------------------- value = GRND6

      IF((NPATCH.EQ.'KESO').AND.(INDVAR.EQ.LBNAME('KEUS'))) THEN
       CDEE=RG(133)
       CMEW=RG(134)
       CCUSER=CMEW/CDEE
       CALL FN31(VAL,GEN1,LEN1,CCUSER,1.0,2.0)
      ENDIF

      IF((NPATCH.EQ.'KESO').AND.(INDVAR.EQ.LBNAME('EPUS'))) THEN
       C1EE=RG(131)
       C2EE=RG(132)
       CCUSER=C1EE/C2EE
       CALL FN21(VAL,GEN1,VIST,0.0,CCUSER)
      ENDIF
      RETURN
```

Fig.3.15: Code in ground.for file. GEN1 is the mean rate of strain defined by (Uij+Uji)^2/2

KELIN=0

$C_k = \nu_t C_d /(L_m^2 C_\mu)$ $\quad V_k = E L_m^2 C_\mu / C_d$

$C_\varepsilon = C_{2\varepsilon} C_d \nu_t /(C_\mu L_m^2)$ $\quad V_\varepsilon = C_{1\varepsilon} \nu_t E / C_{2\varepsilon}$

Fig.3.16: source term for the equations of k and ε.

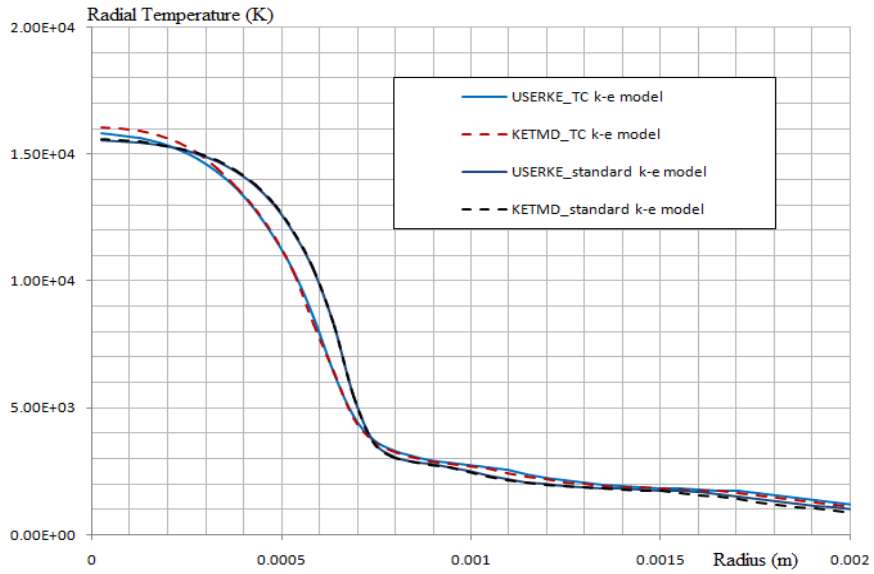

Fig.3.17: comparison of prediction of radial temperature by standard k-ε model with default KETMD and user defined USERKE at nozzle throat in 100A DC current case.

For the nozzle arcs of Aachen nozzle, all three current levels from 100 A to 1800 A can be accurately calculated by using the USERKE. The comparison of radial temperature profiles by using these two calculations of KETMD (PHOENICS default equations) and USERKE (User defined equations) with two turbulence models have been carried out and it is shown in Fig.3.17 for the 100 A case. It is found that the prediction with these two calculations are almost same, it is can be used for the DC steady case like Aachen nozzle arc case shown. However, in the latter studies, it is can be found that this calculation may not calculate accurately for some complex situation, such as transient cases or switching arcs.